Sediment Dynamics of Megaslides along the Svalbard continental Margin and the Relation to paleoenvironmental Changes and Climate History

Dipl.-Geol. Daniel Winkelmann

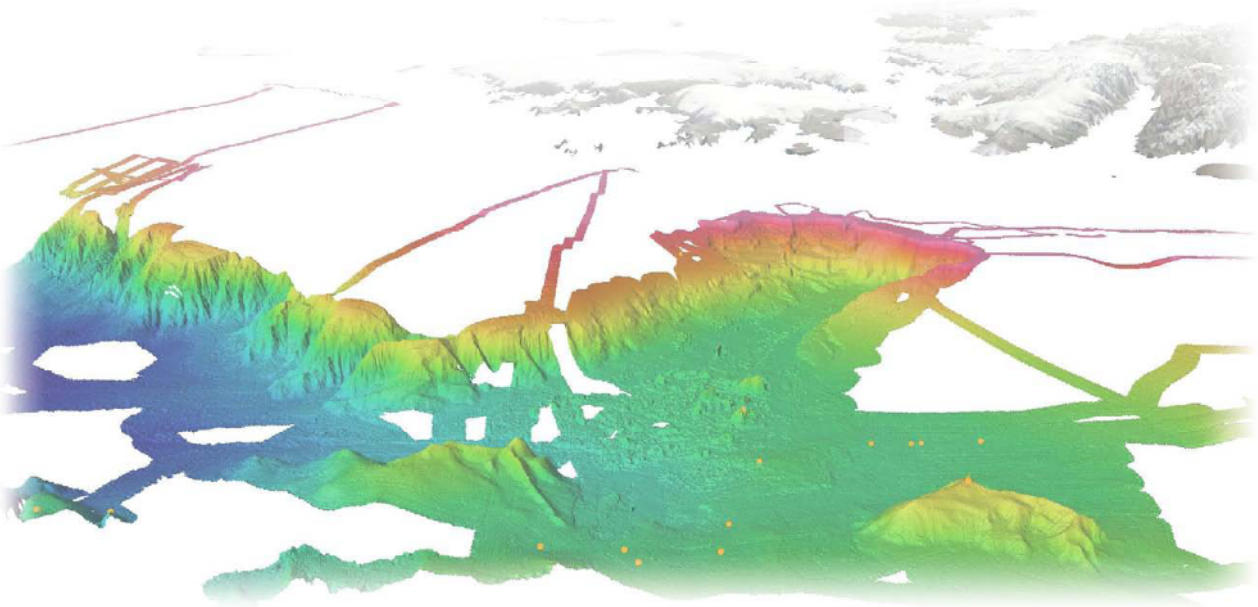

vorgelegt beim Fachbereich Geowissenschaften der Universität Bremen als Dissertation

zur Erlangung des akademischen Grades

eines Doktors der Naturwissenschaften (Dr. rer. Nat.)

Bremerhaven, August 2007

1. Gutachter: Prof. Dr. Rüdiger Stein

2. Gutachter: Prof. Dr. Rüdiger Henrich

Contents

Abstract

With increasing interest in slope stability issues on continental shelves the causes and trigger mechanism of submarine slides get more and more into the scientific focus. Within the ESF EUROMARGINS project “Slope Stabilities on Europe's passive continental Margin” (SPACOMA) sediment dynamics of megaslides along the passive continental margin north of Svalbard have been investigated. The study concentrated on identification and sedimentological characterisation of mega-failure events, their dating and interpretation in relation to paleoceanography and climate history of the Svalbard archipelago.

Integrated interpretation of multi-beam bathymetric, sediment-penetrating acoustic (PARASOUND) and seismic data shows a multiple slope failure on the northern European continental margin, north of Spitsbergen. One huge submarine slide has been identified which was first described by Cherkis et al. (1999) – the Yermak Slide (later named Hinlopen/Yermak Megaslide).

The extent of the Hinlopen/Yermak Megaslide has been revised based on new acoustic and detailed bathymetric data. Details from the side's internal structure give evidence for one main slide event followed by repeated minor events. The first slide event occurred during MIS 3 around 30 cal. kyr. BP and was characterised by highly dynamic and rapid evacuation of ca. 1.250 km³ of sediment from the lower to the upper part of the shelf slope. During this megaslide event, headwalls up to 1600 m have been created and ca. 1150 km³ material from hemi-pelagic sediments and from the lower pre-existing trough mouth fan has been entrained and transported into the semi-enclosed Sophia Basin. This megaslide was followed by a secondary evacuation of debris material to the Nansen Basin accomplished by funnelling of the debris through the Littke Channel between Polarstern Seamount and the adjacent continental slope. The main slide debris is overlain by a set of fining-upwards sequences as evidence for the associated suspension cloud and following minor failure events. Subsequent adjustment of the eastern headwalls led to failure of rather soft sediments and creation of smaller debris flows that followed the main slide superficial topography. Discharge of the Hinlopen ice stream during the Last Glacial Maximum and the following deglaciation draped the central headwalls and created a new trough mouth fan (TMF) deposit of glacigenic debris flows south of the remnants of the original (now abandoned) TMF.

The true geometry, with an affected area of at least 10,000 km^2 and more than 2400 km^3 involved sedimentary material, puts the Hinlopen/Yermak Megaslide among the largest exposed submarine slides worldwide, comparable to the Storegga Slide off central Norway. The side's geometry and internal physical appearance point to a tectonically induced partial shelf collapse.

The timing of the Hinlopen/Yermak Megaslide around 30 cal. kyr. BP coincides with the transition of the Kapp Ekholm Interstadial into Glaciation G of Svalbard (Mangerud et al., 1998) and the build-up phase of the Svalbard-Barents Sea Ice Sheet. Thus, the slide occurred during a period of falling sea level, increasing ice volume and, presumably, increasing glacio-tectonic activity. Following a detailed assessment of the paleo-environmental conditions as well as possible trigger mechanisms of the Hinlopen/Yermak Megaslide, including paleo-sea-level, paleoceanographic circulation, glacial processes, tectonics and earthquakes, it is concluded that the Hinlopen/Yermak Megaslide has been the consequence of the rapid onset of Late Weichselian glaciation resulting in a drastic sea-level drop, asymmetrical ice loading and a fore bulge development. As the final trigger we assume a strong earthquake positioned below or close to the SE-Sophia Basin.

The SW Sophia Basin constitutes an excellent archive in respect to paleo-environmental reconstructions. As a side product of the slide related investigations within the ESF project a number of gravity cores have been recovered containing promising records. Application of established methods as well as the rather new XRF analysis resulted in precious time series of paleo-environmental proxies. As a result of a multi-proxy approach a number of distinct terrigeneous input events and inflow events of Atlantic water into the SW Sophia Basin have been recognised. Highest inflow seems lead to full glacial conditions of MIS 6.2 and the LGM. Newly proposed circulation scenarios associated with built-up and collapse phases of vast ice sheets shed light on the driving forces of the last three glaciations. The major Early Weichselian glaciation (Mangerud et al., 1998) is not recorded in our sediment cores. Therefore, the existence of this glaciation is questioned and a revised glaciation curve based on multi-parameters including Sr/Ca ratios is presented. Further, the Sr content of bulk sediment in the gravity cores correlates to both $\partial^{13}C$ of *N. pachyderma sin.* and $\partial^{18}O$ of Greenland's ice records (GRIP, N-GRIP) and can thus be used for fast establishment of age models.

Kurzfassung

Mit dem steigenden Interesse an der Hangstabilität der kontinentalen Schelfe geraten die Auslösefaktoren und involvierte Mechanismen mehr und mehr in den Fokus wissenschaftlichen Interesses. Im Rahmen des ESF EUROMARGINS Projektes “Slope Stabilities on Europe's passive continental Margin” (SPACOMA) wurde die Sedimentdynamik von submarinen Megarutschungen am passiven Kontinentalrand nördlich von Spitzbergen untersucht. Die Studie konzentriert sich auf die Identifizierung und sedimentologische Charakterisierung von Megaereignissen des Hangversagens, deren Datierung und Interpretation im Hinblick auf die Beziehung zu Paläoozeanographie und Klimageschichte des Svalbard Archipels.

Die integrierte Interpretation von hochauflösenden batymetrischen Fächersonardaten, sedimentdurchdringende akustische (PARASOUND) und seismische Daten zeigt ein mehrfaches Hangversagen am nördlichen europäischen Kontinentalrand, nördlich von Spitsbergen. Eine gewaltige submarine Rutschung, von Cherkis et al. (1999) zuerst beschrieben, wurde identifiziert – die Yermak Rutschung (Yermak Slide, später auch Hinlopen/Yermak Rutschung bzw. Megaslide genannt).

Basierend auf hochauflösenden akustischen Datenmaterial wurde die Hinlopen/Yermak Megarutschung neu kartiert und ihre flächenhafte Ausdehnung revidiert. Details der inneren Rutschungsstruktur kennzeichnen eine einzige Hauptrutschung, welche von mehreren deutlich kleineren Rutschungsereignissen gefolgt wird. Dieses erste Megarutschung ereignete sich im Marinen Isotopenstadium (MIS) 3, vor etwa 30.000 Kalenderjahren, und war von einer hoch dynamischen und rapiden Evakuierung von ca. 1250 km³ Sedimentmaterials vom unteren Kontinentalhang bis zur Schelfkante gekennzeichnet. Während dieser Megarutschung wurden bis zu 1600 m hohe Abrißkanten geschaffen und ca. 1150 km³ Sedimente des unteren preexistenten Hinlopen Trogfächers, sowie hemipelagische Sedimente in die Rutschung einbezogen und ins halb geschlossene Sophia Becken transportiert. Auf diese Megarutschung folgte innerhalb einer sekundären Evakuierungsphase ein kanalisierter Transport des Rutschungsschuttmaterials entlang des Littkekanals zwischen dem Polarstern Seamount und des benachbarten Kontinentalhanges hindurch ins Nansen Becken.

Der Hauptrutschungsschutt wird von einer fining-upwards Sequenz überlagert die Zeugnis der zugehörigen Suspensionswolke sowie späterer kleinerer Rutschungen ist. Die auf die Hauptrutschung folgende dynamische Anpassung der östlichen Hangabrißkanten führte zum Versagen von relative weichen Sedimentschichten und resultierenden kleineren Schuttströmen (debris flows), welche den topographischen Depressionen des Hauptrutschungsschutts folgen.

Die Sedimentausschüttung des Hinlopen Eisstromes während des letzten Glazialen Maximums (LGM) bedeckte den zentralen Teil der Hangabrißkanten und formte einen neuen kleineren Trogfächer von glazigenen Schuttströmen (debris flows) südlich der Relikte des nunmehr abgeschnittenen älteren Hinlopen Trogfächers.

Die wahre Geometrie mit über 10.000 km² Ausdehnung und mehr als 2.400 km³ einbezogenem Sedimentmaterial platziert die Hinlopen/Yermak Megarutschung unter die größten exponierten submarinen Rutschungen weltweit, vergleichbar der Storegga Rutschung vor Mittelnorwegen. Die Rutschungsgeometrie und ihr inneres physikalisches Erscheinungsbild weisen auf einen tektonisch iniziierten Schelfkollaps hin.

Die Datierung der Hinlopen/Yernak Megarutschung mit einem Alter von ca. 30 Jahrtausenden fällt mit dem Übergang des Kapp Ekholm Interstadials ins Glazial G der Vereisungskurve Svalbards (Mangerud et al., 1998) und dem rapiden Aufbau des Svalbard-Barents-See-Eisschildes zusammen. Daher ereignete sich die Megarutschung während einer Periode des Meeresspiegelabfalls, des Eischildwachstums und zugehöriger intensivierter glazio-tektonischer Aktivität.

Nach einer Analyse der in Frage kommenden Auslösemechanismen inklusive Paläomeerespiegeltendenz, Paläoozeanographische Zirkulation, glazialer Prozesse, Tektonik und Erdbeeben wird der Schluß gezogen, dass die Rutschung die direkte Konsequenz der rapiden Spätweichselvereisung, die einen rapiden und drastischen Meeresspiegelabfall, asymmetrische Eislast und eine Fore Bulge Entwicklung zur Folge hat. Als finalen Auslöser wird ein starkes Erdbeeben unterhalb oder nahe des südwestlichen Sophia Beckens angenommen.

Das südwestliche Sophia Beckens stellt ein exzellentes geologisches Archiv für die rekonstruktion von Paläoumweltbedingungen dar. Als Nebenprodukt des rutschungsbezogenen ESF-Projektes wurde eine Anzahl von Sedimentkernen mit viel versprechenden Sedimentabfolgen gewonnen. Die kombinierte Anwendung von einerseits konventionellen etablierten wissenschaftlichen Untersuchungsmethoden, sowie der eher neuen Röntgenfluoreszenzkernanalyse (XRF) resultierte in wertvollen Zeitreihen von Paläoumweltproxis. Als Erggebnis des Multiproxi-Ansatzes, konnte eine Reihe von Ereignissen des intensiven terrigenen Eintrags und des Atlantikwassereinstroms im südwestlichen Sophia Becken identifiziert werden. Dabei scheint höchster Atlantikwassereinstrom zu Hochglazialen des LGM sowie des MIS 6.2 zu führen. Neu vorgeschlagene Zirkulationsszenarios, die mit dem Eisschildaufbau- und Kollapsephasen assoziiert sind, werfen Licht auf die treibenden Kräfte der drei letzten Vereisungen. Die

Frühweichselvereisung (Mangerud et al., 1998) ist nicht als ausgedehnte Vereisung in unseren Kernen dokumentiert. Daher wird die Existenz dieser in Frage gestellt und eine überarbeitete Vereisungskurve basierend auf mehreren Parametern inklusive Sr/Ca-Verhältnisse präsentiert. Darüberhinaus korreliert der Sr-Gehalt der Sedimentkerne sowohl mit den $\partial^{13}C$ von *N. pachyderma sin.* und dem $\partial^{18}O$-Signal grönländischer Eiskerne (GRIP, N-GRIP) und kann daher für die schnelle Erstellung von Altersmodellen genutzt werden.

Chapter I

Introduction

Introduction

Failure Processes – Submarine Slides – Why caring about moving dirt in the dark?

Gravity driven mass movements have been descibed extensively for the subaerial environment. Rockfalls, avalanches and other forms of slope failure have always impacted the human live. It took until 1929 when the "Grand Banks" earthquake caused submarine slope failures including a submarine slide that developed into a turbidity current which destroyed several transatlantic telegraph cables, that public and scientific interest turned towards the gravity driven mass movements in the oceans. Following these investigations, the significance of these submarine slope failures has been identified when their relation to mass movement-induced large scale waves (tsunamis) were found. The Grand Banks earthquake, positioned on the western margin of St. Pierre slope, did not only cut the connection between the American and European continents, it genrated a tsunami that killed 27 people in a coastal village of Newfoundland (e.g. Piper et al., 1985, 1988, 1999). Today, the importance of submarine slope failure processes rises with increasing infrastructure on the seafloor and near the coasts. A variety of socio-economical branches, including energy, communication, navigation, tourism, fisheries, military and science extend their interest further offshore and deeper into the sea.

Submarine slides – or submarine landslides – constitute the most impressive slope failure processes among the variety of submarine sediment transport mechanisms. By removing large amounts of fairly consolidated sedimentary material usually within singular events, they represent an expressed hazard to any seafloor infrastructure as well as to coastal communities by creation of large tsunamis with their far-reaching consequences. Slide volumes can reach more than 3000 km³, large slided blocks are common reaching extensions of up to 25x12x2 km and associated tsunami heigts can exceed 100 m(Takahashi et al., 2002; Locat & Mienert, 2003; Yalciner et al., 2003; and references therein).

Submarine slides are common on the shelves of active continental margins. Their high supply of sediment and their seismic activity appear as a reasonable background for frequent slope failures along the shelf break. However, research of the last ~30 years identified large scale slope failures on the shelves of passive continental margins too. A number of submarine slides have been identified on Europe's passive continental margin (e.g. Vogt et al., 1999; Canals et al., 2004; Evans et al., 2005; Figure 1). Ranging from small scale failures within fjords to main slope failures along the shelf of Scandinavia. Three slides representing three different environments have been chosen to study their nature and relation to environmental conditions within the ESF project “Slope stabilities on Europe's passive continental margin” (SPACOMA) and under the EUROCORES EUROMARGINS programme. The Big 95 Slide in

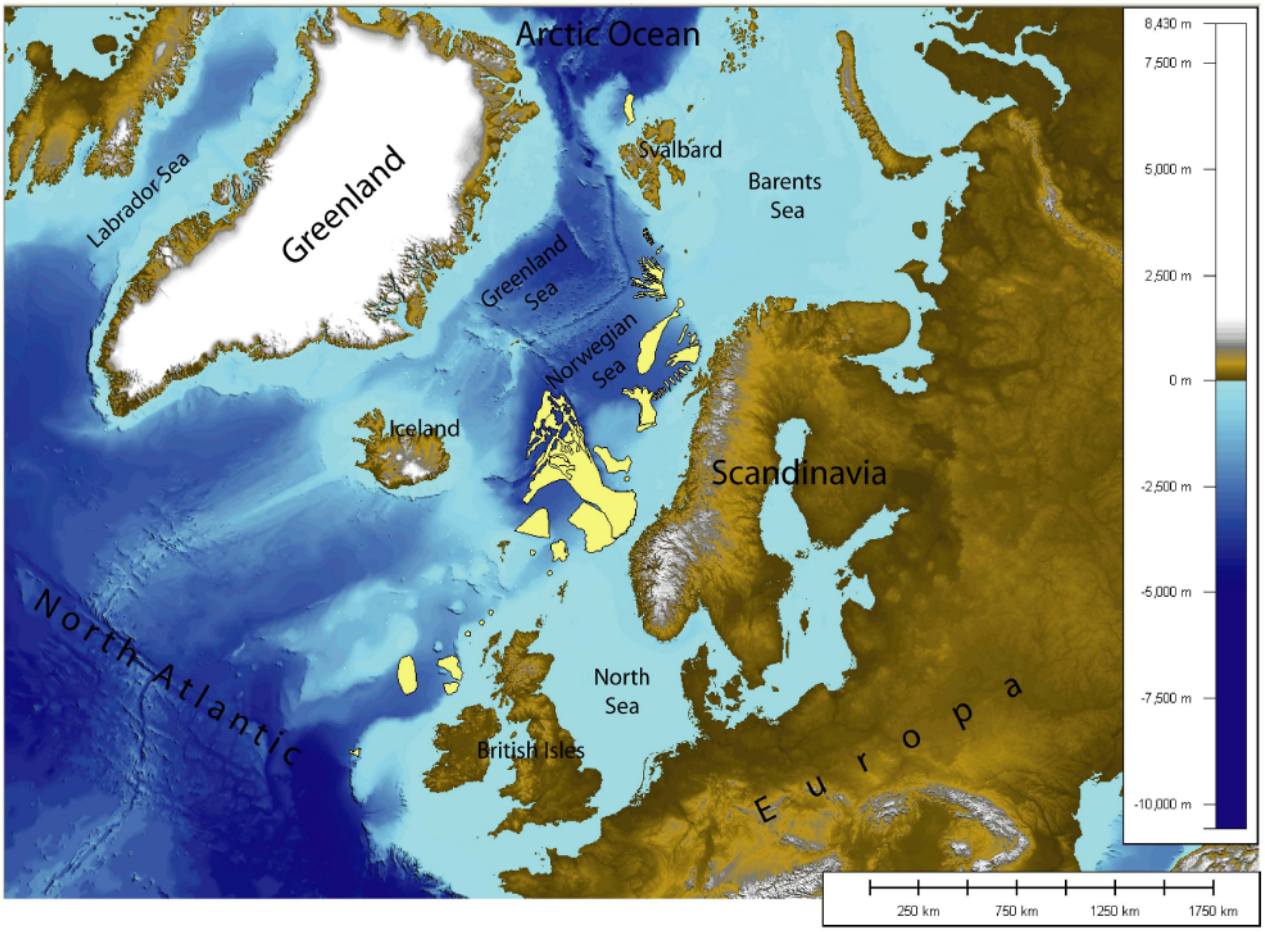

Figure 1: Submarine slide and other gravity driven mass flows on the passive continental margin of NW Europe (according to several authors e.g. Vogt et al., 1999; Evans et al., 2005). Bathymetry / topography: is reproduced from the GEBCO Digital Atlas published by the British Oceanographic Data Centre on behalf of IOC and IHO, 2003.

the western Mediterranean is situated on a river-fed carbonate margin; the Storegga Slide represents a large scale slope failure on the river and glacier-fed siliciclastic margin off Mid-Norway and the Yermak Slide north of Spitsbergen is located on a glacier-fed siliciclastic margin in an Arctic environment.

The following study has been devoted to this northern-most submarine slide. The focus of the investigation has been put on identification of failure events, their sedimentological characterisation, dating of the event(s) and their interpretation in relation to the Quaternary climate history of Svalbard.

Research Area – Svalbard

The Svalbard archipelago is situated on the north-western corner of the European continent. Bordered by the Arctic Ocean, Fram Strait, Norwegian and Barents Sea, its regional Arctic climate is maritime dominated. The change of passing low and high-pressure systems characterise the weather conditions. The atmospheric variations can be explained by the leading empirical orthogonal function of sea level pressure variation for the northern hemisphere described as Arctic Oscillation (AO; Thompson & Wallace, 1998) and an index (AOI) in the style of the North Atlantic Oscillation (NAO) has been introduced. This index more highly correlated with surface air temperatures of the northern hemisphere (Thompson & Wallace, 1998). Despite the fact that Svalbard is surrounded by water masses, it is to be characterised as a semi-dessert due to its high-Arctic temperatures and associated precipitation pattern.

Geological History – Tectonic Evolution – Svalbard, the "northernmost Greenland"

The connection of the Arctic and Atlantic Oceans began with Early Jurassic intra-continental rifting in Northwest Europe (Ziegler, 1988). Progressive rifting separated Greenland and Eurasia from North America and later in Paleocene time Greenland from Europe. Paleocene rifting along the Arctic Mid-Ocean Ridge also initiated separation of the Lomonosov Ridge from the Barents Shelf to create the early Eurasia Basin and a shallow seaway between the Arctic and Atlantic Oceans (Wilson, 1963; Kristoffersen, 1990a, b; Figure 2). The seaway developed into an oceanic rift that separated Svalbard from Greenland, and progressively permitted the interchange of deep water between the Arctic and the Atlantic Oceans by Middle Miocene time.

The initiation of the continental rifting that has lead to the formation of the modern shelves is directly related to the opening of the North Atlantic. The earliest dextral strike-slip movements between Svalbard and Greenland along the Trolle-Land Fault Zone (northeast Greenland) date back into chron 33 around 80 Ma ago (Håkonsson & Pedersen , 1982). Following this rifting and continiuos spreading, the Svalbard archipelago has been separated from Greenland and moved relatively along the (modern) Fram Strait in a dextral strike-slip manner. This process was truncated by a period of compression that affected the young transpressive fold belt of W-Spitsbergen around the Paleocene/Eocene boundary, (chron 25 and 24 between 59-56 Ma ago) following a change of spreading direction in the Labrador Sea during (Müller & Spielhagen, 1990). Synchronously, true seafloor spreading continued at Mohns Ridge and within the juvenile Norwegian-Greenland Seas – there associated with ongoing rifting and crustal extension during chron 25 and 24b. This transpressional regime in western Spitsbergen endured into the Middle Eocene

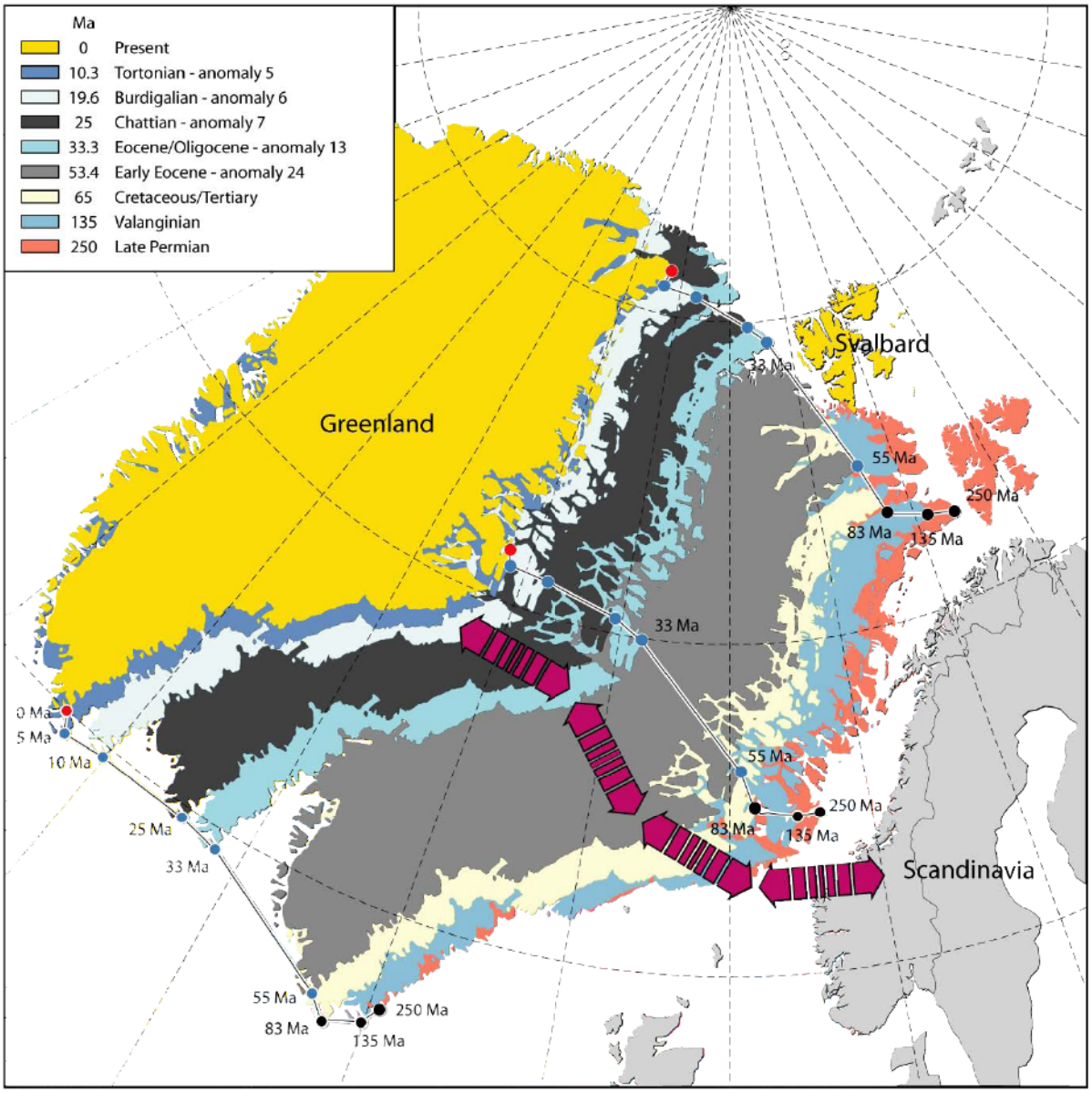

Figure 2: tectonic plate evolution of the Nordic Seas. Greenland's relative movement from NW Europe according to revised rotation poles. Trajectory of three distinct points on Greenland line out the movement between successive positions of Greenland. Arrows qualitatively indicate the main rifting directions. Note that the indicated pre-rifting position of Svalbard for the Late Permian is inferred (modified after Mosar et al., 2002).

(chron 21 around 49 Ma ago) and was followed by transtension. The transtensional regime dominated throughout the last 36 Ma and lead to streched and rifted lithosphere west of the Hornsund Lineament (Eldholm et al., 1987; Müller & Spielhagen, 1990; Crane et al 1991; Boebel 2000). Pull apart structures have formed along this major fault zone as a consequence of strike slip movements (e.g. Eiken, 1993). According to Ritzmann (2003), the western shelf of Spitsbergen is segmented due to step-wise evolving transform faults during the Oligocene and Miocene (36-9,5 Ma ago) and can be structured into a rifted margin, a sheared margin and a very broad rifted margin.

The northern shelf of the Barents Sea and off Svalbard faces the Arctic Ocean. The formation of the adjacent Nansen Basin dates back into chron 24 between 56 and 53 Ma ago and is associated with the earliest rifting of the yet to become Gakkel Ridge around 60 Ma ago (Vogt et al., 1979). The Gakkel Ridge is the northernmost continuation of the Mid Atlantic Ridge. It is connected by a number of smaller ridges (e.g. Knipovich Ridge, Mohns Ridge) and transfer zones (e.g. Jan Mayen Fracture Zone, Spitzbergen Fault Zone). The ridge extends beneath sediments close to the Laptev Shelf and probably much further below the Eurasian continent. Several extensional structures within the Laptev Shelf and the coastal mountains might be related to this slowest Mid Ocean Ridge (Gaina et al., 2002). The Gakkel Ridge is an utra-slow spreading ridge with with modern half-spreading rates of 3 mm/a close the Laptev Shelf and up to 7 mm/a in the Fram Strait (Michael et al., 2003). The basin development of the evolving Ammundsen and Nansen Basins has been outlined by Kristoffersen (1990a, b).

The structure of the northern shelf of Svalbard is less constraint due to its almost perrennial sea ice cover. The first systematic seismic profiles (multi-channel reflection data) have been aquired by RV "Polarstern" (Jokat, 2000) on this margin in 1999, imaging the whole sedimentary strata. The inner shelf east of the Hinlopen Strait is obviously eroded and characterised by a thin veneer of over-consolidated sediments above the acoustic basement. Towards the outer shelf, the acoustic basement is downfaulted and covered by up to 3,5 km of sediments (Geissler & Jokat 2004). The continental slope is heavily incised as a result of repeated slumping and evolving turbidity current-canyon systems (Cherkis et al., 1999; Jokat, 2000). The Nansen Basin displays up to 4,5 km of sedimentary strata close to the shelf. The Sophia Basin, north of Spitsbergen probably contains more than 9 km of sediments (Geissler & Jokat, 2004).

The opening of the Lena Trough is believed to have started during chron 13 around 35 Ma ago. A ridge complex consisting of the Morris-Yesupp Rise and the Yermak Plateau has probably inhibited the exchange of deep water masses until the Miocene and/or Pliocene (Kristoffersen & Husebye, 1985). The final establishment of the Fram Strait as a deep water connection and its consequences for the Arctic Ocean (e.g. Kristoffersen 1990a, b) has been accomplished between 11 – 14 Ma ago (Jokat et al., 2007).

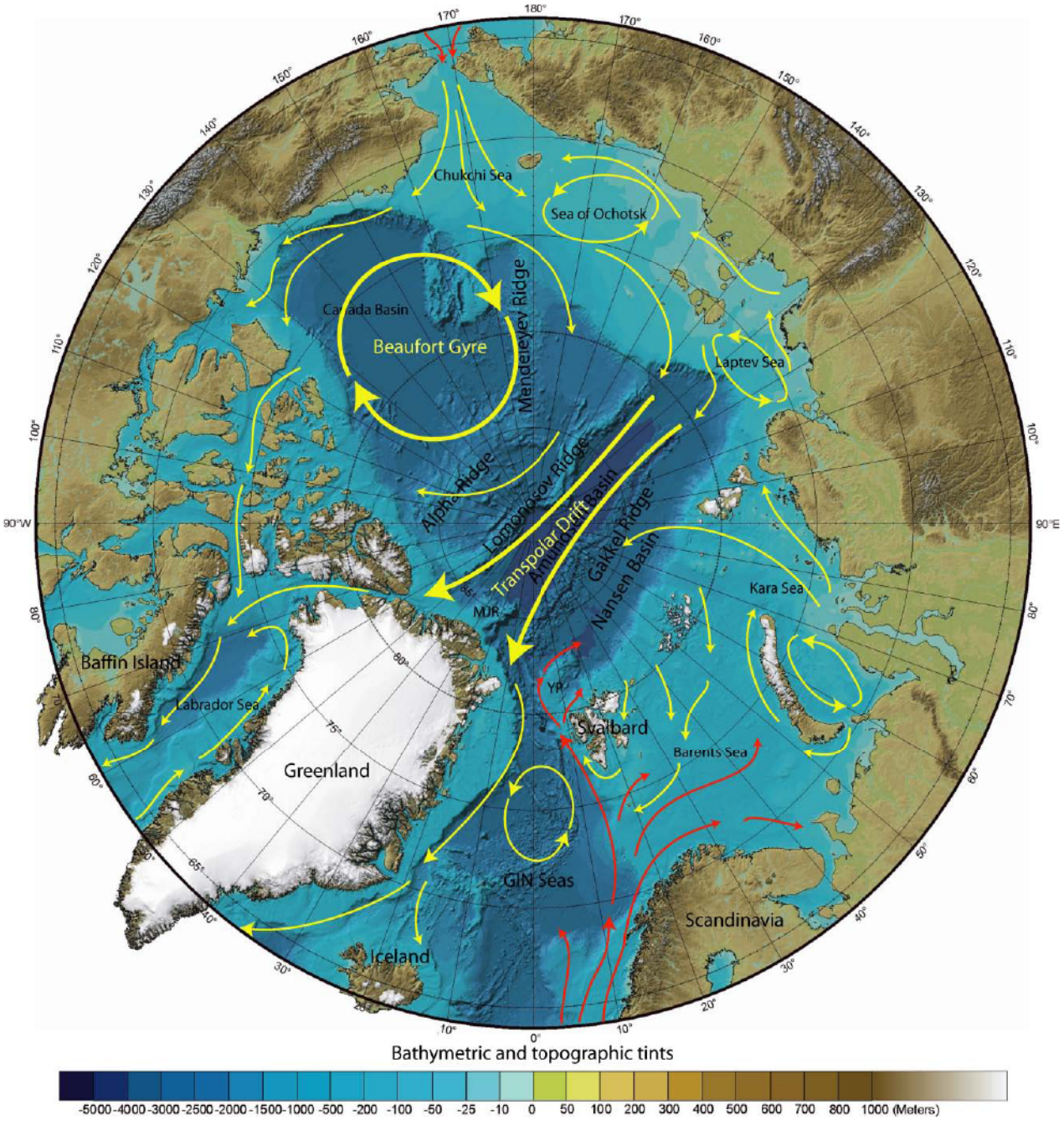

Figure 3: Modern bathymetry (IBCAO, Jakobsson et al., 2000) and surface circulation pattern of the Arctic Ocean with warm (red arrows) and cold (yellow arrows) currents (according to several authors).

Modern Oceanic Circulation

The Arctic Ocean is morphological divided into two major basins – the Amerasian and Eurasian Basin – by the Lomonossov Ridge. Surface circulation pattern are governed by these morphological conditions

and are characterised by two main surface current systems. The Beaufort Gyre positioned above the Amerasian Basin rotates its surface waters clockwise while intermediate and deep waters move counterclockwise (e.g. Rudels et al., 1994; Jones et al., 1995). The Transpolar Drift transports sea ice from the Laptev Sea shelf areas across the North Pole into Fram Strait and Baffin Bay following the Gakkel and Amundsen Ridges (Figure 3).

The Svalbard Archipelago is situated on the north-western edge of the North-European continental shelf, adjacent to the main energy supplier into the Arctic – the Golf Stream. Atlantic Water (AW), a surface water associated with salinity and temperature maxima, enters the Norwegian Sea across the Iceland-Scotland Ridge with temperatures between 6 and 8°C and salinities of 35,1 to 35,3 (Maslowski, 1994). On its way north the AW flows along the continental shelf as the Norwegian Atlantic Current, splits and leaves the eastern current that turns into the Barents Sea (as the North Cape Current) where it is significantly altered before reaching the Arctic Ocean (Hopkins, 1991). The northward extension of the Norwegian Atlantic Current flows along the continental slope of the western Barents Sea and west off Spitsbergen to become the West Spitsbergen Current (WSC). The upper 600 metres of the WSC are occupied by the relative warm and saline Atlantic Water resulting in ice-free western coasts of Spitsbergen during most of the year (Aagaard et al., 1987; Gascard et al., 1995). Elevated mean annual air temperatures (e.g. a long-term average of –6°C at Ny Ålesund; Steffensen, 1982) are a consequence as well. When AW leaves the Nordic Seas through Fram Strait its temperature are lowered by 5°C compared to its entry and salinities are about 35,0 (Maslowski, 1994). It supplies the largest heat, mass and salt amounts to the Arctic Ocean through the Fram Strait (Aagaard & Greisman, 1975).

The WSC divides into three major branches along its northward flow in the Fram Strait area. The western branch or Return Atlantic Current, the northward directed Yermak Branch (Yermak Slope Current and Yermak Plateau Current) and the north- and later eastward flowing Svalbard branch (North Svalbard Current; e.g. Schlichtholz and Houssais, 1999a, 1999b). This branching of the central core of AW as well as modification of its temperature-salinity signature by sea-air-ice interaction and internal mixing processes results in the recirculation of a large portion of Atlantic Water into the Greenland, Iceland, Norwegian and Barents Seas (Manley, 1995). Modelling results supported by results of Bourke et al. (1988), indicating that the Yermak Branch is largely recirculated, estimate the recirculated portion as high as 50 percent (Rudels, 1987). According to Manley (1995) this portion may well account for two thirds of the Atlantic Water masses.

The western branch (Return Atlantic Currents) meets the counterpart of the WSC – the East Greenland Current (EGC) flowing east of Greenland's coasts and transporting sea ice from the Polar Drift into the

Atlantic Ocean. The Arctic Water of the EGC is characterised by low salinities (< 34,4) and low temperatures (< 0°C). The EGC is about 100 kilometres wide and ice drift speeds have been estimated to about 6 km per day (Thorndike & Colony, 1982). The area between these two surface currents (the Arctic Domain) is characterised by mixed waters (Swift & Aagaard, 1981). Variability of the EGC and ice export via Fram Strait have been linked to wind pattern over the major arctic surface circulation systems (e.g. Strübing, 1968) and correlated to the Arctic Oscillation (AO), such that reduced convergence of ice area in the eastern Arctic Ocean, a retreat of sea ice in the Greenland and Barents Sea and increased export of ice area through Fram Strait occur during periods of high AO (Kwok & Rothrock, 1999; Kwok, 2000; Rigor et al., 2002). These findings were supported by modelling results showing a similar relation of atmospheric circulation and ice volume (Zhang et al., 2000).

The waters of the eastern Svalbard Branch enter the Arctic Ocean north-west off Spitsbergen. Its relatively warm (>0°C) and saline (>35) waters are being advected farther East on the continental slope at intermediate depths and delivering energy and nutrients to the Eurasian marginal seas. The remnant core of Atlantic water north-east of Spitsbergen has been detected at 250 metres water depth compared to a few tens of metres water depth along the south-western coast of Spitsbergen. In the western Laptev Sea it can be located as Atlantic Intermediate Water at 400 metres water depth (Manley, 1995).

A second current with arctic type (<0°C and salinities <34,4) waters characterises the Svalbard archipelago. The East Spitsbergen Current (ESC) enters the Barents Sea from north between Franz Joseph Land and Nordaustlandet flows south-west around Edgeøya and Sørkapp then turning north while flowing along the coast of Spitzbergen (cf. Svendsen et al., 2002).

Since the warm Atlantic Water west off Spitzbergen impacts environmental conditions on the Island, changes in supply pattern are recorded in nearby terrestrial and marine archives. Variability of the northward transport of the Atlantic water has been reported for glacial and interglacial periods (e.g. Hebbeln et al., 1994; Knies et al., 1999, 2000) as well as for the Holocene (e.g. Duplessy et al., 2001).

The most modern circulation pattern displays an increasing inflow of Atlantic water into the Arctic Ocean affecting heat and salinity budget, water stratification, sea ice cover and regional climate (e.g. Morison et al., 2000; Polyakov et al., 2005; and references therein).

Sea Ice Conditions

The Svalbard archipelago is seasonally ice-covered (Figure 4). Associated with the Polar Front, the transition of sea ice and open waters – the marginal ice zone (MIZ) – provides favourable conditions in terms of water mixing and is characterised by peak primary productivity (Owrid et al., 2000). Maximum and minimum ice extent north of Svalbard are observed by the end of February and in the middle of September,respectively (Ramseier et al., 2001; Divine & Dick, 2006). However, The relatively warm waters of the WSC keep the western coasts of Spitsbergen essentially free of sea ice for most of the year. The sea ice cover shows a high seasonal, annual, and interannual variability in extent, thickness, and distribution. The sea ice cover variability is largely controlled by ice export conditions from the Arctic Ocean into Fram Strait by the Transpolar Drift (Vinje & Finnekåsa, 1986; Martin & Augstein, 2000; Kwok et al., 2004). This variability has been linked to interannual dynamics of Atlantic water inflow (e.g. Midtun & Loeng, 1987) as well as to the North Atlantic Oscillation (NAO) (e.g. Vinje, 2001) and northern hemisphere temperatures (Vinje, 2001).

The mean travel time of Arctic Ocean sea ice to the Fram Strait varies significantly, ranging from 6 years for ice from the southern Beaufort Sea to 1 year for ice from north of Svalbard (Pfirman et al., 1997). The mean annual ice export from the Arctic Ocean via Fram Strait has been calculated by Vinje et al. (1998) to 2850 km³. This sea ice consists mainly of multi-year pack ice originating from the Siberian continental shelf with an average thickness of 3.27 m in the Fram Strait (Vinje et al., 1998). Micropaleontological and sedimentological studies of sea-ice sediments by several authors conclude that the Laptev Sea is the most important source area for multi-year sea ice found in the Fram Strait (Abelmann, 1992; Nürnberg et al., 1994; Dethleff et al., 2000; Eicken et al., 2000; Dethleff, 2005).

During the last century the Arctic experienced a warming that exceeded the global and even the northern hemisphere warming of average surface temperatures (Eischeid et al., 1995; Jones et al., 1999; Serreze et al., 2000; IPCC-report, 2001). This warming has been attributed to the positive coupling effects (polar amplification) and correlated to many other Arctic climate and environment related variables such as precipitation, sea-ice extent, snow cover permafrost temperature and vegetation distribution (Serreze et al., 2000; Morison et al., 2000; SEARCH SSC, 2001). In recent decades, sea level air pressure decreased in the Arctic more than anywhere else in the northern hemisphere (e.g. Walsh et al., 1996). Sea ice thickness and distribution pattern have already exhibited a strong affection to changing wind and temperature condition and will likely respond more drastically to continued warming (e.g. IPCC-report, 2001; Kerr, 2002). Vinje (2001) for example, report that temperature increase (magnitude in the order of ca. 1°C) since the cooling of the Little Ice Age (LIA) in the upper layers of the northbound warmer ocean

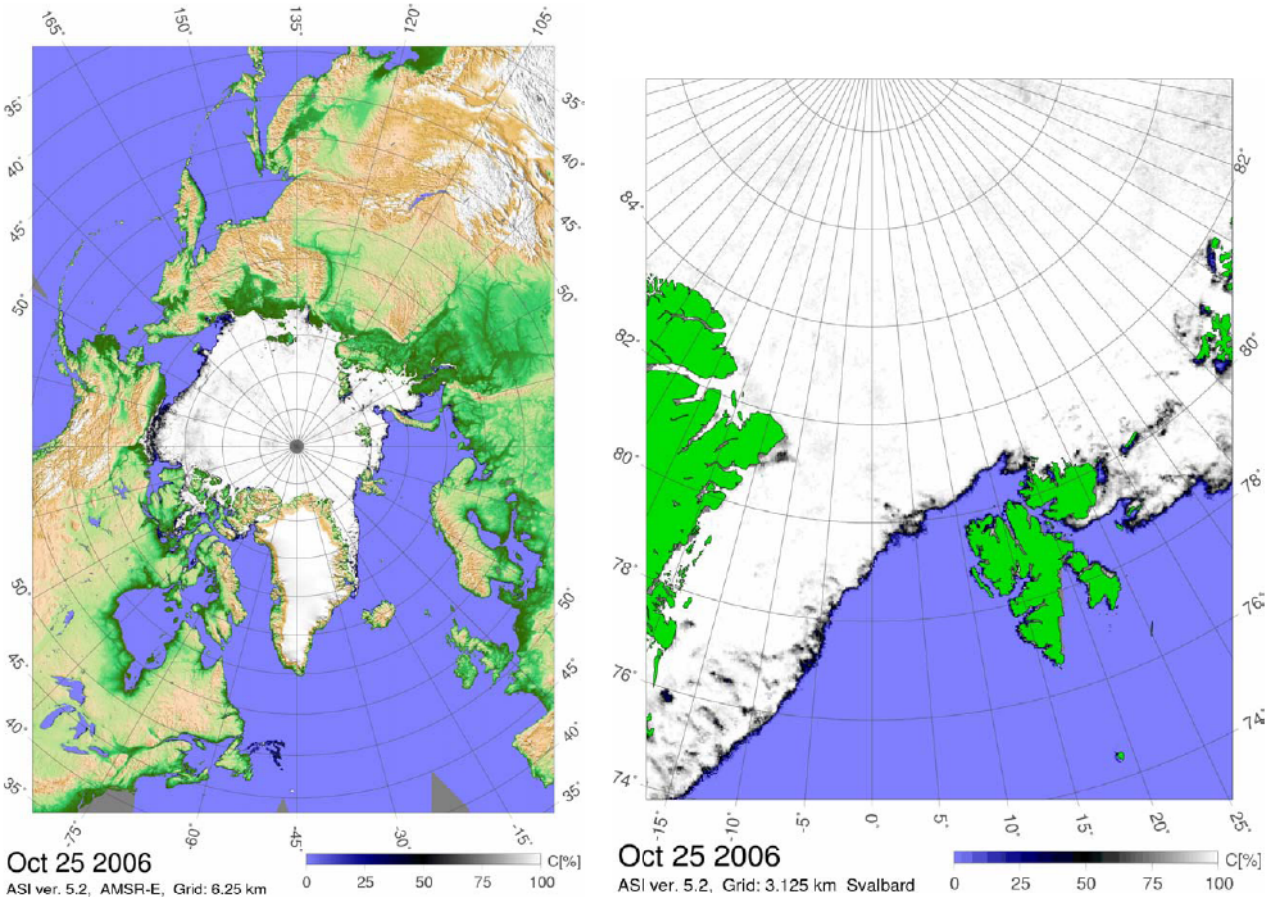

Figure 4: Sea Ice distribution maps for the Arctic (left) and the Fram Strait region and Svalbard (right) based on satellite data for the 25th October 2006 (http://www.seaice.de; http://iup.physik.uni-bremen.de:8084/amsr/amsre.html).

currents accounts for most of the ice extent reduction since the 1860ies. The increased temperature of the Atlantic Water (core of the West Spitsbergen Current) observed during the 1990ies (e.g. Swift et al., 1997) has been considered one cause for the thinning of sea ice in the Arctic (Rothrock et al., 1999, 2003; Morrison et al., 2000; Polyakov et al., 2005). A reduced primary productivity associated with the Marginal ice zone (e.g. Owrid et al., 2000) has been correlated to higher surface air temperatures on Svalbard and point to a reduced annual duration of the sea ice (Winkelmann & Knies, 2005). The reduced sea ice cover will most likely promote future atmospheric warming due to albedo feedback effects (Morales-Maqueda et al., 1999; Polyakov et al., 2005).

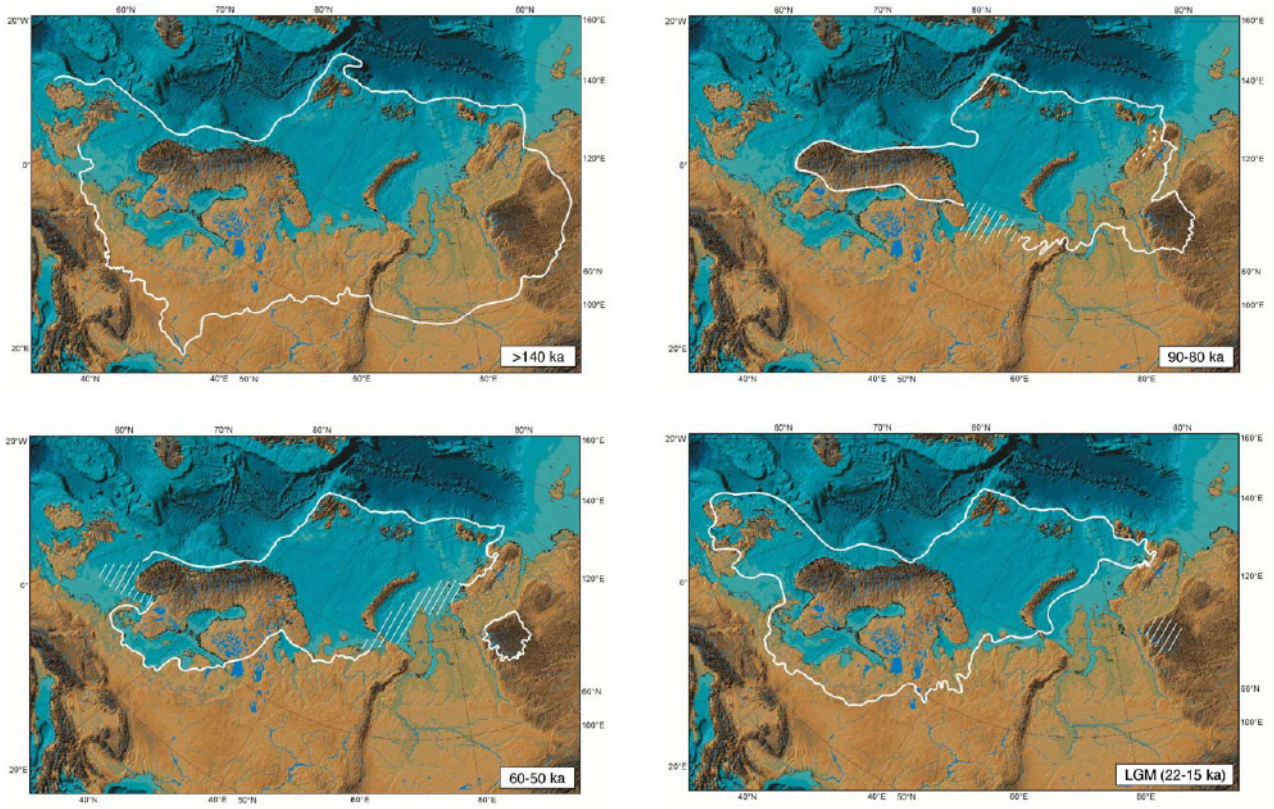

Figure 5: Ice sheet extents during the last glacial cycle including the latest view of the LGM according the QUENN project (Svendsen et al., 2004 and references therein).

Quaternary Climate History

The Arctic Region has been affected by several extensive glaciations. The earliest Cenozoic glacial deposits in the northern hemisphere date middle Miocene age around 4 Ma (Solheim et al., 1996a; Thiede et al., 1998). A further stepwise decrease of northern hemisphere temperature is documented by several IRD pulses during late Miocene around 7.2, 6.8 and 6.3 Ma. The cooling culminated in an intensification of northern hemisphere glaciation during late Pliocene/Early Pleistocene recorded as a intensification of IRD pulses within the eastern Nordic and Barents Seas between 3.2 and 2.7 Ma (Thiede et al., 1998). The interplay of large scale glacials and interglacials shaped the region throughout the last 2.56 Ma. The glacial/Interglacial cycles are orbitally controlled and display an affinity to the 41 kyr obliquity periods between 1.2-0.6 Ma as well as 100 kyr. eccentricity periods for the last 600-700 kyr. of the Milanchovic orbital parameters (Thiede et al., 1998). Between 1.2 to 0.6 Ma, marine sediments show generally high carbonate contents, while the proceeding sediments display high-amplitude oscillations of carbonate contents (e.g. Mangerud et al., 1996; Solheim et al., 1996b).

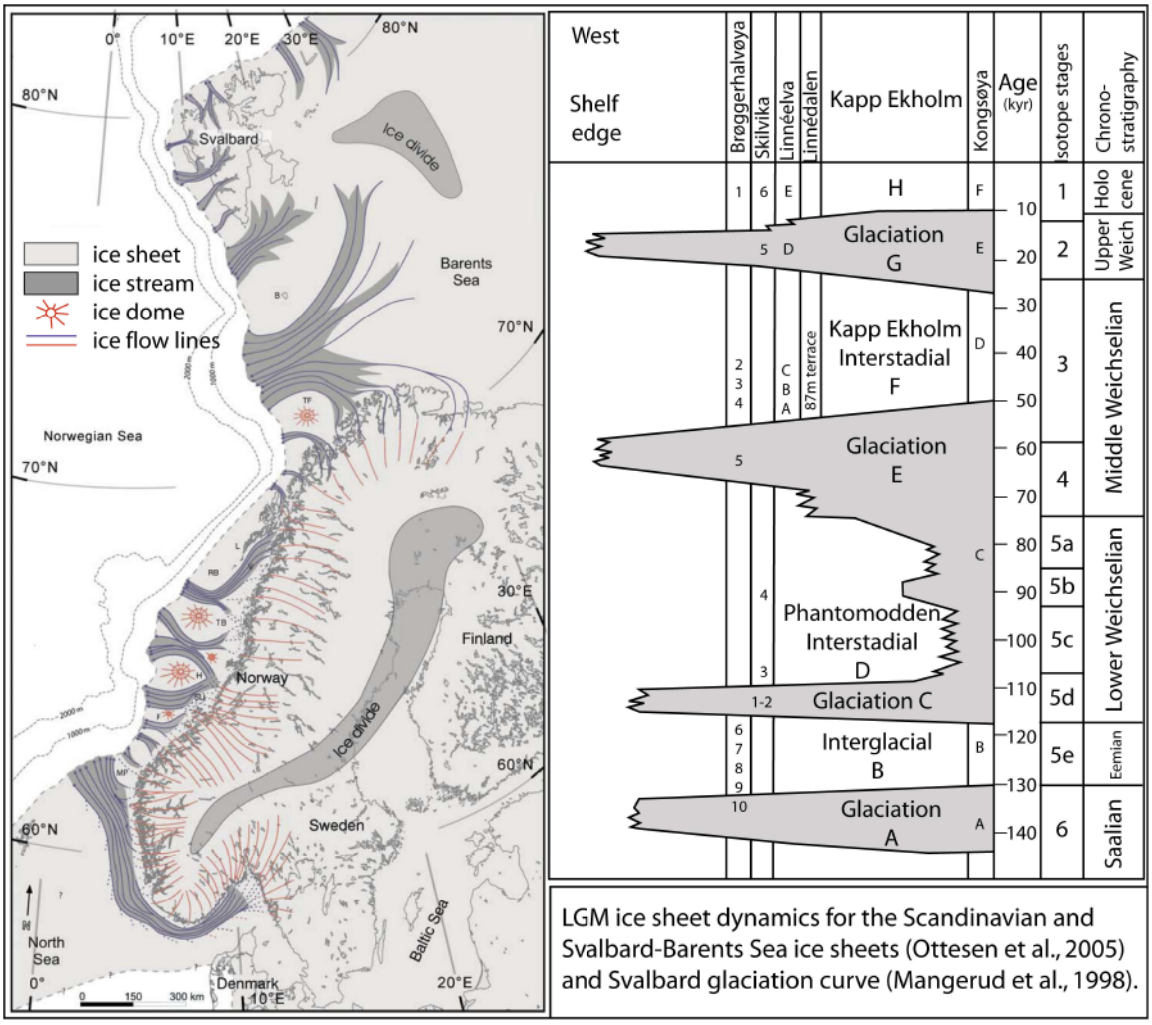

Figure 6: Synthesis of terrestrial and submarine evidence for major ice streams within the Scandinavian and Svalbard-Barents Sea Ice Sheets (Ottesen et al., 2005) and synthesis of terrestrial evidence for major glacial advances on the Svalbard archipelago during the last glacial cycle according to Mangerud et al. (1998).

During the Last glacial cycle three large glaciations have been recognised within the Weichselian (or Wisconsin) glacial that affected large parts of Eurasia and North America. The glaciations ocurred around 140, 90, 60 and 20 kyr BP (see Svendsen et al., 2004 and references therein; Figure 5). According to its maximum extent in NW Europe the latest glaciation is usually referred to as the Last Glacial Maximum (LGM) – a term that largely refers to maximum glacier and ice sheet extents of terrestrial records. Thus, the LGM displays not always a synchronous character and does not coincide with the time of maximum ice volume.

Svalbard has been covered by ice sheets (Svalbard-Barents Sea Ice Sheet – SBIS) during the last glaciations and is still partly glaciated (e.g. Landvik et al., 1998; Mangerud et al., 1998; Knies et al., 2000; Figure 6). The terrestrial records on Svalbard provide evidence at least for three of these advances while

there was only one site found (depending on the intra-site correlation of records) that might give evidence for four advances. According to Mangerud et al., (1998), these four glacial advances occurred roughly between 110-115 (Glaciation C), around 90, between 80-50 (Glaciation E) and 26-10 cal. kyr. BP (Glaciation G). The main three advances (C, E, G) were separated by marine transgressions of the interstadials (Phantom Odden Instadial D and Kapp Ekholm Interstadial F; Figure 6) and their marine sediments allowed relatively precise dating of the stadials. The character of the ice sheet that developed on Svalbard has been described as complex and dynamic with focused ice drainage via ice streams in glacial troughs and outlet glaciers while areas inbetween may had been less dynamic and characterised by nunataks (Landvik et al., 2005). The ice sheet might have been polythermal since evidence for warm as well as cold based ice have been found. The main deposition centres of the SBIS have been inferred from glacial rebound emergence records on Svalbard. They probably were positioned south of Nordaustlandet in the Barents Sea near Kongsøya (e.g. Landik et al., 1998) and mainly drained via fast-flowing ice streams (Landvik et al., 2005; Ottesen et al., 2005).

Following these extensive glaciations, the morphology of Spitsbergen is characterised by sharp mountain ridges (giving the Island's name), steep U-shaped valleys and fjord systems reaching as cross shelf troughs the shelf edge. Minor ice caps on Nordaustlandet, parts of Spitzbergen, Barentsøya and Edgeøya exist while glaciers dominate the archipelago. Most of these glaciers are considered to be the result of the Neoglaciation, polythermal as well as being of surge type due to observations and features that indicating surge behaviour (Hagen et al., 1993; Liestøl, 1993; Lefauconnier & Hagen, 1991; Hamilton & Dowdeswell, 1996). The permafrost layer on Svalbard reaches depths down to 450 metres with an active upper layer of about one metre (e.g. Isaksen et al., 2000a, 2001). Accordingly, periglacial features like ice wedges, polygons and pingos can be found on Spitzbergen as well as rock glaciers (e.g. Liestøl, 1977; Isaksen et al., 2000b).

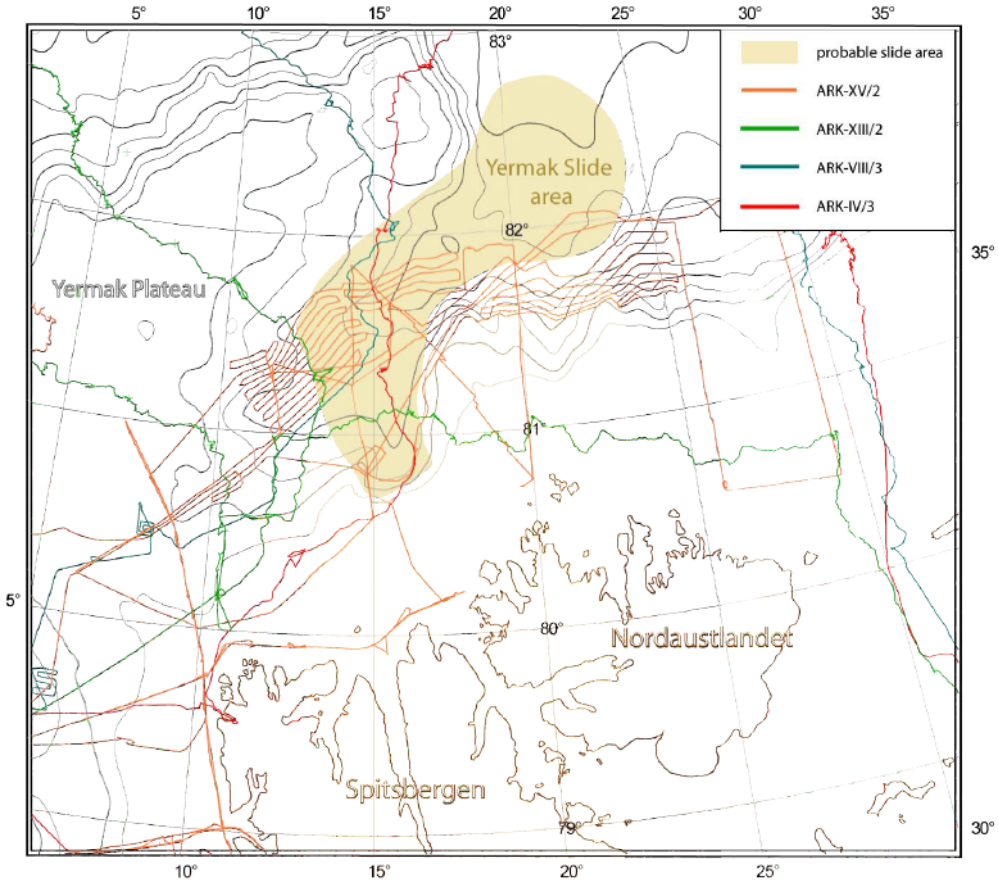

Figure 7: Map of northern Svalbard with previous expeditions by AWI with RV "Polarstern" that crossed the slide area: ARK-IV/3 (Thiede, 1988); ARK-VIII/3 (Fütterer, 1992); ARK-XIII/2 (Stein & Fahl, 1997); ARK-XV/2 (Jokat, 2000).

Previous Work – Some things are too big to be discovered.

In 1989 and 1990, favourable sea-ice conditions gave way to two expeditions along the northern Svalbard continental margin. The survey carried out by the Norwegian Polar Institute (NPI) was using a shallow-towed SeaMARK II side-scan sonar system with RV “Håkon Mosby”. Their results were published within the Norwegian Seafloor Atlas (Crane & Solheim, 1995). The expedition ARK-XV/2 with research icebreaker “Polarstern” equiped with the ATLAS Hydrosweep swath bathymetry system and the parametric echosounding (PARASOUND) surveyed a large part of the continental shelf and the Sophia Basin in 1999 (Figure 7). They discovered and fully mapped two seamounts within the Sophia Basin. The bathymetric maps of the seamounts have been published within the cruise report (Jokat, 2000). Later, this bathymetry data was integrated in the International Bathymetric Chart of the Arctic Ocean (IBCAO, Jakobsson et al., 2000). First indication of a submarine slide was encountered during ARK-VIII/3 (Fütterer, 1992) that crossed one of the main megablocks and recorded its relief in the SEABEAM swath bathymetry data (Figure 7). During ARK-XV/2 (Jokat, 2000) a wide range of the slide was mapped by

high-resolution bathymetry, the transition into normal glacio-marine sediments were found and the first systematic seismic profiles on the continental shelf north of Svalbard were acquired. Despite its dimensions, the evidence of a giant submarine slide was not identified soon, and side-scan images of the slide debris have been interpreted as “Rubble from Glacial Scouring” in the Norwegian Seafloor Atlas. The analouge single-beam bathymetry data of the western headwall was converted into digitally data in cooperation with N. Z. Cherkis but was later classified in the USA. The discovered headwall area was then described as submarine embayment named Malene Bukta on the map published by the Norwegian Hydrographic Survey. However, an integration of indications and interpretation as a submarine slide has been presented by Cherkis et al. (1999). Their work was mainly based upon two side-scan profiles across the Sophia Basin, single beam bathymetry data from the western headwall during a survey of the Norwegian Hydrographic Survey (NSK) and two seismic profiles (survey carried out by the Norwegian Petroleum Directorate, NPD) from the adjacent shelf. Without knowledge of the seamounts, Cherkis et al. (1999) outlined a broad slide structure and concluded a free development of the slide into the Sophia and Nansen Basins. Despite the paper by Cherkis et al. (1999), the presence of a submarine slide or slump was, however, controversially discussed until the beginning of the ESF project “Slope stabilities on Europe's passive continental margin” (SPACOMA). Three cruises with RV “Polarstern” and “Jan Mayen” were planned to survey the slide. While collegues from the University of Tromsö focused on the headwall region with RV “Jan Mayen”, we concentrated investigations with RV “Polarstern” on the ice-covered area above the Sophia and Nansen Basins to yield information on the distal parts of the submarine slide.

Objectives of this Study

The main objectives of this study ("Sediment dynamics of Megaslides along the continental margin north of Svalbard") are (i) to identify, (ii) sedimentologically characterise, (iii) date and (iv) interprete major failure events on the continental shelf north of Svalbard in relation to the climate history of the archipelago.

Aside these main objectives defined by the ESF project, the newly recovered sediment cores that constitute excellent archives within the Sophia Basin for the last ~240 kyr. have been investigated to expand the knowledge of the late Quaternary history in the Fram Strait/Svalbard region and to enhance the interpretation of paleo-environmental changes.

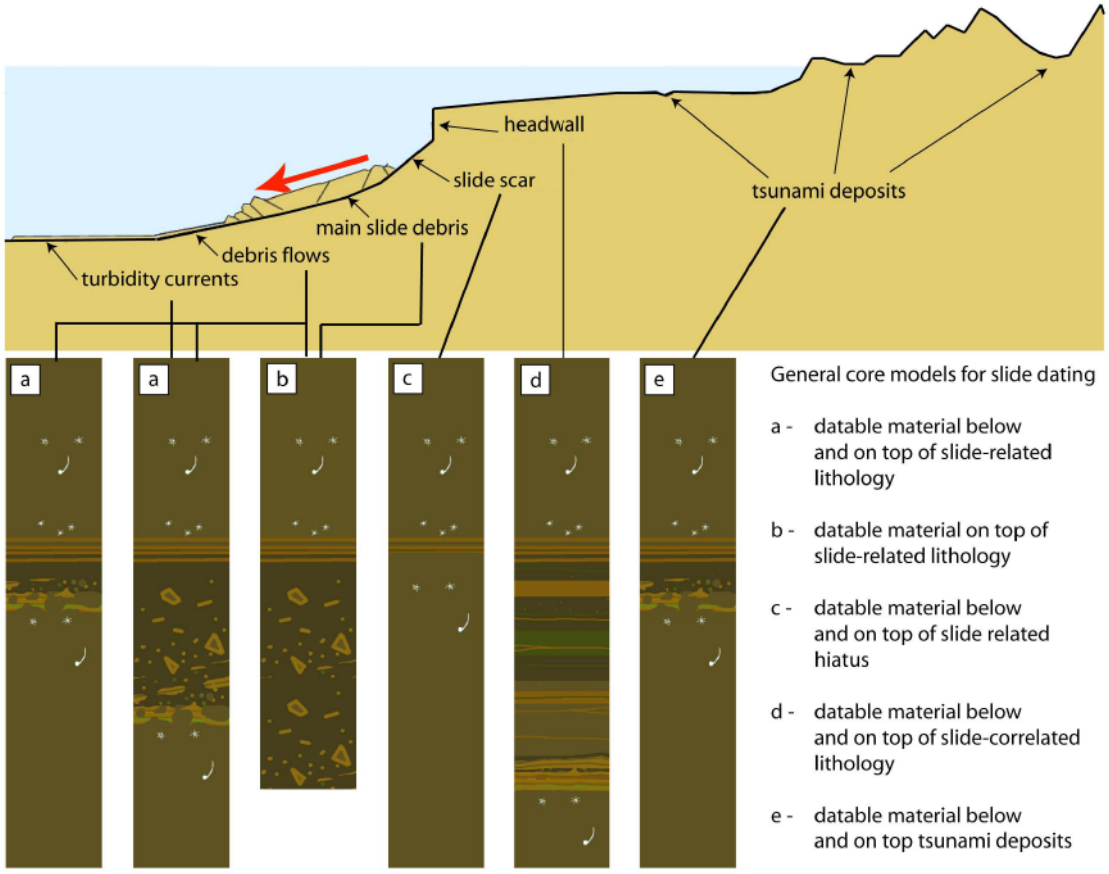

Figure 8: Schematical drawing of a submarine slide with key-core positions and expected core models (categories a to e) with focus on dating of a singular mass failure event. Note that category a can be found distally and laterally. Tsunami deposits on the shelf include the assumption of a lowered sea level during the failure event.

Research Strategy

The sedimentological characterisation and dating of main failure events are two main tasks of the present study. Generally, a mass wasting event can be dated by dating its deposits or hiatus in the corresponding sediment cores (e.g. Rodriguez & Paull, 2000; Haflidason et al., 2004, 2005; Figure 8). For failure events that are not older than 40 – 50 kyr. BP, radicarbon dating of planktic carbonaceous microfossils, in the Arctic realm *Neogloboquadrina Pachyderma sinistralis*, as monospecific samples are to be preferred. *N. Pachyderma sin.* dominates the cold surface waters around Svalbard and thus is regarded to be in equilibrium with athmospheric radiocarbon. Additionally, its stable carbon and oxygen isotopes have been used for establishment of chronologies in the Arctic Ocean beyond 50 kyr. BP. However, many gravity cores from the Arctic Ocean were difficult to date because of low or no concentrations of foraminifera. To overcome this problem and to recover a sufficient amount of foraminifera within our sediment cores, the giant gravity corer (kastenlot) was to be applied for key-locations.

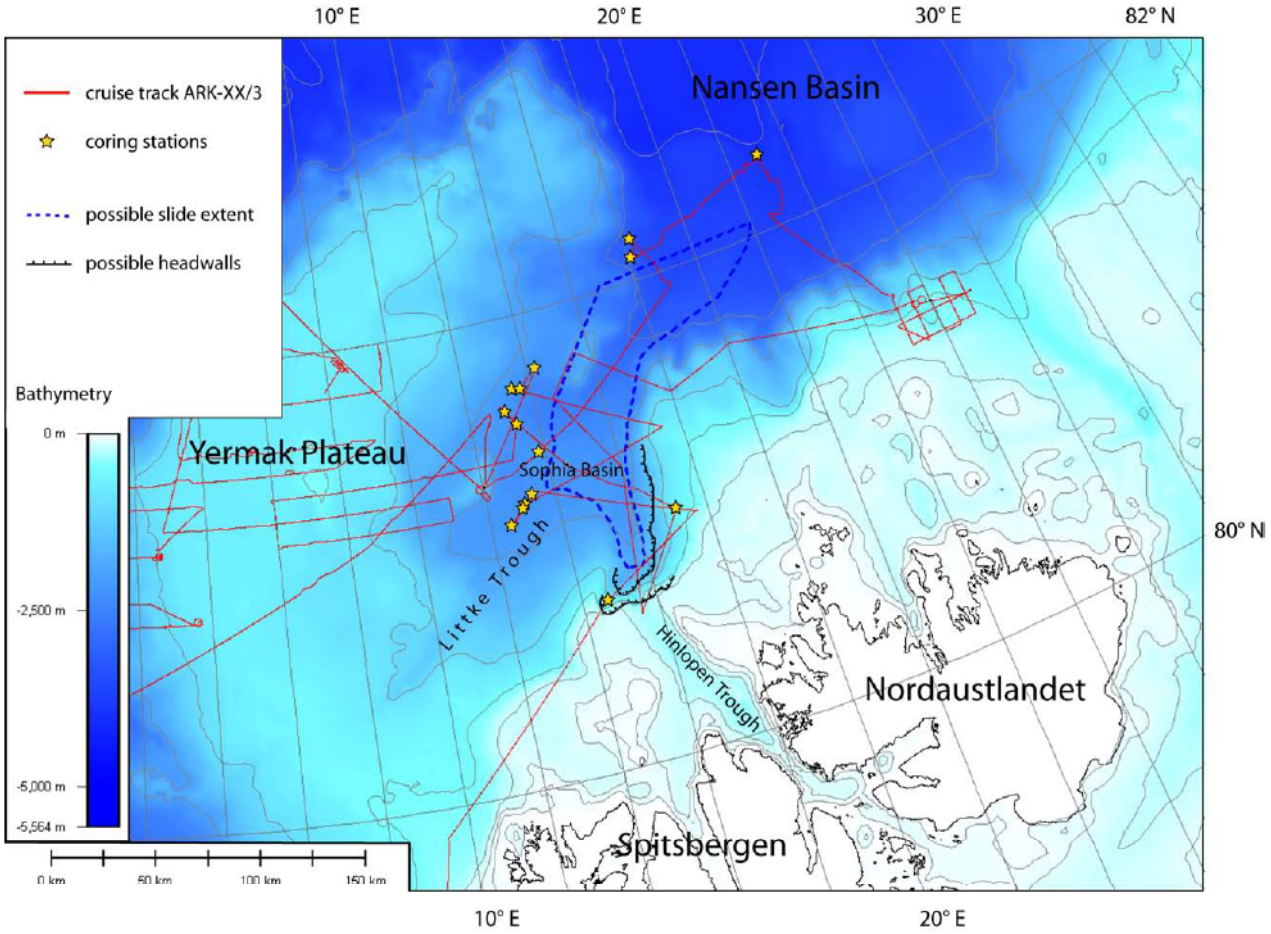

Figure 9: Map of the Sophia Basin north of Svalbard with acoustic profiles and coring stations of expedition ARK-XX/3 with ice-breaking RV "Polarstern" on the Yermak Slide area. The possible slide extent and headwalls are outlined according to Cherkis et al. (1999). Bathymetry: IBCAO (Jakobsson et al., 2000).

In preparation of the cruise ARK-XX/3, a synthesis of already existing geophysical data was necessary. The GIS-based intergration of bathymetry and PARASOUND data of the Alfred Wegener Institute (AWI), published side-scan sonar images of the Norwegian Polar Institute (NPI) and already recovered sediment cores (AWI, NPI and University of Stockholm) from the slide area revealed that the outlined slide extent needed to be revised. In addition this synthesis of existing evidence essentially helped to define key-sites of the Yermak Slide that appeared most promising for recovery of sediment cores for dating of the failure event. In preparation of the scheduled cruise with RV “Polarstern”, a number of profiles were planned across the slide for characterisation of its geometry and related parameters (e.g. drop height, run-out distance etc.; Figure 9) as well as to match with the key-locations targeted for gravity coring of ARK-XX/3 and projected sea ice conditions in an optimum of available ship-time.

Table 1: List of slide-related long gravity cores recovered during ARK-XX/3. Gear abbreviations: GC – gravity corer, KAL – kastenlot; categories according to Figure 8 (letters in brackets indicate failed purpose e.g. zero recovery).

Latitude	Longitude	Station	Depth	Date	Time	Gear	Recovery	Category
80° 43,20' N	14° 38,02' E	PS66/304-3	1095 m	03/09/2004	17:40	GC	4,19 m	c
81° 14,56' N	13° 18,62' E	PS66/306-2	2268 m	04/09/2004	03:34	GC	3,50 m	b
81° 11,94' N	13° 02,68' E	PS66/307-2	2275 m	04/09/2004	06:21	GC	4,57 m	b
81° 07,30' N	12° 35,97' E	PS66/308-3	2218 m	04/09/2004	10:47	GC	5,54 m	a
81° 11,22' N	12° 59,08' E	PS66/309-1	2269 m	04/09/2004	13:44	KAL	7,65 m	a
81° 41,78' N	13° 28,20' E	PS66/311-3	2192 m	05/09/2004	02:53	GC	4,93 m	a
81° 41,24' N	13° 42,65' E	PS66/312-2	2275 m	05/09/2004	05:30	GC	6,33 m	a
81° 45,56' N	14° 16,31' E	PS66/313-1	2298 m	05/09/2004	07:35	GC	4,49 m	a
81° 24.49' N	13° 48.79' E	PS66/319-1	2178 m	12/09/2004	22:26	GC	3,13 m	b
82° 10.27' N	18° 13.47' E	PS66/321-4	2360 m	13/09/2004	11:51	GC	7,11 m	(a)
82° 05.40' N	18° 05.25' E	PS66/322-3	3028 m	13/09/2004	16:16	GC	6,00 m	(a)
82° 18.44' N	22° 59.67' E	PS66/323-3	3913 m	14/09/2004	06:06	GC	0,66 m	b
81° 00.92' N	17° 09.39' E	PS66/327-3	701 m	16/09/2004	17:18	KAL	5,92 m	(d)
81° 19.25' N	14° 30.88' E	PS66/328-1	1979 m	16/09/2004	21:03	GC	0 m	(b)
81° 36.31' N	13° 06.13' E	PS66/329-3	2211 m	17/09/2004	03:44	GC	4,82 m	a
81° 32.88' N	13° 21.71' E	PS66/330-2	2305 m	17/09/2004	06:44	GC	4,54 m	a

Being part of the ESF collaborative project, the expedition ARK-XX/3 with the German research ice breaker “Polarstern” was intended to focus on the distal and sea ice-covered part of the slide while colleagues from the Tromsø University, Norway concentrated their investigations on the headwall area with RV “Jan Mayen”.

During expedition ARK-XX/3 with the ice-breaking RV “Polarstern” systematic PARASOUND profiles across the submarine slide were acquired including profiles from the main headwall to the distal part of the submarine slide in order to establish a run-out profile for a assessment of its geometry (Figure 9). In addition, high-resolution swath-bathymetry mapping was carried out to fill in the gaps of the already existing data (c.f. Jokat, 2000; Stein, 2005). This multi-beam acoustic survey resulted in an almost complete coverage of the Sophia Basin and the continental slope north of Nordaustlandet. The high-resolution PARASOUND data (including the 18 kHz NBS signal of the new PARASOUND system) allowed precise navigation to the targeted key coring stations. Gravity coring along selected key-profiles resulted in a total of 15 long gravity cores and a number of associated short cores from the slide and its adjacent area. First sedimentological investigations including multi-sensor core logging, x-ray radiography and geological core description and sampling were performed directly after recovery onboard the research vessel (c.f. Stein, 2005 and references therein).

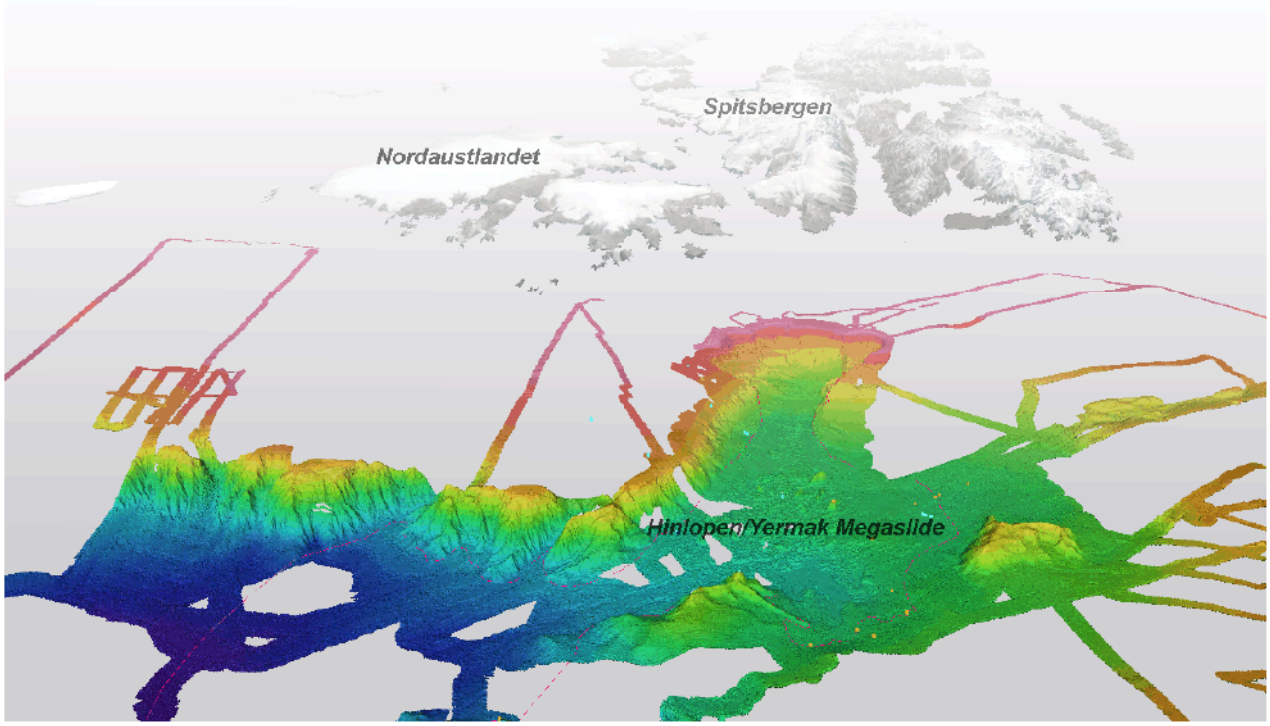

Figure 10: 3D-model of the Sophia Basin north of Svalbard (view towards Svalbard, S) based on high resolution bathymetry (HYDROSWEEP HS DS 2 and SMRAD EM300) with coring stations of expedition ARK-XX/3 with ice-breaking RV "Polarstern" on the Yermak Slide area. The slide extent is outlined according to this study).

The subsequent investigation following the cruise included integration and interpretation of geophysical data, construction of 3D-models of the slide's surface with integration of seismic data, sedimentological characterisation of the recovered sediment cores, establishment of age models for the cores and a slide-related local stratigraphy.

The integration of geophysical data was accomplished by application of standard GIS (ESRI, GM, Panmap). For the 3D-construction the IVS Fledermaus software appeared most promising and was applied (Figures 10 and 11). One key-aspect was the integration of bathymetry data from the headwall area that were recovered with RV “Jan Mayen” in autumn 2004 (Vanneste et al., 2004). This data set was acquired with a SYMRAD EM300 multi-beam system. The two data sets (HYDROSWEEP HS DS 2 from AWI and the SYMRAD EM300) exhibit systematic differences. Apart from the differences arising from different water speeds, the two systems vary in accuracy and noise within the data. In addition, heavy sea ice conditions resulted in poor quality of part of the HYDROSWEEP data. The problem was solved within an iterative process of adjusting both data sets by application of factors and offsets resulting in an grid almost unaffected by this systematic problem.

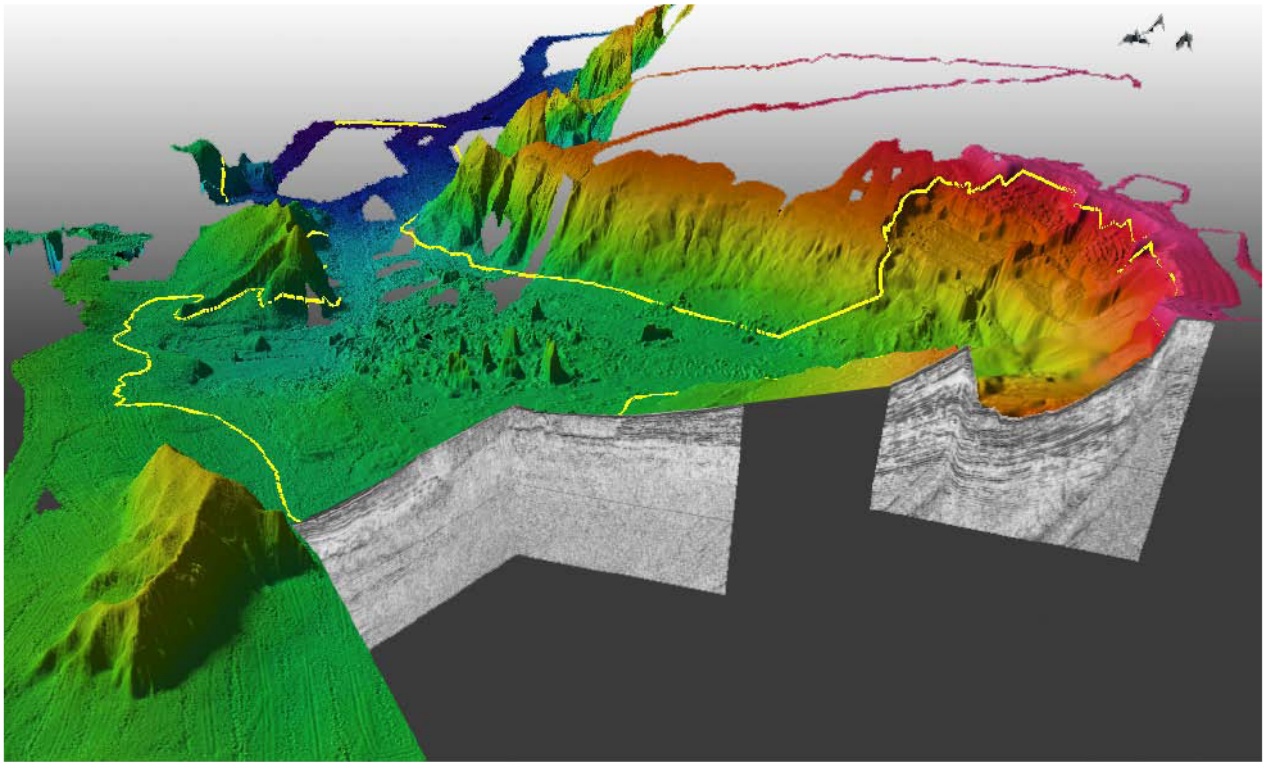

Figure 11: 3D-model of the Sophia Basin north of Svalbard (view towards Nansen Basin, NE) based on high resolution bathymetry with seismic profiles and coring stations of expedition ARK-XX/3 with ice-breaking RV "Polarstern" on the Yermak Slide area. The slide extent is outlined according to this study, seismic data from Jokat (2000) published by Geissler & Jokat (2004). For more details see http://www.awi-bremerhaven.de/GEO/Arctic/SPACOMA/SPACOMA.html.

The sedimentological characterisation was mainly based on interpretation of x-ray radiographs, MSCL data, geochemical bulk parameter and IRD contents. The stratigraphic work was mainly based upon AMS radiocarbon dating of *Neogloboquadrina pachyderma sinistralis* but included stable carbon and oxygen isotopic analysis of the same species, correlation of geochemical bulk parameters, MSCL data and IRD contents. XRF analysis was performed on key-core PS66/308-3 for further characterisation of the paleoceanographic conditions within the Sophia Basin as well as for detailed stratigraphic application.

Outline of the following Chapters

- Chapter 1 gives an introduction to submarine slides and to the research area Svalbard.
- The following Chapter 2 (publication 1) addresses basic questions concerning the Yermak Slide. It will focus on the establishment of the slide's true geometry, extent and volume and will give first indication of its age, mainly based on geophysical data.
- In Chapter 3 (publication 2) is devoted to the slide's dynamics, the timing of the slide's process and process-oriented sedimentary characterisation of its deposits. It is based on the integrated interpretation of geophysical and sedimentological data and represents the main work on the slide. Aside these main investigation the chapter gives implication for the structural framework of the Sophia Basin corroborating the interpretation of the slide's dynamics.
- Chapter 4 (publication 3) focuses on the trigger mechanism of the submarine slide in relation to environmental conditions and the climate history of Svalbard. A new triggering scenario is presented following the discussion on commonly suspected trigger mechanisms.
- Within Chapter 5 (additional work; future publications) credit is paid to fact that cores with excellent proxy records have been recovered from the SW-Sophia Basin during this project, expanding the focus from the slide towards the paleoceanographic history of the entire Sophia Basin throughout the last ~240 kyr. The chronology is refined and a new paleo-proxy is presented in this Chapter.
- Chapter 6 (summary & conclusion) summarises the main results from this work and gives the conclusions.
- Chapter 7 (outlook) addresses open questions and their possible assessment.

References

Aagaard, K. & Greisman, P. (1975): Toward new mass and heat budgets for the Arctic Ocean, Journal of Geophysical Research 80: 3821-3827.

Aagaard, K., Foldvik, A., Hillman, S.R. (1987): The West Spitsbergen Current: disposition and water mass transformation, Journal of Geophysical Research 92(C4), 3778-3784.

Abelmann, A., (1992): Diatom assemblages in Arctic sea ice - indicator for ice drift pathways, Deep-Sea Research, 39(2) S525-S538.

Boebel, T., (2000): Airborne topography and gravimetry: System and application to Fram Strait, Svalbard and Northeast Greenland, Reports on Polar Research, Vol. 366, Alfred Wegener Institute for Polar and Marine Research, Bremerhaven, p. 366.

Bourke, R. H., Weigel, A.M., Paquette, R.G. (1988): The westward turning branch of the West Spitsbergen Current, Journal of Geophysical Research 93, 14.065-14.077.

Canals, M., Lastras, G., Urgeles, R., Casamor, J.L., Mienert, J., Cattaneo, A., De Batist, M., Haflidason, H., Imbo, Y., Laberg, J.S., Locat, J., Long, D., Longva, O., Masson, D.G., Sultan, N., Trincardi, F., Bryn, P. (2004): Slope failure dynamics and impacts from seafloor and shallow sub-seafloor geophysical data: case studies from the COSTA project, Marine Geology 213 (1-4), 9-72.

Cherkis, N.Z., Max, M.D., Vogt, P.R., Crane, K., Midthassel, A., Sundvor, E. (1999): Large-scale mass wasting on the north Spitsbergen continental margin, Arctic Ocean, Geo-Marine Letters, 19, 131-142.

Crane, K., Sundvor, E., Buck, R., Martinez, F., (1991): Rifting in the Northern Norwegian-Greenland sea: Thermal Tests of Asymmetric Spreading, Journal of Geophysical Research, 96(B9), 14 529–14 550.

Crane, K. & Solhein, A. (Eds.) 1995: Seafloor Atlas of the Northern Norwegian-Greenland Sea, Norsk Polarinstitutt Meddelelser 137, Oslo, 1995, ISBN 82-7666-089-4.

Dethleff, D., Rachold, V., Tintelnot, M., Antonow, M. (2000): Sea-ice transport of riverine particles from the Laptev Sea to Fram Strait based on clay mineral studies. International Journal of Earth Sciences, 89(3): 496-502.

Dethleff, D., (2005): Entrainment and export of Laptev Sea ice sediments, Siberian Arctic, Journal of Geophysical Research, 110(C07009), doi: 10.1029/2004JC002740.

Divine, D.V. & Dick, C. (2006): Historical variability of sea ice edge position in the Nordic Seas, Journal of Geophysical Research, 111(C01001): doi:10.1029/2004JC002851.

Duplessy, J.-C., Ivanova, E., Murdmaa, I., Paterne, M., Labeyrie, L. (2201): Holocene paleoceanography of the northern Barents Sea and variations of the northward heat transport by the Atlantic Ocean, BOREAS Volume 30 (1), 2-16, DOI: 10.1080/03009480118702.

Eldholm, O., Faleide, J.I., Myhre, A.M., (1987): Continent-ocean transition at the western Barents Sea/Svalbard continental margin, Geology, 15, 1118–1122.

Eiken, O., (1993): An outline of the northwestern Svalbard continenal margin, in Arctic Petroleum Potential, NPF Special Publication 2, 619–629, eds Vorren, T.O., Bergsager, E., Dahl-Stamnes, Ø.A., et al. Elsevier, Amsterdam.

Eicken, H., Kolatschek, J., Freitag, J., Lindemann, F., Kassens, H. and Dimitrenko, I., (2000): A key source area and contraints on entrainment for basin-scale sediment transport by Arctic sea ice. Geophysical Research Letters, 27(13): 1919-1922.

Eischeid, J.K., Baker, B., Karl, T.R., Diaz, H.F. (1995): The quality control of long-term climatiological data using objective data analysis, Jornal of Applied Meteorolgy 34 (12), 2787-2795, doi: DOI: 10.1175/1520-0450(1995)034<2787.

Evans, D., Harrison, Z., Shannon, P.M., Laberg, J.S., Nielsen, T., Ayers, S., Holmes, R., Hoult, R.J., Lindberg, B., Haflidason, H., Long, D., Kuijpers, A., Andersen, E.S., Bryn, P. (2005): Palaeoslides and other mass failures of Pliocene to Pleistocene age along the Atlantic continental margin of NW Europe, Marine and Petroleum Geology 22, 1131–1148.

Fütterer, D.K. (Ed.) (1992): ARCTIC '91: Die Expedition ARK-VIII/3 mit FS 'Polarstern' 1991, Reports on Polar and Marine Research 107, ISSN 0176-5027.

Gaina, C., Roest, W.R., Müller, R.D. (2002): Late Cretaceous - Cenozoic deformation of northeast Asia. Earth and Planetary Science Letters 197, 273–286.

Gascard, J.-C., Richez, C., Rouault, C. (1995): New insights on large scale oceanography in Fram Strait: the West Spitsbergen Current. Arctic oceanography: marginal ice zones and continental shelves, in W.O. Smith & J.M. Grebmeier (Eds.), Arctic Oceanography: Marginal Ice Zones and Continental Shelves. American Geophysical Union, Washington, DC, pp. 131–182.

Geissler, W. H. & Jokat, W. (2004): A geophysical study of the northern Svalbard continental margin, Geophysical Journal International, 158, 50-66.

Haflidason, H., Sejrup, H., P., Nygard, A., Mienert, J., Bryn, P., Lien, R., Forsberg, C. F., Berg, K., Masson, D. (2004): The Storegga Slide: architecture, geometry and slide development. Marine Geology 213. 201-234.

Haflidason, H., Lien, R., Sejrup, H., P., Forsberg, C. F., Bryn, P. (2005). The dating and morphometry of the Storegga Slide, Marine and Petroleum Geology 22, 123–136.

Håkonsson E. & Pedersen, S.A.S. (1982): Late Paleozoic to Tertiary tectonic evolution of the continental margin in North Greenland, in Arctic Geology and Geophysics, Can. Soc. Pet. Geol. Mem. 8, pp. 331–348, eds Embry, A.F. & Balkwill, H.R. Canadian Society of Petroleum Geologists, Calgary.

Hagen, J. O., Liestøl, O., Roland, E., Jørgensen, T. (1993): Glacier atlas of Svalbard and Jan Mayen, Norsk Polarinstitut Meddeleser 129.

Hamilton, G.S. & Dowdeswell, J.A. (1996): Controls on glacier surging in Svalbard, Journal of Glaciology 42(140): 157-168.

Hebbeln, D., Dokken, T., Andersen, E.S., Hald, H., Elverhøi, A. (1994): Moisture supply for northern ice-sheet growth during the Last Glacial Maximum, Nature 370, 357-360.

Hopkins, T. S. (1991): The GIN Sea - a synthesis of its physical oceanography and literature review 1972-1985, Earth Science Reviews 30: 175-318.

IPCC REPORT, I. W. T. A. (2001): Summary for Policymakers. Shanghai, IPCC.

Isaksen, K., Holmlund, P., Sollid, J., L., Harris, C. (2001): Three deep alpine-permafrost boreholes in Svalbard and Scandinavia, Permafrost and Periglacial Processes 12: 13-25.

Isaksen, K., Vonder Mühll, D., Gubler, H., Kohl, T., Sollid, J., L. (2000a): Ground surface temperature reconstruction based on data from a deep borehole in permafrost at Janssonhaugen, Svalbard, Annals of Glaciology 31, 287-294.

Isaksen, K., Ødegård, R.S., Eiken, T., Sollid, J.L. (2000b): Composition, Flow and Development of Two Toungue-Shaped Rock Glaciers in the Permafrost of Svalbard, Permafrost and Periglacial Processes 11, 241-257.

Jakobsson, M., N. Z. Cherkis, et al. (2000): New Grid of Arctic bathymetry aids scientists and mapmakers, EOS, 81, 89-96.

Jokat, W. (Ed.) (2000): The Expedition ARKTIS-XV/2 of Polarstern in 1999, Reports on Polar and Marine Research 368, 128 pp., ISSN 0176-5027.

Jokat, W., Leinweber, V., Ehlers, B., Boebel, T., Schenke, H.W. (2007): Timing and Geometry of Fram Strait opening, Geophysical Journal International.

Jones, E. P., Rudels, B., Anderson, L.G. (1995): Deep waters of the Arctic Ocean: origins and circulation, Deep-Sea Research 42(5), 737-760 doi: 10.1016/0967-0637(95)00013-V.

Jones, P. D., New, M., Parker, D.E., Martin, S., Rigor, I.G. (1999): Surface air temperature and its changes over the past 150 years, Reviews of Geophysics 37, 173-199.

Kerr, R. A. (2002): A Warmer Arctic Means Change for All, Sience 297, 1490-1492.

Knies, J., Vogt, C., Stein, R. (1999): Late Quaternary growth and decay of the Svalbard/Barents Sea ice sheet and paleoceanographic evolution in the adjacent Arctic Ocean, Geo-Marine Letters 18, 195-202.

Knies, J., Nowaczyk, N. R., Müller, C., Vogt, C, Stein, R. (2000): A multiproxy approach to reconstruct the environmental changes along the Eurasian continental margin over the last 150 000 years. Marine Geology 163, 317-344.

Kristoffersen, Y. & E. Husebye (1985): Multichannel seismic reflection measurements in the Eurasian Basin, Arctic Ocean, from U.S. ice station FRAM-IV. Tectonophysics 114, 1-4, 103–115.

Kristoffersen, Y. (1990a): Eurasia Basin. In The Arctic Ocean Region, Vol. L, the Geology of North America. A. Grantz, G.L. Johnson, and J.F. Sweeney (eds.), The Geological Society of America, Boulder, pp. 365–378.

Kristoffersen, Y. (1990b): On the tectonic evolution and paleoceanographic significance of the Fram Strait gateway. In Geological History of the Polar Oceans: Arctic versus Antarctic: Proceedings of the NATO Advanced Research Workshop on Geological History of the Polar Oceans: Arctic versus Antarctic (1988:Bremen). U. Bleil and J. Thiede, Kluwer Academic Publishers , Dordrecht, pp. 63–76.

Kwok, R. & D. A. Rothrock (1999): Variability of Fram Strait ice flux and North Atlantic Oscillation, Journal of Geophysical Research 104, 5177-5189.

Kwok, R. (2000): Recent changes in Arctic Ocean sea ice motion associated with the North Atlantic Oscillation, Geophysical Research Letters 27, 775-778.

Kwok, R., Cunningham, G.F., Pang, S.S., (2004): Fram Strait sea ice outflow, Journal of Geophysical Research, 109 (C01009), doi: 10.1029/2003JC001785.

Landvik, J. Y., Bondevik, S., Elverhøi, A., Fjeldskaar, W., Mangerud, J., Salvigsen, O., Siegert, M. J., Svendsen J.-I., Vorren, T. O., (1998): The last glacial maximum of Svalbard and the Barents sea area: ice sheet extent and configuration, Quaternary Science Reviews 17, 43-75.

Landvik, J. Y., Ingólfsson, Ó., Mienert, J., Lehman, S. J., Solheim, A., Elverhøi, A., Ottesen, D. (2005): Rethinking Late Weichselian ice-sheet dynamics in coastal NW Svalbard. Boreas, 34, 7–24, ISSN 0300-9483.

Lefauconnier, B. & Hagen, J.O. (1991): Surging and calving glaciers in eastern Svalbard, Norsk Polarinstitut Meddeleser 116.

Liestøl, O. (1969): Glacier surges in West Spitsbergen, Canadian Journal of Earth Science 6 (895), 895-897.

Liestøl, O. (1977): Pingos, springs and permafrost in Spitsbergen, Norsk Polarinstitutt Årbok 1975, Norsk Polarinstitutt.

Liestøl, O. (1993): Glaciers of Europe - Glaciers of Svalbard, Norway, U.S. Geological Survey Prof. Pap. 1386(E), 127-151.

Locat, J., Mienert, J. (Eds.) (2003): Submarine Mass Movements and Their Consequences, Springer, pp. 552, ISBN 1402012446.

Mangerud, J., Jansen, E., Landvik, J.Y., (1996): Late Cenozoic history of the Scandinavian and Barents Sea ice sheets, Global and Planetary Change, 2 (1-4), 11-26.

Mangerud, J., Dokken, T., Hebbeln, D., Heggen, B., Ingólfsson, Ó., Landvik,J.Y., Mejdahl, V., Svendsen, J.I., Vorren, T.O. (1998): Fluctuations of the Svalbard-Barents Sea ice sheet during the last 150 000 years, Quaternary Science Reviews, 17, 11-42.

Manley, T. O. (1995): Branching of Atlantic Water within the Greenland-Spitsbergen Passage: An estimate of recirculation, Journal of Geophysical Research 100(C10), 20.627-20.634.

Maslowski, W. (1994): Numerical modelling study of the circulation of the Greenland Sea, University of Alaska.

Martin, T. & Augstein, E., (2000): Large-scale drift of Arctic Sea ice retrieved from passive microwave satellite data, Journal of Geophysical Research, 05(C4), 8775–8788.

Michael, P. J., Langmuir, C.H., Dick, H.J.B., Snow, J., Goldstein, S.L., Graham, D.W., Lehnert, K., Kurras, G., Jokat, W., Mühe, R., Edmonds, H.N. (2003): Magmatic and amagmatic seafloor generation at the ultraslow-spreading Gakkel Ridge, Arctic ocean. Nature 423, 956–961.

Midttun, L. & Loeng, H. (1987): Climatic variations in the Barents Sea. The Effect of Oceanographic Conditions on Distribution and Population Dynamics of Commercial Fish Stocks in the Barents Sea, Proceedings of the 3rd Soviet-Norwegian Symposium, Bergen, Institute for Marine Research.

Morales-Maqueda, M.A., Willmott, A. J., Darby, M. S. (1999): A numerical model for interdecadal variability of sea ice cover in the Greenland-Iceland-Norwegian Sea, Climate Dynamics 15, 89-113.

Morison, J. H., Aagaard, K., Steele, M. (2000): Recent environmental changes in the Arctic: A review, Arctic 53, 359-371.

Mosar, J., Eide, E.A., Osmundsen, P.T., Sommaruga, A. and Torsvik, T.H., (2002): Greenland - Norway seperation: A geodynamical model for the North Atlantic. Norwegian Journal of Geology, 82: 282-299.

Müller, D. & Spielhagen, R.F. (1990): Evolution of the Central Tertiary Basin of Spitsbergen: towards a synthesis of sediment and plate tectonic history. Paleogeography, Paleoclimatology, Paleoecology 80, 153-172.

Nürnberg, D., Wollenburg, I., Dethleff, D., Eicken, H., Kassens, H., Letzig, T., Reimnitz, E., Thiede, J., (1994): Sediments in Arctic sea ice: Implications for entrainment, transport and release, Marine Geology 119, 185-214.

Ottesen, D., Dowdeswell, J.A., Rise, L. (2005): Submarine landforms and the reconstruction of fast-fl owing ice streams within a large Quaternary ice sheet: The 2500-km-long Norwegian-Svalbard margin (57°–80°N), Geological Society of America Bulletin 117, 7/8, p. 1033–1050, doi: 10.1130/B25577.1.

Owrid, G., Socal, G., Civitarese, G., Luchetta, A., Wiktor, J., Nöthig, E.-M., Andreassen, I., Schauer, U., Strass, V., (2000): Spatial variability of phytoplankton, nutrients and new production estimates in the waters around Svalbard, Polar Research 19(2): 155-171.

Pfirman, S.L., Colony, R., Nürnberg, D., Eicken, H., Rigor, I., (1997): Reconstructing the origin and trajectory of drifting Arctic sea ice, Journal of Geophysical Research, 102(C6): 12,575-12,586.

Piper, D.J.W., Farre, J.A., Shor, A.N. (1985): Late Quaternary slumps and debris flows on the Scotian Slope, Geolocical Society of America Bulletin, 96, 1508-1517.

Piper, D.J.W., Shor, A.N., Hughes-Clarke, J.E. 1988: The 1929 Grand Banks earthquake, slump and turbidity current, in Clifton, H.E., Sedimentologic consequences of convulsive geologic events, Geological Society of America, Special Paper 229, pp.77-92.

Piper, D.J.W., Cochonat, P., Morrison, M.L. (1999): The sequence of events around the epicentre of the 1929 Grand Banks earthquake: initiation of debris flows and turbidity current inferred from sidescan sonar, Sedimentology 46, 79-97.

Polyakov I.V., Beszczynska, A., Carmack, E.C., Dmitrenko, I.A., Fahrbach, E., Frolov, I.E., Gerdes, R., Hansen, E., Holfort, J., Ivanov, V.V., Johnson, M.A., Karcher, M., Kauker, F., Morison, J., Orvik, K.A., Schauer, U., Simmons, H.L., Skagseth, Ø., Sokolov, V.T., Steele, M., Timokhov, L.A., Walsh, D., Walsh J.E. (2005): One more step toward a warmer Arctic, Geophysical Research Letters 32, doi:10.1029/2005GL023740.

Ramseier, R.O., Garrity, C., Martin, T. (2001): An Overview of Sea-Ice Conditions in the Greenland Sea and the Relationship of Oceanic Sedimentation to the Ice Regime, in: Schäfer, P., Ritzrau, W., Schlüter, M., Thiede, J. (Eds.), The Northern North Atlantic, Springer Verlag, Berlin, pp.19-38.

Rigor, I. G., Wallace, J. M. Colony, R.L. (2002): On the Response of Sea Ice to the Arctic Oscillation, Journal of Climate 15 (18), 2546-2663. doi: DOI: 10.1175/1520-0442(2002)015.

Ritzmann, O., (2003): Architecture and geodynamic evolution of the Svalbard Archipelago, the Yermak Plateau and the Fram Strait oceanic province, from deep seismic experiments, Reports on Polar Research, 439, Alfred Wegener Institute for Polar and Marine Research, Bremerhaven.

Rodriguez, N.M., Paull, C.K. 2000: ^{14}C dating of sediment of the uppermost Cape Fear Slide Plain: constraints on the timing of this massive submarine landslide, 32. Data Report in Paul, C.K., Matsumoto, R., Wallace, P.J., Dillon, W.P. (Eds.), Proceedings of the Ocean Drilling Program, Scientific Results, Volume 164.

Rothrock, D.A., Yu, Y., Maykut, G.A. (1999): Thinning of the Arctic Sea-Ice Cover, Geophysical Research Letters 26(23), 3469-3472.

Rothrock, D.A., Zhang, J., Yu, Y. (2003): The Arctic ice thickness anomaly of the 1990s: A consistent view from observations and models. Journal of Geophysical Research, Vol. 108, No. C3, Article No. 3083.

Rudels, B. (1987): On the mass balance of the polar ocean, with special emphasis on the Fram Strait, Skrifter Norsk Polar Institutt 1987(188), 1-53.

Rudels, B. (1990): Haline convection in the Greenland Sea, Deep-Sea Research 37, 1491-1511.

Rudels, B., Jones, E.P., Anderson, L.G., Kattner, G. (1994): On the intermediate depth waters of the Arctic Ocean, The Polar Oceans and their Role in Shaping the Global Environment: The Nansen Centennial Volume. O.M. Johannessen, R.D. Muench and J.E. Overland. Washington D.C., U.S.A., AGU. 85: 33-46.

Schlichtholz, P. & Houssais, M.N. (1999a), An inverse modeling study in Fram Strait, Part 1: dynamics and circulation, Deep-Sea Research II (46), 1083-1135.

Schlichtholz, P. & Houssais, M.N. (1999b), An inverse modeling study in Fram Strait, Part 2: water mass distribution and transports, Deep-Sea Research II (46), 1137-1168.

SEARCH SSC, S. (2001): Study of Environmental Arctic Change, Science Plan,. SEARCH. J. M. e. al. Seattle, University of Washington: 1-89.

Serreze, M. C., Walsh, J.E., Chapin, F.S., Osterkamp, T., Dyurgerov, M., Romanovsky, V., Oechel, W.C., Morison, J., Zhang, T., Barry, R.G. (2000): Observational evidence of recent change in the northern high-latitude environment, Climatic Change 46, 159-207, doi: 10.1023/A:1005504031923.

Solheim, A., Andersen, E.S., Elverhøi, A., Fiedler, A., (1996a): Late Cenozoic depositional history of the western Svalbard continental shelf, controlled by subsidence and climate, Global and Planetary Change, 12 (1-4), 135-148.

Solheim, A., Riis, F., Elverhøi, A., Faleide, J.I., Jensen, L.N., Cloetingh, S., (1996b): Impact of glaciations on basin evolution: data and models from the Norwegian margin and adjacent areas-Introduction and summary, Global and Planetary Change, 12 (1-4), 1-9.

Steffensen, E. L. (1982). The climate at Norwegian Arctic Stations, DNMI Klima, No.5, 3-44.

Stein, R. & Fahl, K. (Eds.) 1997: Scientific Cruise Report of the Arctic Expedition ARK-XIII/2 of RV 'Polarstern' in 1997, Reports on Polar and Marine Research 255, 235 pp., ISSN 0176-5027.

Stein, R. (Ed.) (2005), Scientific Cruise Report of the Arctic Expedition ARK-XX/3 of RV "Polarstern" in 2004: Fram Strait, Yermak Plateau and East Greenland Continental Margin, Reports on Polar Research, 517, 195 pp., ISSN 0176-5027.

Strübing, K. (1968): Eisdrift im Nordpolarmeer, Umschau in Wissenschaft und Technik 21, 662-663.

Svendsen, H., Beszczynska-Møller, A., Hagen, J.O., Lefauconnier, B., Tverberg, V., Gerland, S., Ørbæk, J.B., Bischof, K., Papucci, C., Zajaczkowski, M., Azzolini, R., Bruland, O., Wiencke, C., Winther, J-G., Dallmann, W. (2002): The physical environment of Kongsfjorden-Krossfjorden, an Arctic fjord system in Svalbard, Polar Research 21(1), 133-166.

Svendsen, J.I., Alexanderson, H., Astakhov, V.I., Demidov, I., Dowdeswell, J.A., Funder, S., Gataullin, V., Henriksen, M., Hjort, C., Houmark-Nielsen, M., Hubberten, H.W., Ingólfsson, Ò., Jakobsson, M., Kjær, K.H., Larsen, E., Lokrantz, H., Lunkka, J.P., Lysså, A., Mangerud, J., Matiouchkov, A., Murray, A., Möller, P., Niessen, F., Nikolskaya, O., Polyak, L., Saarnisto, M., Siegert, C., Siegert, M.J., Spielhagen, R.F., Stein, R. (2004): Late Quaternary ice sheet history of northern Eurasia, Quaternary Science Reviews 23, 1229–1271.

Swift, J. H. & Aagaard, K. (1981): Seasonal transitions and water mass formation in the Iceland and Greenland Seas, Deep-Sea Research 28(Part A): 1107-1129.

Swift, J.H., Jones, E.P., Aagaard, K., Carmack, E.C., Hingston, M., MacDonald, R.W., McLaughlin, F.A., Perkin, R.G. (1997): Waters of the Makarov and Canada basins, Deep-Sea Research 44(8): 1503-1529.

Takahashi, E., Lipman, P.W., Garcia, M.O., Naka, J., Aramaki, S. (Eds.) 2002: Hawaiian Volcanoes: Deep Underwater Perspectives, Geophysical Monograph Series, Volume 128, 2002. 418 pages, ISBN 0-87590-987-6.

Thiede (Ed.) 1988: Scientific cruise report of Arctic Expedition ARK IV/3, Reports on Polar and Marine Research 43, 237 pp., ISSN 0176-5027.

Thiede, J., Winkler, A., Wolf-Welling, T., Eldholm, O., Myhre, A.M., Baumann, K.-H., Henrich, R., Stein, R., (1998): Late Cenozoic history of the Polar North Atlantic: results from ocean drilling. Quaternary Science Reviews, 17(-3): 185-208.

Thompson, W.J. & Wallace, J.W. (1998): The Arctic oscillation signature in the wintertime geopotential height and temperature fields, Geophysical research Letters 25, 1297-1300.

Thorndike, A.S. & Colony, R. (1982): Sea ice motion in response to geostrophic winds, Journal of Geophysical Research 87, 5845-5852.

Vinje, T. & Finnekåsa, Ø., (1986): The Ice Transport through the Fram Strait, Skrifter Norsk Polarinstitutt, 186: 1-39.

Vinje, T., Nordlund, N., Kvambekk, Å., (1998): Monitoring ice thickness in Fram Strait, Journal of Geophysical Research, 103(C5): 10437-10449.

Vinje, T. (2001): Anomalies and Trends of Sea-Ice Extent and Atmospheric Circulation in the Nordic Seas during the Period 1864-1998, American Meteorological Society, 225-267.

Vogt, P.R., Taylor, P.T., Kovacs, L.C., Johnson, G.L. (1979): Detailed aeromagnetic investigations of the Arctic Basin. Journal of Geophysical Research 84 (B3), 1071–1089.

Vogt, P.R., Gardner, J., Crane, K. (1999): The Norwegian-Barents-Svalbard (NBS) continental margin: Introducing a natural laboratory of mass wasting, hydrates and ascent of sediment, pore water, and methane, Geo-Marine Letters 19, 2-21.

Walsh, J.E., Chapman, W.L., Shy, T.L. (1996): Recent decrease of sea level pressure in the central Arctic, Journal of Climate 9, 480-486.

Wilson, J.T. (1963): Hypothesis of earth's behaviour. Nature, 198:925–929.

Winkelmann, D., & Knies, J. (2005): Recent distribution and accumulation of organic carbon on the continental margin west

off Spitsbergen, Geochemistry Geophysics Geosystems 6, Q09012, doi:10.1029/2005GC000916.

Yalciner, A.C., Pelinovsky, E.N., Okal, E., Synolakis, C.E., (Eds.) 2003: Submarine Landslides and Tsunamis, NATO Science Series IV Earth and Environmental Sciences 21, Springer, pp. 352, ISBN: 1402013493.

Zhang, J., Rothrock, D.A., Steele, M. (2000): Recent changes in Arctic Sea Ice: The interplay between ice dynamics and thermodynamics, Journal of Climate 13, 3099-3114.

Ziegler, P.A. (1988): Evolution of the Arctic-North Atlantic and the Western Tethys. American Association of Petroleum Geologists Memoir 43, 198 pp.

Chapter II

Age and Extent of the Yermak Slide north of Spitsbergen, Arctic Ocean

Age and Extent of the Yermak Slide north of Spitsbergen, Arctic Ocean

D. Winkelmann, W. Jokat, F. Niessen, R. Stein, A. Winkler

Alfred Wegener Institute for Polar and Marine Research, Columbusstrasse, Bremerhaven, Germany

Published in Geochemistry, Geophysics, Geosystems, Volume 7, number 6, 8th June 2006, Q06007, doi:10.1029/2005GC001130.

Abstract

The extent of the Yermak Slide has been revised based on new acoustic and detailed bathymetric data. The true geometry, with an affected area of at least 10,000 km^2 and more than 2400 km^3 involved sedimentary material, puts the Yermak Slide among the largest exposed submarine slides worldwide, comparable to the Storegga Slide off central Norway. Details from the side's internal structure give evidence for one main slide event during MIS 3 followed by repeated minor events. The timing coincides with the transition of the Kapp Ekholm Interstadial into Glaciation G of Svalbard (Mangerud et al., 1998) and the build-up phase of the Svalbard-Barents Sea Ice Sheet. Thus, the slide occurred during a period of falling sea level, increasing ice volume and, presumably, increasing glacio-tectonic activity. The side's geometry and internal physical appearance point to a tectonically induced partial shelf collapse.

Introduction

Submarine slides (or submarine landslides) play a significant role among the variety of sediment transport processes from continental margins to deep sea environments. By moving large amounts of sediment masses, they are not only an effective mechanism to transport sediment to the abyssal plains, but they are also a substantial hazard to seafloor infrastructure and are able to create tsunamis that have far-reaching consequences. On Europe's continental margins, a number of slides have been discovered by side-scan sonar imaging and detailed bathymetric mapping, ranging from small scale features to mega scale events like the Storegga Slide off Norway, which affected some 95,000 km^2 of the seafloor and involved about 2,400 - 3,200 km^3 of sediment (e.g. Vogt et al. 1999c; Mienert & Weaver, 2002 and references therein; Haflidason et al., 2004). Three of these slides have been chosen to be studied in more detail within the ESF EUROMARGIN project "Slope Stabilities on Europe's passive continental Margin" to shed light on the preconditions, trigger mechanisms and geometrical relations of these events. The COSTA project (Canals et al., 2004) has shown that submarine slides are highly variable in size, position

and setting, exhibit between their geometrical parameters such as headwall height, drop height, run-out distance or total area, and that a trend from carbonate river-fed to glacier-fed continental margins might exist. Geometrical parameters are not yet available for Europe's northernmost identified slide, situated on the glacier-fed, siliciclastic continental margin north of Spitsbergen (Figure 1). This slide was first described by Cherkis et al. (1999) and is situated at the termination of the Hinløpen Strait cross-shelf trough, which hosted an ice stream during glacial times (Ottesen et al. 2005). The slide has been referred to as the Yermak Slide, according to its position adjacent to the Yermak Plateau, or sometimes as Malene Bukta or Malene Slide according to the submarine embayment of its evacuation area (Vogt et al., 1999; Haflidason et al., 2004). Cherkis et al. (1999) used side-scan sonar images and bathymetric data to determine some of its structures (Figure 2).

Physiographic Setting

The surface water circulation around Spitsbergen is characterised by the northward flowing West Spitsbergen Current (WSC) transporting warm and saline Atlantic water into the Arctic Ocean via Fram Strait. Branches of the WSC flush the outer shelf west and north-west of Spitsbergen (North Svalbard Current, NSC) and the Yermak Plateau (Yermak Slope Current, YSC; Yermak Plateau Current, YPC)(Schlichtholz & Houssais, 1999a, b). A counterpart to the WSC, the East Greenland Current (EGC), transports less saline and colder Arctic water into the Greenland Sea (Figure 1).

The archipelago was repeatedly and heavily glaciated during the Weichselian Glacial (Mangerud et al., 1998, Svendsen et al., 2004). Our investigation area is situated on and close to the shelf north of Spitsbergen and Nordaustlandet. These two present-day islands are separated by a deep geologic structure that has been exploited by glacial erosion to form a cross shelf trough. This Hinløpen cross shelf trough hosted an ice stream during glacial times, and probably also during late Weichselian full glacial conditions (Ottesen et al. 2005). The termination of the Hinløpen trough is characterised by a number of submarine embayments and slope escarpments (Cherkis et al., 1999, Vanneste et al., 2004). In contrast to other cross shelf troughs, a trough mouth fan (TMF) is missing. A number of submarine escarpments and headwalls characterise the evacuation area of the Yermak Slide, giving evidence for multiple slope failure events (Cherkis et al., 1999, Vanneste et al., 2004).

In this paper we present new acoustic and detailed bathymetric data that show the first details of the Yermak Slide's internal structure, a much larger extent than previously thought (Figure 2) and the first evidence for a pre-LGM stage of sliding.

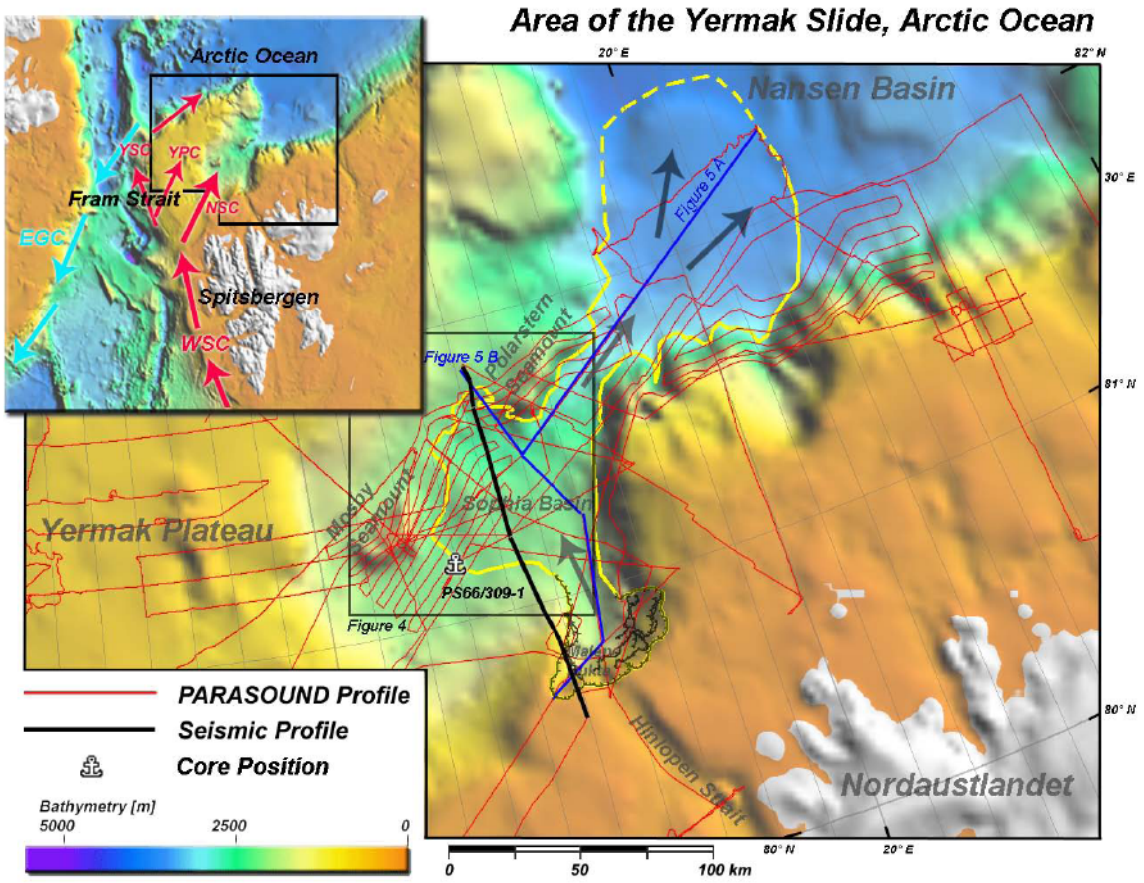

Figure 1: Map of Sophia Basin and the adjacent shelf with position of sediment core PS66/309-1, and PARASOUND and seismic profiles acquired during "Polarstern" Expeditions ARKXV/2 and ARKXX/3. Slide extent according to our study (headwalls partly according to integrated interpretation of Vanneste et al., 2004). Insetmap shows surface water ciculation in the Fram Strait area (WSC: West Spitsbergen Current, NSC: North Svalbard Current, YPC: Yermak Plateau Current, YSC: Yermak Slope Current, EGC: East Greenland Current). Bathymetry from the International Bathymetric Chart of the Arctic Ocen (IBCAO) (Jakobsson et al. 2001).

Material and Methods

Detailed bathymetric data and high resolution ground penetrating echo sounding data were acquired by the HYDROSWEEP DS2 and the PARASOUND Hydromap Control systems, respectively, aboard RV "Polarstern" during cruise ARKXX/3 (Stein, 2005). Additional data from cruise ARKXV/2 of RV "Polarstern" (Jokat, 2000), including marine multichannel seismic profiles (acquired using a 24-litre air gun cluster; see Geissler & Jokat, 2004 for details), have been compiled to analyse the area of the Yermak Slide. Sediment cores, from carefully selected sites, were retrieved using the gravity or giant gravity corer (Stein, 2005). AMS radiocarbon dating was performed on carbonaceous shells from *Neogloboquadrina pachyderma sin.* at the Leibniz-Labor for Radiometric Dating and Isotope Research in Kiel, Germany.

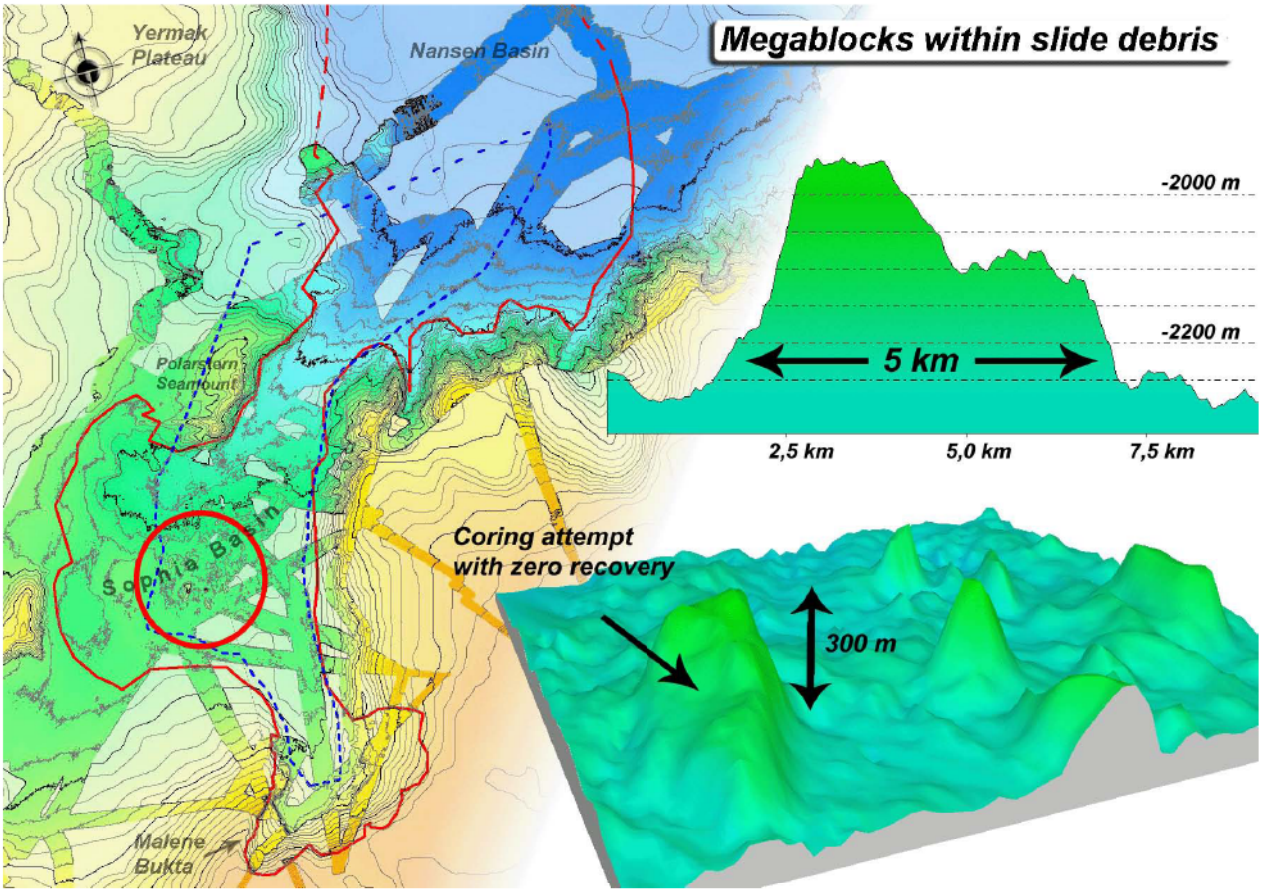

Figure 2: Map with new detailed bathymetry showing offsets to the underlying older IBCAO, slide extent according to Cherkis et al. 1999 (dashed blue line) as well as new slide extent (red line; headwall area according to Vanneste et al., 2004) and closeup of megablocks reaching up to 5 km long and with 300 m relief above the surrounding debris (red encircled area). A coring attempt on the main megablock, with zero recovery (see Stein, 2005) probably points towards a more solid lithology of these blocks.

Results

PARASOUND sediment penetrating acoustic data reveal clear differences in the acoustic facies of slide debris and normal hemi-pelagic glacio-marine sediments. The latter sediments appear as acoustically layered units that permit deep penetration of acoustic waves. The slide related debris is acoustically opaque, revealing no indication of internal structures and almost no penetration of acoustic energy. The absence of internal structures in the PARASOUND imagery (that is, no systematic contrasts in acoustic impedance) points towards a homogeneous debris. This distinction permits a mapping of the slide area, having an inner part within the Sophia Basin and an outer part towards the Nansen Basin (Figure 2). The inner part of the slide is characterised by a mass of dense acoustically opaque material (presumably over-consolidated silty clays). A number of large blocks, with extents of up to 4 km and relief of more than

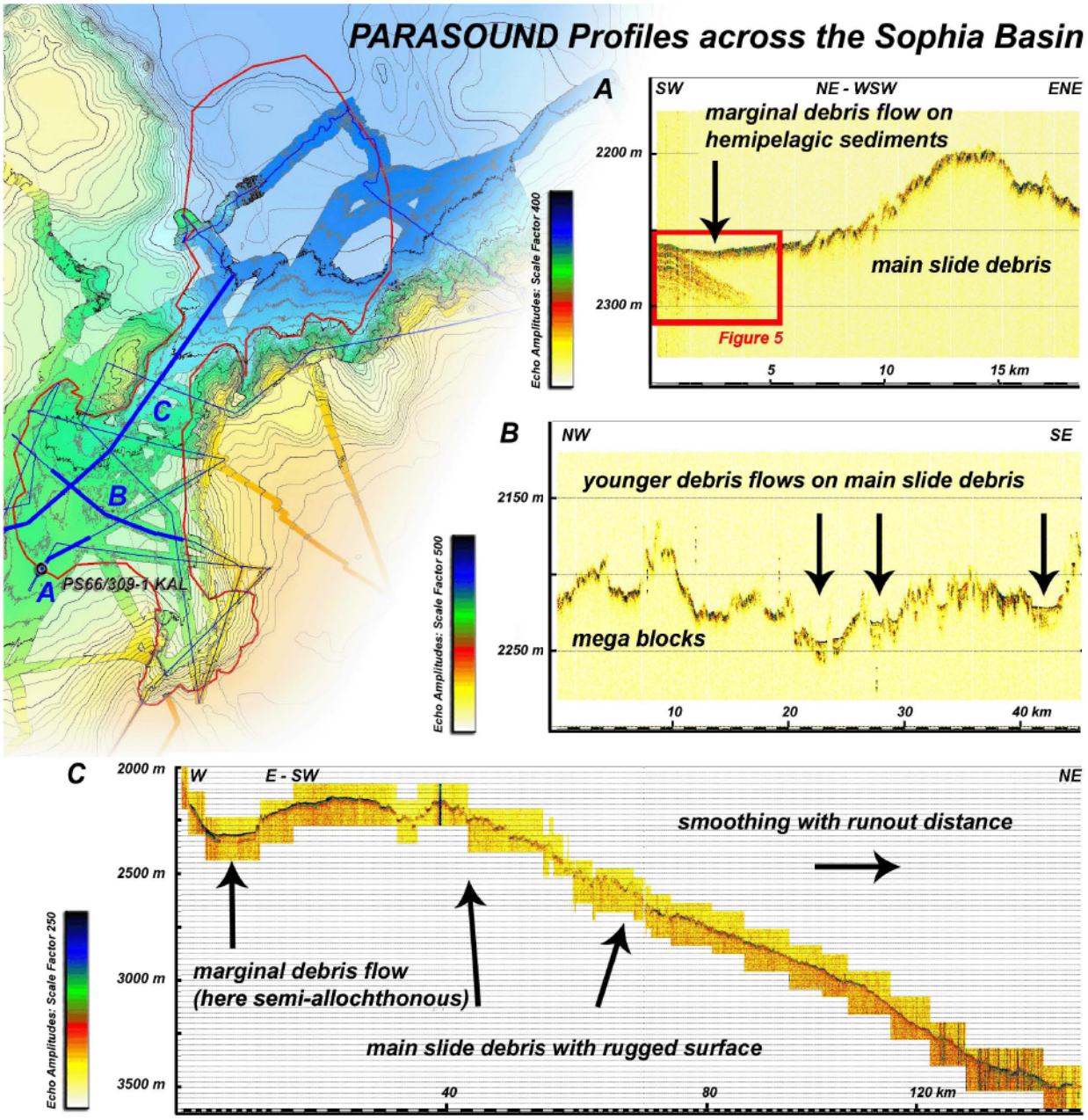

Figure 3: Typical PARASOUND profiles across the western margin of the Yermak Slide within the Sophia Basin, showing the transition from main slide debris into the marginal debris flow (A), the inner slide area with hummocky relief, megablocks and indication of younger debris flows within distinct local depressions (B), and along runout displaying the slide's broad geometric features, as well as smoothing of the surface towards the distal part (C). Note that the marginal debris flow developed a semi-allochthonous appearance in profile C.

300 m above the surrounding hummocky area, are centred within this debris (Figure 2). A coring attempt on the main megablock (Figure 2) resulted in zero recovery (Stein, 2005).

Judging from the rope tension protocol, the gravity core must have jumped back from a presumably hard ground. Therefore, and due to their intact shape, they might represent a second and more solid type of lithology in the slide. Large ridges in front of the blocks suggest that they ploughed up the surrounding debris while travelling, which might point to them having a higher density. Younger debris flows, visible as acoustically transparent units, have been identified in PARASOUND data from some of the topographic depressions in this inner part of the slide (Figure 3). These flows occasionally overlie each other and are likely to correspond to the younger slide scars in the head wall area.

Towards its western margin within the Sophia Basin, the Yermak Slide develops a consistent facies (Figures 3 and 4). Starting from the hummocky slide debris of the inner part of the slide, which appears acoustically opaque and with rough topography, the acoustic character of the slide becomes increasingly transparent, suggestive of debris flows. The marginal debris flows and, presumably, associated turbidites overlie and pinch out into “normal” glacio-marine hemi-pelagic sediments which appear as acoustically layered sequences (Figure 4). The same hemi-pelagic glacio-marine silty clay can be found on top of the debris flows / turbidites (Figures 4 and 5). Thus, our interpretation is that the slide developed into a debris flow with associated turbidites towards its western margin, in accordance with both theory and lithologic evidence from our cores. According to the PARASOUND data, the marginal debris flows did not develop an erosional character. This points towards hydroplaning at the base of the debris flow which may be a common feature for debris flows (e.g., deBlasio et al., 2004). In our interpretation, the western margin of the slide debris lies further west in the Sophia Basin than depicted by Cherkis et al. (1999) (Figure 2).

Originating at the trough mouth of Hinløpen Strait and flowing into Sophia Basin, the slide funnelled out between the shelf and a seamount discovered in 1999 (Polarstern Peak; Daschner et al., 2000; Figure 3) towards the continental slope north of Nordaustlandet and into the Nansen Basin. The slide keeps its hummocky appearance towards its distal part, although in general the surface seems to become smoother with distance. At the north-easternmost station of cruise ARK XX/3 (82°18´N and 23°E; Stein 2005) the slide develops a debris flow-like appearance, and beyond this most likely extends further into the Nansen Basin. However, due to heavy sea ice conditions, resulting in poor quality and coverage of the acoustic data, this remote part of the slide remains poorly constrained. In general, the eastern margins of the slide did not develop a pronounced and characteristic acoustic appearance. Consequently, the distinction of the side's margins from slumps and debris flows from the shelf break north of Nordaustlandet remains difficult. Thus, the actual margin may lie further east, and the slide may be even larger than shown here. However, the probable margin has partly been based on bathymetric information and represents the most

likely extent. Neglecting the debris flows into the Nansen Basin, the Yermak Slide has affected an area of at least 10,000 km^2.

Seismic data from lines AWI-99161 and AWI-99140, collected in 1999 (Geissler & Jokat, 2004), display some deeper features of the slide. A number of reflectors can be observed within the Yermak Slide deposits despite strong seismic energy scattering at the rough seafloor and a pronounced first reflector (Figure 6). The slide debris should have at least an average thickness of 200 m, based on extrapolation of the dipping hemi-pelagic strata below the main debris in PARASOUND images. The character of the 2nd reflector on line AWI-99161 (Figure 6 D) seems to be influenced by bathymetric effects. In addition, the reflector does not match with the PARASOUND data (showing no internal reflectors at this level) and the expected depth interval of the lower slide boundary. Thus, the lower boundary of the slide is most likely represented by the 3rd strong reflector (Figure 6 B). The southern part of line AWI-99140 (Figure 6 A) shows the same three reflectors, but echoes below the rough topography (including the mega blocks) are more scattered. The central part of this line displays a similar sequence, with two reflectors (2nd and 3rd reflectors, Figure 6 C) dipping northward at about 3.6 and 3.7 s TWT. The reflectors seem not to mimic the seafloor and correspond with the expected depth interval for the lower slide boundary; thus, they most likely represent the slide base.

According to the reflector's depths of 275 to 305 m below seafloor, the volume of the sedimentary material from the inner slide can be estimated at between 1100 and 1250 km^3. A volume calculation for the outer part of the slide remains more difficult because seismic information on the slide plane is confined to its southern part, close to the shelf rise north of Nordaustlandet. According to seismic lines AWI-99130 and AWI-99165 the reflector that probably represents the slide base, is located between 230 and 240 m below the seafloor. Assuming this thickness is constant throughout the outer area of at least 4750 km^2 results in a volume estimate of about the same size as that for the inner slide (1100 to 1150 km^3). This gives a total of about 2400 km^3 of sediments for the whole Yermak Slide.

Sediments from carefully selected sites along a representative profile across the western margin were recovered for dating of the main slide (Stein, 2005). Initial AMS radiocarbon dates on planktic foraminifera from core PS66/309-1 KAL give ages of 25,390 $\pm$ 220 ^{14}C-years BP directly on top of the slide-related turbidite and 42,340 + 2020 -1610 ^{14}C-years BP below it (Table 1). Bias of the minimum age by dating foraminifera eroded from older strata exposed in the headwall area can be ruled out because the samples were taken well above the last slide (turbidite) related fining upwards sequences, within silty-clayey material. Thus, the maximum and minimum ages for the slide prove a pre-LGM (Late Glacial Maximum), upper Marine Isotope Stage (MIS) 3 date (Figure 5).

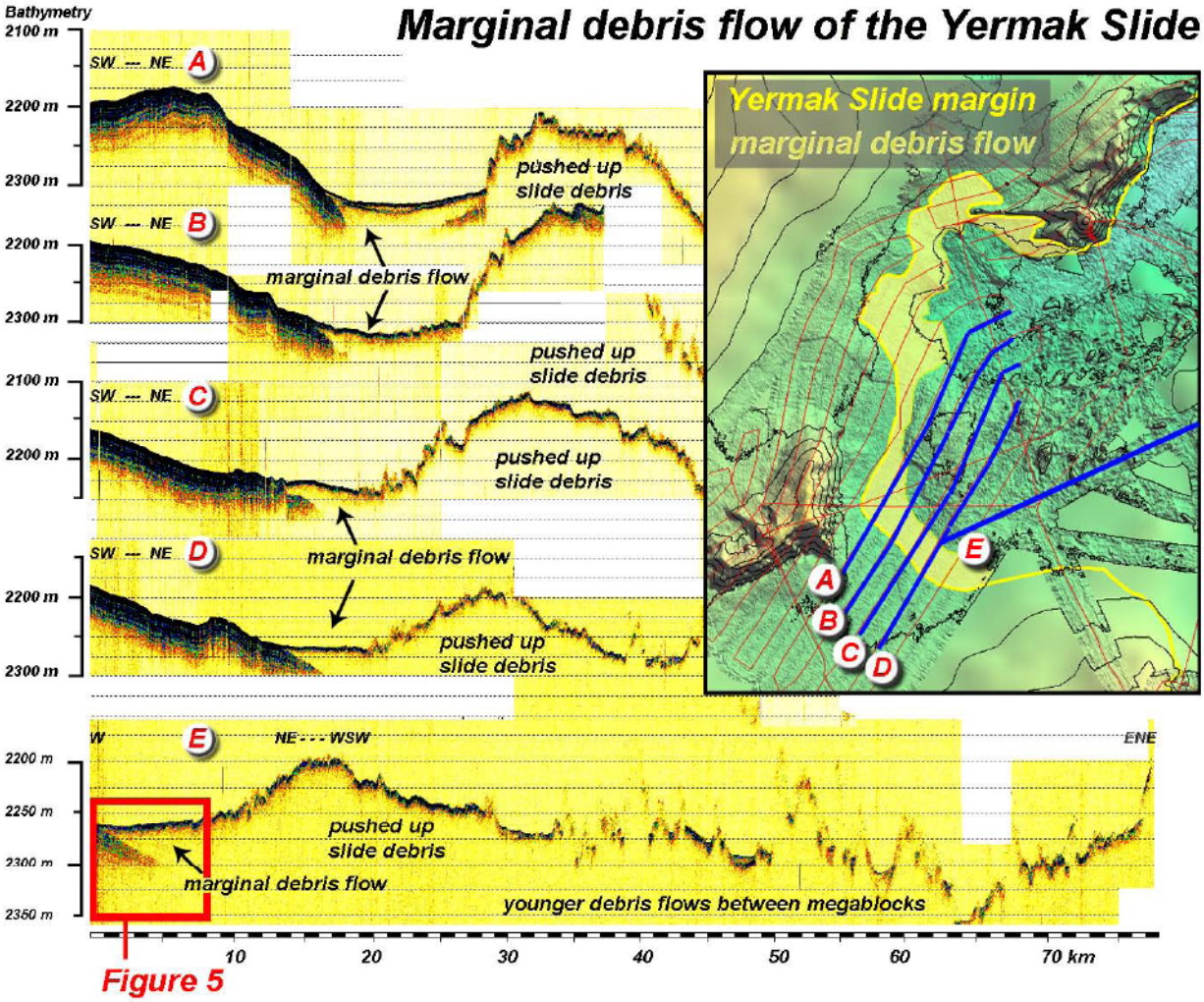

Figure 4: Map of marginal debris flow, with typical PARASOUND profiles across the western margin of the Yermak Slide in the south-western Sophia Basin. Note the consistent transition from pushed-up slide debris into the marginal debris flow in all profiles. Profile A exhibits a semi-allochthonous marginal debris flow with a younger debris flow ontop (for location of map see Figure 1).

Discussion

The physical appearance of the Yermak Slide suggests that one major and catastrophic event occurred on its formation. Failure of the TMF sediments occurred along major lineations, perhaps initiated by an earthquake, leading to a submarine slide which developed into a debris avalanche (according to accepted classification, Canals et al., 2004 and references therein). Tectonic triggering of the main event seems to be the most likely explanation in view of straight and sharp walls formed along major lineations on shelf.

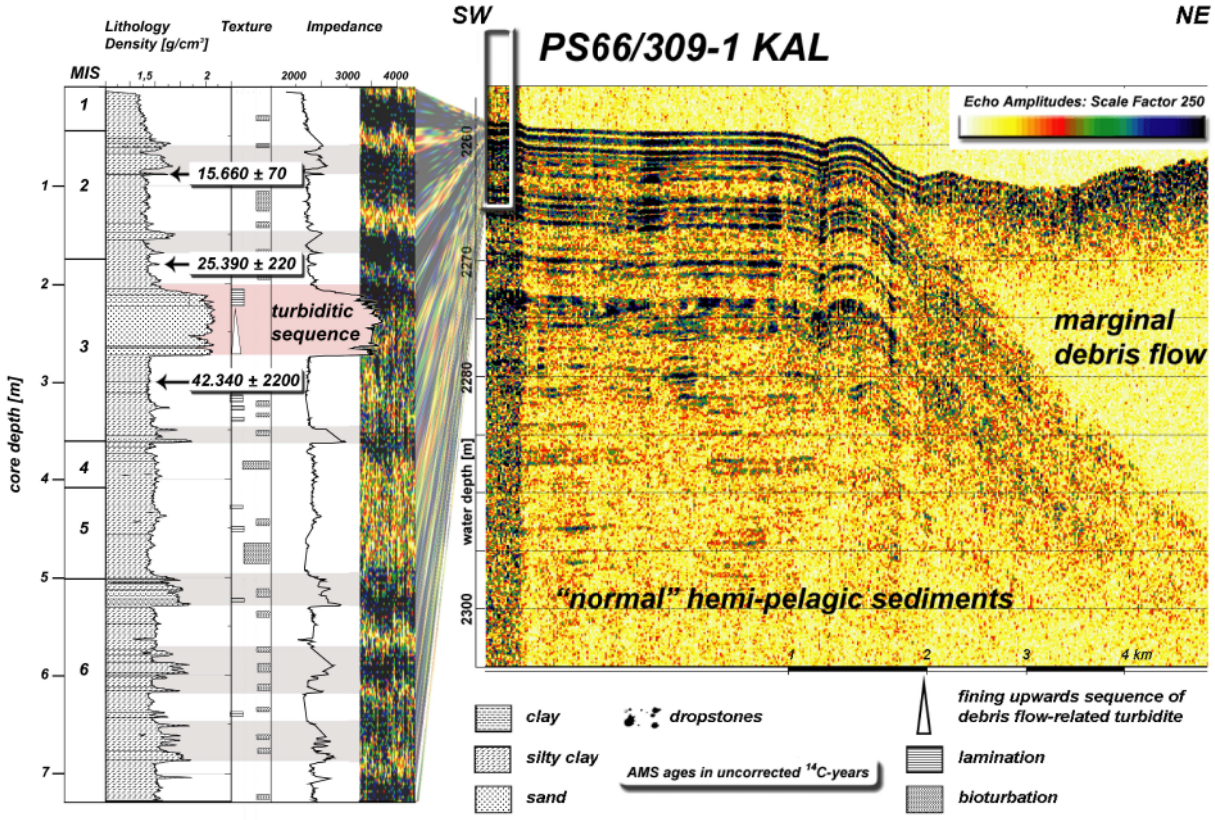

Figure 5: Closeup of PARASOUND data showing marginal debris flow pinching out into hemi-pelagic sediments; position of key core PS66/309-1 KAL (giant gravity corer, 81° 11.22´ N, 12° 59.07´ E, 2270 m water depth, 7,29 m recovery; see Stein 2005 for details) including lithology, density, texture and acoustic impedance of core logging. AMS radiocarbon ages above and below the debris flow-associated turbidite are depicted as 14C years BP, uncorrected for the marine reservoir effect. Marine Isotope Stages (MIS) are based on preliminary correlation of magnetic susceptibility from core logging to cores with existing isotopic stratigraphy. For position of profile and core see Figures 4 and 1 respectively.

The younger slide events that left debris flows on the main slide debris likely correspond to smaller and presumably younger slide scars or escarpments and exhibit a retrogressive character. The scars seem to be related to weak layers or horizons on the shelf (Vanneste et al., in prep.) and may be the consequence of adjusting to a new equilibrium of the physical environment following the main event.

Although volume calculation remains a general problem (Canals et al., 2004), the size of the Yermak Slide at more than 10,000 km^2 affected area and up to 2400 km^3 of involved sedimentary material is comparable to the Storegga Slide (95,000 km^2 and 2400 – 3200 km^3 according to Haflidason et al. 2004). The coincidence of head and sidewalls with major shelf lineations seems however less pronounced in the Storegga Slide than in the Yermak Slide. Some of the typical parameters used to describe landslides exhibit the difference of this Arctic slide to other slides. Although the comparison of submarine

Table 1: Dating results for core PS66/309-1 KAL[a)]

Sample ID	Core depth	^{14}C-age	Corr. ^{14}C-age	calendar age	Dated material
KIA 25699	088 – 091 cm	15660 ± 70	15240 ± 70	16491 ± 237 BP	*N. pachyderma sin.*
KIA 25700	179 – 182 cm	25390 ± 200	24970 ± 200	29928 ± 310 BP	*N. pachyderma sin.*
KIA 27116	299 – 302 cm	42340 ± 2020	41920 ± 2020	45858 ± 1898 BP	*N. pachyderma sin.*

[a]: Water depth 2270 m, recovery 765 cm. AMS radiocarbon dating was on carbonaceous shells of *Neogloboquadrina pachyderma sinestralis* at the Leibniz-Labor for Radiometric Dating and Isotope Research in Kiel, Germany. Conversion to calendar ages was done using the CalPal online software (www.calpal-online.de) with the CalPal2005_SFCP calibration curve. A standard reservoir age of 420 years has been applied for all dates.

landslides is a complicated affair (e.g. Canals et al., 2004) there seems to be a trend towards increasing maximum height of headwalls and major escarpments from river-fed to glacier-fed margins. A second trend towards larger total areas from low to high latitudes on the European shelves might exist too. The BIG´95 Slide in the western Mediterranean Sea constitutes a slide representative of those occurring on river-fed, siliciclastic, progradational continental slopes (Canals et al., 2004). With headwall heights of up to 200 m and ca. 2000 km^2 total area (Lastras et al., 2004), this slide is comparably small.

The headwalls of the Storegga Slide off Mid Norway are up to 120 m high, and the total area accounts for 95,000 km^2 (Haflidason et al., 2004). In contrast the headwalls of the Yermak Slide reach heights of up to 1400 m, more than ten times higher, while the total area, of at least 10,000 km^2, appears to be smaller. Even when excluding the giant turbidite and compressional area of the Storegga Slide, the area of ca. 53,000 km^2 is still five times greater. A possible reason for this difference is the fact that the Yermak Slide developed into the relatively small Sophia Basin, and was forced to funnel out into the Nansen Basin, a process which likely consumed a substantial part of its kinetic energy. A similar scenario defined the changing flow direction of the BIG`95 Slide (Canals et al., 2004). However a cross plot of geometric parameters (run-out distance, headwall height and total area, as well as the ratio of drop or headwall height and run-out distance) show the Yermak Slide to resemble any of of the lobes of the Storegga Slide (Haflidason et al., 2004) (Figure 7). The volume of sedimentary material moved in the Yermak Slide, at about 2400 km^3, is well in the range of the Storegga Slide lobes.

Given the volume of the evacuation area (950 to 1000 km^3) the Yermak Slide seems to have incorporated substantial amounts of sedimentary material on its way. This phenomenon has been reported from several other sites as well (e.g. Gee et al., 1999, 2005; Canals et al. 2004) and may be a common feature of slides involving large detached blocks (Gee et al., 2005). The head walls are situated at the mouth of a cross shelf trough, the Hinløpen Strait, where the usually associated TMF is missing. The unknown volume of

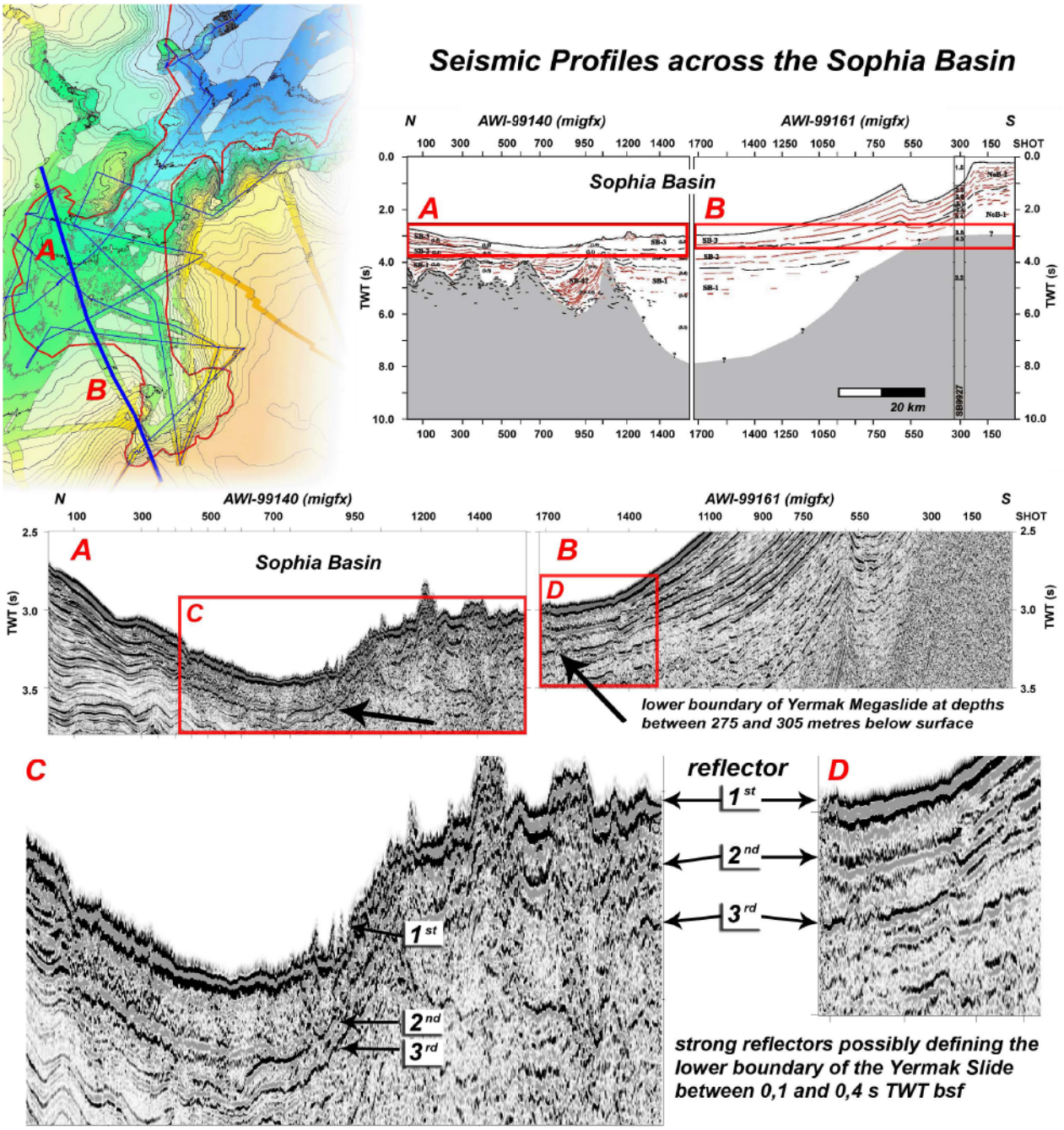

Figure 6: Seismic profiles AWI-99140 and AWI-99161 across the Sophia Basin showing reflectors which most likely represent the lower boundary of the Yermak Megaslide between 275 and 305 metres below seafloor. Modified line drawing from Geissler & Jokat (2004).

the TMF has not been taken into account, but nevertheless, the total volume of the slide (including its entire outer part) would still exceed the volume of the evacuation area.

Considering the removed volume, the megablocks, and the bathymetric appearance of the shelf edge in the area, the main slide event must have involved a substantial part of the shelf proper. Whether these megablocks represent intact parts of the shelf moved from positions close to the headwall, or whether they have been pushed out to the shelf edge by the Hinløpen Ice Stream (Ottesen et al., 2005) and buried within the TMF, as has been reported for the Bear Island TMF (large scale glacio-tectonic features; Andreassen et al., 2004), remains unclear since no information about their full vertical extension nor lithology is available yet. The solid lithology and their physically intact shapes may support the latter suggestion.

The transition from the rather stable shelf north of the Spitsbergen mainland to a shelf with decollements and indications of deformed sediments north of Nordaustlandet, as seen in seismic (Norwegian Petroleum Directorate Survey 1990; Cherkis et al. 1999; Geissler & Jokat, 2004) and acoustic profiles and core material from the shelf (Stein, 2005 and further references therein), is located in the Hinløpen Strait area. This is interpreted as an adjustment following the removal of the TMF. It may also point towards a differing deep structures and tectonic behaviours of the shelf north of Spitsbergen and the shelf edge bordering the Sophia and Nansen Basin north of Nordaustlandet. The decollements may have played a crucial role in preconditioning, at least for the younger events. These often low permeability clayey "weak layers" are supposed to commonly correspond to slip planes beyond the headwalls and their formation, as well as the preconditioning of slides in general, is climatically controlled (Canals et al. 2004). The trigger mechanism for a preconditioned submarine slide is usually assumed to be an earthquake (especially in high latitude margins where post glacial rebound intensifies magnitude) but destabilisation of hydrates has also been suggested (Canals et al. 2004).

The timing of the main slide event in MIS 3 around 30,000 calendar years BP (25,390 $\pm$ 200 ^{14}C years) (Figure 5, Table 1), coincides with the transition of the Kapp Ekholm Interstadial into Glaciation G of Svalbard (Mangerud et al., 1998) and the build-up phase of the Svalbard-Barents Sea Ice Sheet (SBIS). Thus, the TMF collapsed during a period of overall falling sea level, increasing ice volume, and presumably increasing glacio-tectonic activity (Chapell & Shackleton, 1986; Chapell et al., 1996; Svendsen et al., 2004 and references therein). One implication of such a setting is gasification of potential gas-hydrates, due to lowering of the hydrate stability zone (HSZ) as a consequence of lowered pressure. The possibility of post-glacial hydrate dissociation following reduction of shear strength within "weak layers", promoting failure, has been proposed for the Norwegian margin (e.g. Posewang & Mienert; Mienert et al., 2001). In addition, the build-up of the SBIS required a moisture supply, which has been attributed to intervals of inflow of (warmer) Atlantic water into Fram Strait and associated open water

conditions during the LGM (Hebbeln et al., 1994; Nørgaard-Pedersen et al., 2003). A corresponding peak in abundance of foraminifera between 30,000 – 27,000 calendar years BP in the Yermak Plateau region (high productivity zone 2; Dokken and Hald 1996; Hald et al. 2001) points towards such conditions in the slide area. Thus, elevated water temperatures may have contributed to a lowering of the HSZ. A possible relation of hydrate stability and slope failure due to warm water influx onto the headwall region has been modelled and discussed for the Storegga Slide (Mienert et al., 2005). To what extent warmer surface waters influence the stability field of the underlying shelf strata in the Yermak Slide's headwall area is difficult to access since information on the thickness of the (paleo-) warm water layer is not available.

At the present day, the warm and saline Atlantic water west and north of Spitsbergen reaches depths down to ca. 700 m water depth on the shelf and within Sophia Basin (Schlichtholz & Houssais, 1999a, b; Rudels et al., 2000; Saloranta & Haugan, 2004). Given a lowered and steadily falling sea-level, warm surface waters might have had an significant impact on the HSZ and thus slope stability in the headwall area of the Yermak Slide. In addition, investigations of a small area near the Storegga Slide headwall, showed abundant pockmarks and linear depressions probably related to pore water or gas escape, but do not prove a direct connection between extensional features and gas seepage (Parsons et al., 2005). However, we see no indications of either shallow gas, de-gassing features like pockmarks or bottom simulating reflectors (BSRs) in the headwall area of the Yermak Slide. Nevertheless, there are some striking similarities between the Storegga and the Yermak Slides. Both developed on the right flank of a TMF, and their flow paths consequently turned right. Both exhibit a retrogressive character. In both cases, major lineations are present and probably intrinsic to the trigger mechanism. To what extent the probable development of a fore-bulge from increasing load on the lithosphere may have affected the conditioning and/or trigger mechanism north off Svalbard remains difficult to asses, since information on the lithospheric rheology is not available. In addition, the physical behaviour of a shelf corner in response to waxing and waning ice sheets is poorly understood.

Given that the consistent appearance of the slide in the Sophia Basin points towards one main slide event, and the large amount of mass moved in this event, at least one big tsunami can be postulated. Possible tsunami deposits, as have been identified for the Storegga Slide tsunami (e.g. Bondevik et al., 2005), may be expected in the adjacent fjords or on the shelf proper. Whether tsunami deposits will be identified on the Spitsbergen archipelago remains open to question, given that ice coverage close to the archipelago may have hampered the wave propagation. In addition, the potential pre-LGM tsunami deposits on land or on the shelf may not have survived the subsequent glaciation, deglaciation and flooding of the shelf.

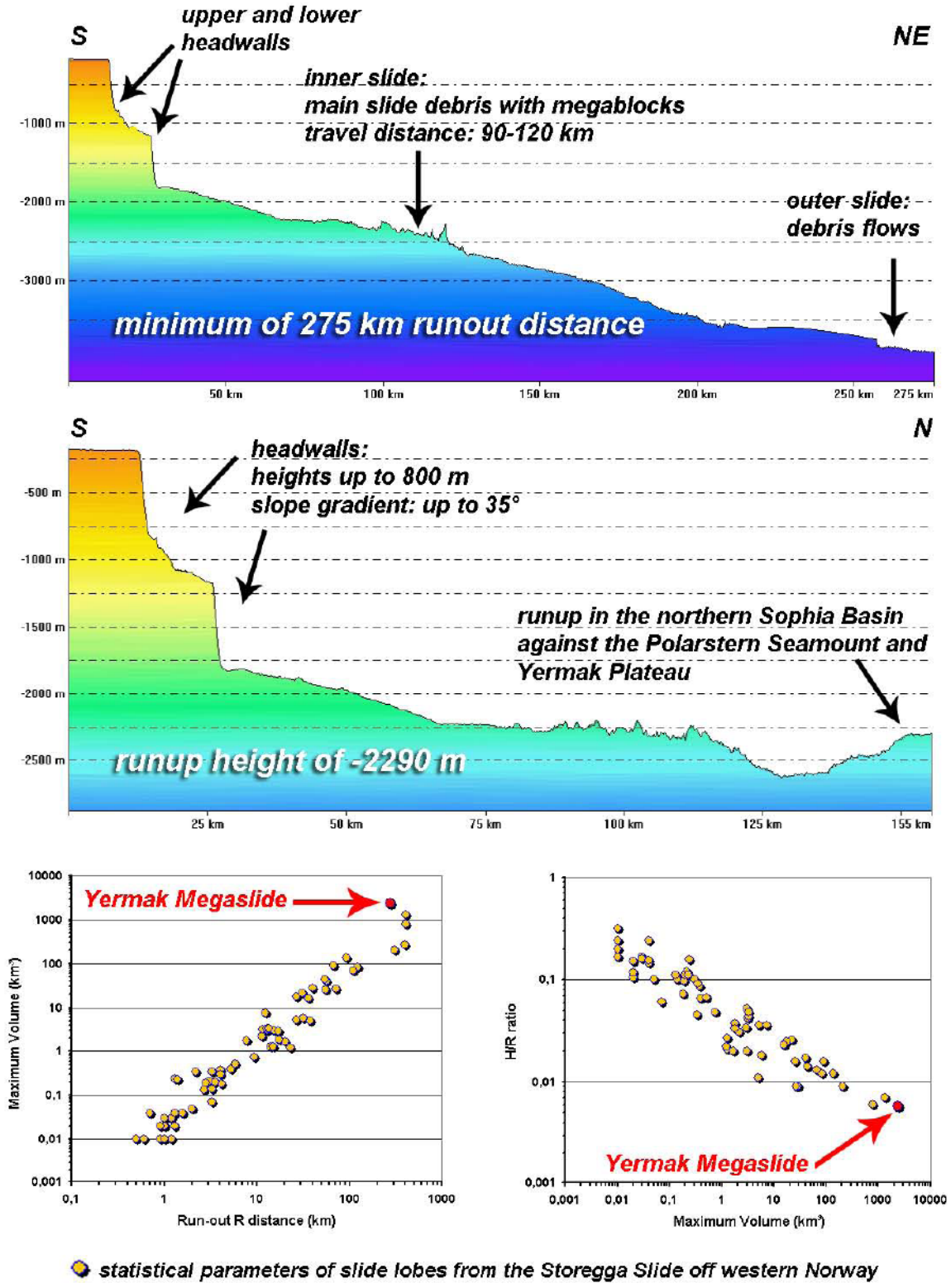

Figure 7: Bathymetric profiles (see Figure 1 for location) and geometrical parameters of the Yermak Megaslide: headwall height, runout distance, transport distance of mega blocks, slope gradients of headwalls, compared to parameters from the Storegga Slide (Haflidason et al. 2004).

Cores taken from carefully selected sites (Stein, 2005) will be used for further characterisation of the slide process concerning preconditioning, trigger mechanisms and timing in relation to the climate history of this Arctic area. Numerical modelling, based on geometrical parameters will shed light on the actual mass movement mechanism in terms of speed and internal dynamics with its further implications for a tsunami model.

Conclusion

- The Yermak Slide extends further west and further into the Nansen Basin than reported by Cherkis et al. (1999). The slide affected an area exceeding 10,000 km^2 and involved more than 2400 km^3 sedimentary material. Thus, it is to be ranked among the largest exposed submarine slides.
- The slide consists at least of one main event, judging by its consistent appearance within the Sophia Basin and towards the Nansen Basin, that occurred during MIS 3. Repeated minor slide events followed this major event.
- The physiographic appearance, together with the character and volume of the involved material (e.g. tens of megablocks), rather points towards a partial shelf collapse than a submarine slide within less consolidated material. This may favour a tectonic preconditioning and triggering mechanism.

Acknowledgements

This study is part of the ESF EUROMARGINS Project Slope Stabilities on Europe's passive continental margins (SPACOMA) and funded by the German Research Foundation (DFG, STE 412/17). We are thankful to the scientific shipboard party and the captain and crew of RV “Polarstern” during ARK-XX/3. We thank Dr. G. Eagles for improvement of the English manuscript.

References

Andreassen, K., Nilssen, L.C., Rafaelsen, B., Kuilman, L.W. (2004): Three-dimensional seismic data from the Barents Sea margin reveal evidence of past ice streams and their dynamics, Geology, 38, 729-732.

Bondevik, S., Løvholt, F., Harbitz, C., Mangerud, J., Dawson, A., Svendsen, J.I. (2005): The Storegga Slide tsunami – comparing field observations with numerical simulations, Marine and Petroleum Geology 22, 195-208.

Canals, M., Lastras, G., Urgeles, R., Casamor, J.L., Mienert, J., Cattaneo, A., de Batist, M., Haflidason, H., Imbo, Y., Laberg, J.S., Locat, J., Long, D., Longva, O., Masson, D.G., Sultan, N., Trincardi, F., Bryn, P. (2004): Slope failure dynamics and impacts from seafloor and shallow sub-seafloor geophysical data: case studies from the COSTA project, Marine Geology 213, 9-72.

Chapell, J. & Shackleton, N.J. (1986): Oxygen isotopes and sea level, Nature 324, 137-140.

Chappell J, Omura, A., Esat, T., McCulloch, M., Pandolfi, J., Ota, Y., Pillans, B. (1996): Reconciliation of late Quaternary sea levels derived from coral terraces at Huon Peninsula with deep sea oxygen isotope records, Earth and Planetary Science Letters 141, 227-236.

Cherkis, N.Z., Max, M.D., Vogt, P.R., Crane, K., Midthassel, A., Sundvor, E. (1999): Large-scale mass wasting on the north Spitsbergen continental margin, Arctic Ocean, Geo-Marine Letters 19, 131-142.

Daschner, S., Hohmann, C., Voß, W. (2000): Hydrosweep DS2 Bathymetry, in The Expedition ARKTIS-XV/2 of "Polarstern" in 1999, Berichte zur Polar- und Meeresforschung 368, edited by W. Jokat, pp. 71-76, Alfred-Wegener-Institut, Bremerhaven.

De Blasio, F. V., L. Engvik, C.B. Harbitz and A. Elverhøi (2004): Hydroplaning and submarine debris flows, Journal of Geophysical Research 109, C01002, doi:10.1029/2002JC001714.

Gee, M.J.R., Gawthorpe, R.L., Friedmann, J.S. (2005): Giant striations at the base of a submarine landslide, Marine Geology 214, 287-294.

Geissler, W.H. & Jokat, W. (2004): A geophysical study of the northern Svalbard continental margin, Geophysical Journal International 158, 50-66.

Haflidason, H., Sejrup, H.P., Nygard, A., Mienert, J., Bryn, P., Lien, R., Forsberg, C.F., Berg, K., Masson, D. (2004): The Storegga Slide: architecture, geometry and slide development, Marine Geology 213, 201-234.

Jakobsson & IBCAO Editorial Board Members (2001): Improvement to the International Bathymetric Chart of the Arctic Ocean (IBCAO): Updating the Data Base and the Grid Model., Eos Trans. AGU 84.

Jokat, W. (Ed.) (2000): The Expedition RKTIS-XV/2 of Polarstern in 1999, Berichte zur Polar- und Meeresforschung 368, 128 pp, Alfred-Wegener-Institut, Bremerhaven.

Lastras, G., Canals, M., Urgeles, R., De Batist, M., Calafat, A.M., Casamor, J.L. (2004): Characterisation of the recent BIG`95 debris flow deposit on the Ebro margin, Western Mediterranean Sea, after a variety of seismic reflection data. Marine Geology 213, 235-255.

Mangerud, J., Dokken, T., Hebbeln, D., Heggen, B., Ingólfsson, Ó., Landvik, J.Y., Mejdahl, V., Svendsen, J.I., Vorren, T.O. (1998): Fluctuations of the Svalbard-Barents Sea ice sheet during the last 150 000 years, Quaternary Science Reviews 17, 11-42.

Mienert, J., Posewang, J., Lukas, D. (2001): Changes in the hydrate stability zone on the Norwegian margin and their consequences for methane and carbon releases into the oceanosphere, in The Northern North Atlantic, edited by P. Schäfer, W. Ritzrau, M. Schlüter and J. Thiede, pp. 259–280, Springer-Verlag, Berlin.

Mienert, J. & Weaver, P.P.E. (Eds.) (2002): European Margin Sediment Dynamics, Side-Scan Sonar and Seismic Images, 309 pp., Springer-Verlag, Berlin.

Mienert, J., Vanneste, M., Bünz, S., Andreassen, K., Haflidason, H., Sejrup, H.P. (2005): Ocean warming and gas hydrate stability on the mid-Norwegian margin at the Storegga slide. Marine and Petroleum Geology 22(1-2), 233-244.

Ottesen, D., Dowdeswell, J.A., Rise, L. (2005): Submarine landforms and the reconstruction of fast flowing ice sheet: The 2500-km-long Norwegian-Svalbard margin (57°-80°N), Geological Society of America Bulletin 117(7/8), 1033-1050.

Parsons, B.S., Vogt, P.R., Haflidason, H., Jung, W.Y. (2005): Sidescan and video exploration of the Storegga slide headwall region by submarine NR-1. Marine Geology 219, 195-205.

Posewang, J. & Mienert, J. (1999): The enigma of double BSRs: indicators for changes in the hydrate stability field. Geo-Marine Letters 19, 157–163.

Rudels, B., Meyer, R., Fahrbach, E., Ivanov, V., Osterhus, S., Quadfasel, D., Schauer, U., Tverberg, V., Woodgate, R.A.(2000): Water mass distribution in Fram Strait and over the Yermak Plateau in summer 1997, Ann. Geophys-Germany 18(6), 687-705.

Saloranta, T. M. & Haugan, P.M. (2004): Northward cooling and freshening of the warm core of the West Spitsbergen Current, Polar Research 23(1), 79–88.

Schlichtholz, P. & Houssais, M.N. (1999): An inverse modeling study in Fram Strait, Part 1: dynamics and circulation, Deep-Sea Research II(46), 1083-1135.

Schlichtholz, P. & Houssais, M.N. (1999): An inverse modeling study in Fram Strait, Part 2: water mass distribution and transports, Deep-Sea Research II(46), 1137-1168.

Stein, R. (Ed.) (2005): Scientific Cruise Report of the Arctic Expedition ARK-XX/3 of RV "Polarstern" in 2004: Fram Strait, Yermak Plateau and East Greenland Continental Margin, Berichte zur Polar- und Meeresforschung 517, 195 pp, Alfred-Wegener-Institut, Bremerhaven.

Svendsen,J. I., H. Alexanderson, V.I. Astakhov, I. Demidov, J.A. Dowdeswell, S. Funder, V. Gataullin, M. Henriksen, C. Hjort, M. Houmark-Nielsen, H.W. Hubberten, Ingólfsson, Ó., Jakobsson, M., Kjær, K.H., Larsen, E., Lokrantz, H., Lunkka, J.P., Lysså, A., Mangerud, J., Matiouchkov, A., Murray, A., Möller, P., Niessen, F., Nikolskaya, O., Polyak, L., Saarnisto, M., Siegert, C., Siegert, M.J., Spielhagen, R.F., Stein, R. (2004): Late Quaternary ice sheet history of northern Eurasia, Quaternary Science Reviews 23, 1229–1271.

Vanneste, M., Bünz, S., Iversen, S., Yang, S. (Eds.) (2004): R/V Jan Mayen Cruise Report, NFR Strategisk Universitets prosjekt (SUP) – Slope Stability, 52 pp., Institutt for Geologi, Universitetet I Tromsö.

Vogt, P.R., Gardner, J., Crane, K. (1999): The Norwegian-Barents-Svalbard (NBS) continental margin: Introducing a natural laboratory of mass wasting, hydrates and ascent of sediment, pore water, and methane, Geo-Marine Letters 19, 2-21.

Vogt, P.R., J. Gardner, J., Crane, K., Sundvor, E., Bowles, F., Cherkashev, G. (1999b): Ground-Truthing 11- to 12-kHz side-scan sonar imagery in the Norwegian-Greenland Sea: Part I: Pockmarks on the Vestnesa Ridge and Storegga slide margin, Geo-Marine Letters 19, 97-110.

Vogt, P.R., Gardner, J., Crane, K., Sundvor, E., Hjelstuen, B.O., Bowles, F., Cherkashev, G. (1999c): Ground-Truthing 11- to 12-kHz side-scan sonar imagery in the Norwegian-Greenland Sea: Part II: Probable diapirs on the Bear Island fan slide valley margins and the Vøring Plateau, Geo-Marine Letters 19, 111-130.

Chapter III

Dynamic and Timing of the Hinlopen/Yermak Megaslide north of Spitsbergen, Arctic Ocean

Dynamic and Timing of the Hinlopen/Yermak Megaslide north of Spitsbergen, Arctic Ocean

D. Winkelmann, W. Geissler, J. Schneider, R. Stein

Alfred Wegener Institute for Polar and Marine Research Bremerhaven, Germany
Submitted for publication in Marine Geology 28th November 2006; under revision.

Abstract

Integrated interpretation of multi-beam bathymetric, sediment-penetrating acoustic (PARASOUND) and seismic data show a multiple slope failure on the northern European continental margin, north of Spitsbergen. The first slide event occurred during MIS 3 around 30 cal. kyr. BP and was characterised by highly dynamic and rapid evacuation of ca. 1.250 km³ of sediment from the lower to the upper part of the shelf slope. During this event, headwalls up to 1600 m have been created and ca. 1150 km³ material from hemi-pelagic sediments and from the lower pre-existing trough mouth fan has been entrained and transported into the semi-enclosed Sophia Basin. This megaslide event was followed by a secondary evacuation of material to the Nansen Basin by funnelling of the debris through the channel between Polarstern Seamount and the adjacent continental slope. The main slide debris is overlain by a set of fining-upwards sequences as evidence for the associated suspension cloud and following minor failure events. Subsequent adjustment of the eastern headwalls led to failure of rather soft sediments and creation of smaller debris flows that followed the main slide surficial topography. Discharge of the Hinlopen ice stream during the Last Glacial Maximum and the following deglaciation draped the central headwalls and created a fan deposit of glacigenic debris flows.

Introduction

With increasing human interest in accessing natural resources on continental margins and growing infrastructure on the shelves, slope stability has become a more and more important issue. Submarine slides (or submarine landslides) play a significant role among the variety of sediment transport processes at continental margins. They are the most prominent and spectacular slope failure events, often associated with tsunamis that have far-reaching socio-economic consequences (e.g. Bondevik et al., 2005).

Slide complexes, especially at the termination of major paleo-ice streams, characterise the Norwegian-Barents-Svalbard passive continental margin (e.g. Vogt et al 1999; Hühnerbach et al., 2004; Evans et al.,

2005). The exposed and buried slides on this margin range from small-scale features to mega-scale events like the Storegga Slide off Norway, which affected some 95,000 km^2 of the seafloor and involved about 2,400 - 3,200 km^3 of sediment (e.g. Vogt et al. 1999; Laberg et al., 2000; Laberg & Vorren, 2000; Mienert & Weaver, 2002 and references therein; Haflidason et al., 2004; 2005). Large slide events have been associated with regular glacial advances to the shelf break during the last 500 kyr. (e.g. Bryn et al., 2003; Nygård et al., 2005; Evans et al., 2005; Sejrup et al., 2005) but also with deglaciation scenarios (e.g. Haflidason et al., 2004, 2005; Laberg & Vorren, 2000; Mienert et al., 2005).

The major slide on the continental slope north of Svalbard has first been described by Cherkis et al. (1999). Its true extent and a first calculation of its volume as well as first indication of its (age around 30 cal. kyr. BP) have been presented by Winkelmann et al. (2006a, b; Figure 1). Vanneste et al. (2006) interpreted seismic and detailed bathymetric data from the headwall area as indication for a retrogressive and multiple slope failure event at the trough mouth. In contrast, Winkelmann et al. (2006) found indication for a single main slide event. In this paper, we present new constraints on timing and evidence for a highly dynamic single catastrophic megaslide event during MIS 3 from acoustic, seismic and sedimentological data. Aside elucidating the dynamics of the slide, an outline of the basin structure of the Sophia Basin is presented as well.

The slide has been referred to as the Yermak Slide, according to its position adjacent to the Yermak Plateau (Winkelmann et al., 2004, 2005, 2006a, b; Vanneste et al., 2005b), as Arctic Slide (Vanneste et al., 2005a), as Hinlopen Slide according to its position at the termination of the Hinløpen Strait cross-shelf trough (Vanneste et al., 2006), or sometimes as Malene Bukta or Malene Slide according to the submarine embayment of its evacuation area (Vogt et al., 1999; Haflidason et al., 2004). In credit of both, source area (Hinlopen cross-shelf trough) and accumulation area (east and south-east of the Yermak Plateau) we propose the term Hinlopen/Yermak Megaslide according to Vanneste et al., (2006) to be applied for the entire megaslide complex.

The Svalbard archipelago was affected by several extensive glaciations including the Weichselian (Mangerud et al., 1998, Svendsen et al., 2004). Our investigation area is situated on and close to the shelf north of Spitsbergen and Nordaustlandet (Figure 1). These two present-day islands are separated by a deep geologic structure that has been exploited by glacial erosion to form a cross shelf trough. This Hinløpen cross-shelf trough hosted an ice stream during glacials, and probably also during Late Glacial Maximum (LGM) (Ottesen et al. 2005). In contrast to other cross-shelf troughs (CSTs), a trough mouth fan (TMF) is missing. The termination of the Hinløpen trough is characterised by a number of submarine embayments and slope escarpments.

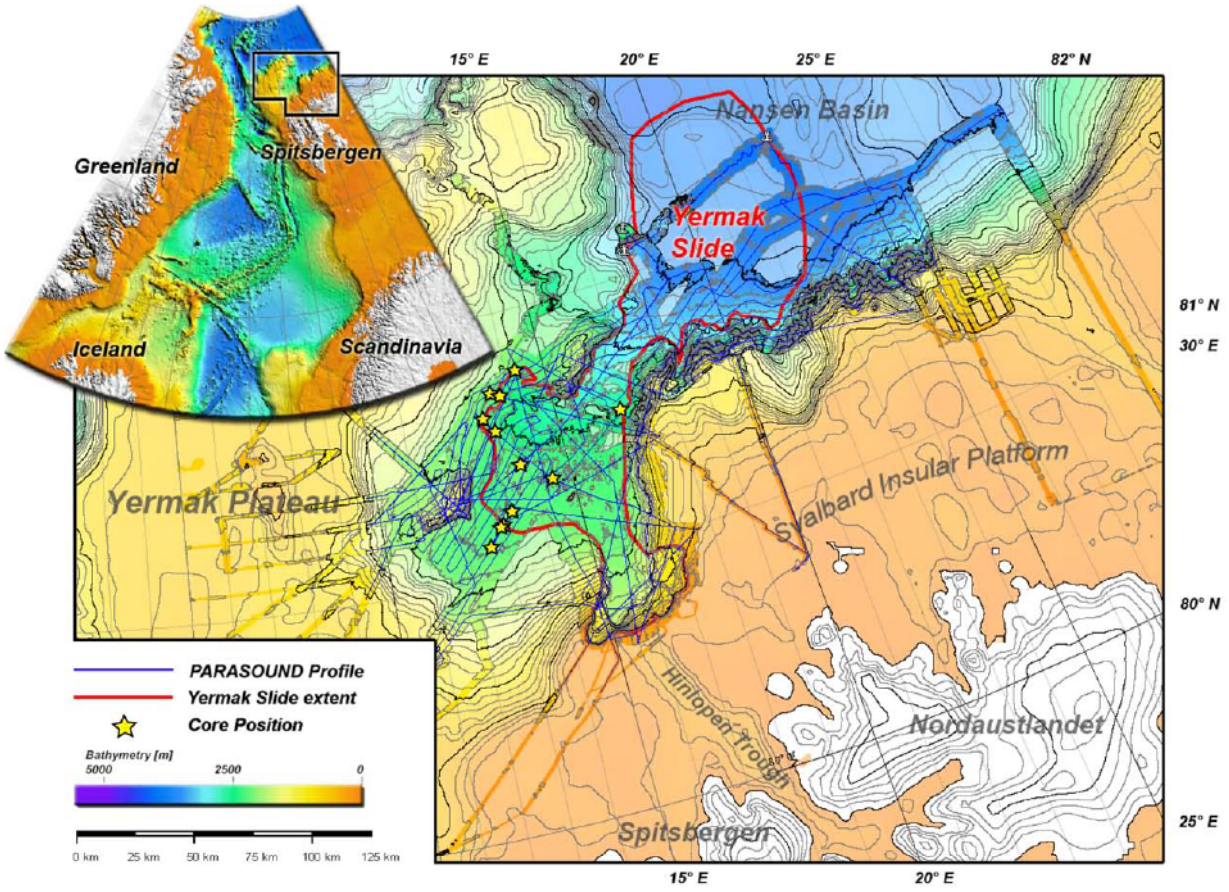

Figure 1: Overview map of the Hinlopen/Yermak Megaslide region (detailed bathymetry on IBCAO) with location of acoustic (PARASOUND) and seismic profiles, core stations and slide extent (headwall data from Vanneste et al., 2006).

Cherkis et al. (1999) first mapped this headwall area and postulated a huge mass-wasting event with large rafted blocks within the Sophia Basin. Vanneste et al. (2004), however, fully mapped the headwall area in greater detail during their cruise. The presented data showing a number of submarine escarpments and headwalls characterising the evacuation area of the Hinlopen/Yermak Megaslide, give evidence for multiple slope failure events (Cherkis et al., 1999; Vanneste et al., 2004).

Material and Methods

Within the ESF EUROMARGINS project slope stability on Europe's passive continental margins (SPACOMA) new surveys of the Hinlopen/Yermak Megaslide area have been carried out. While project partners from the university of Tromsø focused on the headwall area (Vanneste et al., 2006), we concentrated on the more distal, ice-covered part using RV “Polarstern”. Detailed bathymetric data and high-resolution ground-penetrating echo-sounding data were acquired by the HYDROSWEEP DS2 and

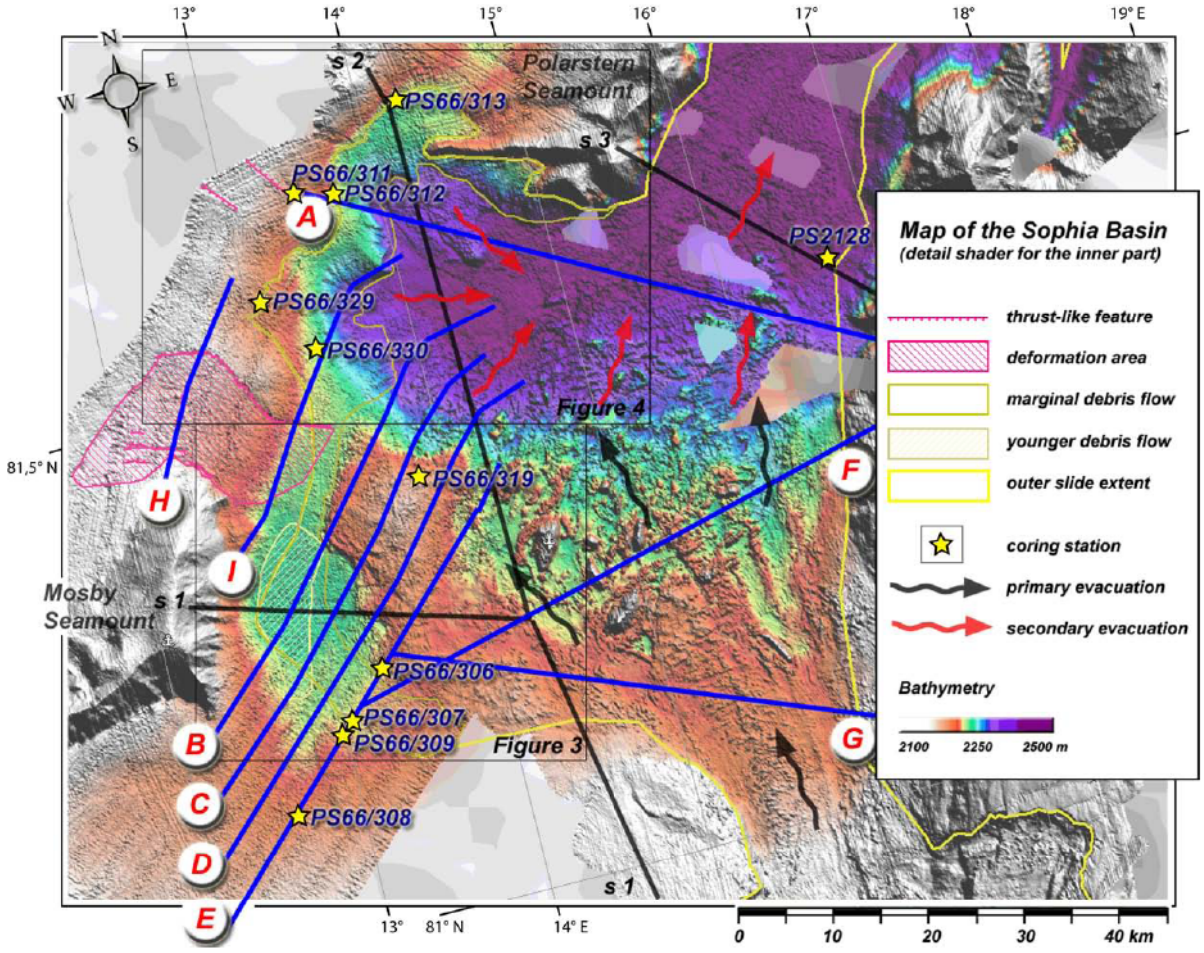

Figure 2: Map of the Sophia Basin (detailed bathymetry on IBCAO; note the detail shader), location of PARASOUND (blue lines) and seismic (black lines) profiles, core stations, slide extent and indication of primary and secondary evacuation directions (arrows), compressional area and younger debris flow.

the PARASOUND Hydromap Control systems, respectively, aboard RV "Polarstern" during cruises ARKXV/2 in 1999 (Jokat, 2000) and ARKXX/3 in 2004 (Stein, 2005). Additional bathymetric data from cruise of RV "Jan Mayen" in 2004 (Vanneste et al., 2004) have been compiled to analyse the area of the Hinlopen/Yermak Megaslide (Figure 1).

Based on high-resolution acoustic (PARASOUND) data, the main slide debris and younger debris flows were fully mapped inside the Sophia Basin, and coring sites were carefully selected along profiles crossing the well developed marginal facies of the mega slide. A total number of 15 gravity cores were taken from key locations (Figures 1 and 2). Two coring attempts were made on the inner slide debris and one pre-existing core opened for integration of information on material properties. Multi-sensor core logging (MSCL) was performed onboard RV "Polarstern" approximately 24 hours after recovery to allow temperature equilibration.

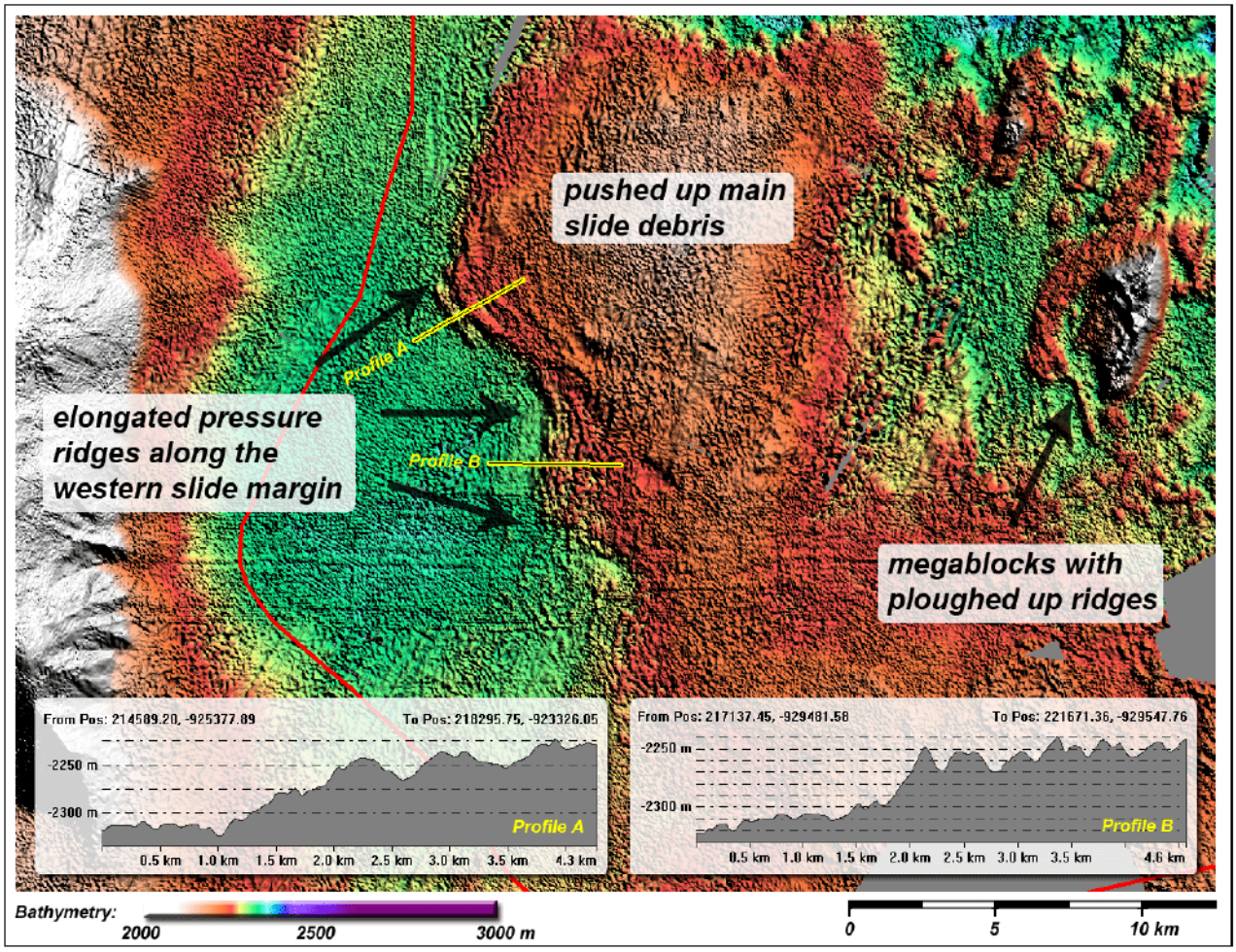

Figure 3: Detailed bathymetry data of the central Sophia Basin showing pushed up main slide debris with elongated pressure ridges along the western slide margin, megablocks with their ploughed up ridges and profiles across the pressure ridges.

AMS radiocarbon dating was performed on carbonaceous shells of *Neogloboquadrina pachyderma sinistralis* at the Leibniz-Laboratory for Radiometric Dating and Isotope Research at the Christian Albrecht University in Kiel, Germany. ^{14}C ages were converted to calendar ages using the CalPal online software (www.calpal-online.de) with the CalPal2005_SFCP calibration curve and a correction for the reservoir effect of 420 years.

Results

A number of PARASOUND profiles across the Hinlopen/Yermak Megaslide region revealed a distinct and typical pattern of the slide which led to a distinction of internal areas. In general the slide can be divided into four broad areas: The headwall area, an inner slide debris area within the Sophia Basin, a transitional

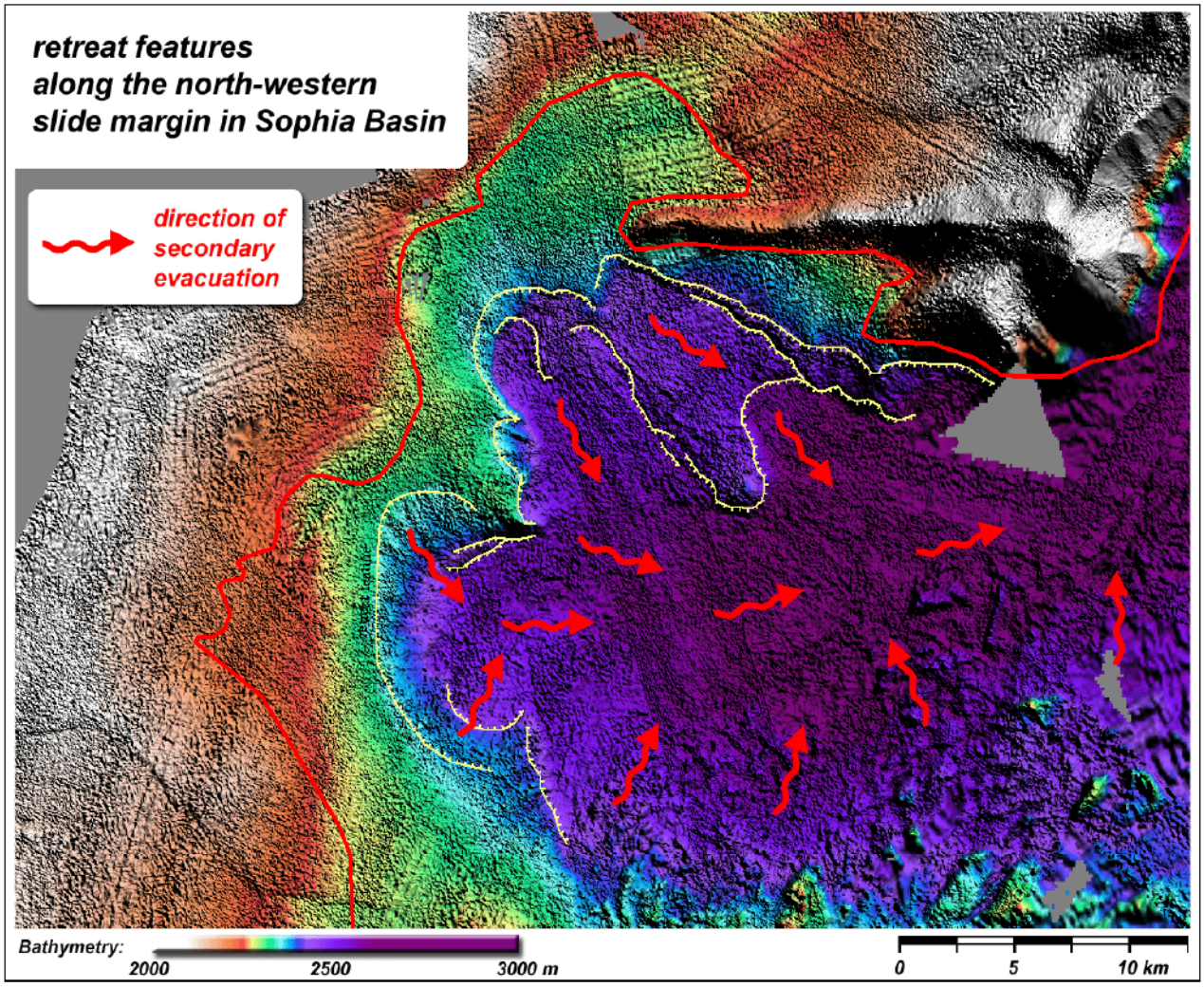

Figure 4: Detailed bathymetry data showing retreat features as escarpments and trim lines close to the north-western slide margin within the Sophia Basin. The red arrows indicate the direction of secondary evacuation.

area between the Polarstern Seamount (Daschner et al., 2000) and adjacent continental slope along the Littke Trough, and an outer debris area neighboring the transitional area and extending towards the Nansen Basin.

The headwall area can be subdivided into a western part west of the Hinlopen (CST), a central part, in front of the Hinlopen CST, and an eastern part, comprising headwalls and escarpments east of the Hinlopen CST (cf. Vanneste et al., 2006).

The inner slide debris area can be subdivided into three different areas: a central part containing a field of megablocks (Winkelmann et al., 2006) with younger debris flows in topographic lows, an area of debris with generally elevated morphology and indication of pushed structures (Figure 3). These structures include a set of elongated ridges running parallel to the western slide margin. Up to 5 parallel or sub-

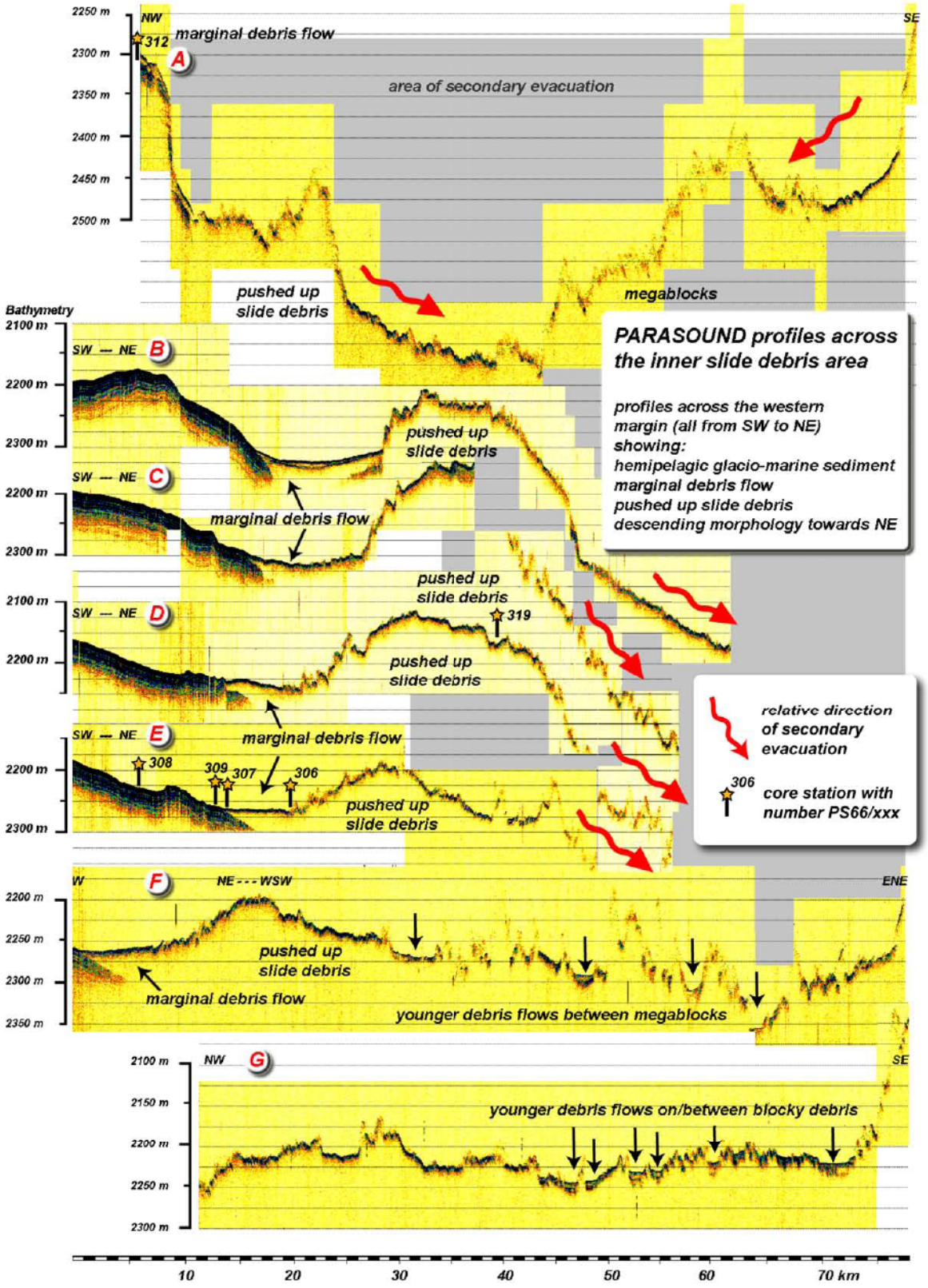

Figure 5: PARASOUND profiles across the inner slide area within the Sophia Basin (see Figure 2 for location). Profiles A-F of the western and northern margin show the marginal debris flow, pushed up slide debris and descending slide surface towards the NE. Note younger debris flows, hummocky slide debris and megablocks in profiles F and G.

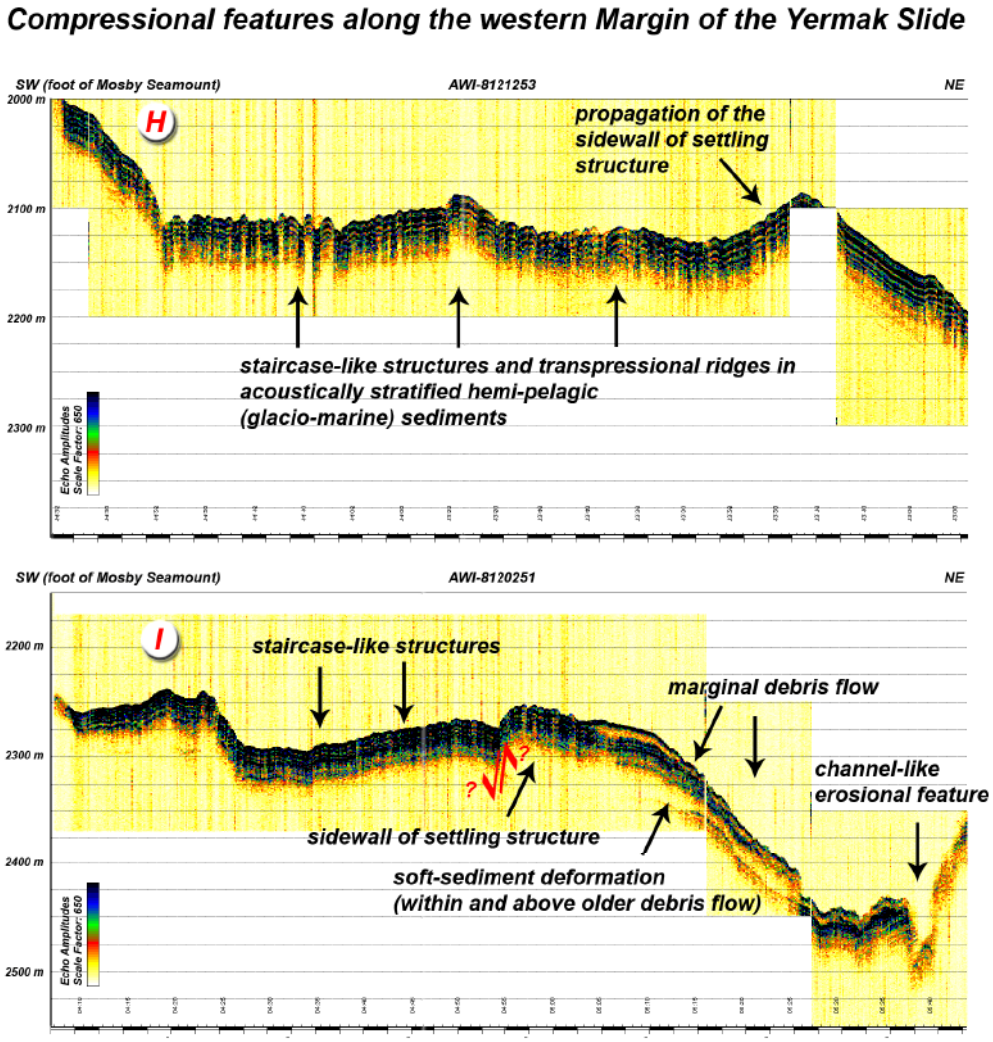

Figure 6: PARASOUND profiles along the western margin of the Hinlopen/Yermak Megaslide and across the compressional area showing staircase-like structures of transpressional ridges, soft sediment deformation and thrust-like features. The staircase-like structures are interpreted as a consequence of settling in combination with evacuation down slope. The reason for this is seen as a remobilisation of an older debris flow (probably pre-MIS 6) due to its overburden of younger sediments. They now creep unequally down-slope and deform the overlaying strata. Note the debris flow-like appearance (acoustically transparent) of deformed sedimentary material and the erosional feature following the secondary evacuation phase of the slide process from the Sophia Basin. For location of profiles see Figure 2.

parallel ridges can be identified at the western margin of the pushed-up main slide debris and are obviously related to the compressional environment in this area. These pressure ridges are typically 200 to 600 m wide and 20 to 30 m high but can reach extensions of up to 40 m height and up to 15 km length. The area further comprises the marginal debris flow, that has been mapped along the south-western, western and northern margin of the slide. We identified an area adjacent to the west of the slide, bordering

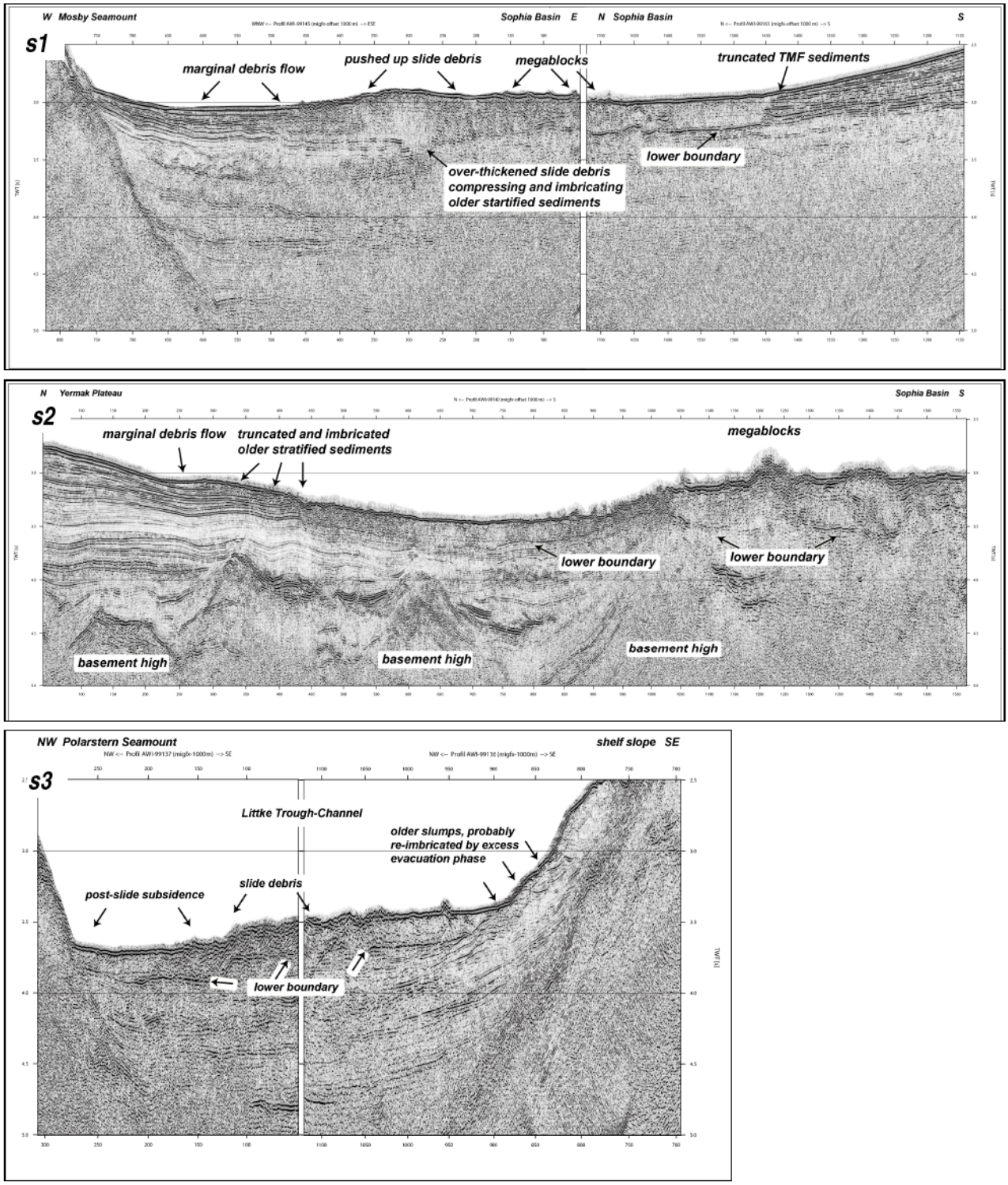

Figure 7: Seismic profiles AWI-99145 and AWI-99161 across the Sophia Basin showing over-thickened slide debris that truncates the TMF-sediments (upper right) and erodes (upper centre), compresses and imbricates (upper centre towards left) the underlying sedimentary strata. Profile AWI-99140 across the Sophia Basin displays lower boundary (middle centre), erosion and imbrication of older sediments (middle left). Profiles AWI-99137 and AWI-99136 across the Littke Trough-Channel display re-imbricated older slumps (lower right), slide debris with lower boundary and indication of post-slide subsidence (lower left). For location of profiles (s1-s3) see Figure 2.

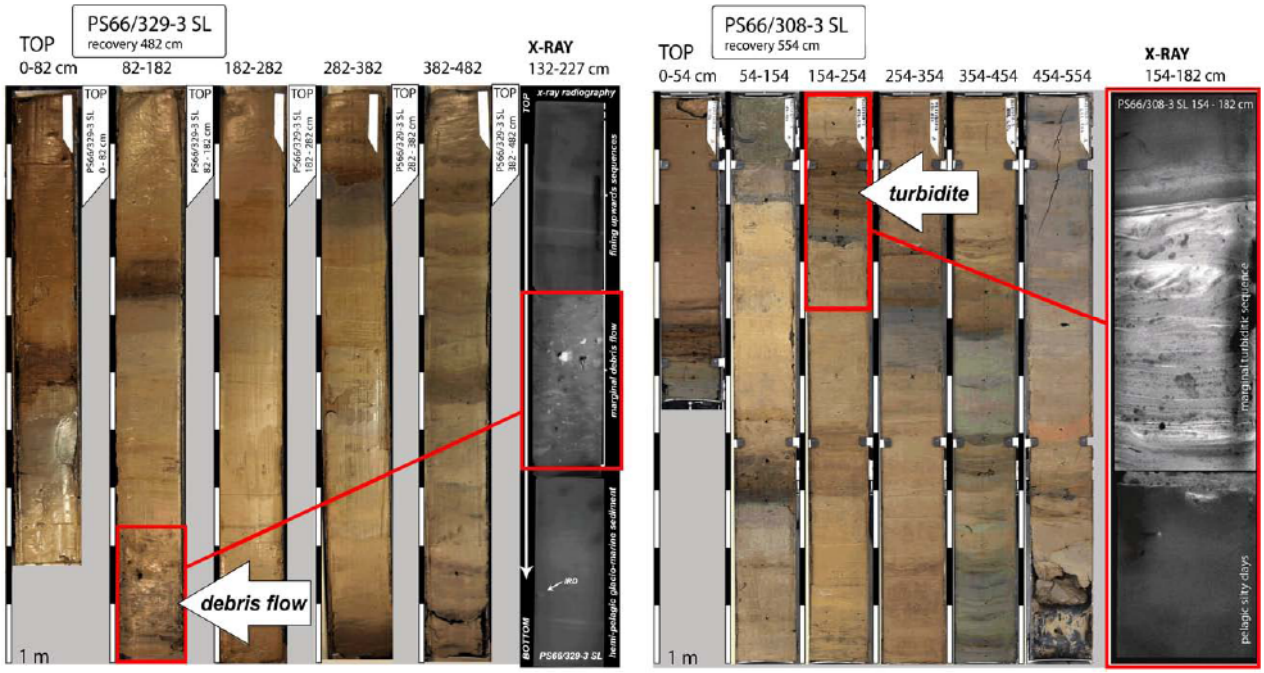

Figure 8: Example of slide related lithology. Left: core sections of core PS66/329-3 SL showing the slide related marginal debris flow between 157 and 180 cm core depth, and x-ray radiographies of the interval 132 - 207 cm core depth shows a the typical debris flow mosaic structure and fining upwards sequences silty clayey material. Right: core sections of core PS66/308-3 SL showing the slide related marginal turbidite between 158 and 180 cm core depth and x-ray radiographs of the interval with a set of sequences starting from gravely coarse sand with erosive base and fining upwards into fine sands and finally silty clays.

the Mosby Seamount to the north and north-east, with compressional features as well as staircase structures. We term it deformational area. This area includes a younger debris flow resting partly on the marginal debris flow which deloped a semi-allochthonous character close to the deformational area (Figure 2, 5B and 6). There is, however, a turbiditic sequence which is related to the marginal debris flow that extend even further SW, but due to the low thickness it is difficult to map based on the PARASOUND data. As seen in cores PS66/308-3 and PS66/309-1 this turbiditic sequence reaches far into the Sophia Basin and thins towards the SW (Figure 2).

The outer slide-debris area and the transitional area have not been further subdivided due to the lack of either different features or data coverage. This area is characterised by up to 275 m thick slide debris with generally more smooth surface. Towards its distal part the debris developed more into common thinner debris flows (Winkelmann et al., 2006a) and presumably into turbidites that may reach far into the Nansen Basin.

A number of acoustic profiles across the western and northern slide margin have been acquired and sampled by gravity cores with the intention to recover hemi-pelagic sediments ontop as well as below the slide-related lithologies. The slide-related lithologies at the slide's margin comprise thick debris flows that

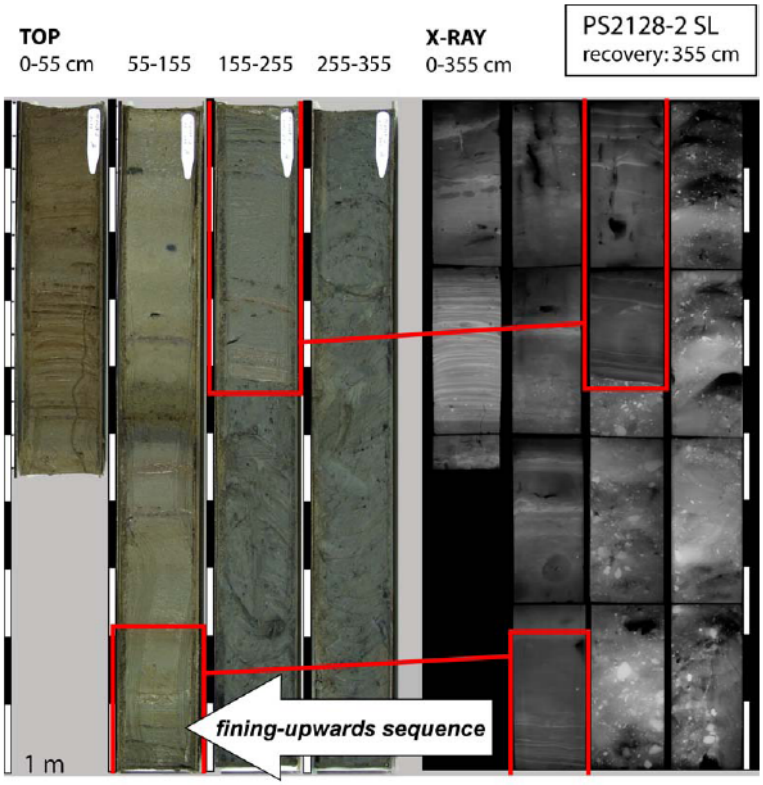

Figure 9: Example of slide related lithology. Left: core sections from core PS2128-2 SL showing the main slide debris (debris flow) with sharp contact to a fining upwards sequence on top. Right: x-ray radiographs of the core showing diamict-like over-consolidated silty sandy clays containing gravel and stones with turbulent structures of the main slide debris below approx. 195 cm core depth and sharp contact to slide related fining upwards, silty-clayey sequences until 136 cm core depth. The AMS radiocarbon date (*N. pachyderma sin.*, 124-125 cm core depth) is given in uncorrected ^{14}C-years BP.

were not cored trough (cores PS66/306, PS66/307, PS66/313), rather thin turbidites (cores PS66/308-2, PS66/309-1, Figure 8) or thin debris flows (e.g. core PS66/329-3) that were successfully cored through. The main slide debris consists of diamict-like over-consolidated stiff clays that are overlain by a series of fining-upwards sequences of silty-clayey sediment (core PS2128-2, Figure 9). Occasionally, younger debris flows overlie these lithological units in topographic depressions. However, debris flow-like deposits with chaotic internal structures, that are probably related to the hummocky slide debris surface (e.g. core PS66/319-1, cf. Stein, 2005), are also observed on top of the main slide debris.

Chronology

The application of acoustic and multi-sensor core-logging data in concert with radiocarbon dating for the spacial and temporal characterisation has been demonstrated elsewhere (e.g. Silva et al., 2004). Based on integrated interpretation of high-resolution acoustic and bathymetric data, a representative profile across

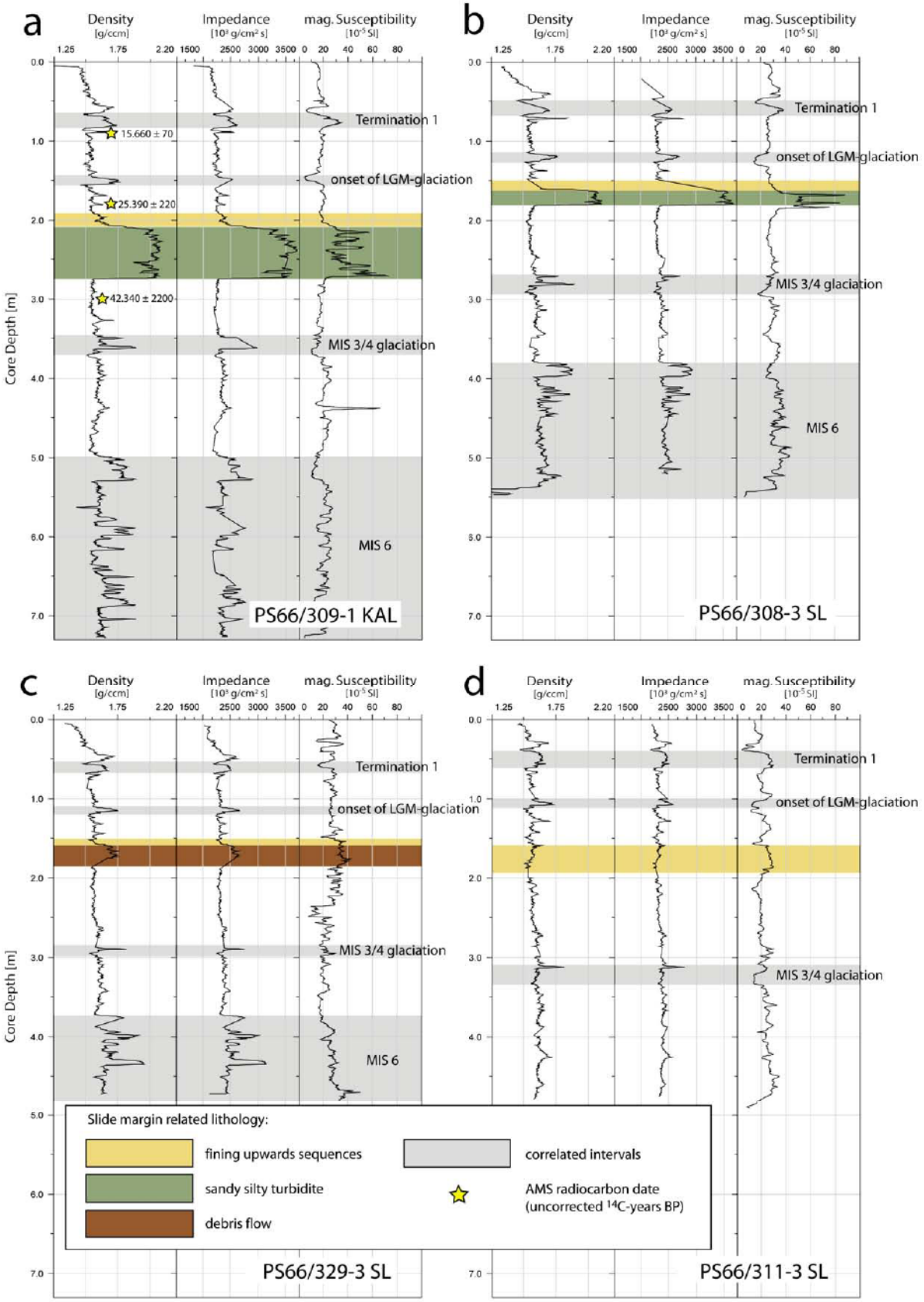
a
Density [g/ccm]
Impedance [10³ g/cm² s]
mag. Susceptibility [10⁻⁵ SI]
Core Depth [m]
15.660 ± 70
25.390 ± 220
42.340 ± 2200
Termination 1
onset of LGM-glaciation
MIS 3/4 glaciation
MIS 6
PS66/309-1 KAL
b
PS66/308-3 SL
c
PS66/329-3 SL
d
PS66/311-3 SL
Slide margin related lithology:
fining upwards sequences
sandy silty turbidite
debris flow
correlated intervals
AMS radiocarbon date (uncorrected ¹⁴C-years BP)

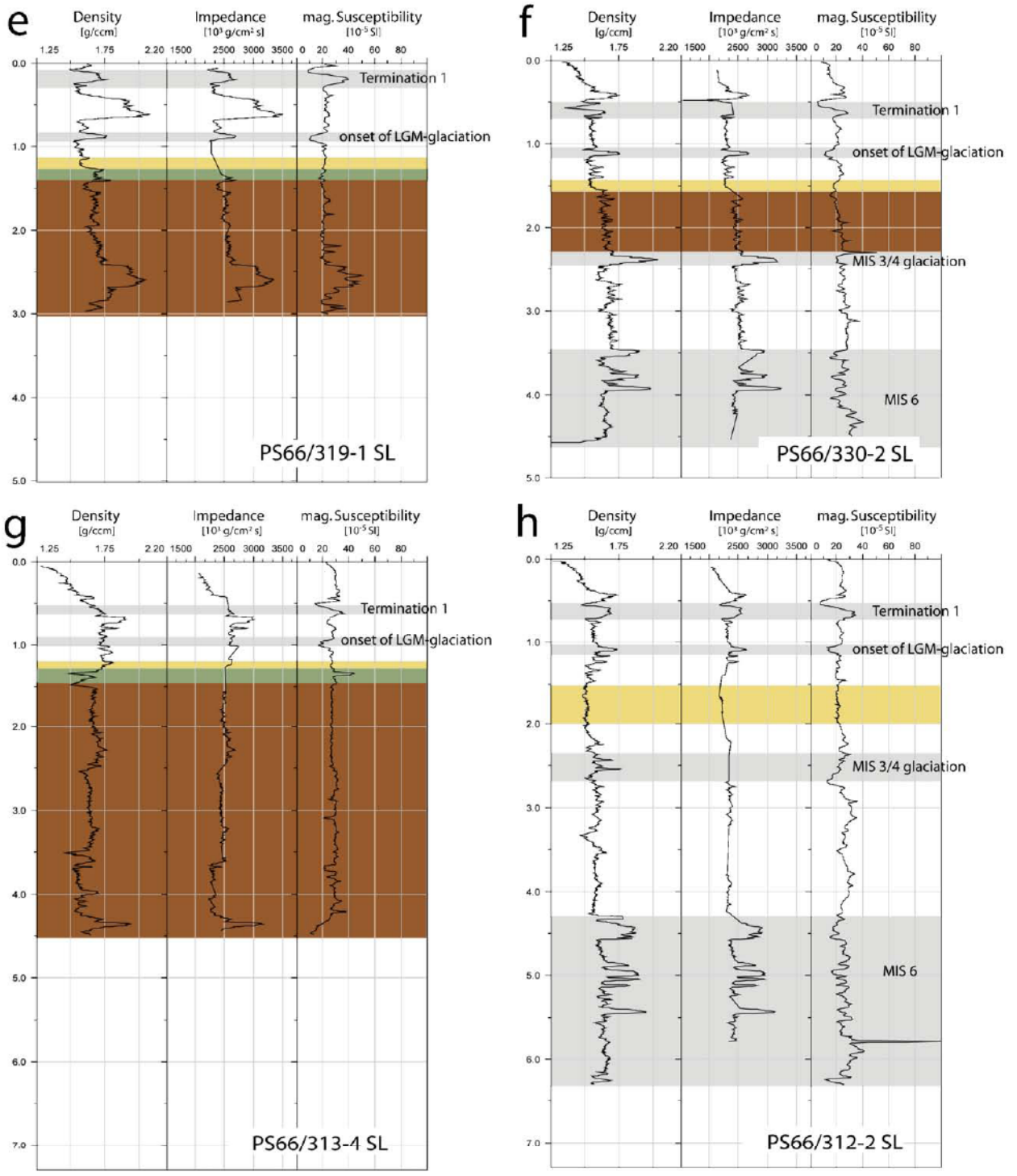

Figure 10: Correlation of cores PS66/308 (b), PS66/309 (a), PS66/311 (d), PS66/312 (h), PS66/313 (g), PS66/319 (e), PS66/329 (c) and PS66/330 (f) based upon multi-sensor core logging data (density, impedance and magnetic susceptibility). Slide related lithologies are indicated as marginal debris flow, turbidite and slity-clayey fining upwards sequences. AMS radiocarbon dates for PS66/309-1 KAL (a) are plotted as uncorrected ^{14}C-years BP.

Table 1: Dating results* for core PS66/309-1 KAL (water depth 2270 m, recovery 765 cm) and PS2128-2 SL (water depth 2528 m, recovery 355 cm; KIA 27117).

Sample ID	Core depth	^{14}C-age BP	Corr. ^{14}C-age BP	calendar age BP	Dated material
KIA 25699	088 – 091 cm	15660 ± 70	15240 ± 70	18491 ± 237	*N. pachyderma sin.*
KIA 25700	179 – 182 cm	25390 ± 200	24970 ± 200	29928 ± 310	*N. pachyderma sin.*
KIA 27116	299 – 302 cm	42340 ± 2020	41920 ± 2020	45858 ± 1898	*N. pachyderma sin.*
KIA 29238	142 – 144 cm	20020 ± 140	18000 ± 140	21527 ± 486	*N. pachyderma sin.*
KIA 27117	124 – 125 cm	24850 ± 220	24430 + 220	29388 ± 466	*N. pachyderma sin.*

*: AMS radiocarbon dating was on carbonaceous shells of *Neogloboquadrina pachyderma sinistralis* at the Leibniz-Laboratory for Radiometric Dating and Isotope Research in Kiel, Germany. Conversion to calendar ages was done using the CalPal online software (www.calpal-online.de) with the CalPal2005_SFCP calibration curve. A standard reservoir age of 420 years has been applied for all dates.

the western margin of the main slide debris within the Sophia Basin has been chosen as a key profile for establishment of a chronology. Cores PS66/308-3 and PS66/309-1 from carefully selected sites along this key profile have successfully penetrated and recovered the marginal turbidite of the main slide debris showing hemi-pelagic glacio-marine sediments beneath and on top of a turbiditic sequence (Figure 8 and 10). Since core PS66/309-1 showed a slightly higher sedimentation rate, this core has been selected as the key core for dating. First dating results point towards a pre-LGM date of this event (Winkelmann et al., 2006a).

The cores of the western and north-western margin within the Sophia Basin can be lithologically correlated showing slide related lithologies in the same stratigraphic position of their upper core sections (Stein, 2005). This relation is also documented in an excellent correlation of multi-sensor core logging data (Figure 10). Thus, a local stratigraphic model was established relating the age model of the key-core (PS66/309-1) to the cores on transects of the western and northern margin within the Sophia Basin (Figure 10).

The result gives evidence for a single megaslide event that created the slide margin within Sophia Basin. This interpretation is supported by correlation of core PS66/319-1 on the main debris and dating results of core PS2128-2 retrieved from the main slide debris close to the eastern margin (Figure 9). Additional support comes from dating of core NP94-20 (Leirdal, 1997) situated on the outer slide debris. The radiocarbon dates of this core are situated slightly further up in the core but gives a similar minimum age for the slide event.

Discussion

Headwall Area – Bottle Neck

The configuration of the headwall area resembles a cauliflower structure with headwalls in two distinct levels (see Cherkis et al., 1999; Vanneste et al., 2006) and with a pronounced bottle neck. More complex headwall configuration and detached sediment ridges characterise the eastern headwall area. This morphological appearance resemble headwall areas of the Traenadjupet Slide or Storegga Slide of Norway (Laberg & Vorren, 2000; Haflidason et al., 2005). The dynamic implication from this physical appearance can be postulated as a retrogressive slope failure that originated somewhere in the bottle neck area and developed further up-slope with retrograding headwalls that cut more and more into the shelf strata while turning their orientation laterally from the original failure centre (towards east and west respectively). A slide model that incorporates excess pore pressure (due to rapid sedimentation during glacials) and strain softening, explains retrogressive sliding even at low inclinations (Kvalstad et al., 2005) and appears applicable for the multiple eastern headwalls.

The geometry and vertical position of the detached sliding slabs can be inferred from the erosion levels (side walls) at the bottle neck. Like trimlines of valley glaciers or ice streams they can be used to reconstruct the upper vertical limit of the moving mass within a morphological negative structure. The erosional level of the side walls lays between 1600 and 1625 m water depth on both sides of the bottle neck. The semi-transparent appearance in seismic data (Vanneste et al., 2006) suggest that either a debris flow or rotated slump blocks characterise this western side wall. If this structure really is a debris flow, the elongated depression in its surface can be interpreted as a plough mark of a sliding block. If true, it would give an idea of the geometry of the sliding mass during failure. Following this interpretation, the plough mark indicates that the sliding material escaped laterally on the slope and turned downwards as soon as the lateral pressure decreased. In case this structure constitutes rotated slump blocks, the actual sidewall would lie further down at around 2000 m water depth. The erosion of sedimentary material at the side wall (unloading/evacuation) would have caused the slumps. Both interpretations are in accordance with the vertical position of the sidewalls further up-slope in the bottle neck.

The seismic structure of the highest western headwalls shows well-stratified sequences, typical for an alternation of glacigenic debris flows and glacio-marine sedimentation (e.g. Laberg & Vorren, 1995; Nygård et al., 2002). In addition, the slope to the north of the western headwalls shows morphology and backscatter of glacigenic debris flow with their flow paths pointing towards the Hinlopen trough mouth (its former position in the central headwall area). Thus, we interpret them as a remnant of the Hinlopen Trough Mouth Fan. Interestingly, these western headwalls show developing canyons as a result of repeated

turbidity current activity. Considering their age of 30 kyr., they appear as very stable in contrast to the eastern headwalls. Slope stability issues have been attributed to this lithological environment due to their different physical properties, as well as to accumulation of free gas or gashydrates (Mienert et al., 2005a, b). We see strong reflectors as well as blanketing within the headwalls and below the glide plane. The glide plane is visible as a strong reflector that can be traced into the neighbouring strata (Figure 7). However, a clear bottom simulating reflector (BSR) does not seem to exist.

Sophia Basin – Inner Slide Debris

The central part of the Sophia Basin is characterised by humocky surface of blocky debris including a field of megablocks, younger debris flows within topographic lows and a marginal debris flow. Like other slides (eg. Gee et al., 2005), the Hinlopen/Yermak Megaslide eroded the underlying and adjacent sediments. Close to its western margin the slide debris formed an area of generally elevated morphology adjacent to the field of megablocks in the central part. It appears that the slide debris was pushed up against the western margin from its central part. The slided debris over-thickened (Figures 5 and 7) and created the elongated pressure ridges in this area (Figure 3) as a consequence of this transpression. The erosion ascended into shallower levels towards the east as the transpression reached the boundary of lateral extent. The underlying strata were therefore compressed and imbricated close to the western margin (Figure 7). Dewatering effects might have contributed to the imbrication due to the higher density of the overlying main slide debris. The transpression appears to be closely related to the establishment of the marginal debris flow which constitutes the western border of the Hinlopen/Yermak Megaslide in the Sophia Basin (Figure 2).

Interpretation of the related turbiditic lithological unit gives a dynamic scenario of the marginal turbidite. The turbidite only occurs along the south-western and northern slide margin within the Sophia Basin and is spatially related to the marginal debris flow. According to the PARASOUND data it developed from the marginal debris flow (Winkelmann et al., 2006a; Figure 5). However, there is only one core (PS66/307-2; Stein, 2005) that recovered both lithological units. In this core, at the lateral termination of the marginal debris flow, the turbiditic sands seem to erode the uppermost parts of the debris flow. Following this geologic evidence, the debris flow must have been in place before the turbidite followed. Because the turbidite occurs at the same core intervals as the marginal debris flows, and since there is no evidence for another source, this turbidite must be related to the sediment processes of the Hinlopen/Yermak Megaslide's margin.

Our interpretation of the related dynamic process puts the marginal debris flow ahead the turbulent suspension cloud that led to the turbidite (Figure 11). The head of the debris flow, presumably

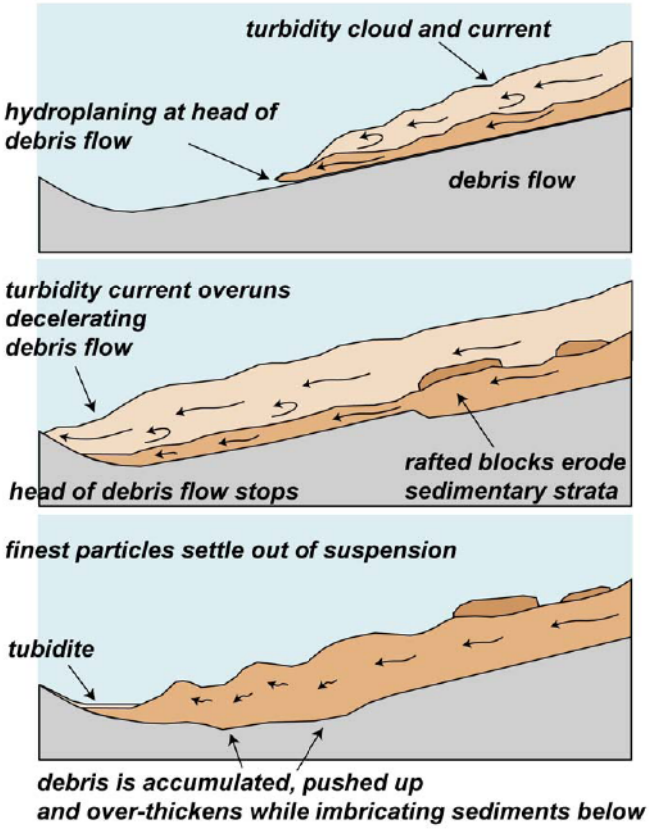

Figure 11: Simplified dynamic model for the genesis of marginal debris flow and the associated turbiditic sequences. In this three-step scenario, the debris flow is faster than the suspension cloud and is overrun by the turbidity currents after it came to a halt. The main slide debris with its rafted blocks erode the underlying strata and over-thickens which leads to imbrication in the sediments beneath. Following the less dynamic conditions, the finer sediment settles out and creates the slide related fining upward sequences. The result of this process corresponds to the interpretation of seismic line AWI-99145 (see Figure 7 s1). Note that motions of the drawing are lateral and accordingly relative (adapted and modified from Ilstad et al., 2004a,b).

characterised by hydroplaning (De Blasio et al., 2004), would be faster than the water-sediment suspension which followed and overruns the marginal debris flow as soon as it comes to a halt. This scenario stands in accordance with laboratory studies of Ilstad et al. (2004a, b). Their debris flow experiments show that the upper surface of the debris flow is being eroded while the head of a the debris flow pushes into the water column down-slope. Due to friction, this (eroded) debris material mixes with the water above and creates the water-sediment suspension of an associated turbidity current. The head of a strongly coherent debris flow would be faster than the suspension cloud (Ilstad et al., 2004a, b). This scenario, however, gives some indication of the original debris composition with a low sand-clay ratio and strongly coherent mass movement. Both assumptions stand in accordance with our core data, showing clays with some gravel, sand and silt within the debris flow deposits, and a dense, consolidated rather diamict-like sediment of the main slide debris (Figures 8 and 9).

The height of pushed up debris coincides with the vertical limit of slide-related debris at the northern slide's margin within the Sophia Basin. The morphology of the inner slide is characterised by a descending surface towards the axis of the Littke Trough leading into the Nansen Basin (Figures 2, 4 and 5). The slide debris on this axis exhibits no essential thinning based on reflector interpretation of seismic lines (AWI-99140; AWI-99137; Geissler & Jokat, 2004; Winkelmann et al., 2006a; Figure 7). It appears as a cover of blocky debris with more or less constant thickness of about 275 - 305 m. Thus, we speculate that tectonic activity repeatedly activated the debris and induced a movement towards the Nansen Basin repeatedly. Whether this process is still operating due to neo-tectonic seismic events remains unclear. Shape of the debris as well as retreat features along the northern and north-western margin of the slide (secondary headwalls or escarpments; Figure 4) indicate that the debris has been evacuated in a secondary phase.

The area with deformational features (Figure 2) borders the Hinlopen/Yermak Megaslide's debris to the west. These features include sediment wave-like stair case structures on a weak plane which is acting as detachment. The imbricated blocks cover an area north/north-east of the Mosby Seamount (Figure 2 and 6). The high-resolution bathymetry data display transpressional ridges almost perpendicular to the slope. These ridges seem to be the result of down-slope evacuation of sedimentary material within confined borders. The younger thin debris flow resting on the marginal debris flow (Figures 2 and 5B) seems to be related to this compressional feature and indicates that the compressional phase must have followed the establishment of the western slide margin. Thrust-like features indicating the start of soft sediment displacement adjacent to the north-east point towards a compression along the western and north-western slide margin (Figures 2 and 6).

A relation of the compressional area to the slide process can not be proofed nor ruled out. However, we speculate that this area is related to a secondary evacuation phase of the slide. The compressional features could have been created during a first emplacement of dense debris, pushing towards the adjacent sediments. The removal of excess debris during a secondary evacuation phase could have triggered a failure of layered hemi-pelagic glacio-marine sediments with subsequent creation of staircase structures, ridges and a generation of a debris flow.

Our interpretation includes the existence of an old debris flow (probably pre-stage 6) that is visible on profile AWI-8120251 (Figure 6I). It appears as has been remobilised and therefore as reason for the settling and evacuation structures within the overlying soft sediments. These old debris flows are common at the shelf slopes of Greenland, Siberia, the Svalbard-Barents margin and on the slope of the Yermak Plateau (Niessen pers. com.). They commonly exhibit higher porosities and due to that a lower density. As

a consequence of overburden from younger sediments, they can be remobilised, creep unequally downslope and deform the overlaying strata. Diapirs, flexures and tension cracks can be attributed to this phenomenon. However, the mobilisation of this old debris flow might stand in close relationship with the emplacement of the Hinlopen/Yermak Megaslide's debris. If true, this interpretation marks an area of ca. 240 km² and ca. 20 - 25 km³ of sedimentary material that is prone to failure. Dating of the younger debris flow will result in a better understanding of the relation between Hinlopen/Yermak Megaslide and this slope failure.

The western shelf slope north of Nordaustlandet (east and north-east of the Hinløpen Lineament) is characterised by weak layers acting as decollements. These horizons can be seen in seismic lines (Cherkis et al. 1999) and the shallower ones in our PARASOUND data (Stein, 2005). An impressive example of this deformation was recovered with the giant gravity core (kastenlot) PS66/327-3 that showed soft sediment deformation including folding of glacio-marine sediments in its lower part (Stein, 2005). The deformation throughout this shelf part has been interpreted as adjustment following the removal of the Hinlopen TMF by the slide process (Winkelmann et al., 2006a).

Dynamic of the Hinlopen/Yermak Megaslide

As a result of core correlation, being in accordance with the PARASOUND data, and our stratigraphic model, we are confident that the western, northern and, presumably, eastern margins of the Hinlopen/Yermak Megaslide within the Sophia Basin have been created during a single event. Additional support for a single main slide event comes from core PS2128-2 at the eastern border of the transitional area. The uncorrected AMS radiocarbon date directly above the slide related sediments gives 24.850 $\pm$ 220 kyr BP, corresponding to 29,388 $\pm$ 466 cal. kyr. BP (Figure 9, Table 1). As a summary of our integrated interpretation, the highly dynamic morphology of the slide as seen in the bathymetric data and in acoustic images (Figures 2-5), supported by geological evidence from our sediment cores and in concert with radiocarbon dating, points towards a single catastrophic main slide event.

A series of 18 small-scale fining upward sequences in core PS2128-2 within silty-clayey material (up to 136 cm core depth, Figure 9) directly above the diamict-like main slide debris shows that the first event was subsequently accompanied by a suspension cloud and followed by a set of minor turbidity currents at this site. The sequence's internal structure points to rhythmic pulses of sediment-loaded bottom waters. We interpret the fining-upwards sequences as last stage of the main slide event when velocities of sediment and water masses decreased and the near bottom water conditions became less dynamic. This

interpretation is supported by a AMS radiocarbon age of 24850 ± 220 ^{14}C-years BP directly on top of the fining-upwards sequence. Thus, their genesis is equal to the turbidite that is associated with the marginal debris flow at the slide's south-western margin.

Based on morphologic evidence a chronology of the slide-related processes can be established as follows:

Phase 1 – Initiation of Megaslide around 30 kyr BP:

A tectonically induced shelf collapse (Winkelmann & Stein, 2007) led to failure of a trough mouth fan and to the submarine slide along major lineations of the continental shelf. The failure started in the area of the bottle neck and developed retrogressive with back-cutting headwalls. The event led to formation of the cauliflower configuration of the headwalls and might have had several stages but in a close time window. The slide ran through the bottle neck into Sophia Basin with high speed and created steep erosional sidewalls. The slide material ran up against Polarstern Seamount and Yermak Plateau.

Phase 2a – primary Evacuation:

Due to funnelling effects out of the Sophia Basin (NE) and ongoing sliding (evacuation from headwalls exceeds evacuation from the Sophia Basin), the main debris was pressed laterally against the side walls. As a consequence, the northern and western margins extended further west, accompanied by over-thickening of the main slide debris, compression and imbrication of underlying older strata, the development of pressure ridges and establishment of the marginal debris flow with its consistent facies. The funnelling creates steep walls and higher erosional levels at the sidewalls within the eastern and north-eastern Sophia Basin. Re-imbrication of an older slump on the shelf slope along the border of the Littke Trough Channel seems to be related to the funnelling.

Phase 2b – deformational Period

The consequent compression of slide debris within the Sophia Basin led to the creation of deformational features along NW margin. A pre-existing older debris flow beneath this escape structure was probably remobilised and evacuated overlying sediments. Associated staircase structures appeared indicating this escape feature, and a related younger debris flow was initiated and emplaced.

Phase 3 – secondary Evacuation:

Evacuation from headwalls was no longer exceeding evacuation from the Sophia Basin resulting in a draw-back of the main debris from the NW margin and from the inner parts leaving the area of pushed-up debris as well as megablocks outstanding. Oriented features along the Littke Trough were established.

This evacuation may have taken longer and could have been motivated by tectonic activity along the Littke Trough. The ploughed-up ridges in front of single megablocks were created following gravitational moving of the blocks.

Phase 4 – post Phase, 30 – ca.18 kyr BP:

After the main event the eastern headwalls started adjusting to their new physical equilibrium resulting in secondary or tertiary escarpments and slumps. Associated debris flows started to run out onto the main slide debris and took place within topographic lows. LGM and deglaciation-related debris fan blanketed the central headwall area. Sedimentation rates were high but comparatively low considering other TMFs. The fan-related turbidity currents and debris flows followed the bathymetric features. The secondary evacuation might still go on as a consequence of seismic activity (e.g. IRIS, 2000) along the Littke Trough. Post-slide subsidence within the northern Sophia Basin and Littke-Trough-Channel probably contributed to this process.

Phase 4b – modern sub recent Phase:

Normal hemipelagic glaciomarine sedimentation was further blanketing the area during late/post glacial conditions and the Holocene. Variations in sedimentation rates results from a concert of oceanic circulation, glacial input and winnowing on the mega-blocks due to higher current speeds. Adjustment of the shelf to the east of the Hinløpen Trough, especially in the eastern part of the headwall area, continued and led to deformational features within soft sediment, tertiary escarpments and ridges of detached sediment.

The unusual geometry of the Hinlopen/Yermak Megaslide with rather thick debris deposits and rather high volume in comparison to its total area, can be attributed to several conditions. The first and probably most important reason seems to be the morphological configuration of the accumulation area. The semi-enclosed Sophia Basin with its narrow channel (Figure 1 and 2), connecting it to the Nansen Basin, constitutes both a first accumulation area and an obstacle that consumes a significant part of kinetic energy of the moving debris. A second reason is more related to the debris rheology. According to our findings of gravity cores taken from the main slide debris, this material consists of over-consolidated clays with high amounts of silt, sand, gravel, stones and probably even boulders. This rather diamict-like material constitutes a rather stiff sediment and might be responsible for shorter run-out distance and minor total area of the slide. A similar relation has been inferred from a collection of submarine landslide data of the North Atlantic (Hühnerbach et al., 2004).

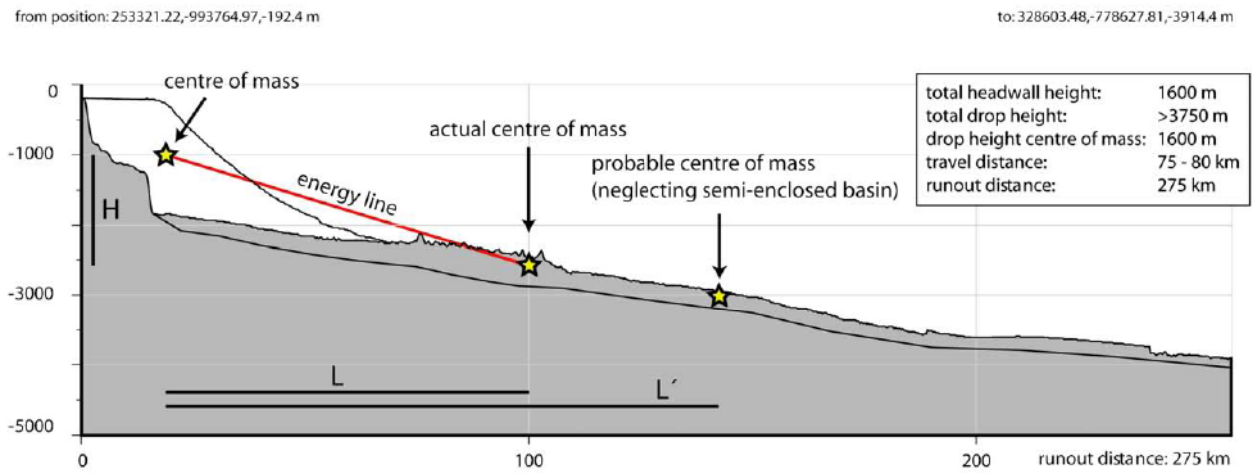

Figure 12: Energy line concept, incorporating the centre of mass of a landslide, applied to the runout profile of the Yermak Slide. Drop height (H) and travel distance (L) are based on the actual most likely centre of mass of the slided debris (area of megablocks) and the assumed shelf geometry. The travel distance for the centre of mass (L´) indicates a possible position of this centre if the slide would have developed into a non enclosed area. Thus L´ is not constrained but remains to be modelled. Note, that the centre of mass from the evacuation area lies further to the shelf since the lateral extent is higher towards the shelf (based on Straub, 1997; modified).

An approach towards the predictability of long runout landslide motion under sub-aerial conditions has been based upon the energy line concept which uses the line (energy line) from the centre of mass within the body of material that is going to slide and the centre of mass of the slided debris (e.g. Straub, 1997 and references therein; Figure 12).

A calculation for kinetic energy for the Hinlopen/Yermak Megaslide appears to be possible considering runout distance (>275 km), run-up height of the slide along the western and northern margin within the Sophia Basin (2290 m bsl.) and total drop height (>3750 m). The field of megablocks, 90 to 120 km away from the headwalls, probably indicates the centre of mass of the slided debris (Figure 12; cf. Straub, 1997 and references therein). Although important parameters (including bathymetry of the area) are established, a fully assessment of the kinetic process of this submarine slide into the semi-enclosed Sophia Basin, however, would require numerical modelling and scaling according to the submarine environment. Following this kinetic model, a reasonable tsunami scenario could be established, which should allow the prediction of areas of potential tsunami deposits on Svalbard and/or on the shelf. Sites for recovery of such deposits might be predicted after an evaluation of both a possible sea ice cover, that may have hampered to some degree the tsunami's wave propagation, and erosion scenarios of warm or cold based ice during the subsequent Late Weichselian Glaciation and termination. Discovery and characterisation of related tsunami deposits contributed significantly to the tsunami model of the Storegga Slide (Bondevik et al., 2005).

Implications for the Tectonic Framework

Based on integrated interpretation of acoustic, morphological and seismic data, a deep structure of the Sophia Basin can be postulated. The overall genetic structure of this morphological deep is a pull-apart basin as a consequence of bi-directional extension along the Littke Trough. The transition from the inner slide debris area to the area most affected by the secondary evacuation can be drawn as a line from 81° 28 ´N, 13° 30´E to 81°22N, 16° 22´E (Figure 13). This line B crosses the northern megablock field and constitutes the north-eastern border of the compressional area, identical with a thrust-like feature within soft sediments close to the western border of the slide. The nature of line B is most likely explained by a basement high that can be identified in seismic profile AWI-99140 (Figures 2 and 7). The corresponding lines A and C to the north and south, respectively, in concert with lines -1 to 6 and lines define areas with tectonically different features (Figure 13).

Lines A-C striking NW-SE define a couple of large-scale features within the Sophia Basin. Line A defines the western ridge of Polarstern Seamount as well as morphological depressions to the west. Line B defines an overall bathymetric step and separates the area of pronounced secondary evacuation from the adjacent southern main debris area. It also defines the lowermost part of the north-eastern soft sediment thrust-like feature of the re-mobilised older debris flow as well as the ridge orientation within this area. Line C defines a flank of the Mosby Seamount, bathymetric depressions to the east and is visible in seismic line AWI-99161 (Geissler & Jokat, 2004, Winkelmann et al., 2006a; Figures 7 and 13). This line played an essential part in defining debris movement of the slide (truncating older TMF-sediments) and thus coincides with the slide's lateral extent close to the headwall area.

The lines -1 to 6 (striking SW-NE) define features along the Littke Trough. Lines 4 to 6 define the lineament in the south-western part of the basin, well in accordance with the bathymetric trough (Figure 1 and 13). A switch to lines 2 to 4 in the north-eastern basin (defining the eastern flank of the Polarstern Seamount and the adjacent shelf) characterise the transformation within the Sophia Basin and constitute a first hint of its pull-apart structure. The transform faults are probably indicated by lines t to z. A first trend towards a transitional character might be visible for line s too.

A set of N-S (or NNE-SSW) striking linear elements (Figure 13) define prominent features like the eastern flank of the Mosby Seamount, bathymetric features in the south-western Sophia Basin as well as some flanks of the Polarstern Seamount. The changing in strike of the northern thrust-like feature within soft-sediments of the remobilised older debris flow seems to be controlled by the same line that defines the eastern flank of Mosby Seamount. To minimize confusion, we do not assign numbers or letters to this set of lines.

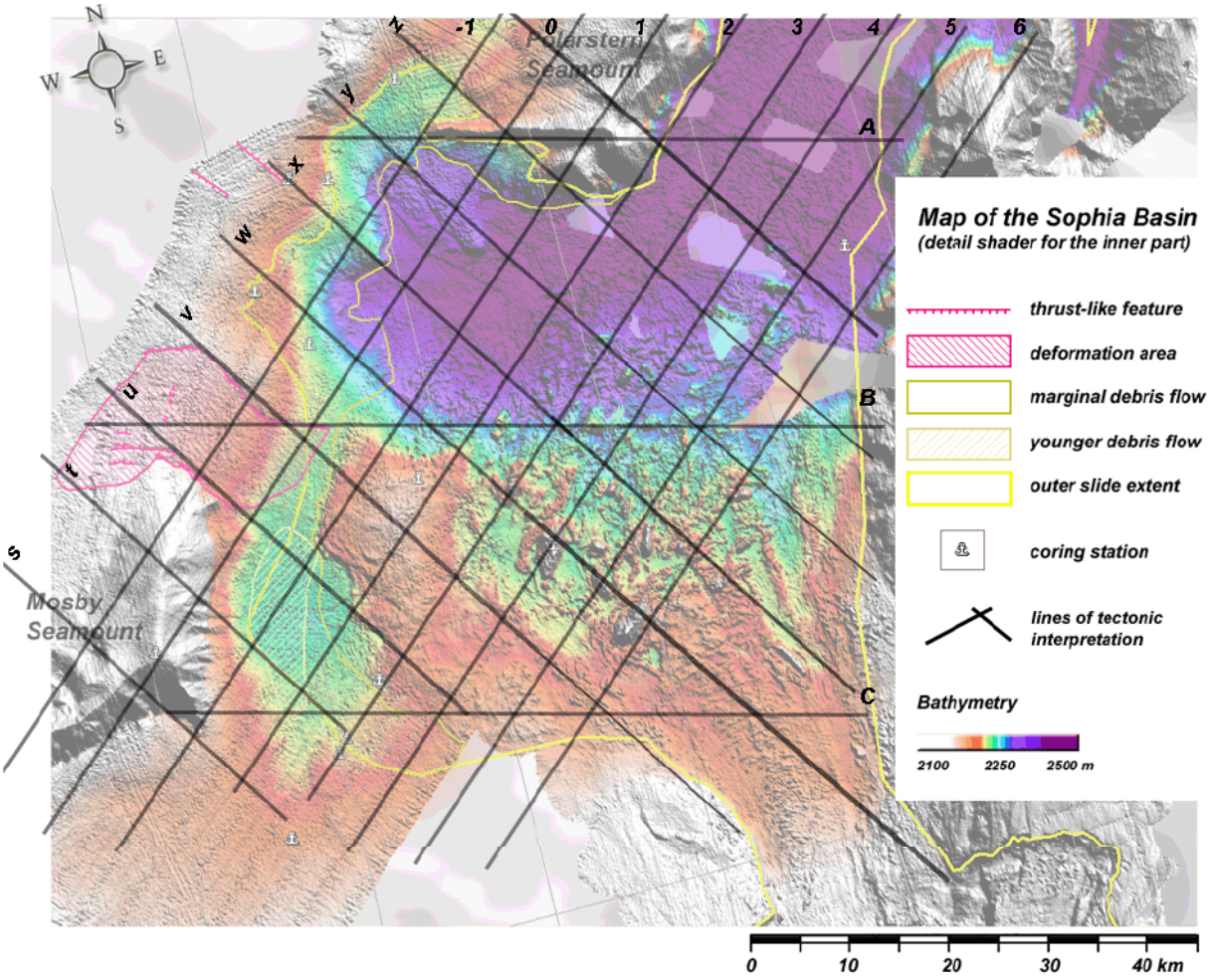

Figure 13: map with lines of tectonic interpretation (see text for explanation). The term line is used to describe a liner element that is morphologically evident and geologically most likely represented as a set of faults striking along this direction.

A tertiary set of linear elements striking WSW-ENE (no numbers/letters and no lines assigned) might be seen in Figure 13. These lines seem to be of minor priority concerning postulated movements in the Sophia Basin, but still define large-scale features like the western flank of Mosby Seamount as well as bathymetric elements along the western slide margin.

As a consequence of the morphological interpretation of the defined elements above, we can postulate their different tectonic behaviour and speculate about their timing and relation to regional tectonics. The Sophia Basin shows subsidence along the Littke Trough but most prominent between lines A to C and -1 to 6 (7). The northern part (defined by lines -1 to 6 and A to B) is characterised by the secondary evacuation and probably affected by more intensive tectonic activity as well as higher subsidence.

Subsidence along the northern Sophia Basin and Littke Trough Channel is evident in seismic profiles AWI-99140 and AWI-99137 (Figure 7), most prominent within the northern part of the Littke Trough Channel (between lines 1 and 2, Figures 7 and 13). Assuming a temporal equilibrated morphology established by the slide debris within the basin as indicated by the more or less very low dipping trim lines, the differences in morphology should indicate evacuation and/or subsidence of the basin. Neglecting evacuation, a loss of 400 m in relief during 30.000 years would account for 1.3 cm of annual subsidence for the northern part of the Sophia Basin. To put this into context with the basin history (initial rifting probably started within chron 24 around 56 Ma ago and modern sediment filling of more than 9 km; Geissler & Jokat, 2004), this calculated subsidence pattern is not in accordance with crustal extension and sedimentary infill. Therefore, a substantial part of the slide debris must have been removed towards the Nansen Basin during the secondary evacuation phase, consistent with the presence of secondary headwalls (Figure 4). The area between the elevated debris and the Mosby Seamount (lines t-u and -1-1) displays indication of subsidence too (see semi-allochthonous marginal debris flow; Figure 5b). However, in concert with neo-tectonic activity the basin appears to be active throughout the last 30 kyr.

With high subsidence, high sedimentation rates and lithologies that include organic carbon-rich sediments, turbidites and sealing slide debris, the Sophia Basin gives an impressive example of a hydrocarbon-generating polar environment.

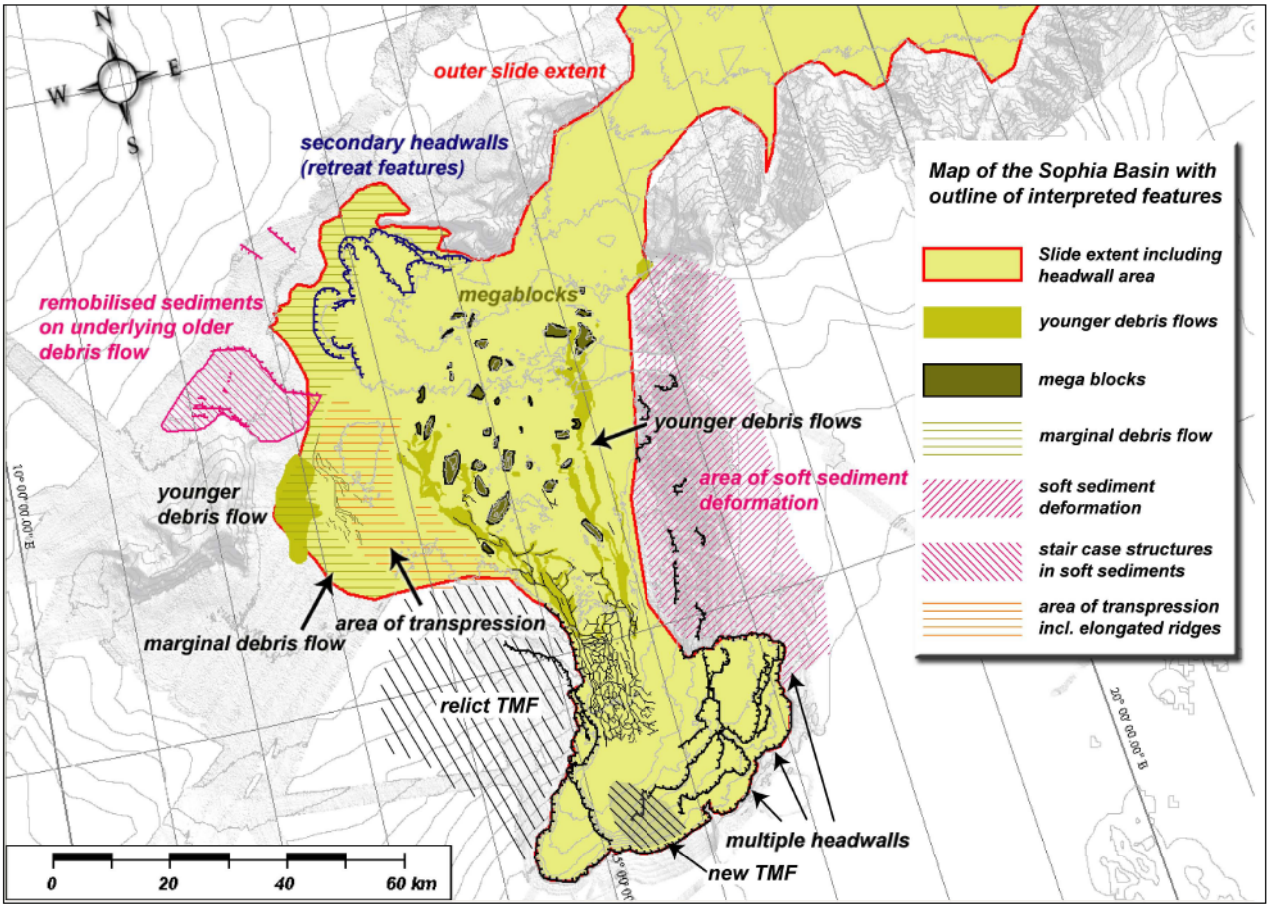

Figure 14: map with outline of interpreted features within Sophia Basin.

Conclusion

- The Hinlopen/Yermak Megaslide is one slide event. The major failure event rapidly evacuated sediment volumes of about 1200 to 1350 km³ into the Sophia Basin. Entrainment of sedimentary material on its way resulted in a total volume of ca. 2.400 km³ and a total affected area of more than 10.000 km².
- The only source region for this megaslide is the termination of the Hinlopen cross shelf trough and its TMF. Minor headwalls in the north-western Sophia Basin are of secondary origin and represent retreat features of a later slide evacuation stages (phase 3). Thus, we can rule out other main failure events from the Yermak Plateau for this megaslide.
- A secondary evacuation phase from Sophia Basin into the Nansen Basin is probably related to tectonic activity and contemporaneous subsidence along the Littke Trough. This process seems to affect parts of Sophia Basin unequally and might not be finished.
- Minor slide events followed the major event as a result of an adjustment to a new morphological

equilibrium. These events are likely represented as the adjusting headwalls and escarpments east of the Hinlopen Lineament and there deposits as younger debris flows on top of the blocky debris within the Sophia Basin. The continental slope east of the lineament adjusts as well to a new equilibrium as a results of the TMF removal.

- Deposits from the Late Weichselian Glaciation and subsequent deglaciation are blanketing the headwalls at the present-day mouth of the Hinlopen cross-shelf trough. Some related small scale debris flows can be traced into the Sophia Basin as well where they overly the hummocky slide debris of the first event and occasionally the older debris flows.
- A quantitative approach of these deposits will shed light on deposition rate and thus erosion rate of the drainage area of the Hinlopen trough. An evaluation of this data should give indication of the possible existence of an ice stream in the Hinlopen CST during the LGM.

Acknowledgement

This study is part of the ESF EUROMARGINS Project Slope Stabilities on Europe's passives continental margins (SPACOMA) and funded by the German Research Foundation (DFG, STE 412/17). We are thankful to scientific shipboard party as well as captain and crew of RV “Polarstern” during ARK-XX/3. We thank M. Vanneste (Tromsø University) for providing the bathymetry data of the headwall area.

References

Bondevik, S., Løvholt, F., Harbitz, C., Mangerud, J., Dawson, A., Svendsen, J.I. (2005): The Storegga Slide tsunami – comparing field observations with numerical simulations, Marine and Petroleum Geology 22, 195-208.

Bryn, P., Solheim, A., Berg, K., Lien, R., Forsberg, C.F., Haflidason, H., Ottesen, D., Rise, L. (2003): The Storegga Slide Complex: repeated large scale sliding in response to climatic cyclicity, in: Locat, J., Mienert, J. (Eds.), Submarine Mass Movements and their Consequences Advances in Natural and Technological Hazards Research, vol. 19. Kluwer Academic Publishers, Dordrecht, pp. 215–222.

Cherkis, N.Z., Max, M.D., Vogt, P.R., Crane, K., Midthassel, A., Sundvor, E. (1999): Large-scale mass wasting on the north Spitsbergen continental margin, Arctic Ocean. Geo-Marine Letters 19, 131-142.

Daschner, S., Hohmann, C., Voß, W. (2000): Hydrosweep DS2 Bathymetry, in Jokat, W. (Ed.) The Expedition ARKTIS-XV/2 of "Polarstern" in 1999, Reports on Polar Research, 368, Alfred Wegener Institute for Polar and Marine Research, Bremerhaven, 128 pp. (2000), 71-76.

De Blasio, F.V., Engvik, L., Harbitz, C.B., Elverhøi, A. (2004): Hydroplaning and submarine debris flows, Journal of Geophysical Research 109, C01002, doi:10.1029/2002JC001714.

Evans, D., Harrison, Z., Shannon, P.M., Laberg, J.S., Nielsen, T., Ayers, S., Holmes, R., Hoult, R.J., Lindberg, B., Haflidason, H., Long, D., Kuijpers, A., Andersen, E.S., Bryn, P. (2005): Palaeoslides and other mass failures of Pliocene to Pleistocene age along the glaciated European margin, Marine and Petroleum Geology 22, 1131–1148.

Gee M.J.R., Gawthorpe, R.L., Friedmann, J.S. (2005): Giant striations at the base of a submarine landslide, Marine Geology 214, 287-294.

Geissler, W.H., & Jokat, W. (2004): A geophysical study of the northern Svalbard continental margin, Geophysical Journal International 158, 50-66, doi: 10.1111/j.1365-246X.2004.02315.x.

Haflidason, H., Sejrup, H.P., Nygard, A., Mienert, J., Bryn, P., Lien, R., Forsberg, C.F., Berg, K., Masson, D. (2004): The Storegga Slide: architecture, geometry and slide development, Marine Geology 213, 201-234.

Haflidason, H., Lien, R., Sejrup, H.P., Forsberg, C.F., Bryn, P. (2005): The dating and morphometry of the Storegga Slide, Marine and Petroleum Geology 22, 123–136.

Hühnerbach, V., Masson, D.G. and partners of the COSTA-project (2004): Landslides in the North Atlantic and its adjacent seas: an analysis of their morphology, setting and behaviour, Marine Geology 213, 343-362.

Ilstad, T., Marr, J.G., Elverhøi, A., Harbitz, C.B. (2004a): Laboratory studies of subaquaeous debris flows by measurements of pore-fluid pressure and total stress, Marine Geology 213, 403-414.

Ilstad, T., Elverhøi, A., Issler, D., Marr, J.G. (2004b): Subaquaeous debris flow behaviour and its dedependence on the sand/clay ratio: a laboratory study using particle tracking, Marine Geology 213, 415-438.

Jakobsson & IBCAO Editorial Board Members (2001): Improvement to the International Bathymetric Chart of the Arctic Ocean (IBCAO): Updating the Data Base and the Grid Model. Eos, Transactions, American Geospysical Union, Vol. 84.

Jokat, W. (Ed.) (2000): The Expedition RKTIS-XV/2 of Polarstern in1999, Reports on Polar Research, 368, Alfred Wegener Institute for Polar and Marine Research, Bremerhaven, 128 pp.

Kvalstad, T.J., Andresen, L., Forsberg, C.F., Berg, K., Bryn, P., Wangen, M. (2005): The Storegga slide: evaluation of triggering sources and slide mechanics, Marine and Petroleum Geology 22, 245–256.

Laberg J.S. & Vorren T.O. (1995): Late Weichselian submarine debris flow deposits on the Bear Island Trough Mouth Fan, Marine Geology 127, 45-72.

Laberg J.S., Vorren T.O., Dowdeswell J.A., Kenyon N.H., Taylor, J. (2000): The Andøya Slide and the Andøya Canyon, north-eastern Norwegian–Greenland Sea, Marine Geology 162, 259–275.

Laberg, J.S. & Vorren T.O. (2000): The Trænadjupet Slide, offshore Norway – morphology, evacuation and triggering mechanisms, Marine Geology 171, 95-114.

Leirdal, G. (1997): Senkvartaer utvikling av kontinentalmarginen nord for Svalbard, M.S. Thesis, 141 pp., Institutt for Geologi, University of Oslo, 1997.

Mangerud, J., Dokken, T., Hebbeln, D., Heggen, B., Ingólfsson, Ó., Landvik, J.Y., Mejdahl, V., Svendsen, J.I., Vorren, T.O. (1998): Fluctuations of the Svalbard-Barents Sea ice sheet during the last 150 000 years, Quaternary Science Reviews 17, 11-42.

Mienert, J. & Weaver, P.P.E. (Eds.), (2002): European Margin Sediment Dynamics, Side-Scan Sonar and Seismic Images. Springer-Verlag, Berlin. 309 pp.

Mienert, J., Bünz, S., Guidard, S., Vanneste, M., Berndt, C. (2005a): Ocean bottom seismometer investigations in the Ormen Lange area offshore mid-Norway provide evidence for shallow gas layers in subsurface sediments, Marine and Petroleum Geology 22, 287–297.

Mienert, J., Vanneste, M., Bünz, S., Andreassen, K., Haflidason, H., Sejrup, H.P. (2005b): Ocean warming and gas hydrate stability on the mid-Norwegian margin at the Storegga Slide, Marine and Petroleum Geology 22, 233–244.

Nygård, A., Sejrup, H.P., Haflidason H., King, E.L. (2002): Geometry and genesis of glacigenic debris flows on the North Sea Fan: TOBI imagery and deep-tow boomer evidence, Marine Geology 188, 15-33.

Nygård, A., Sejrup, H.P., Haflidason, H., Bryn, P. (2005): The glacial North Sea Fan, southern Norwegian Margin: architecture and evolution from the upper continental slope to the deep sea basin, Marine and Petroleum Geology 22, doi: 10.1016/j.marpetgeo.2004.12.001.

Ottesen, D., Dowdeswell, J.A., Rise, L. (2005): Submarine landforms and the reconstruction of fast flowing ice sheet: The 2500-km-long Norwegian-Svalbard margin (57°-80°N), GSA Bulletin 117 (7/8), 1033-1050.

Sejrup, H.P., Hjelstuen, B.O., Dahlgren, K.I.T., Haflidason, H., Kuijpers, A., Nygård, A., Praeg, D., Stoker, M.S., Vorren T.O. (2005): Pleistocene glacial history of the NW European continental margin, Marine and Petroleum Geology 22, 1111–1129.

Silva, A.J., Baxter, C.D.P., LaRosa, P.T., Bryant, W.R. (2004): Investigation of mass wasting on the continental slope and rise, Marine Geology 203, 355-366.

Stein, R. (Ed.) (2005): Scientific Cruise Report of the Arctic Expedition ARK-XX/3 of RV "Polarstern" in 2004: Fram Strait, Yermak Plateau and East Greenland Continental Margin, Reports on Polar and Marine Research, 517, Alfred Wegener Institute for Polar and Marine Research, Bremerhaven, 188 pp.

Straub, S. (1997): Predictability of long runout landslide motion: implications from granular flow mechanics, Geologische Runschau 86, 415-425.

Svendsen, J.I., Alexanderson, H., Astakhov, V.I., Demidov, I., Dowdeswell, J.A., Funder, S., Gataullin, V., Henriksen, M., Hjort, C., Houmark-Nielsen, M., Hubberten, H.W., Ingólfsson, Ó., Jakobsson, M., Kjær, K. H., Larsen, E., Lokrantz, H., Lunkka, J.P., Lyså, A., Mangerud, J., Matiouchkov, A., Murray, A., Möller, P., Niessen, F., Nikolskaya, O., Polyak, L., Saarnisto, M., Siegert, C., Siegert, M.J., Spielhagen, R.F., Stein, R. (2004): Late Quaternary ice sheet history of northern Eurasia, Quaternary Science Reviews 23, 1229–1271.

Vanneste, M., Bünz, S., Iversen, S., Yang., S. (2004): R/V Jan Mayen Cruise Report, NFR Strategisk Universitets prosjekt (SUP) – Slope Stability, Institutt for Geologi, Universitetet I Tromsö, 52 pp.

Vanneste, M., Bünz, S., Mienert, J. (2005a): Multi-phase submarine mega-slide development on the Arctic continental margin north of Svalbard. Edvard Suess session - EUROMARGINS, EGU2005, 24-29 April, Vienna, Austria, Geophysical Research Abstracts 7.

Vanneste, M., Bünz, S., Mienert, J. (2005b): Multi-phase submarine mega-sliding on the Arctic Continental Margin north of Svalbard: characteristics, morphology and volume estimates, NGF Abstracts and Proceedings of the 2nd International Conference “Submarine Mass Movements and Their Consequences”, 5-7 September 2005, Oslo, Norway.

Vanneste, M., Mienert, J., Bünz, S. (2006): The Hinlopen Slide: A giant, submarine slope failure on the northern Svalbard Margin, Arctic Ocean, Earth Planetary Science Letters 245, 373-388.

Vogt, P.R., Gardner, J., Crane, K. (1999): The Norwegian-Barents-Svalbard (NBS) continental margin: Introducing a natural laboratory of mass wasting, hydrates and ascent of sediment, pore water and methane, Geo-Marine Letters 19, 2-21.

Winkelmann, D., Stein, R., Niessen, F. (2004): The Yermak Slide north of Svalbard (Arctic Ocean) - Preliminary Results, 2nd EUROMARGINS Conference, Palau de les Heures, 11-13 Nov., Barcelona, Spain.

Winkelmann, D., Jokat, W., Niessen, F., Stein, R., Winkler, A. (2005): The Yermak Slide - New Constraints on Extent and Age, 22nd International Polar Meeting German Society of Polar Research, 18-24 September 2005, Jena, Germany.

Winkelmann, D., Jokat, W., Niessen, F., Stein, R., Winkler, A. (2006a): Age and extent of the Yermak Slide north of Spitsbergen, Arctic Ocean, Geochemistry Geophysics Geosystem, 7, Q06007, doi:10.1029/2005GC001130.

Winkelmann, D., Jokat, W., Niessen, F., Stein, R., Winkler, A. (2006b): Dynamic and Timing of the Yermak/Hinlopen Slide, Arctic Ocean, European Geosciences Union General Assembly 2006 Vienna, Austria, 02 – 07 April 2006.

Winkelmann, D. & Stein, R. (2007): Triggering of the Hinlopen/Yermak Megaslide in relation to paleoceanography and climate history of the continental margin north of Spitsbergen, Geochemistry, Geophysics, Geosystems 8, Q06018, doi:10.1029/2006GC001485.

Chapter IV

Triggering of the Hinlopen/Yermak Megaslide in relation to paleoceanography and climate history of the continental margin north of Spitsbergen

Triggering of the Hinlopen/Yermak Megaslide in relation to Paleoceanography and Climate History of the continental Margin north of Spitsbergen

Daniel Winkelmann & Ruediger Stein

Alfred Wegener Institute for Polar and Marine Research, Columbusstrasse, Bremerhaven, Germany
Published in Geochemistry, Geophysics, Geosystems, Volume 8, number 6, 29th June 2007, Q06018, doi:10.1029/2006GC001485.

Abstract

On the basis of the detailed sedimentological record of the key-core PS66/309-1 and a review of open literature, we present an assessment to the paleo-environmental conditions as well as trigger mechanism of the Hinlopen/Yermak Megaslide north of Spitsbergen. The Svalbard archipelago is characterised by strong inflow of Atlantic water accompanied by rapidly falling sea-level, rapidly growing Svalbard-Barents Sea-Ice Sheet and associated increasing glacio-tectonic activity during the time window around 30 cal. kyr. PB of this catastrophic failure event. Thus, the potential trigger mechanisms include sediment buoyancy and excess pore pressure, hydrate stability and tectonic/glacio-tectonic processes. While the common scenarios seem to fail to explain this unique submarine megaslide, we focus on glacial processes and their consequences for the regional tectonic framework. We conclude that the Hinlopen/Yermak Megaslide has been the consequence of the rapid onset of Late Weichselian glaciation resulting in a drastic sea-level drop, asymmetrical ice loading and a forebulge development leading to enhanced tectonic movements along the Hinlopen fault zone. As the final trigger we assume a strong earthquake positioned below or close to the SE-Sophia Basin.

Introduction

Causes of submarine slides and factors that control slide frequencies remain poorly understood despite the fact that submarine slides represent a hazard to seafloor structures and are able to generate tsunamis with far-reaching consequences (e.g. Baptista et al., 1998; Bondevik et al., 1997, 2005; Garcia et al., 2003). On the European glacially influenced continental margins, slide frequency has been related to repeated ice sheet advances to the shelf (Haflidason et al., 2005) implying a lithologic and thus climate-dependant control. Theories that tried to associate submarine slides to sea level changes range from falling to rising sea level scenarios (e.g. McMurtry et al., 2004, Mienert et al., 2005b; Haflidason et al., 2005), from high stand to low stand sea level. This paper deals with a major submarine slide that occurred on the continental slope north of Svalbard first described by Cherkis et al. (1999). To give credit to the source area (Hinlopen Trough and Trough Mouth Fan) and the deposition area of the megaslide (east and

southeast of the Yermak Plateau) (see below), we propose to name it "Hinlopen/Yermak Megaslide". Based on the description of Winkelmann et al. (2004, 2006a) (Figure 1), this slide can be classified as a megaslide and it represents an end-member concerning geometrical parameters like headwall heights, volume, size and geometry of slided blocks. In this paper we present new constraints on environmental and paleoceanographic conditions of this area with focus on the most likely environmental conditions that favoured the triggering of the highly dynamic catastrophic first slide event of the Hinlopen/Yermak Megaslide.

Modern oceanographic Setting

The modern surface water circulation pattern around Spitsbergen is characterised by the northward flowing West Spitsbergen Current (WSC). It transports warm and saline Atlantic water into the Arctic Ocean via Fram Strait where it branches into the North Svalbard Current (NSC) flushing the shelf of NW- and N-Spitsbergen, the Yermak Plateau Current (YPC) and the Yermak Slope Current (YSC) that follows the bathymetric contours of the submarine plateau into the Arctic Ocean (Schlichtholz & Houssais, 1999a, b). East Greenland Current (EGC), as counterpart to the WSC, transports colder and less saline Arctic water into the Greenland Sea (Figure 1).

Glacial History of the Study Area

The Svalbard archipelago with its main islands Spitsbergen and Nordaustlandet was repeatedly affected by major glaciations during the Weichselian (Mangerud et al., 1998, Svendsen et al., 2004). Extent and character of these glaciations have been extensively studied and summarised within the QUEEN (Quaternary Environments of the Eurasian North) project (e.g. Svendsen et al., 2004 and further references therein). The Hinlopen/Yermak Megaslide headwall is situated on the continental shelf between Spitsbergen and Nordaustlandet islands which are separated by a deeply routed fault zone along which persistent glacial erosion has formed a cross-shelf trough. This Hinløpen cross shelf trough hosted an ice stream during glacial times, and probably also during the Last Glacial Maximum (LGM) (Ottesen et al. 2005). In contrast to other cross shelf troughs, the termination of the Hinløpen trough is characterised by a number of submarine slide headwalls that form the Hinlopen/Yermak Megaslide (Cherkis et al., 1999, Vanneste et al., 2004, 2006; Winkelmann et al., 2006a, b) rather than a Trough Mouth Fan (TMF).

Material and Methods

Detailed bathymetric data and high-resolution ground-penetrating echo sounding data were acquired by the HYDROSWEEP DS2 and the PARASOUND Hydromap Control systems, respectively, aboard RV

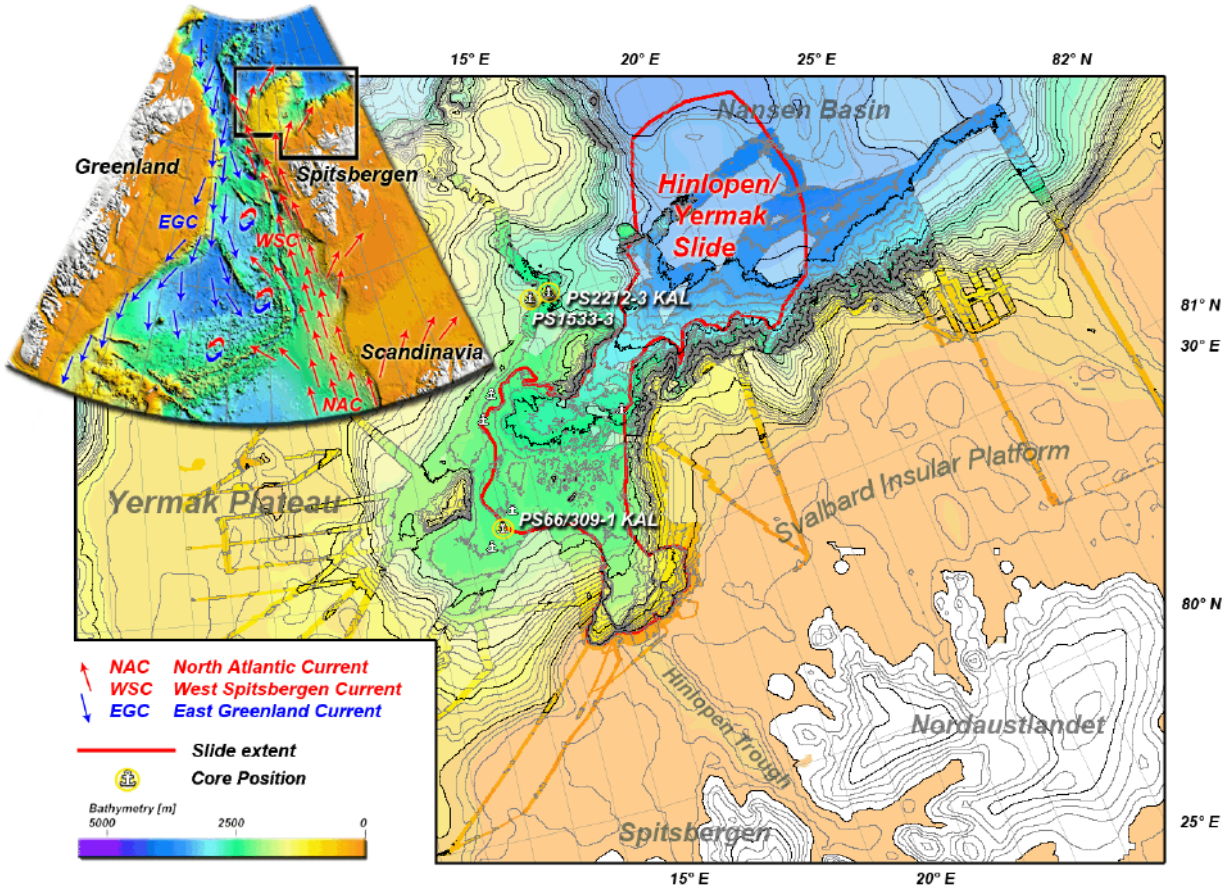

Figure 1: overview map of the Spitsbergen area with (modern) oceanic circulation, ice sheet extent during Saalian and Weichselian Glaciations, LGM (according to Landvik et al 1998; Svendsen et al., 2004) and Ice streams (according to Ottesen et al 2005), location of cores and extent of the Hinlopen/Yermak Megaslide (according to Winkelmann et al., 2006a, b). Bathymetry: high-resolution Swath-bathymetry (Winkelmann et al., 2006a; Vanneste et al., 2006) on IBCAO (Jakobsson et al., 2001).

"Polarstern" during cruise ARKXX/3 (Stein, 2005). Additional data were collected during cruises ARKXV/2 of RV "Polarstern" (Jokat, 2000) and RV "Jan Mayen" (Vanneste et al., 2004; 2006). Preliminary data compilation on the structure of the Hinlopen/Yermak Megaslide were performed by Winkelmann et al. (2006a, b). Based on the PARASOUND record, coring sites were selected along a representative key-profile crossing the well developed marginal facies of the mega slide during cruise ARKXX/3 (Stein, 2005; Winkelmann et al., 2006a). Multi-sensor core logging, core description, x-ray radiography and standard geological sampling were performed aboard RV Polarstern (Stein, 2005). Core PS66/309-1 KAL was sampled continuously at 2-3 cm intervals for stable isotope analysis of *N. pachyderma (sin.)* Stable oxygen and carbon isotopes were measured by standard techniques (Duplessy, 1978) on the automated Carbo-Kiel device connected to a Finnigan MAT 251 mass spectrometer. The external analytical reproducibility is 0.08‰ and 0.04‰ for $\partial^{18}O$ and $\partial^{13}C$, respectively. Total organic carbon and total nitrogen were determined by means of a LECO CNS analyser (Schäfer, 2005).

Table 1: Dating results for core PS66/309-1 KAL (water depth 2270 m, recovery 765 cm).*

Sample ID	Core depth	^{14}C-age BP	Corr. ^{14}C-age BP	calendar age BP	Dated material
KIA 25699	088 – 091 cm	15660 ± 70	15240 ± 70	18541 ± 237	*N. pachyderma sin.*
KIA 29238	142 – 144 cm	20020 ± 140	19600 ± 140	23379 ± 394	*N. pachyderma sin.*
KIA 25700	179 – 182 cm	25390 ± 200	24970 ± 200	29928 ± 310	*N. pachyderma sin.*
KIA 30396	182 – 184 cm	25310 ± 210	24890 ± 210	29876 ± 312	*N. pachyderma sin.*
KIA 27116	299 – 302 cm	42340 ± 2020	41920 ± 2020	45858 ± 1898	*N. pachyderma sin.*

*: AMS radiocarbon dating was on carbonaceous shells of *Neogloboquadrina pachyderma sinistralis* at the Leibniz-Labor for Radiometric Dating and Isotope Research in Kiel, Germany. Conversion to calendar ages was done using the CalPal online software (www.calpal-online.de) with the CalPal2005_SFCP calibration curve. A standard reservoir age of 420 years has been applied for all dates.

AMS radiocarbon dating was performed on carbonaceous shells of *N. pachyderma sinistralis* at the Leibniz-Laboratory for Radiometric Dating and Isotope Research at the Christian Albrecht University in Kiel, Germany. ^{14}C ages have been converted to calendar ages using the CalPal online software (www.calpal-online.de) with the CalPal2005_SFCP calibration curve and a correction for the reservoir effect of 420 years (Table 1).

Stratigraphy

A first characterisation of the age of the Hinlopen/Yermak Megaslide has been presented by Winkelmann et al. (2006a) which was mainly based upon AMS radiocarbon dates directly below and above the slide related turbidite in core PS66/309-1. The slide's minimum age was defined by the closest AMS date above the turbidite. This minimum age around 30 calendar (cal.) kyr. BP still represents the best datum of the slide's actual age. However, for further characterisation of the trigger mechanism (e.g. timing and trends in environmental conditions), the stratigraphy of this study has been focused on MIS 3. The final age model of core PS66/309-1 KAL was deduced from its oxygen and carbon isotope records (Figure 2), which, in general, can be correlated with the global isotope curve SPECMAP stack (Martinson et al., 1987). AMS ^{14}C dates at 90, 143, 180, 183 and 300 cm core depth helped to pinpoint Marine Isotope Stages (MIS) 2 and 3. The stratigraphic framework is further supported by correlation to core PS1533-3 and PS2212-3 KAL which have established age models ranging from MIS 1 into 6 (Spielhagen et al., 2004; Vogt et al., 2001; Figure 2). In core PS66/309-1 KAL a series of melt water peaks characterise the MIS 2. We date the most prominent peak at 15,66 + 70 ^{14}C-kyr BP (18,541 ± 237 cal. kyr. BP; Figure 2). Well-dated melt water events during Termination I have been recognised in the adjacent areas (cf. Hebbeln et al., 1994). The MIS 3/2 boundary is characterised by a well defined association of sedimentological, mineralogical

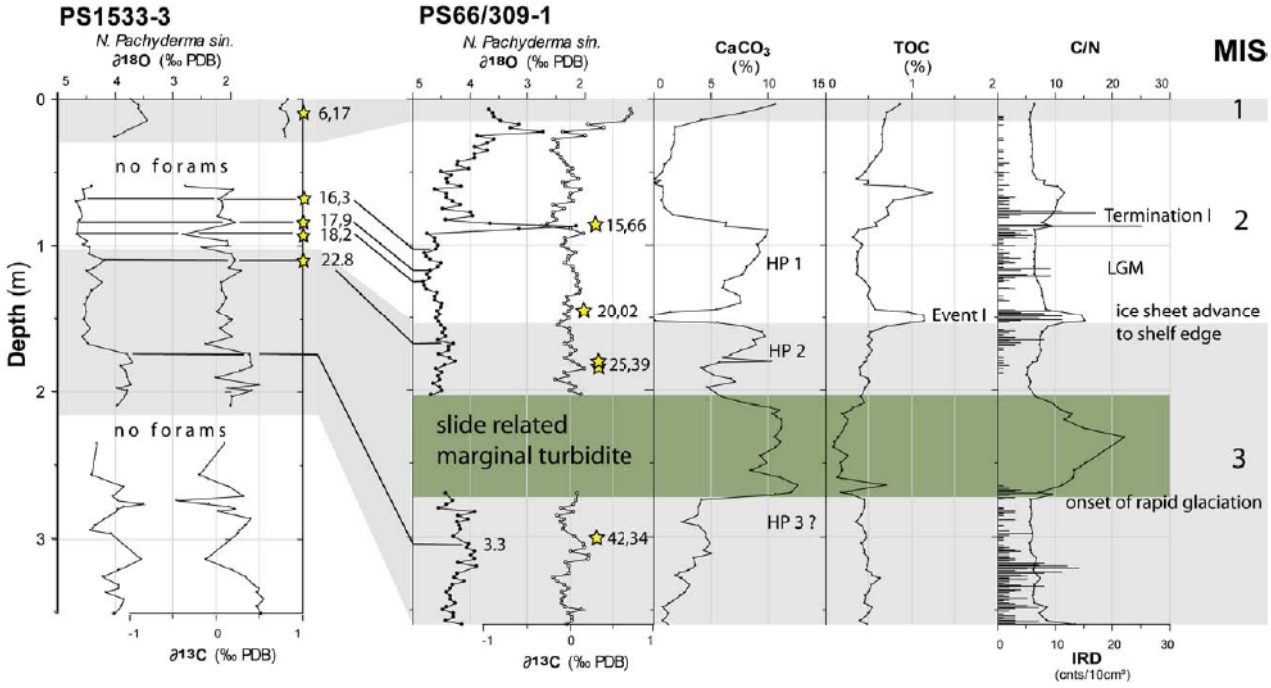

Figure 2: Proxy record of core PS66/309-1 KAL including bulk parameter and IRD for MIS 3 within Sophia Basin showing heavy stable oxygen isotope values above 4 ‰, relatively high carbonate contents during onset of Late Weichselian Glaciation and Hinlopen/Yermak Megaslide failure event. The advance to the shelf edge by the SBIS is reflected in Event I at the MIS 3/2 boundary. The interval of the Hinlopen/Yermak Megaslide failure event (marginal turbidite, green box, cf. Winkelmann et al., 2006a) follows a sudden drop to heavy $\partial^{18}O$ values around 45 kyr. BP (MIS sub-stage 3.3). This drop might indicate the onset of the rapid glaciation. HP events (1-3) according to Hald et al. (2001). The chronostratigraphy of core PS66/309-1 KAL is based on the $d^{18}O$ and $d^{13}C$ record of N. pachyderma sin., the correlation to core PS1533-3 (Spielhagen et al., 2004) and AMS radiocarbon dating. Marine Isotope Stage (MIS) assignments are based on Martinson et al. (1987). AMS-^{14}C dates from PS1533-3 (Nørgaard-Pedersen et al., 2003; Spielhagen et al., 2004) are correlated to PS66/309-1 KAL (left; corrected ^{14}C-kyr.). New AMS-^{14}C dates (right; given in uncorrected ^{14}C-years BP) were measured on N. pachyderma sin. at the Leibniz Laboratory, Kiel University.

and organic–geochemical parameters in all sediment cores in the region (cf. Andersen et al., 1996; Vogt et al 2001; Figure 2). The layer exhibits lamination and contains high amounts of mature terrestrial organic material and very low carbonate contents (Vogt et al., 2001). This layer has been described as Event I (Knies & Stein, 1998) and has been deposited between 22.5 and 19.5 ^{14}C kyr. BP as based on several AMS ^{14}C-ages. In core PS66/309-1 KAL the closest AMS ^{14}C date directly above this layer gives an age of 20,02 ± 140 ^{14}C kyr. BP (21,527 ± 486 cal. kyr. BP, Table 1, Figure 2). According to the published interpretation, we assume it to be a synchronous deposit and use it as one indicator of the lowermost MIS 2 (Figure 2).

Paleo-environmental setting for the triggering of the Hinlopen/Yermak Megaslide

The Late Weichselian Glaciation

A drop to heavy $\partial^{18}O$ preceding the megaslide (Figure 2) indicate the pre-slide onset of glaciation and increasing ice volume with its implication for sea level changes. Global sea level data suggest a rapid approach of near maximum volumes around 30 cal. kyr. BP (e.g. Lambeck et al., 2002). The rapid establishment of maximum ice volume and extent of this Late Weichselian Glaciation, which has been the largest of the Weichselian ones on Svalbard, is documented as strong IRD peaks accompanied by higher sedimentation rates, C/N ratios and TOC contents. This integrated signal occurs around 23,4 cal. kyr. BP when the outlet glaciers reached the shelf edge and post-slide intensive terrigenous sediment input commenced (Event I according to Knies & Stein, 1998; Figure 2). The Hinlopen/Yermak Megaslide occurred around 30 kyr. BP. Thus, it coincides with the transition from the Kapp Ekholm Interstadial into glaciation G of the Svalbard glaciation curve i.e. the onset of the major Late Weichselian glaciation that lead to maximum extents of the Last Glacial Maximum (LGM)(Figure 3; Mangerud et al., 1998, Svendsen et al., 2004).

The major element driving this rapid glaciation has been attributed to the higher influx of Atlantic water masses leading to open water conditions and the corresponding moisture supply to build-up of the SBIS (e.g. Hebbeln et al., 1994; Dokken & Hald, 1996). Paleoceanographic proxies show a high productivity zone (HP 2) and point to an increased warm water influx to the area west and north of Spitsbergen between 32 and 26 cal. kyr. BP (Dokken & Hald, 1996; Hald et al., 2001; Hebbeln et al., 1994, 1998; Spielhagen et al., 2004). The associated meridional surface circulation pattern (paleo-WSC) might have not differed drastically from the modern pattern (e.g. Hebbeln et al 1998).

Eustatic versus isostatic Sea Level Changes on Svalbard

The paleo-sea level and isostatic position of Svalbard is a crucial factor in discussing the possible trigger mechanisms of the megaslide. Sea level changes (Figure 3) directly influence the pressure field, buoyancy and thus stability of sediments as well as hydrate stability. The assessment of an isostatic sea level and position of the paleo-shore line of North-Spitsbergen is, however, complicated. Raised beaches (for location of sites see Figure 7) have been found e.g. on Reinsdyrflya at 90 m a.s.l. (Salvigsen & Österholm, 1982) and on the west coast of Phippsöya at 20 m a.s.l. (Forman & Ingolfsson, 2000) with ages >40 ^{14}C kyr. BP, at the south shore of Isfjorden dated to 36 ^{14}C kyr. BP (Mangerud et al., 1992), on northern Prins Karls Forland at 30 to 40 m a.s.l. with ages between 30 and 40 ^{14}C kyr. BP (Andersson et al., 1999). A morainic ridge in Lifdefjorden contains sublittoral sands below the till and date to 36 ^{14}C kyr. BP (Landvik

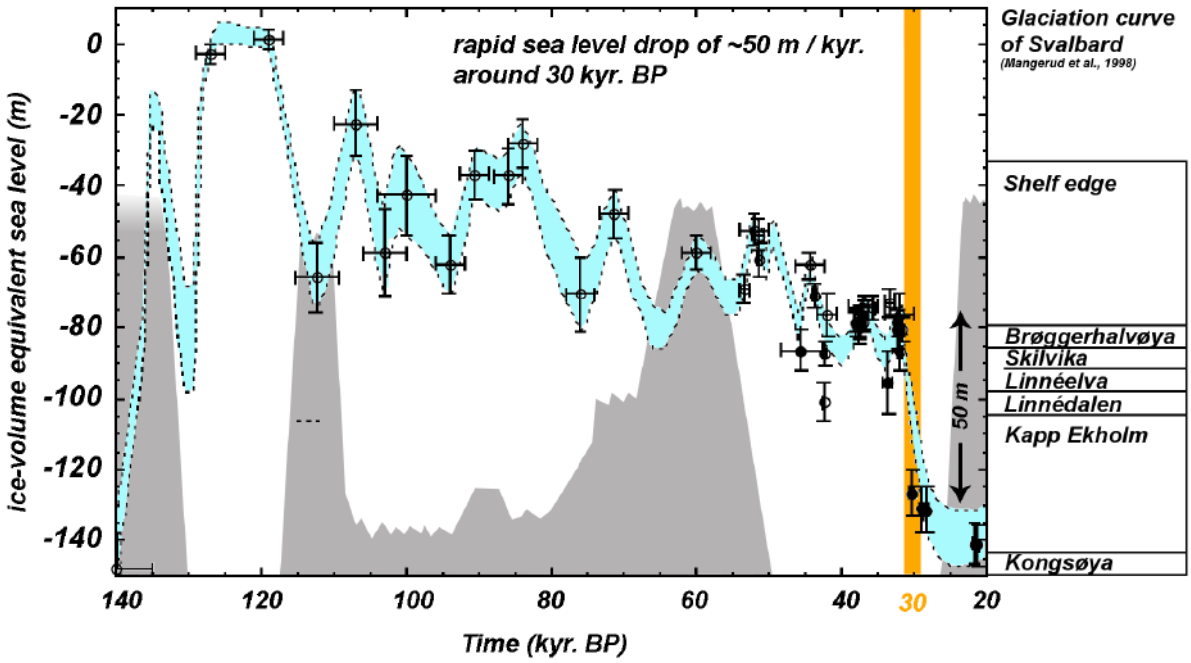

Figure 3: Sea Level curve (light blue) showing a drastic drop in global sea level around 30 kyr. BP during the time window of the Hinlopen/Yermak Megaslide (modified from Lambeck et al., 2002) and Glaciation curve of Svalbard (according to Mangerud et al., 1998, modified).

et al., 1998). Raised marine sediments below a till bed in Linnédalen, West-Spitsbergen gave ages of 40 and 36 ^{14}C kyr. BP. The youngest radiocarbon dates below the LGM associated till on north-west Spitsbergen of calcerous algae gives 33,9 ^{14}C kyr. BP while the youngest marine fossils incorporated in the till date to 28,5 ^{14}C kyr. BP (Landvik et al., 1998).

Summarising the terrestrial geologic evidence, Svalbard must have experienced an isostatic sea level rise prior to 30 cal. kyr. BP (Kapp Ekholm Interstadial; cf. Mangerud et al., 1998) and a following drastic drop before the LGM. In Linnédalen a local sea level drop of at least 87 m can be inferred from raised marine sediments in a terrace at 87 m a.s.l. (Mangerud et al., 1998). However, precise information on both local isostatic sea level and shore lines on N-Spitsbergen are not available so far. Thus, the discussion on changes in the pressure field (from relative sea level changes) and consequently increasing or decreasing buoyancy of the sediment prone to failure is dependant on information of the global sea level.

Lambeck et al. (2002) defined the onset of the LGM as the time when sea level first approached their minimum levels at ca. 30 cal. kyr. BP. The LGM ice volumes were approached at about 30 cal. kyr. BP too and increased only slowly during the following 10 kyr. (Figure 3). The onset of the LGM was thus accompanied by a rapid fall in sea level with ca. 50 m in less than 1000 years. A similar high rate in

falling sea level has only been reported for an interval during the early MIS 3 (Figure 3). The subsequent cold period leading into the LGM was characterised by rapid oscillations in sea level, with magnitudes of tens of metres in time intervals of 1000 years or less. This oscillations were superimposed on a gradually falling sea level (Lambeck et al., 2002).

The direct consequence of such a sea level drop is a change in the pressure field within the TMF sediments by ca. -500 Pa (502,7 Pa; equivalent to 50 m of sea-level drop) resulting in a decrease in buoyancy by 0,21 % of a single particle with given volume at 2000m modern water depth (MWD). The change in buoyancy of -0,21 % results in a higher gravity-driven particle support within the sediments leading to increased stability in an open (connected pores) particle-supported system (e.g. sand). Under sealed conditions, or semi-sealed conditions within clay-rich sediments (pore volume is less efficiently connected), a drop in water column pressure (sea-level drop) can result in hydrostatic overpressure within the pore space, thus, reducing the shear strength of the sediment. The pressure equilibration within the pore volume is dependant on the permeability of the actual sediments and might be retarded accordingly, especially between sedimentary strata of different physical properties (e.g. clay rich sediments with varying grain size spectra). Therefore, elevated pore water pressure might have contributed to reduced stability, even though this contribution appears comparably small at 2000 m water depth. Considering the nature of the TMF sediments (glacigenic debris flows), most of them deposited during active glacial discharge from the Hinlopen ice stream (Ottesen et al., 2005) a drop in pressure should approach conditions under which these sediments have been deposited (lowered sea-level during major glaciations), thus stabilising them.

However, these considerations are based on the calculated compressibility of seawater which is very small and usually neglected for a porous media (even if it is characterized by a very low permeability) and long-term processes like sea-level changes. A falling sea level should therefore be directly accompanied by a decrease of the total stress and the hydrostatic pressure proportional to the sea level drop. Thus, the sea level drop should not have generated excess pore pressure in the submerged and saturated TMF sediments and, therefore, it cannot be considered as the slope triggering mechanism. However, in the case of dissolved or free gas or hydrate phases within the pore volume, the pore pressure would be very sensitive to pressure changes, generating excess pore pressure for a falling sea level scenario.

Stability of potential Gashydrates

Given the presence of gashydrates on Svalbard (e.g. Vanneste et al., 2005) and the potential presence within the TMF sediments before failure, both falling sea level and higher water temperatures could have contributed to a Thinning of the hydrate stability zone (HSZ) and may have affected the slope stability of the headwall region north of Spitsbergen.

The relationship of methane and/or gas hydrates to submarine slides is in contrast to other possible causes so far hypothetical. One of the best studied submarine slides that was extensively investigated towards this relationship is the Storegga Slide off Mid Norway (e.g. Mienert et al., 2005a, b; Sultan et al., 2004). Despite these investigations, a clear causal relationship could not be established so far. Mienert et al. (2005b) tried to relate ocean warming of the upper layer to destabilisation of hydrates within the headwall area of the Storegga Slide. The calculated change within the pressure and temperature field due to ocean warming for the Storegga Slide (Mienert et al., 2005b) probably lead to an displacement of the HSZ between 400 to 750m of modern water depth (MWD). This change was accomplished between 12 and 9 cal. kyr. BP., well before the Storegga Slide (8.2 cal. kyr. BP). However, Mienert et al. (2005b) demonstrated that gas hydrate melting on top of the hydrate occurrence zone (HOZ) could have an essential impact on slope stability in relation to giant submarine slides.

Considering a similar scenario for the Hinlopen/Yermak Megaslide, we can take the modern circulation pattern as an analogue for the warm water inflow north of Svalbard around 30 cal. kyr. BP. (end-member scenario). The warm waters would have flushed the outer shelf and thus affected sediments in depth down to 400 m. This excludes the thermally forced hydrate destabilisation as the trigger since the initial slope failure of the retrogressive Hinlopen/Yermak Megaslide was positioned well below (>2000 m MWD) this impacted shelf area.

However, the warm waters might have had an impact on (potential) gashydrates within the upper headwall areas. The warming of these sediments could have led to reduced thickness of the HSZ thus leading to a shoaling of the bottom of the (hypothesised) HOZ with associated possible hydrate melting on its top. In analogue to the Storegga Slide, this scenario would have contributed to instability within the upper headwall area (400-200 m) impacting horizons that were to fail. Especially the geometry of detached sediment slabs during failure might have been affected by this process.

A model that incorporates the knowledge on gashydrate evidence around Svalbard is given in Figure 4. The gas would migrate along structures like fractures and fault zones (e.g. Knies et al., 2004) to finally escape to the surface, where it is recordable within clayey surface sediments due to adsorbtion effects. The sediments between these structures act as barriers and according to their physical properties, the allow gas

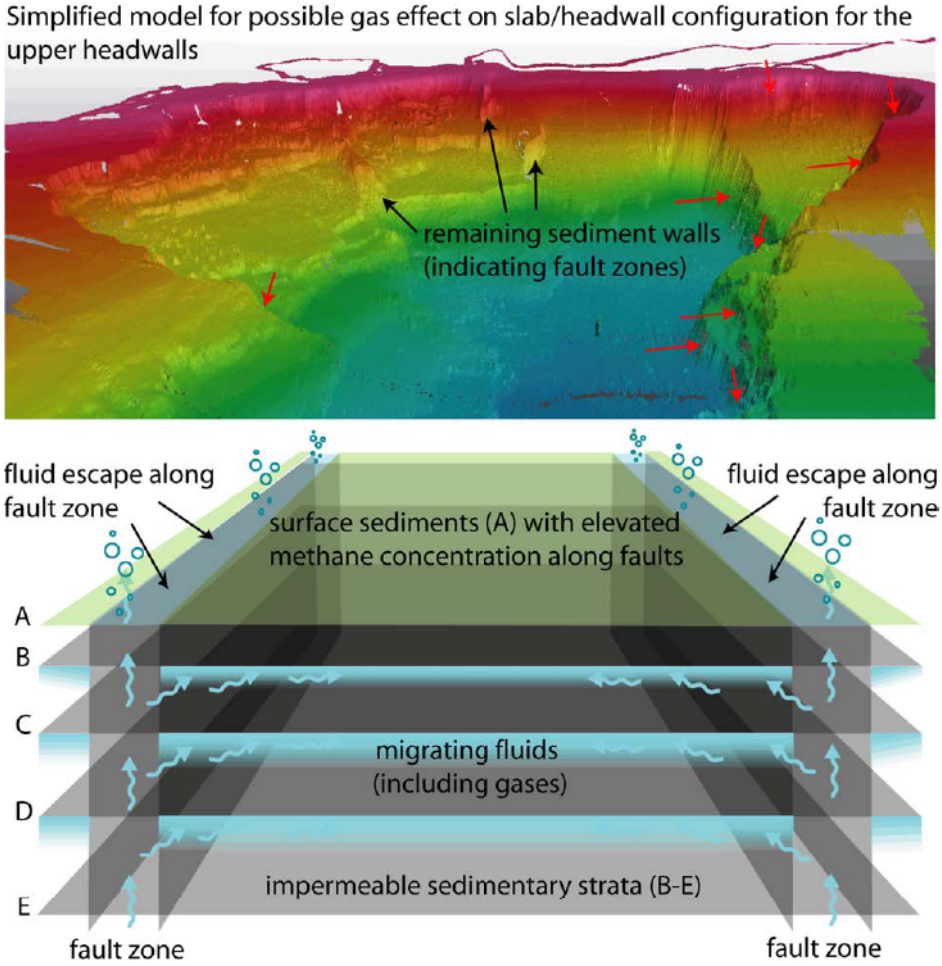

Figure 4: Simplified effect of fluids and gases migrating along structures (fractures and faults, especially major fault zones) within the sedimentary strata on the geometry of sediment slabs that are prone to failure. The model included two processes, both identified on the continental shelf of western Svalbard: (i) fluid escape and venting of gases along structures on the seafloor as reported by Knies et al. (2004) and (ii) accumulation of gases or gas hydrates along sedimentary strata bound by major fault zones as described by Vanneste et al. (2005). The remaining seafloor topography after an slide related evacuation will include exposed glide planes (representing the sediments directly below the weakened layers) and outstanding sediment walls (that represent sediment bound by fault zones that were able to release the fluids and gases). Both morphological features can be seen in the 3D model in the background showing the multiple headwalls of the Hinlopen/Yermak Megaslide (view from the north; high-resolution bathymetry data of Vanneste et al., 2006). Black arrows indicate remnant sediment walls. Red arrows indicate distinct planar elements (faults) that define the geometry of head- and sidewalls. Note the sharp and steep flanks on the lower right. These sidewalls constitute prolongations of the Hinlopen Fault Zone (striking almost NNW-SSE).

to migrate into distinct horizons as has been reported by Vanneste et al., 2005. The consequence during a major slope failure like the Hinlopen/Yermak Megaslide would be that slabs with their geometries defined by structures and weak horizons (possibly weakened by over-pore pressure from hydrate melting and/or gas enrichment) would slide out in an retrogressive style following an initial failure. The headwall area especially in the eastern part provides morphological evidence of such a scenario (Figure 4).

However, in deeper water depths (no direct impact of warm surface waters; in our case >400m MWD) the HSZ is pressure-controlled (e.g. Mienert et al., 2005b). In contrast to the Storegga Slide environmental condition with accomplished ocean warming (12-9 cal. kyr. BP) during a sea-level rise (most of it preceding the failure), the Hinlopen/Yermak Megaslide occurred during rapidly falling sea-level and ocean warming. Therefore the effects of lowered pressure and ocean warming both result in a thinning of the HSZ with consequent destabilisation of possible gas hydrates. The drastic sea-level drop of at least 50m in less than 1 kyr. (Lambeck et al., 2002) could have had an influence on the HSZ in the lower part of the pre-slide slope too, thus being interesting for the trigger mechanism.

Missing the relevant information on sediment properties, geothermal gradient, pressure distribution and gas composition, the calculation of a hypothetical gas hydrate stability field (GHSF) remains speculative. However, assuming lithostatic pressure distribution for the pre-existing Hinlopen TMF and taking -0,8°C of modern bottom water temperature (Schauer et al., 2004) as well as the Storegga Slide area as an analogue (assuming methane hydrate, a geothermal gradient of 0.056°C/m for lithostatic pore pressure and application of associated parameters; c.f. Bouriak et al., 2000, 2003), we can calculate a possible GHSF depth as a function of pressure and temperature (Figure 5a).

The relatively fast sea-level drop of 50 m would have caused the base of the GHSF to ascend. The lower boundary of the GHSF would have shallowed by ca. 21 m (163 to 142 m sub-bottom depth), 7 m (250 to 243 m sub-bottom depth) 5 m (296 to 291 m sub-bottom depth) and 2 m (351 to 349 m sub-bottom depth) at 400, 800, 1200 and 2000 m MWD respectively (Figure 5a).

The resulting higher pore pressure from dissociating gases might certainly have contributed to a possible destabilisation of sedimentary strata. Considering the amount and geometry of destabilised gas hydrates, a causal relation to the megaslide appears reasonable. Contrary, the geometry of evacuated slabs (upper headwall heights up to 600 m) does not coincide with the calculated lower boundary of the GHSF (163 to 256 m sub-bottom depth between 400 and 800 m MWD; Figure 5b) and might confirm that neither an ascending GHSF base nor its an descending top (from surficial thermally induced melting) did configure the detached slabs. The initial slope failure, however, must have been positioned even deeper (between 2000 and 2300m MWD; Winkelmann et al., *submitted*) and below the calculated GHSF base.

However, these considerations should be regarded with care since no information on the real thermal gradient, the (paleo-TMF) sediment's properties, gas composition and pressure distribution are available. Especially the thermal gradient and the sedimentary properties might vary significantly. Furthermore, the applied formula for the methane-seawater-hydrate equilibrium curve (Bouriak et al., 2000) is only valid within the temperature range of -2°C to 15°C. In addition, this hydrate hypothesis remains theoretical

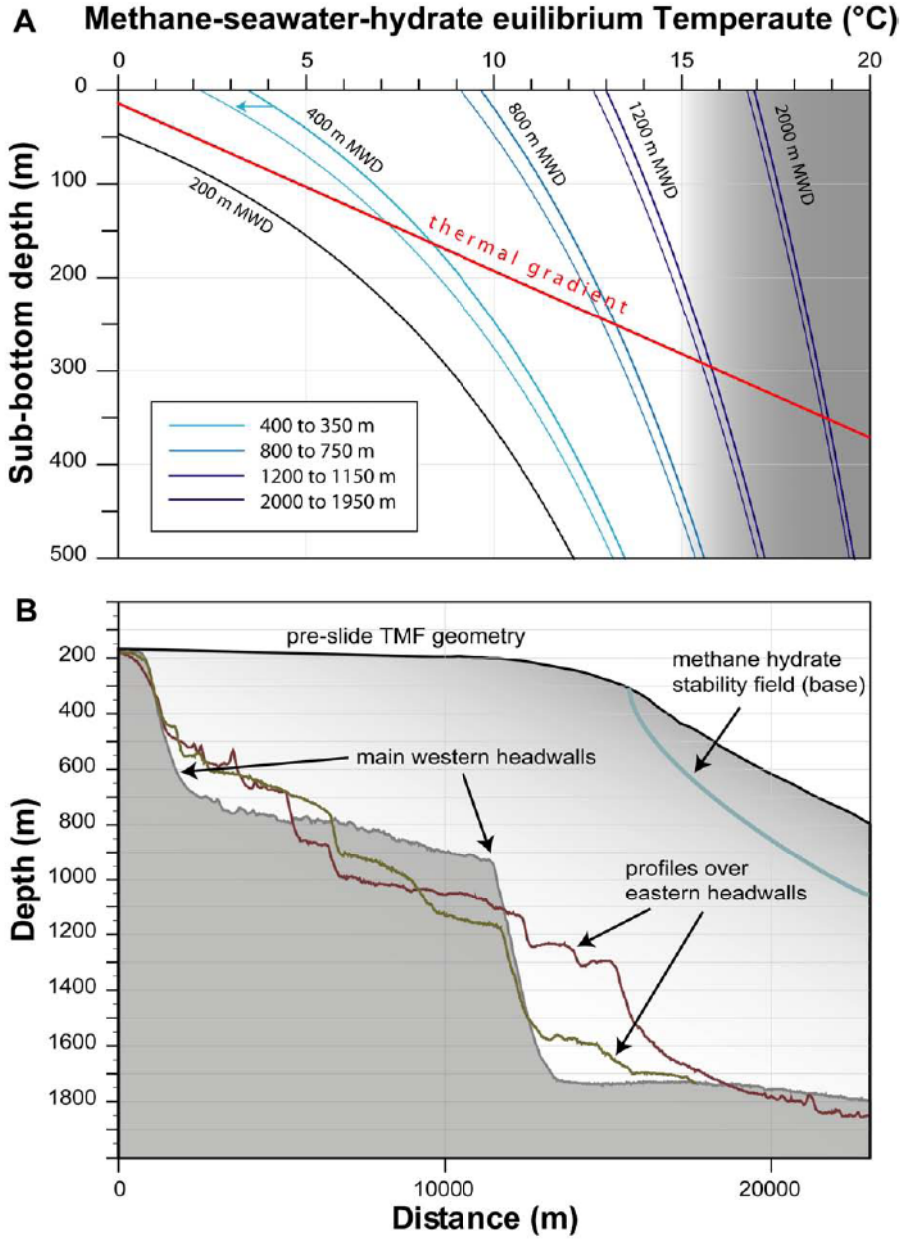

Figure 5: A: Methane-seawater-hydrate equilibrium temperature (MSHT, calculated according to Bouriak et al., 2000; see text) curves at 400, 800, 1200, and 2000 m modern water depth (MWD) before and after a 50 m sea-level drop. For MSHTs below the thermal gradient instability for methane hydrates can be expected. B: Bathymetry profiles across the main western (grey) and eastern (brown and olive) headwalls in relation to pre-slide bathymetry of the TMF with indicated methane hydrate stability zone (MHSZ). Note that the headwall geometries and depths do not coincide with the MHSZ.

since in contrast to the Storegga Slide area neither bottom simulating reflectors (BSR's), degassing features nor other evidence of free gas or gas hydrates have been recognised so far north of Spitsbergen that would corroborate it.

Additional doubt on the gashydrate hypothesis as the slide trigger comes from another consideration. Large amounts of gas (in case of the potential hydrate north of Svalbard mainly methane) hydrates would have been necessary to destabilise the Hinlopen TMF in a sufficient way to reach such a shelf collapse. If large amounts of methane clathrates would be involved in a submarine slide (c.f. Paull et al., 2003), an altered isotopic signature ($\partial^{13}C$ of methane is < -60 ‰ vs. PDB) can be expected in the dissolved carbon pool of the (local) ocean recorded as peaks in foraminiferal tests (e.g. Smith et al., 2001; Millo et al., 2005). The $\partial^{13}C$ record of planktic *N. pachyderma sin.* from nearby cores does not show light $\partial^{13}C$ events and thus, indication of a bigger methane release (Figure 2).

Whether or not gashydrates contributed to the Hinlopen/Yermak Megaslide, however, remains unclear. Despite the fact that methane was found to be concentrated along major geological structures on W-Spitsbergen (e.g. Knies et al., 2004), hydrate accumulation zones are bound by major geological structures (Vanneste et al., 2005) and in contrast to Cherkis et al. (1999) who showed a possible BSR in the headwall region, there is no direct evidence for methane, hydrates (BSR's) nor degassing features in or close to the headwall area of the Hinlopen/Yermak Megaslide (Figure 6). The headwall morphology exhibits a strong tectonic control as head- and sidewalls can be related to fault zones (Figures 4 and 6). However, considering a complete removal of potential hydrates (as the entire HSZ might have slid away), the absence of proof in our data does not proof absence of hydrates in MIS 3.

Glacio-tectonic Activity

The transition from the Kapp Ekholm Interstadial into glaciation G of the Svalbard glaciation curve (Mangerud et al., 1998) must have been rapidly and accompanied by rapid Ice loading onto the Svalbard archipelago. LGM-related moraines on north-western Spitsbergen have been described by Listøl (1972). Salvigsen (1977) dated bivalves from marine sediments that have been incorporated into the related till. They display middle Weichselian ages, the youngest of 28,5 ^{14}C kyr. BP which gives indication for marine transgression at around 33,2 cal. kyr. BP and glacial activity shortly after. Thus, an increasing glacio-tectonic activity probably characterised the time window of the slide event.

Given the spatial offset from the moisture sources close to the shelf edge and the main deposition centres on Svalbard and the Barents Sea (around Kongsøya; e.g. Ingolfsson et al., 1995; Lambeck, 1996; Svendsen et al., 2004), an uneven loading of ice onto the lithospheric crust in the area can be postulated (Figure 7). The corresponding gradients in load would run from depo-centres near Kongsøya on Svalbard to open waters near the western and north-western regions of Spitsbergen. Thus areas to the west and to the east of the Hinløpen cross shelf trough might have experienced a different loading history which can be termed asymmetrical. Increasing asymmetrical ice loading during intensification of Late Weichselian Glaciation

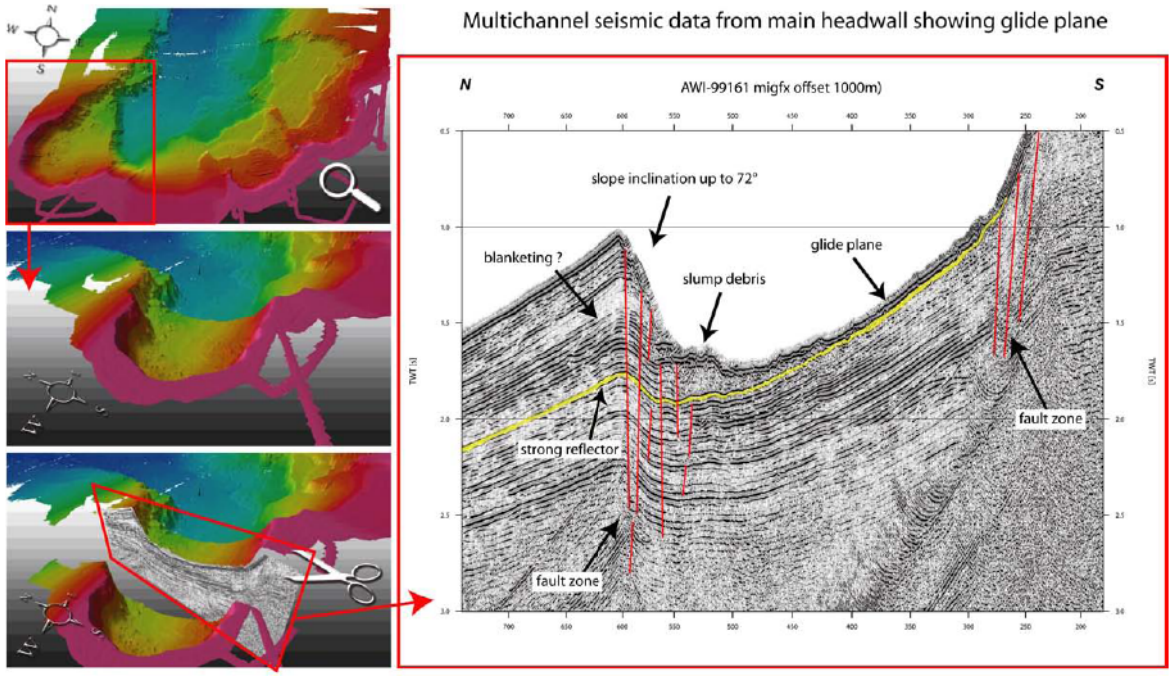

Figure 6: Seismic line AWI-99161 across the main headwall of the Hinlopen/Yermak Megaslide showing slide debris on glide plane which can be traced into the adjacent fan sediments of the old Hinlopen Trough Mouth Fan. There it constitutes a strong reflector. Note that the evacuated sediment slab is bound by fault zones. The indicated blanketing results at least partly from AGC-filtering. See 3D model (view towards NE) on the left for location (seismic data from Geissler & Jokat, 2004; bathymetry data from Vanneste et al., 2006).

adjacent to the Hinløpen cross shelf trough might have caused an additional tectonic stress along this major fault zone leading to higher mechanical activity in the headwall area. Neo-tectonic activity and faulting due to subsequent isostatic adjustment following the last deglaciation have been described for Scandinavia and the Baltic Sea (e.g. Kotilainen & Hutri, 2004; Bungum et al., 2005).

Forebulge Development

In addition, the rapid growth of the SBIS must have had an impact on the isostatic equilibrium in the area. A developing forebulge (Figure 7) is a physical consequence of ice loading onto the lithosphere and probably contributed to the slope instability leading to the Hinlopen/Yermak Megaslide.

However, the lack of reliable information on the lithospheric rheology makes the forebulge assessment a complicated affair. The assessment of local isostatic effects of a forebulge development is heavily dependent on the lithospheric flexural rigidity. Unfortunately, this parameter is not well known and uncertainty on it remains. Fjeldskaar (1994) estimated lithospheric flexural rigidity in Scandinavia to be between 1 x 10^{24} and 1 x 10^{25} Nm. Howell et al. (2000) applied sensitivity tests for their numerical model for the SBIS during the Late Weichselian Glaciation (including the LGM). Depending on the applied

rigidities, the associated forebulges vary between narrow isostatic effects close to the ice load (lithospheric flexural rigidity 1 x 10^{24}Nm) and wide with no overall uplift within the Barents Sea (lithospheric flexural rigidity 1 x 10^{26}Nm) in their model. Howell et al. (2000) concluded with a possible scenario for the central Barents Sea that forebulge development due to early glaciation from the Arctic archipelagos (including Svalbard) and Scandinavia (80m) in combination with global sea-level fall (120m) would be capable to expose parts of the central Barents Sea subaerially. This would be enough to form glaciation nuclei on the Central Bank and would have aided grounded ice sheets from Scandinavia and the Arctic archipelagos to merge in the central Barents Sea. This modelled scenario stands in accordance with geomorphological evidence and has been accomplished by application of a rigidity of 1 x 10^{25} Nm.

Beside the fact that a forebulge is a direct physical consequence of a growing ice sheet, there is additional evidence within the geological archive. At Linnédalen, a terrace at 87m a.s.l. has been described by Mangerud et al. (1998). The minimum ages of marine sediments below the LGM-associated till gave a finite age of 35.9 ^{14}C-kyr. BP. Thus, the sediments were deposited at a global sea level at -80m (Lambeck et al., 2002) which results consequently in an depression of W-Spitsbergen of at least 167m around 40 kyr. BP. The lithological sequence at Linnéelva (20-30 m a.s.l.; Mangerud et al., 1998) shows coarsening upwards and shore face sediments just below the LGM-till. This indicates a local (isostatic) sea level drop shortly after marine sedimentation and before the LGM (at least until 22 kyr.). Considering the global sea level drop of ca. 50 m (from -80 to -130 m around 30 kyr. BP), W-Spitsbergen should have experienced an uplift of at least 7-17 m to reach sea-level at Linnédalen. The actual uplift was probably higher due to the fact that the marine sediments of the 87m-terrace had been deposited well below sea-level. This uplift can be interpreted as an indication of a forebulge development around 30 kyr. BP. This interpretation coincides with the latest view on the LGM ice sheet conditions on Spitsbergen, suggesting highly dynamic and focused ice drainage via ice streams and the existence of nunataks in W and NW Spitsbergen (Landvik et al., 2005). Sea level records of Svalbard's post-glacial emergence (dating of raised beach deposits) indicate a short-lived temporary uplift and following subsidence of sites that were positioned close to the maximum ice sheet extent (Forman & Ingólfsson 2000; Lambeck 1996; Landvik et al., 1998). This can be interpreted as an indication of a retrograding forebulge.

Considering the possible asymmetrical loading, associated forebulge development might have been different to the west and east of the Hinlopen cross-shelf trough leading to enhanced stress and movements along the fault zone.

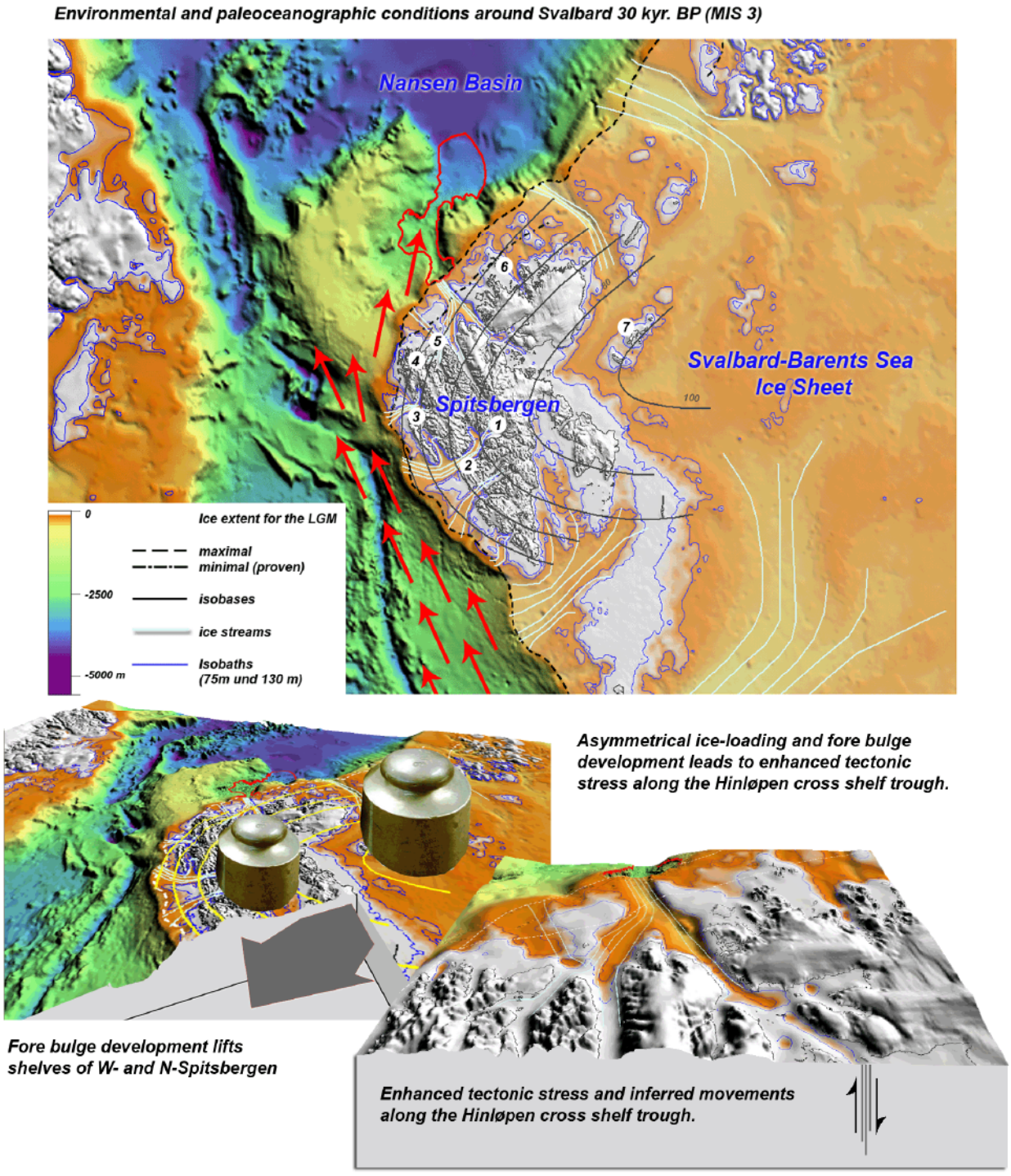

Figure 7: Map with palaeo-environment during MIS 3, sea level between -75 and -130m (according to Lambeck et al., 2002; blue isobaths of today´s topography/bathymetry), ice sheet extent close to maximum (LGM, according to Landvik et al., 1998) and isobases fairly indicating LGM depo-centres (based on relative sea level data from post-LGM emergence; Landvik et al., 1998) ice sheet thickness, oceanic circulation (inflow of Atlantic water masses during HP events, red arrows), ice streams (Ottesen et al 2005). Triggering model for the Hinlopen/Yermak Megaslide showing warm water inflow, increasing asymmetrical ice loading (weights), fore bulge development and inferred movements along the Hinløpen Strait / Hinløpen Trough. (Site names: 1 Kapp Ekholm, 2 Linnédalen/Linnéelva, 3 N-Prins Karls Forland, 4 Lifdefjorden, 5 Reinsdyrflya, 6 Phippsøya, 7 Kongsøya.).

Seismic Rate and Earthquake Amplification

The combination of rapid glaciation and rapid loading on the corner of continental lithosphere has likely played a significant role for the seismic rate too. Sauber & Molnia (2004) reported that earthquake frequency and magnitude might be influenced by climatic factors. They showed on data from southern Alaska that melting of glaciers due to global warming is accompanied by reduced loading of the lithosphere, leading to an increase in the number of earthquakes ($ML \geq 2.5$) and seismic rate associated with ice thinning and a decrease in the number of earthquakes and seismic rate associated with ice thickening (Sauber & Molnia, 2004). Thus, cooling of the lithosphere in concert with loading from ice-sheets and glaciers can be expected to hamper the crustal movements which leads to accumulation of tectonic strain. This process would lead to earthquakes with higher amplitudes on a lower frequency. An earthquake could have been the final trigger leading to failure of the TMF sediments east of the Hinløpen fault zone and to creation of the steep western headwalls of this megaslide.

The Importance of the Rate of environmental Changes

The Hinlopen/Yermak Megaslide as a single major failure event and its physical configuration as a partial shelf collapse with combined headwalls heights of 1600 m, is a rather unique slide event. Therefore, triggering as well as slope stability conditions might be regarded as unique or at least special too. An increasing asymmetrical ice loading and falling sea level seems not enough to explain an apparently singular event. Intensive glaciations have been recorded before the Weichselian (e.g. Svendsen et al., 2004) and a similar failure event has not been reported so far. A possible answer to that might be the rapidity of involved processes. The speed of environmental changes is a crucial factor for stability related processes. An unprecedented speed would be able to exceed a threshold in the stability system resulting in sediments prone to failure. Rapid sea-level drop and rapid glaciation with its consequences (forebulge development) for the tectonic activity characterise the time of the Hinlopen/Yermak Megaslide shelf collapse. Finally, the position of the shelf failure on a major fault zone on a continental corner with two extensional stress fields seems a special factor too. In concert with the lithological properties of the glacial/interglacial sediments this factor might explain the enormous headwall heights.

Favoured Triggering Scenario

Following the considerations on environmental conditions, their effects and possible triggers of the Hinlopen/Yermak Megaslide, we can approach a likely triggering scenario.

The pressure induced changes within particle buoyancy (0,21 %) appear insufficient for a submarine megaslide. Hydrate destabilisation from ocean warming on the upper slope and shelf could not have

affected the area of initial failure. Hydrate destabilisation from pressure drop can not be ruled out but appears insufficient to result in megascale failure. In addition, we found no evidence for hydrates (escape features, hydrates, free gas, BSR's etc.) near the slide. The headwall configuration clearly displays sharp planar elements that defined the slided sediment slabs. The more or less vertical planar elements can directly be related to minor and major structures (fault zones) on the Svalbard archipelago (*Winkelmann et al., submitted*; Figure 4 and 6). As discussed above, this morphology points to a tectonic control of the Hinlopen/Yermak Megaslide. The fact that part of the former TMF west of the Hinlopen fault zone is still present and exhibits the most stable side and headwalls (including highest inclinations; Figures 4 and 6) corroborates the tectonic control interpretation (If hydrates or pressure and/or temperature changes would be the cause, the full TMF should have failed).

Thus, the most probable trigger is to be seen within the spectrum of glacio-tectonic activity arising from asymmetrical ice loading and forebulge development. An amplified earthquake along the Hinlopen fault zone positioned near the bottle neck of the headwall area is the most likely candidate for the final trigger leading to initial failure.

Conclusions: Triggering Scenario for the Hinlopen/Yermak Megaslide

The Hinløpen TMF and parts of the adjacent continental slope collapsed around 30 cal. kyr. BP. Pre-conditioning and trigger mechanism appear to be special to explain the unprecedented geometry and physical configuration of the Hinlopen/Yermak Megaslide.

The lithological (climatically controlled) preconditions are: (i) intercalation of interglacial and glacial sediments of the Pleistocene strata on the shelf; (ii) transition of glacigenic debris flows of a TMF into normal glacio-marine sediments.

The environmental (climatically controlled) preconditioning of the Hinlopen/Yermak Megaslide include (i) higher influx of warm Atlantic water by the paleo-WSC (HP 2) accompanied by (ii) a rapid drop in sea level as inferred from terrestrial geologic evidence as well as global data forcing the (iii) HSZ to thin and large isostatic movements along the Hinlopen cross-shelf trough resulting from ice loading of the rapidly growing SBIS.

The changes in sediment buoyancy of ~0,21 % (2000 m water depth) appear to small for explain the initial failure. Excess pore water pressure due to pressure changes within semi or fully closed pore space sediment systems appears unlikely as the trigger since the TMF sediments have been deposited during sea level low stands and should therefore approach equilibrium.

Despite the absence of hydrate indications, we can not tell from our data whether or not gashydrates contributed to less slope stability within the pre-slide Hinlopen TMF. However, gashydrates might not explain the initial slope failure although they possibly contributed to less slope stability within the upper slope.

Considering that only part of the Hinlopen TMF collapsed (along a major fault zone), theories based on changes in the temperature and/or pressure field fail to explain the stability within the remaining TMF.

Asymmetrical loading on the continent corner by rapid onset of the Late Weichselian Glaciation around 30 cal. kyr BP accompanied by a forebulge development and a strong earthquake, probably positioned below or close to the bottle neck of the headwall region probably resulted in unprecedented movements along the Hinlopen cross shelf trough. The subsequent sediment failure along this major fault zone appears to be the favourite triggering scenario for the Hinlopen/Yermak Megaslide. Thus the trigger is external and not internal (lithological, compensating overburden) as has been proposed for other slides.

Acknowledgement

This study is part of the ESF EUROMARGINS Project Slope Stabilities on Europe's passive continental margins (SPACOMA) and funded by the German Research Foundation (DFG, STE 412/17). We are thankful to the scientific shipboard party and the captain and crew of RV “Polarstern” during ARK-XX/3. We thank Dr. W. H. Geissler for providing the seismic data from the main headwall and Dr. M. Vanneste for the bathymetry data of the headwall area.

References

Andersen, E.S., Dokken, T.M., Elverhøi, A., Solheim, A., Fossen, I. (1996): Late Quaternary sedimentation and glacial history of the western Svalbard margin. Marine Geology 133, 123–156.

Andersson T., Forman, S. L., Ingolfsson, O., Manley, W. (1999): Late Quaternary environmental history of Prins Karls Forland, western Svalbard, Boreas 28, 292-307.

Baptista, M.A., Miranda, P.M.A., Miranda, J.M., Mendes Vistor, L. (1998): Constrains on the source of the 1755 Lisbon tsunami inferred from numerical modeling of historical data; Journal of Geodynamics 25 (2): 159-174.

Bondevik, S., Svendsen, J.I., Johnsen, G., Mangerud, J., Kaland, P.E., (1997): The Storegga tsunami along the Norwegian coast, its age and runup, Boreas 26, 29-53.

Bondevik, S., F. Løvholt, C. Harbitz, J. Mangerud, A. Dawson, and J. I. Svendsen (2005): The Storegga Slide tsunami—Comparing field observations with numerical simulations, Marine and Petroleum Geology 22, 195–208.

Bouriak, S., Vanneste, M., Saoutkine, A., (2000): Inferred gas hydrates and clay diapirs near the Storegga Slide on the southern edge of the Vøring Plateau, offshore Norway, Marine Geology 163, 125-148.

Bouriak,S., Volkonskaia, A., Galaktionov, V. (2003): 'Split' strata-bounded gas hydrate BSR below deposits of the Storegga Slide and at the southern edge of the Vøring Plateau, Marine Geology 195, 301-318.

Bungum, H. Lindholm, C., Faleide, J.I. (2005): Postglacial seismicity offshore mid-Norway with emphasis on spatio-temporal–magnitudal variations, Marine and Petroleum Geology 22, 137–148.

Cherkis, N.Z., Max, M.D., Vogt, P.R., Crane, K., Midthassel, A., Sundvor, E. (1999): Large-scale mass wasting on the north Spitsbergen continental margin, Arctic Ocean, Geo-Marine Letters 19, 131-142.

Dokken, T.M. & Hald, M. (1996): Rapid climatic shifts during isotope stages 2–4 in the Polar North Atlantic. Geology 24 7 , 599–602.

Duplessy, J.C. (1978): Isotope studies, in Gribbin, J., ed., Climatic change: Cambridge, UK, Cambridge University Press, p. 46–67.

Fjeldskaar, W. (1994): Viscosity and thickness of the asthenosphere detected from the Fennoscandian uplift, Earth and Planetary Science Letters 126, 399–410.

Forman, S. & Ingólfsson, Ó (2000): Late Weichselian glacial history and postglacial emergence of Phippsöya, Sjuöyane, northern Svalbard: a comparison of modelled and empirical estimates of a glacial-rebound hinge line, Boreas 29, 16-25.

Garcia, E., Dañobeitia, J.J., Verges, J. and PARSIFAL Team, (2003): Mapping active faults offshore Portugal (36°N–38°N): Implications for seismic hazard assessment along the southwest Iberian margin; Geology, 31 (1), 83–86.

Geissler, W.H. & Jokat, W. (2004): A geophysical study of the northern Svalbard continental margin, Geophysical Journal International, 158, 50–66.

Grobe, H. (1987): A simple method for determination of ice rafted debris in sediment cores. Polarforschung 57 3 , 123–126.

Haflidason, H., Lien, R., Sejrup, H.P., Forsberg, C.F., Bryn, P. (2005): The dating and morphometry of the Storegga Slide, Marine and Petroleum Geology 22, 123–136.

Hald, M., Dokken, T., Mikalsen, G. (2001): Abrupt climatic change during the last interglacial–glacial cycle in the polar North Atlantic, Marine Geology 176, 121-137.

Hebbeln, D., Dokken, T., Andersen, E.S., Hald, M., Elverhøi, A. (1994): Moisture supply for northern ice-sheet growth during the Last Glacial Maximum. Nature 370, 357–359.

Hebbeln, D., Henrich, R., Baumann, K.H. (1998): Paleoceanography of the last Interglacal/Glacial Cycle in the Polar North Atlantic, Quaternary Science Reviews 17, 125-153.

Howell, D., Siegert, M.J., Dowdeswell, J.A. (2000): Modelling the influence of glacial isostasy on Late Weichselian ice-sheet growth in the Barents Sea, Journal of Quaternary Science 15 (5), 475–486.

Ingólfsson, Ó., Rögnvaldsson, F., Bergsten, H., Hedenäs, L., Lehmdal, G., Lirio, J. L., Sejrup, H. P. (1995): Late Quaternary glacial and environmental history of Kongsøya, Svalbard, Polar Research 14, 123-129.

Jakobsson, M., Cherkis, N. Z, Woodward, J., Macnab, R., Coakley, B. (2000): New grid of Arctic bathymetry aids scientists and mapmakers; Eos, Transactions, American Geophysical Union, v. 81 (9), p. 89, 93, 96.

Jokat, W. (Ed.) (2000): The Expedition RKTIS-XV/2 of Polarstern in 1999, Berichte zur Polar- und Meeresforschung, 368, 128 pp, Alfred-Wegener-Institut, Bremerhaven.

Knies, J. & Stein, R. (1998): New aspects of organic carbon deposition and its paleoceanographic implications along the northern Barents Sea margin during the last 30,000 years, Paleoceanography 13 4 , 384–394.

Knies, J., Damm, E., Gutt, J., Mann, U., Pinturier, L. (2004): Near-surface hydrocarbon anomalies in shelf sediments off Spitsbergen: Evidences for past seepages, Geochemistry Geophysics Geosystem 5, Q06003, doi:10.1029/2003GC000687.

Kotilainen, A. & Hutri, K.-L. (2004): Submarine Holocene sedimentary disturbances in the Olkiluoto area of the Gulf of Bothnia, Baltic Sea: a case of postglacial palaeoseismicity, Quaternary Science Reviews 23, 1125-1135.

Lambeck, K. (1996): Limits on the areal extent of the Barents Sea ice sheet in Late Weichselian time, Global and Planetary Change 12, 41-51.

Lambeck, K., Yokoyama, Y., Purcell, T. (2002): Into and out of the Last Glacial Maximum: sea-level change during Oxygen Isotope Stages 3 and 2, Quaternary Science Reviews 21, 343-360.

Landvik, J.Y., Bondevik, S., Elverhøi, A., Fjeldskaar, W., Mangerud, J., Salvigsen, O., Siegert, M.J., Svendsen J.I., Vorren, T.O. (1998): The last glacial maximum of Svalbard and the Barents sea area: ice sheet extent and configuration, Quaternary Science Reviews 17, 43-75.

Landvik, J. Y., Ingólfsson, Ó., Mienert, J., Lehman, S. J., Solheim, A., Elverhøi, A., Ottesen, D. (2005): Rethinking Late Weichselian ice-sheet dynamics in coastal NW Svalbard. Boreas, 34, 7–24, ISSN 0300-9483.

Listøl, O. (1972): Submarine moraines off the west coast of Spitsbergen, Norsk Polarinstitutt Årbok 1970, pp. 165-168, Norsk Polarinstitutt, Oslo.

Mangerud, J., Bolstad, M., Elgersma, A., Helliksen, D., Landvik, J. Y., Lønne, I., Lycke, A. K., Salvigsen, O., Sandahl, T., Svendsen J.I. (1992): The last glacial maximum on Spitsbergen, Svalbard, Quaternary Research 38, 1-31.

Mangerud, J., Dokken, T., Hebbeln, D., Heggen, B., Ingólfsson, Ó., Landvik, J. Y., Mejdahl, V., Svendsen, J. I., Vorren, T. O. (1998): Fluctuations of the Svalbard-Barents Sea ice sheet during the last 150 000 years, Quaternary Science Reviews 17: 11-42.

Martinson, D.G., Pisias, N.G., Hays, J.D., Imbrie, J., Moore, T.C., Shackleton, N.J. (1987): Age dating and the orbital theory of the ice ages: development of a high-resolution 0 to 300,000 years chronostratigraphy. Quaternary Research 27, 1–27.

McMurtry, G. M., Watts, P., Fryer, G. J., Smith, J. R., Imamura, F. (2004): Giant landslides, mega-tsunamis, and paleo-sea level in the Hawaiian Islands, Marine Geology 203, 219-233.

Mienert, J., Bünz, S., Guidard, S., Vanneste, M., Berndt, C. (2005a): Ocean bottom seismometer investigations in the Ormen Lange area offshore mid-Norway provide evidence for shallow gas layers in subsurface sediments, Marine and Petroleum Geology 22, 287–297.

Mienert, J., Vanneste, M., Bünz, S., Andreassen, K., Haflidason, H., Sejrup, H.P. (2005b): Ocean warming and gas hydrate stability on the mid-Norwegian margin at the Storegga Slide, Marine and Petroleum Geology 22, 233–244.

Millo, C. , Sarnthein, M. , Erlenkeuser, H. , Grootes, P.M. , Andersen, N. (2005): Methane-induced early diagenesis of foraminiferal tests in the southwestern Greenland Sea, Marine Micropaleontology, 58 (1), 1-12.

Nørgaard-Pedersen, N., Spielhagen, R.F., Erlenkeuser, H., Grootes, P.M., Heinemeier, J., Knies, J. (2003): The Arctic Ocean during the Last Glacial Maximum: Atlantic and Polar domains of surface water mass distribution and ice cover. Paleoceanography 18 (3), 1063, doi:10.1029/2002PA000781.

Ottesen, D., Dowdeswell, J.A., Rise, L. (2005): Submarine landforms and the reconstruction of fast-fl owing ice streams within a large Quaternary ice sheet: The 2500-km-long Norwegian-Svalbard margin (57°–80°N), GSA Bulletin, 117 (7/8), 1033–1050, doi: 10.1130/B25577.1.

Paull, C.K., Brewer, P.G., Ussler, W. III, Peltzer, E.T., Rehder, G., Clague, D. (2003): An experiment demonstrating that marine slumping is a mechanism to transfer methane from seafloor gas-hydrate deposits into the upper ocean and atmosphere, Geo-Marine Letters, 22 (4), 198-203.

Salvigsen, O. (1977): Radiocarbon datings and the extensions of the Weichselian ice-sheet in Svalbard, Norsk Polarinstitutt Årbok 1976, pp. 209-224, Norsk Polarinstitutt, Oslo.

Salvigsen, O. & Österholm, H. (1982): Radiocarbon dated raised beaches and glacial history of the northern coast of Spitsbergen, Svalbard, Polar Research 1, 97-115.

Sauber, J. M., Molnia, B. F. (2004): Glacier ice mass fluctuations and fault instability in tectonically active Southern Alaska, Global and Planetary Change 42, 279–293

Schäfer, C. (2005): Untersuchungen zu Menge und Zusammensetzung des Organischen Kohlenstoffs in spätquartären Sedimenten des Yermak-Plateaus (Arktischer Ozean) und Umweltbedingungen. Master thesis, Univ. of Trier, 105 pp.

Schauer, U., Fahrbach, E. Osterhus, S, Rohardt, G. (2004): Arctic warming through Fram Strait: Ocean heat transport from 3 years of measurement, Journal of Geophysical Research 109 (C06026), doi: 10.1029/2003JC001823.

Schlichtholz, P. and M.N. Houssais (1999a): An inverse modeling study in Fram Strait, Part 1: dynamics and circulation, Deep-Sea Research II(46), 1083-1135.

Schlichtholz, P. and M.N. Houssais (1999b): An inverse modeling study in Fram Strait, Part 2: water mass distribution and transports, Deep-Sea Research II(46), 1137-1168.

Smith, L.M., Sachs, J.P., Jennings, A.E., Anderson, D.M., deVernal, A. (2001): Light ^{13}C events during deglaciation of the East Greenland continental shelf attributed to methane release from gas hydrate, Geophysical Research Letters, 28 (11), 2217-2220.

Spielhagen, R. F., Baumann, K.-H., Erlenkeuser, H., Nowaczyk, N. R., Nørgaard-Pedersen, N., Vogt, C., Weiel, D. (2004): Arctic Ocean deep-sea record ofnorthern Eurasian ice sheet history, Quaternary Science Reviews 23, 1455-1483.

Stein, R. (Ed.) (2005): Scientific Cruise Report of the Arctic Expedition ARK-XX/3 of RV "Polarstern" in 2004: Fram Strait, Yermak Plateau and East Greenland Continental Margin, Reports on Polar and Marine Research 517.

Sultan, N., Cochonat, P., Foucher, J.P., Mienert, J. (2004): Effect of gas hydrates melting on seafloor slope instability, Marine Geology 213, 379– 401.

Svendsen, J.I., Alexanderson, H., Astakhov, V.I., Demidov, I., Dowdeswell, J.A., Funder, S., Gataullin, V., Henriksen, M., Hjort, C., Houmark-Nielsen, M., Hubberten, H.W., Ingólfsson, Ó., Jakobsson, ́M. Kjær, K.H., Larsen, E., Lokrantz, H., Lunkka, J.P., Lysså, A., Mangerud, J., Matiouchkov, A., Murray, A., Möller, P., Niessen, F., Nikolskaya, O., Polyak, L., Saarnisto, M., Siegert, C., Siegert, M.J., Spielhagen, R.F., Stein, R. (2004): Late Quaternary ice sheet history of northern Eurasia, Quaternary Science Reviews 23, 1229–1271.

Vanneste, M., S. Bünz, S. Iversen, and S. Yang (Eds.) (2004): R/V Jan Mayen Cruise Report, NFR Strategisk Universitets Prosjekt (SUP)–Slope Stability, 52 pp., Inst. for Geol., Univ. I Tromso¨ , Tromso¨ , Norway.

Vanneste, M., Guidard, S., Mienert, J. (2005): Bottom-simulating reflections and geothermal gradients across the western Svalbard margin, Terra Nova, 17 (6), 510-516, doi: 10.1111/j.1365-3121.2005.00643.x.

Vanneste, M., J. Mienert, Bünz, S. (2006): The Hinlopen Slide: A giant, submarine slope failure on the northern Svalbard Margin, Arctic Ocean, Earth and Planetary Science Letters 245, 373-388.

Vogt, C., Knies, J., Spielhagen, R. F., Stein, R. (2001): Detailed mineralogical evidence for two nearly identical glacialrdeglacial cycles and Atlantic water advection to the Arctic Ocean during the last 90,000 years, Global and Planetary Change 31, 23-44.

Winkelmann, D., Stein, R., Niessen, F. (2004): The Yermak Slide north of Svalbard (Arctic Ocean) - Preliminary Results, 2nd EUROMARGINS Conference, Palau de les Heures, 11-13 Nov., Barcelona, Spain.

Winkelmann, D., W. Jokat, F. Niessen, R. Stein, and A. Winkler (2006a): Age and extent of the Yermak Slide north of Spitsbergen, Arctic Ocean, Geochemistry Geophysics Geosystems 7, Q06007, doi:10.1029/2005GC001130.

Winkelmann, D., Jokat, W., Niessen, F., Stein, R., Winkler, A. (2006b): Dynamic and Timing of the Yermak/Hinlopen Slide, Arctic Ocean, European Geosciences Union General Assembly 2006 Vienna, Austria, 02 – 07 April 2006.

Winkelmann, D., Geissler W., Schneider, J., Stein, R. (2007): Dynamic and Timing of the Hinlopen/Yermak Megaslide north of Spitsbergen, Arctic Ocean, (submitted to Marine Geology).

Chapter V

Terrigeneous Events and Paleoceanography of the Sophia Basin north of Spitsbergen, Arctic Ocean

Comments on Chapter V

Within the following chapter V credit is paid to the recovery of sediment cores with excellent records of paleo-environmental changes within the Sophia Basin north of Svalbard during the ESF project. Since the main focus of this study lays on the Hinlopen/Yermak Megaslide, the content of the following chapter should therefore be considered as *additional work*. However, the chronology of events and paleo-environmental interpretation of the megaslide presented within chapters II to IV benefited strongly from this work.

The chapter contains three more or less individual topics that originate from the methodical section and are presented subsequently. The part on terrigeneous events within the Sophia Basin and their implication for the glaciation history of Svalbard is very well constraint and will be prepared for publication later this year. The following part on Atlantic water inflow and primary productivity needs corroboration from mineralogical analysis which will be a future topic. The later, more conceptual part on circulation scenarios represents both a possible interpretation of our data presented before and its corroboration from published work.

Despite its in parts preliminary character, the layout of chapter V has been adjusted to a publication style to keep a consistent appearance of this dissertation.

Terrigeneous Events and Paleoceanography of the Sophia Basin north of Spitsbergen, Arctic Ocean

Daniel Winkelmann

Alfred Wegener Institute for Polar and Marine Research
Additional work; to be prepared for future publications later this year.

Abstract

Here we present a suite of new sediment cores from the Sophia Basin north of Svalbard that recorded a consistent climate history. The records can be directly correlated to Greenland's ice core data and give evidence for fluctuations in terrigeneous input into the Sophia Basin. By application of combined parameters (Sr/Ca, C/N, IRD etc.) we identified a number of terrigeneous input events throughout the last 240 kyr. BP. These events can be considered synchronous and used as time markers. The Sr contents from XRF scanning probably reflect primary productivity due to inflow of Atlantic water in this region. Their fairly good correlation to planktic $\partial^{13}C$ of *N. Pachyderma sin.* can be used for fast establishments of age models for sediment cores. Based on a conceptual circulation model, the North Atlantic climate system changed between circulation-controlled and solar-forced modes during the last 240 kyr. BP. Peak glaciations of the Late Saalian and Late Weichselian occurred during and probably due to a circulation-driven mode. The early Weichselian glaciation is not documented in our sediment cores. Thus, Svalbard was probably not experiencing an extensive glaciation between 115-100 kyr. BP (Glaciation C of the Svalbard glaciation curve; cf. Mangerud et al., 1998), perhaps due to remnant glacial inundation. The Mid Weichselian glaciation (MIS4/3) occurred during the solar-forced mode and minimum insolation.

Introduction

The relevance of past climate behaviour becomes evident in the view of future global warming perspectives. Coupled ocean-atmosphere numeric models and their computed climate climate predictions depend heavily on the input of the base-line starting conditions (c.f. CLIMAP 1976, 1981; GLAMAP, Pflaumann et al., 2003). Thus, the reliability of these scenarios is limited with confidence that the starting scenario is correct. As a consequence, scientists concentrated on the establishment of a synthesis of paleo-environmental conditions at precise temporal windows such as the LGM (Mix et al., 2001; de Vernal et al., 2006). In this context, well-dated high or ultra-high-resolution records of paleo-proxies from terrestrial,

marine and cryogenic archives obtained from globally distributed keey-ares are of major importance. One of these key-areas is certainly the Fram Strait/Yermak Plateau area, i.e. the only deep water conection between the Arctic and the North Atlantic Oceans.

The semi-enclosed Sophia Basin, positioned between the Yermak Plateau and the adjacent shelf of Spitsbergen (Figure 1), constitutes an excellent sedimentary archive recording environmental changes. Within the ESF project "Slope stability on Europe's passive continental margins" Winkelmann et al., (2006a) investigated the Hinlopen/Yermak Megaslide north of Svalbard that covers most of the basin's surface. During ARK-XX/3 we recovered a total number of 14 gravity cores from the Sophia Basin (Stein, 2005) to characterise extent, dynamics and paleo-environmental conditions of this megaslide (Winkelmann et al., 2006a, b) and to study the past oceanography and glacial history of the Sophia Basin and adjacent northern Svalbard, the main focus of this paper.

Modern Surface Circulation Pattern

The surface water circulation pattern around Svalbard and its main island Spitsbergen is characterised by the northward flowing West Spitsbergen Current (WSC) transporting warm and saline Atlantic water into the Arctic Ocean via Fram Strait (Schlichtholz & Houssais, 1999; Figure 1). This current is separated from the archipelago by Arctic type waters of the East Spitsbergen Current (ESC; Svendsen et al., 2002). The East Greenland Current (EGC) acting as a counter part to the WSC, transports less saline and colder Arctic water via Fram Strait into the Greenland Sea (Figure 1). The polar front is accordingly situated along these water boundaries and its seasonal variation characterise the Fram Strait region. Branches of the WSC flush the outer shelf west and north-west of Spitsbergen (North Svalbard Current, NSC) and the Yermak Plateau (Yermak Slope Current, YSC; Yermak Plateau Current, YPC)(Schlichtholz & Houssais, 1999). Especially the NSC transports Atlantic water into the Sophia Basin (Schauer et al., 2004; Figure 1) keeping the south-eastern part of the basin seasonally free of ice.

Glacial History

Following the large Late Saalian glaciation, the archipelago has been repeatedly and heavily glaciated during the Weichselian Glacial, i.e. between 115-105, 75-50 and 25-10 kyr. BP (Mangerud et al., 1998, Svendsen et al., 2004). These glaciations have been reconstructed mainly on the basis of terrestrial and marine geologic evidence (Mangerud et al., 1992, 1996, 1998; Landvik et al., 1998). Svalbard experienced a warm period with accompanied by marine transgression during early Marine Isotope Stage (MIS) 5, its earliest onset probably synchronous with the Eemian interglacial. At the end of this period, a glacial

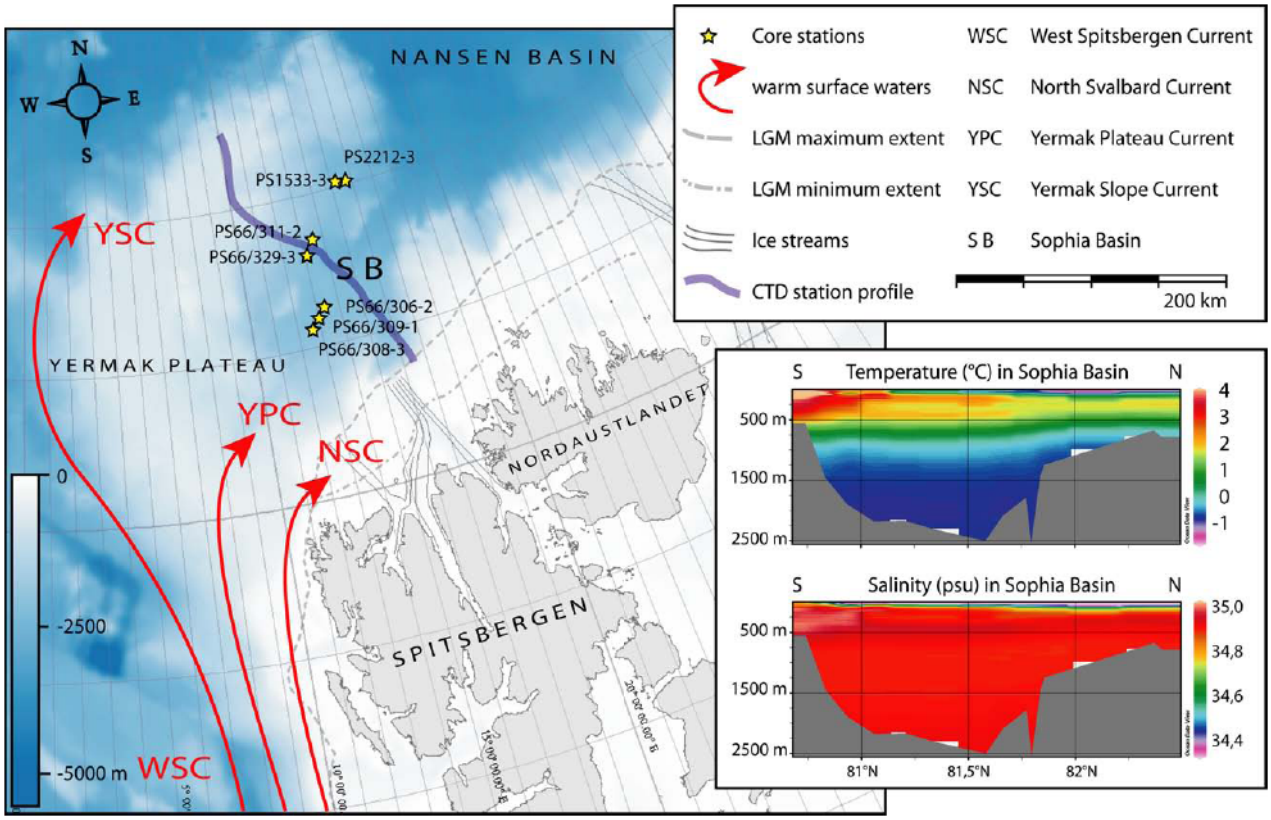

Figure 1: Map of N-Svalbard with (modern) surface circulation, ice sheet extent during the LGM (according to Landvik et al 1998; Svendsen et al., 2004), ice streams north of Svalbard (according to Ottesen et al 2005), location of gravity cores. Water temperature and salinity distribution within the Sophia Basin (Schauer et al., 2004). Bathymetry: IBCAO (Jakobsson et al., 2000).

advance and sea level retreat culminating around 115 kyr. BP. is documented elsewhere and has been termed the Early Weichselian Glaciation. On Svalbard, however, this glaciation is not well constraint and under discussion. The subsequent cold period led with moderate ice extent into another extensive glaciation that peaked during the MIS3/4 boundary around 60 kyr. BP (the Mid Weichselian Glaciation; Glaciation E on Svalbard according to Mangerud et al., 1998; Figure 6). Following global sea-level rise and probably still inundated morphology on Spitsbergen, a local transgression is documented as marine sediments in a number of sites on modern Svalbard (e.g. Landvik et al., 1998; Mangerud et al., 1998 and references therein). Around 30 kyr. BP a drastic drop in sea-level accompanied with the rapid and extensive onset of the Late Weichselian Glaciation, is recorded in the terrestrial and marine archives and led to a major slope failure event north of Svalbard (Hinlopen/Yermak Megaslide) which affected most of the semi-enclosed Sophia Basin (Lambeck et al., 2002, Mangerud et al., 1998, Winkelmann & Stein, 2007). This Late Weichselian Glaciation culminated with maximum ice sheet extents around 23-19 cal. kyr. BP and is usually referred to as the Late Glacial Maximum (LGM; e.g., Schneider et al., 2000; Mix et

al., 2001). The termination of this last glacial was characterised by a rapid deglaciation and transgression and led via a climate oscillation (Bølling/Allerød and Younger Dryas) into the modern interglacial, the Holocene. Emergence pattern of coast lines, documented as raised beaches, during the last ~20 kyr. BP give some hints on the largest glacial deposition centres on Svalbard and the Barents Sea (e.g. Landvik et al., 1998 and references therein, Forman & Ingólfsson, 2000).

Material and Methods

Detailed bathymetric data and high-resolution ground-penetrating echo-sounding data were acquired by the HYDROSWEEP DS2 and the PARASOUND Hydromap Control systems, respectively, aboard RV "Polarstern" during cruise ARKXX/3 (Stein, 2005). Additional data from cruise ARKXV/2 of RV "Polarstern" (Jokat, 2000) have been compiled to analyse the area and structure of the Hinlopen/Yermak Megaslide (Winkelmann et al. 2006a, b). Based on this synthesis, coring sites have been carefully selected along PARASOUND profiles crossing the well developed marginal facies of the mega slide during cruise ARKXX/3 (Stein, 2005). A total number of 14 gravity cores has been taken from key locations. Beside the standard gravity coring equipment the giant gravity corer (Kastenlot, 30x30x1500cm) has been applied to yield sufficient sedimentary material for dating from key sites (Stein, 2005). Multi-sensor core logging (MSCL), opening of cores, core description, x-ray radiography and standard sampling have been performed aboard RV "Polarstern".

We chosed two cores PS66309-1 KAL (giant gravity core) and PS66/308-3 SL as key-cores for the paleoceanographic characterisation. Both cores appear not affected by gravity-driven sediment flows (debris flows, slumps etc.) except for the slide-related marginal turbidite and the following fining-upwards sequence (which they were intended to recover, c.f. Winkelmann et al., 2006a). Recovered ~10 km away from each other, they show an excellent correlation of all measured parameters (MSCL, bulk parameters, IRD) confirming a joint history of paleo-environmental changes.

Core	Latitude	Longitude	Waterdepth	Recovery	Type
PS1533-3	82° 01,9' N	15° 10,7' N	2030 m	477 cm	Gravity core
PS2212-3	82° 04.2' N	15° 43,0 E	2550 m	735 cm	Giant kasten core
PS66/306-2	81° 14,5' N	13° 18,6' E	2268 m	350 cm	Gravity core
PS66/308-3	81° 07,3' N	12° 35,9' E	2218 m	554 cm	Gravity core
PS66/309-1	81° 11,2' N	12° 59,1' E	2269 m	765 cm	Giant kasten core
PS66/311-2	81° 41,8' N	13° 28,2' E	2192 m	493 cm	Gravity core
PS66/329-3	81° 36.3' N	13° 6.1' E	2211 m	482 cm	Gravity core

Table 1: Gravity cores of this study.

Core PS66/309-1 was sampled continuously at 2-3 cm intervals for tests of *Neogloboquadrina pachyderma (sin.).* Stable oxygen ($\partial^{18}O$) and carbon ($\partial^{13}C$) isotopes were measured by standard techniques (Duplessy, 1978) on the automated Carbo-Kiel device connected to a Finnigan MAT 251 mass spectrometer. The external analytical reproducibility is 0.08‰ and 0.04‰ for $\partial^{18}O$ and $\partial^{13}C$, respectively. Total carbon, total organic carbon and total nitrogen were determined by means of a LECO CNS analyser (Schäfer, 2005). IRD was counted according to Grobe (1987) as lithogenic particles from the x-ray radiographies.

X-ray Fluorescense analysis was performed on a Avaatech automated (XRF) core scanner at the Alfred Wegener Institute in Bremerhaven, Germany. Split core segments were scanned at 10 and 30 KV. The standard model for marine sediments including Al, Si, P, S, Cl, K, Ca, Ti, Cr, Mn, Fe, Co, Rh, Ba, Cu, Zn, Ga, Br, Rb, Sr, Y, Zr, Au, Pb, Bi was used for calculation of elemental activities. A density correction for light elements (Al, Si) of the core top (c.f. Tjallingii et al., 2007) was not applied.

Stratigraphy

The stratigraphy of core PS66/309-1 KAL was deduced from its oxygen and carbon isotope records (Figure 2), which were correlated to the global isotope curve SPECMAP stack (Martinson et al., 1987).Ages of MIS boundaries and events have been corrected according to Lisiecki & Raymo (2005) and Thompson & Goldstein (2006). Four AMS ^{14}C dates of *N. pachyderma (sin.)*(Winkelmann et al., 2006a, b) helped to pinpoint MIS 2 and 3 and one has been correlated from core PS1533-3 (Spielhagen et al., 2004) to pinpoint MIS1 (Table 2). The stratigraphic framework is also supported by correlation to PS2212-3 KAL which has an established stratigraphic model ranging from MIS 1 to 6 (Vogt et al., 2001). Although characterised by core intervals with no foraminifers, e.g. Termination 1, its stratigraphic model was additionally based on the occurrence of the benthic foraminifera *Pullenia bulloides*, a stratigraphic marker for the MIS 5/4 boundary in the Nordic Seas (cf. Haake & Plaumann, 1989) and correlation of geochemical and mineralogical parameters (Vogt et al., 2001).

Well-dated melting events during Termination I, e.g. at 14.5 ^{14}C-kyr BP have been recognised in the adjacent areas (cf. Hebbeln et al., 1994). In core PS66/309 a series of meltwater peaks characterise the MIS 2. We date the most prominent peak at 15,66 ± 70 ^{14}C-kyr BP (18,491 ± 237 cal. kyr. BP).

The MIS 3/2 boundary is characterised by a well-defined sequence of sedimentological, mineralogical and organic–geochemical parameters in all sediment cores in the region (cf. Andersen et al., 1996; Vogt et al 2001; Figures 2 and 3). The middle part of this interval exhibits lamination and contains high amounts of mature terrestrial organic material and among other, very low carbonate contents (Vogt et al., 2001). This

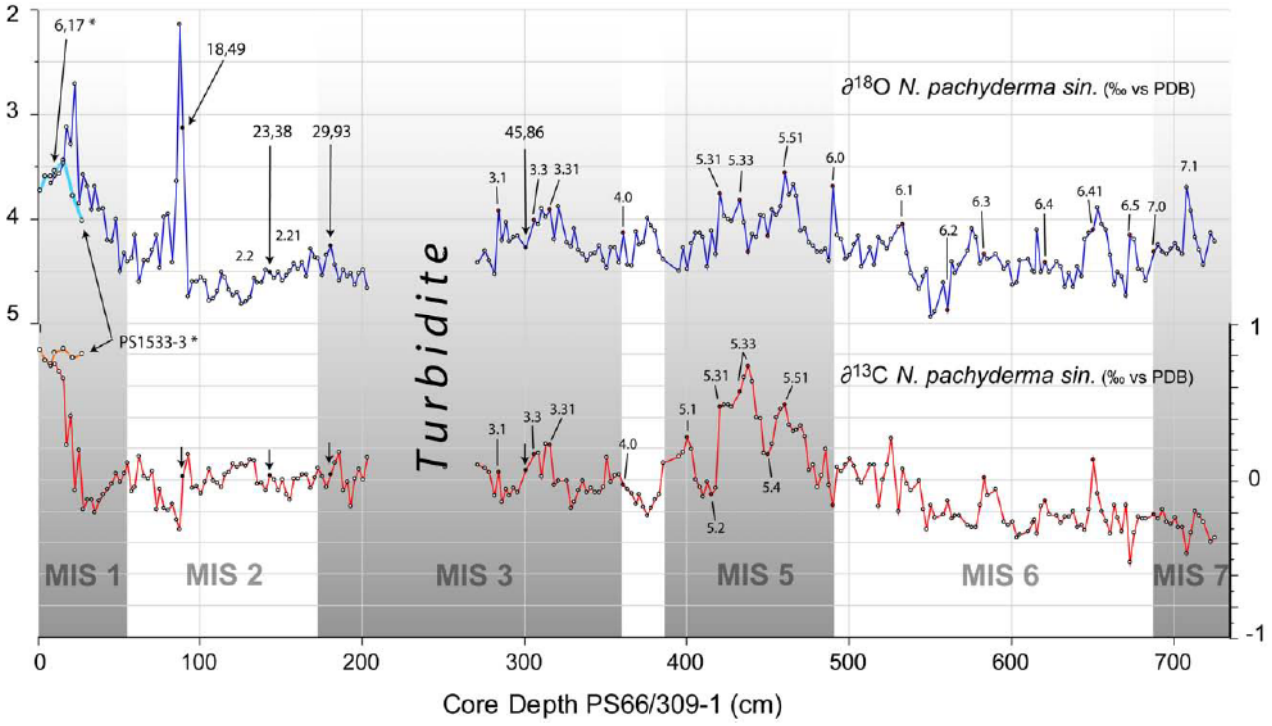

Figure 2: Stratigraphy based on ∂^{18}O of *N. pachyderma sin.* and AMS radiocarbon dates of core PS66/309-1 KAL (indicated slide related turbidite of the Hinlopen/Yermak Megaslide; cf. Winkelmann et al., 2006a). * The youngest radiocarbon date (6,17 ^{14}C kyr. BP) has been correlated from PS1533-3 (Spielhagen et al., 2004; light blue and orange lines for the upper core).

layer has been labelled Event I according to Knies & Stein, 1998 and has been deposited between 22.5 and 19.5 ^{14}C ka BP as based on several AMS ^{14}C-ages; approximately 26–22 kyr. cal. BP according to Voelker et al., 1998. In core PS66/309-1 KAL the closest AMS ^{14}C date directly above this layer gives an age of 20,02 ± 140 ^{14}C kyr. BP (23379 ± 394 cal. kyr. BP, Table 2, Figure 3). Assuming it to be a synchronous deposit in all sediment cores we use it as one indicator of the lowermost MIS 2 (Figure 2). However, following the age correction (Lisiecki & Raymo, 2005), the MIS2/3 boundary is best defined by our closest AMS date (Table 2). The MIS3/4 boundary is based upon an increase to peak values in ∂^{13}C in the early MIS 3 shortly after a typical peak in the C/N ratios that is not reflected in the TOC signal and the onset of intensive ice rafting at the MIS4/3 boundary. This interval is characterised by a carbonate minimum too. A typical decrease of the ∂^{13}C values from late MIS 5 to lowest values in early MIS 4 is observed and used as a regional stratigraphic fixpoint for the MIS4/5 boundary (cf. Dokken & Hald, 1996; Nørgaard-Pedersen et al., 1998; Spielhagen et al., 2004). The MIS5/6 boundary is based on the ∂^{18}O melt water peak that is accompanied by peak IRD concentration shortly after a characteristic C/N peak (that again is not reflected in the TOC record), a distinct carbonate minimum and a density maximum, indicating Termination II.

Age (cal. kyr. BP)	*MIS**	*PS66/309-1 (cm core depth)*	*PS66/308-3 (cm core depth)*	*Reference #*
10,9		***15,5***		***6***
18,49	-	***89,5***	72,6	4
23,38	-	***143***	111,2	5
29,93	-	***180,5***	141,8	4
31,1	3.1	283,0		1
45,86	-	***300,5***	216,8	4
47,8	3.3	305,5	224,8	1
52,2	3.31	315,5	234,8	1
57	4.0	360,0	279,8	2
67,7	4.23	385,0 ?	290,4	1
71	5.0	385,5	299,0	2
80,5	5.1	400,5	312,2	1
91,3	5.2	415,5	324,6	1
100,3	5.31	420,5	330,8	1
104,0	5.33	433,0	335,0	1
108,5	5.4	450,5	351,4	1
122,6	5.51	460,5	357,8	1
129,3	6.0	490,5	381,4	1
135	6.2	560,5	408,0	3
142	6.3	583,0	416,0	3
153,9	6.4	620,5	428,8	1
164,0	6.41	650,5	441,6	1
172,9	6.5	673,0	451,4	1
179,2	7.0	688,0	457,2	1
190,8	7.1	708	463,8	1

Table 2: Age fix points of refined age models for both cores. AMS radiocarbon dates from PS66/309-1 were correlated to PS66/308-3 by their Ca and carbonate records. References for MIS event ages: 1: Thompson & Goldstein (2006); 2: Lisiecki & Raymo (2005); 3*: SPECMAP event numbers from Martinson et al. (1987); 4: AMS radiocarbon dates (bold italic) from Winkelmann et al. (2006a); 5: Winkelmann et al. (2007); 6: Spielhagen et al. (2004).

The definition of MIS boundaries is further supported by a correlation to the Greenlands ice core data (N-GRIP and GRIP), which was used for a refined correlation within the isotope stages (see below).

The stratigraphic model for the sediment cores from transsects across the Hinlopen/Yermak Megaslide's western margin in Sophia Basin has been established by correlation to PS66/309-1 KAL (Winkelmann et al., 2006a, b; Figure 3). Further support of this correlation comes from core PS2128-2 SL (Winkelmann et al., 2007).

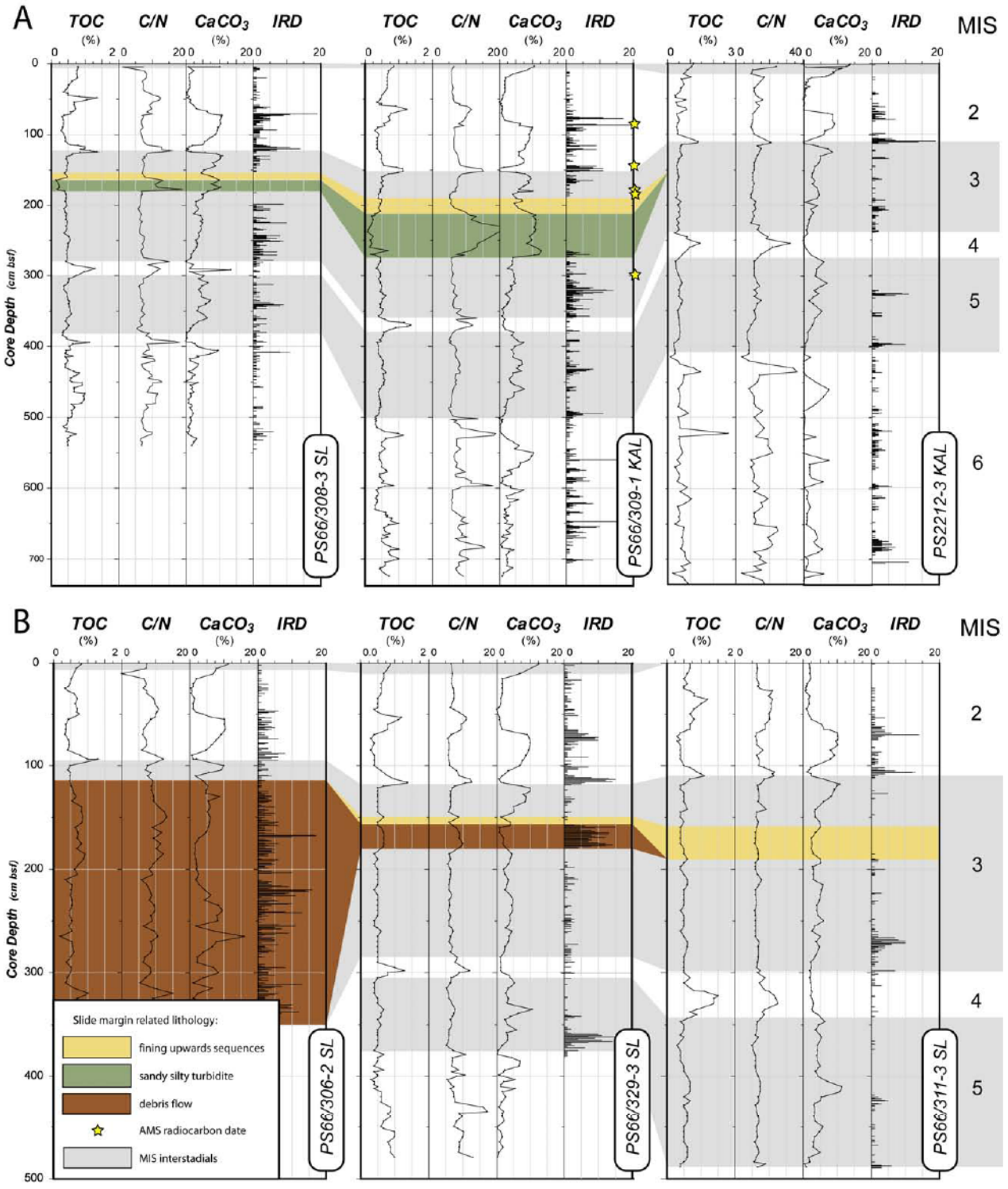

Figure 3: Stratigraphical correlation of core records (geochemical parameters, IRD) of A: cores PS66/308-3 SL, PS66/309-1 KAL from the western Sophia Basin and PS2212-3 KAL (Vogt et al., 2001) from the north-eastern Yermak Plateau; B: of cores PS66/306-2 SL, PS66/329-3 SL and PS66/311-3 SL from the western Sophia Basin. For location see Figure 1.

Ca and Sr recorded in the SW Sophia Basin

Key core PS66/308-3 has been scanned (XRF) for a set of elements including Sr and Ca for a detailed paleo-environmental / paleoceanographic interpretation. First results indicate a complex pattern of variable element distribution within the SW-Sophia Basin during the last ~240 kyr. Here, we focus on the Ca and Sr-record as well as a set of elements that mark certain core intervals by peak concentrations. Considering the complexity of this relative new XRF method with respect to minimum Sr activity (statistical error relative to detected counts: $n^{0,5}/n$), possible interference of element spectra, density and water content changes we stress that the presented XRF data should be treated with care. We are aware that further studies are needed to corroborate the relationships presented in this study to verify our interpretations. However, since the Sr and Ca activity and the calculated carbonate contents exhibit systematic variations in trends and variability we feel confident that the measured Ca and Sr activities reflect the elemental bulk contents and can be used as such for interpretation.

As glacial/interglacial cycles are reflected in stable oxygen isotopes of carbonaceous shells of foraminifera, they influence the Sr budget of the ocean (Stoll & Schrag, 1996). Compared with Sr/Ca variability in modern marine sediments of less than 2% (de Villiers et al., 1994; de Villiers, 1999), Sr/Ca ratios vary between 1-3% over Quaternary glacial/interglacial cycles (Stoll & Schrag, 1998). Sr/Ca ratios of biogenic carbonate has been used for reconstruction of lacustrine paleo-salinities (Chivas et al., 1985; 1986), for temperature calibration and reconstruction (Shen et al., 1996; Elderfield et al., 2000; Haase-Schramm et al., 2003; Swart et al., 2002; Sosdian et al., 2006), reconstruction of paleo-sea-water Sr/Ca (e.g. Stoll et al., 1999; Elderfield et al., 2000) or reconstruction of marine paleo-productivity (Stoll & Bains, 2003). A good correlation between Sr/Ca record from XRF analysis of marine bulk sediment and the SPECMAP $\partial^{18}O$ curve has been reported by Wien et al. (2005) for sediment cores from the Cape Basin of the southern Benguela upwelling system.

Sr is known to substitute Ca within biogenic calcites, a process which is temperature dependent (e.g. Shen et al., 1996; Elderfield et al., 2000; Swart et al., 2002; Rosenthal et al., 2006; Sosdian et al., 2006). Larger cations like Ba and Sr form exclusively orthorhombic carbonates (Gabitov & Watson, 2006) and hence substitute the Ca much easier in aragonite than in calcite. Gaetani & Cohen (2006) demonstrated that during pure chemical precipitation, aragonite displays a negative correlation of temperature and trace metal concentration (Mg, Ba, Sr). This stands in clear contrast to observed positive correlations in biogenic carbonates and thus, highlights the importance of the “vital effect” of living organisms (Rickaby et al., 2002; Gabitov & Watson, 2006; Gaetani & Cohen, 2006). Quaternary changes in the ocean's Sr budget have been attributed to recrystallisation of aragonite to calcite on the exposed shelves during

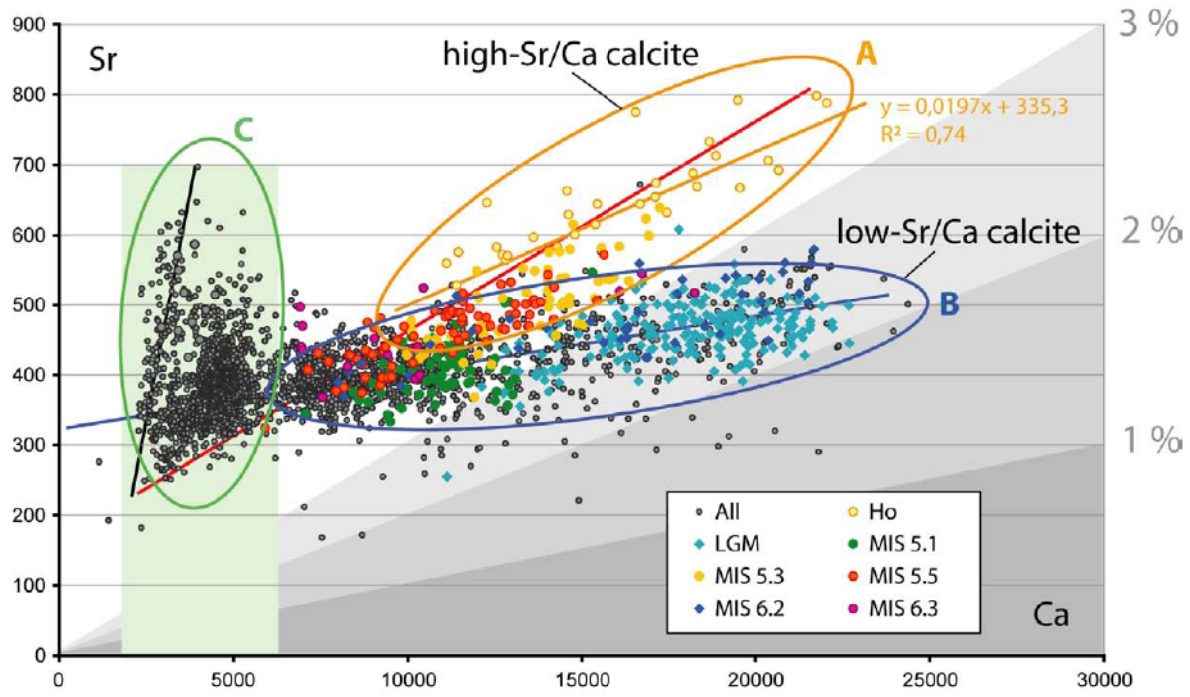

Figure 4: Relation of Sr to Ca from XRF elemental analysis. The distribution pattern clearly shows two linear relationships of Sr to Ca (group A and B; blue and orange ovals) indicating a joint mineralogical source (calcite) and a group of points with very low/no linear relationship (group C; green oval), indicating an additional mineralogical Sr-source. This latter group constitutes the input of terrigeneous Sr-rich minerals. The indicated strong linear relation (black line) for a sub-suite of this group might point towards aragonite (but might also be an artefact, thus pointing to silicates, see text for discussion). The second group (orange oval) displays a slightly higher Sr/Ca ratio and thus might indicate a higher temperature during calcification. Their members date mostly into the Early Holocene and MIS 5.3 – the warmest intervals in our record (coloured indication only for prominent and Early Holocene samples).

glacials leading to elevated Sr/Ca ratios in the ocean contemporaneous with $\partial^{18}O$ changes (Schlanger, 1988; Stoll & Schrag, 1998; Martin et al., 1999). In addition to the oceanic Sr budget, the Sr/Ca ratio of biogenic carbonate appears to be influenced by species-specific incorporation of Sr (e.g. Elderfield et al., 2000; Anand & Elderfield, 2005), growth-/calcification rate (Stoll & Schrag, 2000; Rickaby et al., 2002, Gabitov & Watson, 2006), shell size (Elderfield et al., 2002) and temperature (e.g. Elderfield et al., 2000; Rosenthal et al., 2006). The interpretation of the Sr/Ca record of bulk marine sediment is therefore a complicated affair, but can still gives valuable insight into past environmental changes (e.g. Wien et al., 2005).

The Ca record of core PS66/308-3 correlates perfectly with the measured carbonate contents. Thus, the Ca record is interpreted to be mainly controlled by the concentration of $CaCO_3$ in the record. Therefore a bias of terrigeneous dolomite (c.f. Vogt et al., 2001) appears unlikely or only of minor importance. The Sr record displays a clear positive correlation with the Ca and the $CaCO_3$ record. Therefore, we interpret the Sr as dominantly hosted within calcite and the Sr-concentration record in bulk sediment mainly controlled

by:

i the concentration of calcite (the dominant Ca-bearing mineral in our case);

ii the temperature during calcification;

iii the availability of Sr during calcification; and

iv the input of terrigenous Sr-bearing minerals.

The calcite concentration (i) is controlled by (a) primary productivity, (b) dilution and (c) dissolution. In our study area, the record appears not to be affected by dissolution (c). All intervals with low carbonate concentrations contain foraminifera and coincide with intervals of higher C/N ratios, TOC contents and density, all pointing towards higher terrigeneous input. Thus, the carbonate record appears free of dissolution effects (c) and is mainly controlled by primary productivity (a) and dilution (b).

Primary productivity (a) north of Svalbard is related to higher influx of Atlantic water and associated open water conditions (e.g. Hebbeln et al., 1994; Knies et al., 2000; Hald et al., 2001; Nørgaard-Pedersen et al., 2003) which involves the proximity of the marginal ice zone (MIZ; e.g. Owrid et al., 2000). The main biogenic carbonate-producing component aside coccolithophorida of these Arctic high productivity events is *N. pachyderma*. Both exhibit a positive correlation of their carbonate Sr/Ca to calcification temperature. The Sr/Ca ratio of *N. pachyderma* displays the strongest impact (9,7%) during glacial/interglacial cycles in the Nordic Seas, similar in character with the carbonate's $\partial^{18}O$ (Elderfield et al., 2000) which might point towards a dominant temperature control (ii).

The Sr/Ca ratios of foraminifera and coccolithophorids are additionally affected by the calcification rate (Rickaby et al., 2002; Stoll et al., 2002). The relationship appears to be controlled by kinetic effects (to a minor degree) and the availability of dissolved inorganic and particulate inorganic and organic carbon and carbon dioxide ($CO_2(aq)$) in surface waters. This relation has been reported for $\partial^{13}C$ too (e.g. Rickaby et al., 2002). The probable positive relation between Sr/Ca ratios of biogenic carbonate, productivity, temperature availability of carbon species has been related to the biological pump of membranes (see discussion in Rickaby et al., 2002) and might explain partly the positive correlation of bulk sediment Sr and the $\partial^{13}C$ of *N. pachyderma sin*. Therefore, the Sr/Ca ratios of coccoliths can serve as an sedimentation rate-independent productivity proxy once other affecting factors including assemblage changes, Sr/Ca seawater changes, changes in SST and post-depositional alteration can be constrained (Stoll & Bains, 2003).

Whether the Sr/Ca changes are due to variable ratios of coccolithophorida to *N. pachyderma sin.* or whether they are caused directly by temperature changes appears of minor importance because

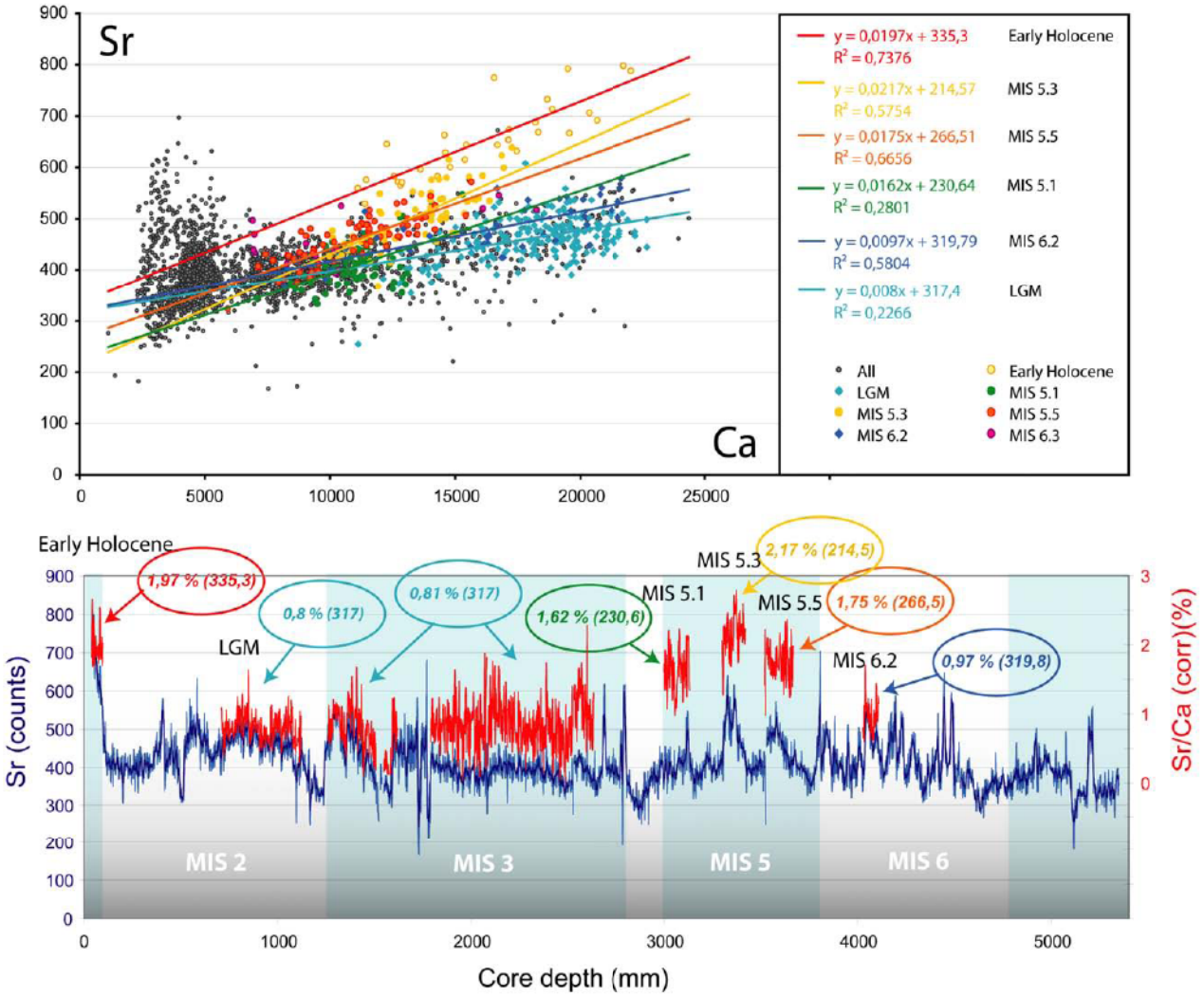

Figure 5: Sr-Ca scatter plot with linear regression of stratigraphic sub-groups. Exemplified, the offsets are used for correction of the associated calcite Sr/Ca ratios. The corrected Sr/Ca ratios represent a qualitative (non-calibrated) SST proxy and are plotted along with the Sr record indicating Atlantic water inflow into Sophia Basin (see text for explanation).

coccolithophorida characterising the higher temperature regime (e.g. Holocene sediments) exhibit the stronger positive relation to temperature with higher ratios. Therefore, we interpret the amount of Sr in bulk sediment as indication for productivity (resulting from Atlantic water inflow and associated open water conditions) and the higher corrected ratios (Sr_{corr}/Ca) of bulk sediment to reflect mainly surface temperature changes. However, the Sr_{corr}/Ca ratios in our bulk sediment might remain difficult to calibrate for a quantitative approach (see below).

The bulk sediment approach of Sr/Ca ratios offers the opportunity to neglect pore water exchange processes (c.f. Schrag et al., 1995) even though authigenic precipitation (e.g. of celestite, SrSO4) may have little influence on the bulk calcite Sr/Ca (c.f. Hampt & Delaney, 1997).

The grouping of our samples around two linear trends within the Sr versus Ca plot (group A and B, Figure 4) indicates the presence of a joint mineral (calcite) which exhibits a low-Sr/Ca and a high-Sr/Ca version. This might point to a temperature control on the Sr/Ca between these groups. However, the detailed effect of the other controlling factors like salinity, carbonate ion effects (Rosenthal et al., 2006) sea-water Sr/Ca (e.g. Martin et al., 1999) and growth parameter (calcification speed and depth, cell size; c.f. Elderfield et al., 2000, 2002; Nyland et al., 2006 and references therein) remains difficult to access.

The dilution aspect (b) of the record is more complex. Intervals with low carbonate concentrations coincide with intervals of higher density, C/N ratios (>9) and TOC contents all pointing towards higher terrigeneous input. In addition these intervals exhibit higher Sr/Ca ratios (>6%) which point to the presence of Sr-rich minerals. In contrast to detrital carbonates of Heinrich layers (IODP Site 1308, re-occupation of DSDP Site 609; c.f. Hodell et al., 2005) that exhibit peaks in the Ca/Sr ratio due to less Sr of the terrigeneous carbonates from the Hudson region, peaks in Sr/Ca measured on bulk sediment reflect enhanced terrigeneous input in our cores.

On Svalbard, and especially within the drainage area of the Hinlopen Trough Sr-containing carbonates crop out (e.g. Halverson et al., 2007). However, at least for the Neoproterozoic carbonates investigated by Halverson et al. (2007), the Sr/Ca ratios (median: 0,059 %; Halverson, pers. comm.) range below the typical marine values of 1-2 % (de Villiers et al., 1994; de Villiers, 1999) and not above. The indicated strong linear relation (black line, Figure 4) might point to a Sr-rich carbonate (aragonite) but might also be an artefact of the sample distribution, having no importance at all. Alternatively, and in accordance with the Sr-Ca plot, the higher amounts of Sr might be hosted within minerals of the plagioclase group as indicated by Siegel et al. (2000) for sediments of the Isfjorden, W-Spitsbergen. With Sr of group C being hosted within silicates, this would explain the missing relation to Ca (Figure 4) since the (higher) Ca concentration is explained by calcite. Alternatively this “Sr-bearing” mineral is zircon which would point to the fact that the the typical spectral peaks of Sr and Zr around 15,6 keV cannot be resolved sufficiently by the WINAXIL software.

With the linear regression line, trend and offset of the calcites (groups A and b, Figure 4) are given. The Sr offset (between 210 and 340 counts) indicates the presence of a non-calcite mineral and can be used for a correction of the individual Sr/Ca values for related core intervals. The trend or inclination is equivalent to the actual mean Sr/Ca ratio of the calcite group. Since the calcite concentration is, aside coccolthophorida, dominated by *N. pachyderma* (which is corroborated by the Sr/Ca range between 1-2 %; c.f. de Villiers et al., 1994; de Villiers, 1999), we might use the corrected Sr/Ca ratios for qualitative and approximated (semi-quantitative) temperature reconstruction as discussed above (Figure 5). The

corrected Sr/Ca ratios range between 1,4 and 2,8 (mean: 1,97) for the Early Holocene and thus approaching the range of modern *N. pachyderna* from core top samples (1,381 mmol/mol; c.f. Elderfield et al., 2000). In contrast to measured Sr/Ca (range: 0,12 mmol/mol) in *N. pachyderna* from core records spanning the last glacial-interglacial transition (Elderfield et al., 2000), our corrected Sr/Ca ratios display a stronger absolute glacial-interglacial range of 1 %. Therefore we consider our corrected Sr/Ca ratios as a qualitative, semi-quantitative temperature proxy.

The (questionable) trend in group C (black line; Figure 4) might further indicate the presence of a Sr-bearing non-carbonate mineral, probably silicate (perhaps plagioclase; c.f. Siegel et al., 2000), during intervals of enhanced terrigeneous input. This is corroborated by a positive linear trend in the Sr-Al scatter plot of a sample sub-group. Therefore, we interpret the Sr/Ca-peaks (>6%) in our cores as a result of higher input of Sr-rich terrigeneous minerals (likely not carbonates) from Svalbard. Thus, the intervals of dilution can be characterised as terrigeneous events leaving the remaining Sr-record to be explained predominantly by productivity.

Since higher productivity north of Svalbard is usually explained by higher influx of Atlantic water with higher temperature and salinity leading to higher production of foraminifera (cf. HP-events; e.g. Hald et al., 2001; Nørgaard-Pedersen et al., 2003), we interpret the Sr-record as indicator for Atlantic water inflow, indirectly mirroring sea surface temperatures with some uncertainties during the terrigeneous events which, however, can be determined by the (uncorrected) Sr/Ca ratio (>6%). The uncertainties during these intervals arise from the lack of terrestrial data that would allow a two-end-member mixing model (c.f. Winkelmann & Knies, 2005 for organic carbon). However, the indirect temperature interpretation (due to higher Atlantic water influx) is able to explain the positive correlation to the $\partial^{18}O$ record of Greenland ice cores (see Figures 7 and 10 below) and corroborated by positive linear trends in the Sr-Ca scatter plot (Figure 4). This correlation is supported by the positive correlation of the Sr record with the isotopic signal of $\partial^{13}C$ *N. Pachyderma sin.* in core PS66/309-1 (Figure 7). Additional support comes from the good correlation of this $\partial^{13}C$ record to the $\partial^{13}C$ of PS2644 which has been correlated to the GRIP ice core in great detail (Voelker 1999, Voelker et al., 1998, 2000).

The $\partial^{13}C$ signal is considered to reflect the ventilation of the ocean (Kroopnick, 1980; Duplessy, 1982; Duplessy et al., 1984; Duplessy & Shackleton, 1985). Thus it can be used as an indication of the intensity of the thermo-haline circulation (THC) that drives the overturning of the North Atlantic. (Duplessy, 1982; Shackleton et al., 1984; Duplessy & Shackleton, 1985; Mix & Faibanks 1985). In addition, the $\partial^{13}C$ signal of planktic foraminifera can be affected by shell size, calcification depth, food $\partial^{13}C$ and changes in primary productivity (resulting in extraction of ^{12}C from the surface waters)(Jansen, 1989 and references

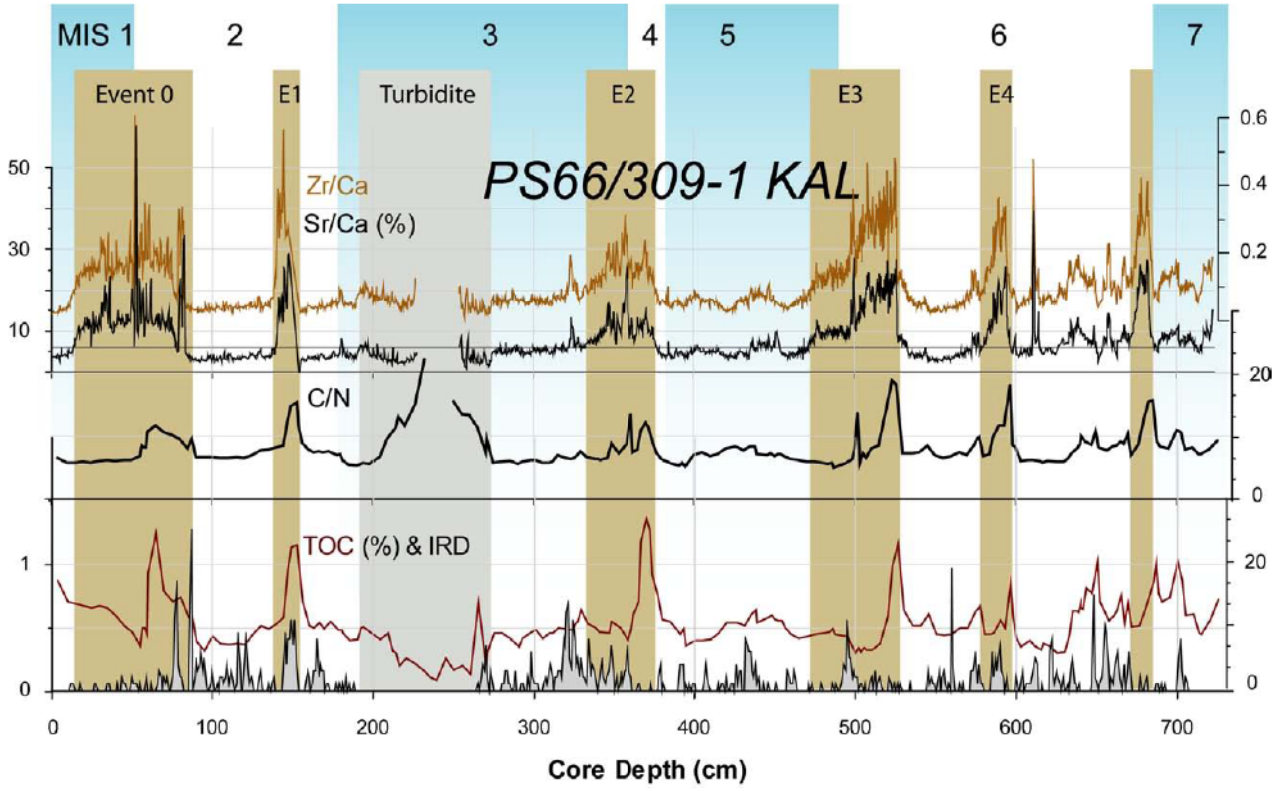

Figure 5: Terrigeneous events (brown boxes) within the Sophia Basin in key core PS66/309-1. Core record of geochemical bulk parameters (TOC, C/N, $CaCO_3$), Sr/Ca, Zr/Ca (XRF ratios) and IRD including indication of slide related lithological units (marginal turbidite; grey box). The peaks of the Sr/Ca ratio indicate increased input of detrital terrigeneous minerals (probably plagioclase; or zircon as indicated by the Zr/Ca record, see text for explanation), from outcropping lithological strata on Svalbard (see text). Thus, the Sr/Ca ratio, here, can be used as proxy for glacial activity. Event 0 reflects Termination I; Event 1 (E1) the Late Weichselian glacial advance to the shelf edge; Event 2 (E2) the onset and termination of the Mid Weichselian Glaciation; Event 3 (E3) Termination II; and Event 4 (E4) reflects the Late Saalian glacial advance to the shelf edge during MIS 6.2. Further events within MIS 6 (e.g. Event 5, etc.) have not been named since they are less consistently recorded in our sediment cores. Note the signal offsets between C/N and Sr/Ca ratios indicating different timing of the sources (Bear Island Trough and Storfjord Trough for C/N and NE-Svalbard for the Sr/Ca ratios).

therein). Despite these difficulties, Labeyrie & Duplessy (1985) showed that the $\partial^{13}C$ records of *N. pachyderma sin.* from high latitudes of both hemispheres provide many similarities.

The Sr record of bulk sediments mirrors primary productivity (with uncertainties for the terrigeneous input events) and likely reflects the inflow of Atlantic water into the Sophia Basin which in return is controlled by the intensity of the Atlantic's THC. Sr and $\partial^{13}C$ records, thus, reflect ocean circulation. The records display joint trends but exhibit distinct differences within certain intervals (e.g. the LGM). In analogue to Wien et al. (2005), Ca and Sr records obtained by XRF scanning may, thus, be used instead of stable isotopic data as a method for fast establishment of age models. In this context, the Sr record seems to be preferable rather than Sr/Ca at least for sediment cores from north of Svalbard.

Terrigeneous Events

As discussed above, the Sr/Ca ratio of bulk sediment in our cores might be less indicative for water temperature rather than changes in the distribution pattern of terrigeneous minerals. Positive excursions of Sr/Ca ratios (>6% to 30%) characterise certain intervals suggesting higher terrigenous input of Sr-rich silicates (perhaps aside aragonite from older carbonaceous rocks cropping out on Nordaustlandet and East Spitsbergen, Edgeøya, Barentsøya; e.g. Halverson et al., 2007 and references therein). The same intervals are characterised by excursions towards lower Rb, Ca, and Sr contents, towards higher Zr, Pb, TOC and IRD contents as well as higher C/N and Ti/Rb ratios (>9; >12 respectively) pointing to episodes of higher terrigeneous sediment supply (Figures 3 and 5).

According to our age model, these intervals of enhanced terrigeneous input of Sr-rich lithogenic material from central Svalbard correspond to the Termination II into MIS 5e, MIS 4 with a strong peak at the MIS 3/4-boundary, the Event 1 near the MIS3/2 boundary (c.f. Knies & Stein, 1998) and Termination I (Figure 5). Further events within MIS 6 can be identified and labelled (Figure 5). These periods are characterised by higher terrigeneous input due to deglaciation into the Eemian warm period, the Mid Weichselian (MIS 3/4) glaciation, the rapid onset of the Late Weichselian (LGM) glaciation and its subsequent de-glaciation respectively. Therefore these terrigeneous events within Sophia Basin reflect higher glacier discharge due to either onset (the SBIS reaches the shelf edge resulting in intensive calving of ice bergs) or termination of a major glaciation (rapid ice-sheet desintegration with following intensive ice berg discharge).

An Early Weichselian Glaciation on Svalbard?

The early Weichselian glaciation described by Mangerud et al. (1996; 1998) as a major glacial advance to the shelf edge is not documented as a terrigeneous event in our sediment cores. These results are in accordance with findings of Knies et al. (1999, 2000, 2001) from the northern Barents Sea Margin and Severnaya Zemlya. The synthesis of terrestrial evidence for a Early Weichselian major ice sheet advance on Svalbard is essentially based on the site interpretation at Kapp Ekholm. There, the identification of this early Weichselian till is based upon intra-site correlation of outcrops (see Mangerud et al., 1998). The wider correlation of the corresponding marine sediments of the Phantom Odden Interstadial is based on luminescence dates. This correlation appears tentative, since the luminescence dates do not show significantly different values for marine sediments of the Interglacial B (Eemian) and the Phantomodden Interstadial that would enclose a diamicton from glacial advances (cf. Mangerud et al., 1998; Forman, 1999). Therefore we question the existence of an Early Weichselian glaciation on Svalbard (Glaciation C of the Svalbard glaciation curve cf. Mangerud et al., 1998) that is still included in the recent view of the

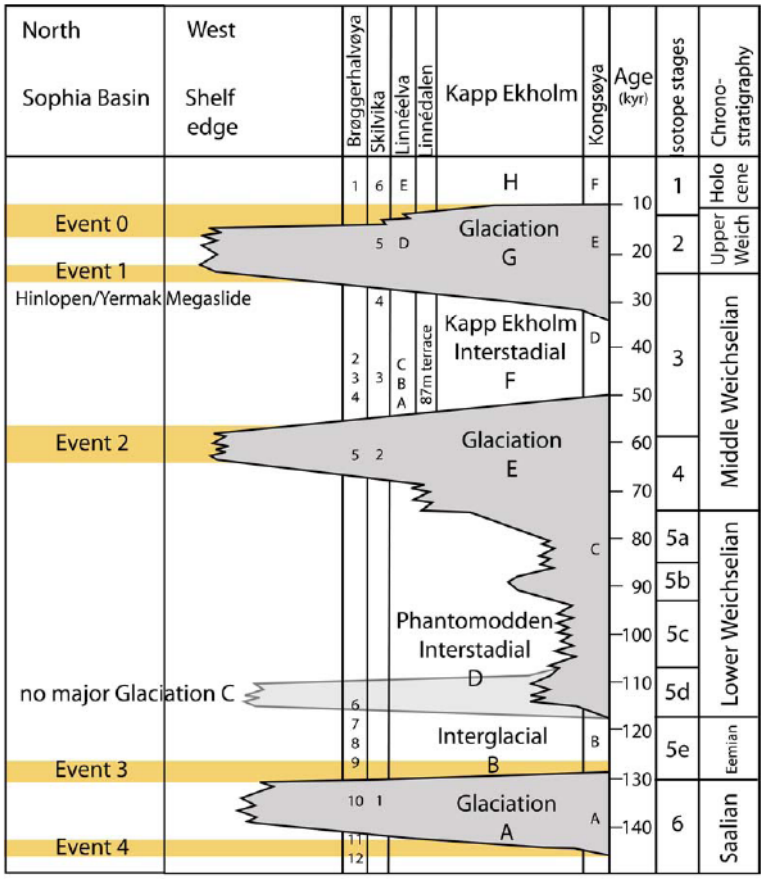

Figure 6: Revised glaciation curve for Svalbard during the last glacial cycle (after Mangerud et al., 1998; modified; for location names and associated numbering see Mangerud et al., 1998 and references therein).

Weichselian glaciation history (c.f. Svendsen et al., 2004) and the associated Phantom Odden Interstadial as a separate unit. Due to the fact that an early Weichselian glaciation is recorded in other (remote) terrestrial archives as well as in sea level changes (e.g. Lambeck et al., 2002), we rather see Svalbard being still inundated following the Late Saalian glaciation during the early MIS 5. Northern Svalbard was probably not experiencing an extensive glaciation between 115-100 kyr. BP and rather was moderately glaciated during MIS5 (Figure 6). This conclusion is supported by the terrestrial records in Brøggerhalvøya, Kapp Ekholm, Skilvika, Hidalen (Kongsøya) depending on their interpretation (see Mangerud et al., 1998 and references therein) as well as geological evidence from marine records (e.g. Knies et al., 2000, 2001) and, thus, revises the current glaciation curve of Svalbard (Mangerud et al., 1998). In analogue to Severnaya Zemlya (Möller et al., 2006), the Svalbard archipelago probably constituted glaciation nuclei for the subsequent growths of the SBIS during the MIS 5 and for the preceding and proceeding glaciations.

High Atlantic Water Influx leading to Glacials?

The periods around 180, 177 and between 162-166, 152-159, 142-150, 124-129, (115-125) 107-115, 93-100 (104-109) 70-82, 30-24 and closely after Event 1 ~23-18 cal. kyr. BP (LGM) are characterised by high Sr concentrations as a consequence of higher Atlantic water influx (The ages in brackets are derived from correlation to GRIP; Figure 7). As has been described for the LGM, enhanced Atlantic water inflow with associated high productivity and open waters probably contributed to the rapid ice-sheet growth of the Barents-Svalbard Ice Sheet (SBIS) by enhanced moisture supply (Hebbeln et al., 1994; Dokken & Hald, 1996; Knies et al., 2000; Hald et al., 2001). We basically see pulses of Atlantic water influx into the Sophia Basin throughout the last ~240 kyr (Figures 7 and 10). The intervals during the LGM and MIS 6.2, meaning peak glaciations, are characterised by a significant increase in Atlantic water influx reaching a maximum before terminating rather abrupt into the Terminations (Figure 7). A shut-down of the thermo-haline circulation during the termination with their extensive ice-berg discharge and fresh water supply to the North Atlantic appears a suitable explanation. Similar events can be found in lower MIS 5, and throughout MIS 3. While the transitions from MIS 7 into 6 and MIS 5 into 4 appears rather similar, the transitions from MIS 6 into 5 and 2 into 1 exhibit some differences. One peak in upper MIS 6 (ca 142-150 kyr. BP) appears to be very similar to one in upper MIS 3 (33-24 kyr. BP). Both represent the strong warm water inflow associated with a rapid built-up phase of the SBIS into maximum glaciations.

This is not well expressed within the Greenland ice core records. Only the GISP2 record shows a warmer interval between 28-26 cal. kyr. BP. Taken the new age-model for the last ~40 kyr. BP of the new N-GRIP ice core (N-GRIP Ice Core Project members, 2004) and the revised Greenland ice core chronology (Andersen et al., 2006; Svensson et al., 2006; Figure 10) into account, the interval's age might be slightly shifted. A possible explanation could be the altitude effect (c.f. Ritz et al., 1997; 2001; Huybrechts et al., 2002) during the rapid built-up phase of the Greenland ice sheet. A rapid increase in ice volume would lead to a vertical displacement of the drilling sites which would have an impact on the isotopic signature, leading to lower values in the $\partial^{18}O$ record. Some indication for this relation might be seen in the relation between annual snow/ice layer thickness and $\partial^{18}O$ (e.g. Svensson et al., 2006) pointing to the relation between temperature and snow accumulation which in turn affects the maximum altitude (Ritz et al., 1997). An alternative explanation of the signal offset during peak glaciations refers to a more complex mechanism and is strongly related to the North Atlantic's circulation pattern.

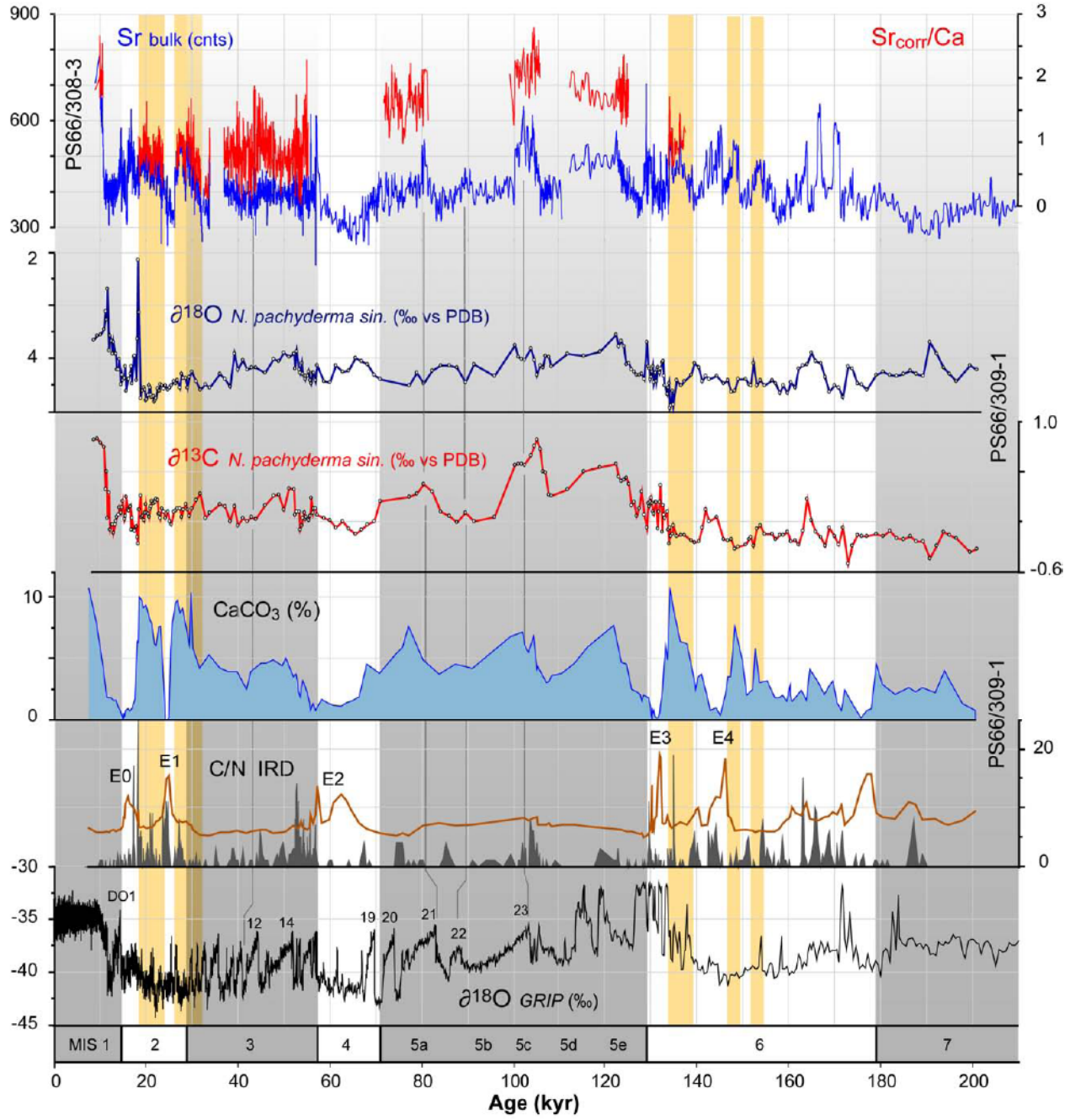

Figure 7: Core records of Sophia Basin and correlation to GRIP (Johnsen et al., 1997) showing Atlantic water inflow during high glacials (orange boxes). Note that the correlation to DO events (lines) are based on the new age model of N-GRIP (N-GRIP Ice Core Project members, 2004).

Circulation Scenarios

Based on the transferred age model, a broad correlation of the Sr record with the Greenland's $\partial^{18}O$ ice records can be observed (Figure 7). Due to this broad correlation, a tentative correlation of intervals within the isotope stages resulting in a tuned age model seems possible. However, this would be based upon the assumption that maxima within the Greenland isotope records correspond to maxima of the Sr

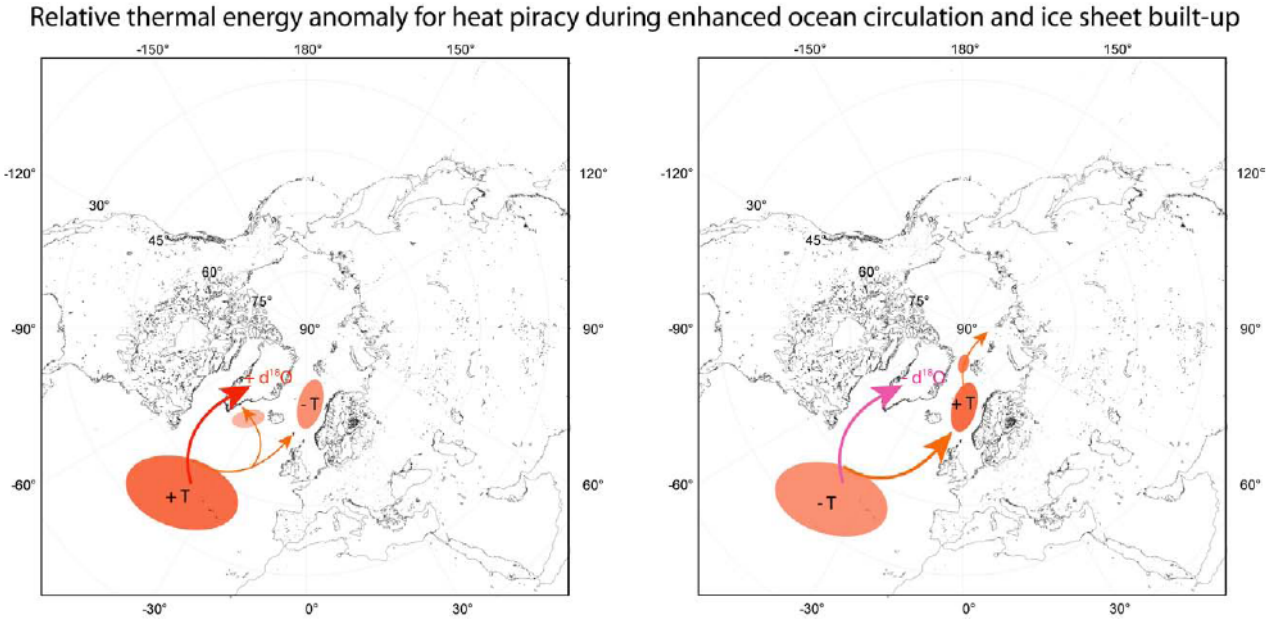

Figure 8: map with conceptual circulation models and associated thermal anomalies during step 1 and 2a: Step 1 – reduced circulation results in lighter $\partial^{18}O$ on Greenland's ice, positive thermal anomalies in the sub-tropical N-Atlantic, SW and central Europe, negative thermal anomalies in the GIN Seas and Arctic Ocean. Step 2a – enhanced circulation cools the N-Atlantic (dynamic) heat reservoir and leads to heavier $\partial^{18}O$ on Greenland's ice, positive thermal anomalies on NW and central Europe, within the Gin Seas and Arctic Ocean.

record, thus implying a synchronous relationship. Following this approach we encountered two distinct intervals, where the positive correlation seems to be reversed. These periods are MIS 6.2 and between 30-20 kyr. BP when global ice volumes approached their maximum during full glacial conditions (c.f. Lambeck et al., 2002).

Given our interpretation that the Sr record reflects productivity and therefore Atlantic water inflow into the Sophia Basin, the result is the coincidence of relatively warm water inflow and heaviest stable oxygen values on Greenland. This idea is not new and has been reported for the region by several authors (e.g. Hebbeln et al., 1994; Dokken & Hald, 1996; Knies et al., 2000; Hald et al., 2001; Spielhagen et al., 2004). The Greenland stable oxygen isotopes of the Greenland ice sheet have been interpreted to reflect the temperature of the moisture source area which was basically assumed to be constant in space and time even though there might have been a variable contribution from the Norwegian and Greenland Seas (e.g. Charles et al., 1994; Crüger et al., 2004; Jouzel et al., 2007). However, putting the Atlantic water inflow idea into context of the basic assumption of these ice core records, we feel the need of adding the ocean circulation compound. Introducing the idea of heat piracy (Stocker, 1998; Stocker & Marchal, 2000), we would like to discuss the different proxy records in terms of heat anomalies (Figures 7 and 8). Following the assumption for Greenland's ice cores, the main source area of their record would be the tropical North

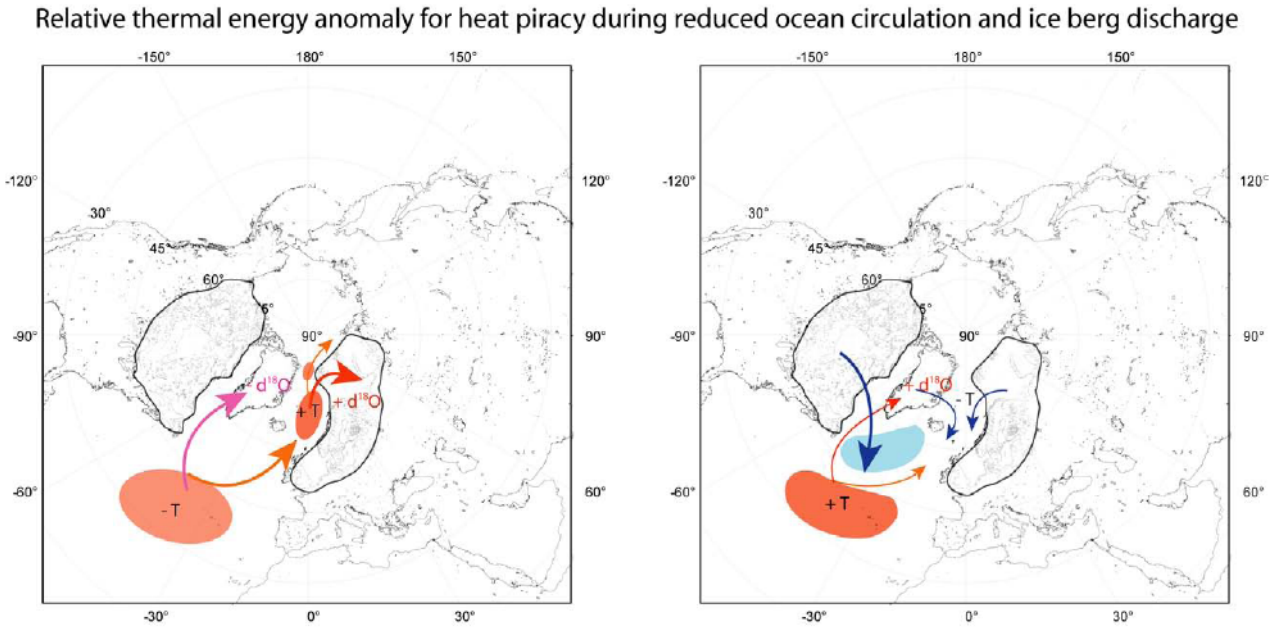

Figure 9: map with conceptual circulation models and associated thermal anomalies during step 2b and 3: Step 2b – enhanced circulation further cools the N-Atlantic (dynamic) heat reservoir and leads to heavier $\partial^{18}O$ on Greenland's ice. Rapidly growing ice sheets alter the regional positive thermal anomalies on NW and central Europe towards negative. Positive anomalies prevail within the Gin Seas and Arctic Ocean.
Step 3 – shut down circulation results in first in heavier (later lighter) $\partial^{18}O$ on Greenland's ice, negative (later positive) thermal anomalies in the sub-tropical N-Atlantic, SW and central Europe, negative thermal anomalies in the GIN Seas and Arctic Ocean. This scenario reflects Heinrich events.

Atlantic, the heat distribution can be configured as mainly atmospheric or (oceanic) circulation dominated. Thus, a number of scenarios can be established based on different intensities of the North Atlantic's thermo-haline circulation (THC):

- Starting with a weak circulation pattern, the heat of the tropical Atlantic would be mainly transferred to lower latitudes by the THC and by low pressure systems travelling north (scenario 1, Figure 7). This scenario results in positive thermal anomalies in central and south Europe, in elevated $\partial^{18}O$ on Greenland and in negative thermal anomalies within the GIN Seas an d the entrance to the Arctic Ocean. Heat would be "accumulated" in the tropical (c.f. Grimm et al., 2006) and adjacent northern Atlantic.
- The next step would be an enhanced circulation pattern (scenario 2, Figure 7). In this scenario, heat is mainly transported by the THC (which now reaches far into the Norwegian Sea) and further distributed into the Arctic Ocean. Atmospheric low pressure systems would now be more frequent in northern Eurasia and able to travel much further east. Thermal anomalies would be negative in the tropical and northern E-Atlantic (resulting in heavier $\partial^{18}O$ on Greenland), positive within the Gin Seas and Arctic Ocean and positive in Eurasia. This enhanced circulation scenario should be seen as the most effective

energy transportation status which consequently equilibrates the inter-latitudinal thermal gradients. Cooling of lower and warming of high latitudes is a direct consequence. The rapid built-up of Eurasian ice sheets is favoured during this scenario by excessive snow fall during winter (c.f. Gildor & Tziperman, 2001 and refernces therein; Figure 8). Following this rapid ice sheet growth, the regional climate pattern of NW Europe and other ice proximal locations would change towards negative thermal anomalies and probably associated precipitation pattern (c.f. Manabe & Broccoli, 1985). A highly dynamic environmental response might be seen locally too. Thus, this scenario has to be separated into two phases – a warm onset and a progressively cooler trend (in NW-European terrestrial records and Atlantic's SST). This enhanced circulation scenario does not stand in contrast to recent LGM reconstructions for the North Atlantic (e.g. SST reconstruction by Weinelt et al., 2003, reduced sea ice c.f. Nørgaard-Pedersen et al., 2003; de Vernal et al., 2006) though maximum ice volumes were reached earlier (e.g. Lambeck et al., 2002).

- The last scenario is a strongly reduced circulation pattern (scenario 3, Figure 8). The THC is more or less shut down within the Norwegian and Greenland Seas and the remnant heat of the tropical Atlantic would be distributed solely by atmospheric low pressure systems. This scenario corresponds to excessive ice berg discharge of Heinrich events (e.g. Bond et al., 1992) that terminate the THC by large fresh water layers (cf. Review by Rahmsdorf 2002). The regional thermal anomalies would all be negative including heavy $\partial^{18}O$ on Greenland. The intensity of this short-lived shut-down scenario would be modified depending upon the regional distribution of the ice bergs, sea ice and associated fresh water layers. On its process, this scenario leads to accumulation of heat within the tropical and subtropical Atlantic as described within scenario 1. A drastic warming (scenario 2) within the Norwegian and Greenland Seas (c.f. SST reconstructions by Weinelt et al., 2003) and probably western Europe follows this shut-down scenario as a result of the re-establishment of the THC transporting (accumulated) heat from lower latitudes in combination with the disappearance of the extensive sea ice cover (allowing for the enhanced ocean-atmosphere exchange; c.f. Gildor & Tziperman, 2001, 2003; Li et al., 2005).

There are several circulation models for the North Atlantic during the Late Pleistocene (c.f. Henrich, 1998 and references therein; Stocker & Marchal, 2000; see review by Rahmstorf, 2002).

The first indication that large scale northern hemispheric glaciations are coincident with open water conditions (within Fram Strait and the adjacent areas at least for the LGM) have been given by Hebbeln et al. (1994) followed by work of several authors (e.g. Dokken & Hald, 1996; Knies et al., 2000; Hald et al., 2001; Spielhagen et al., 2004) that related this fact to the rapid built-up of the SBIS by enhanced moisture

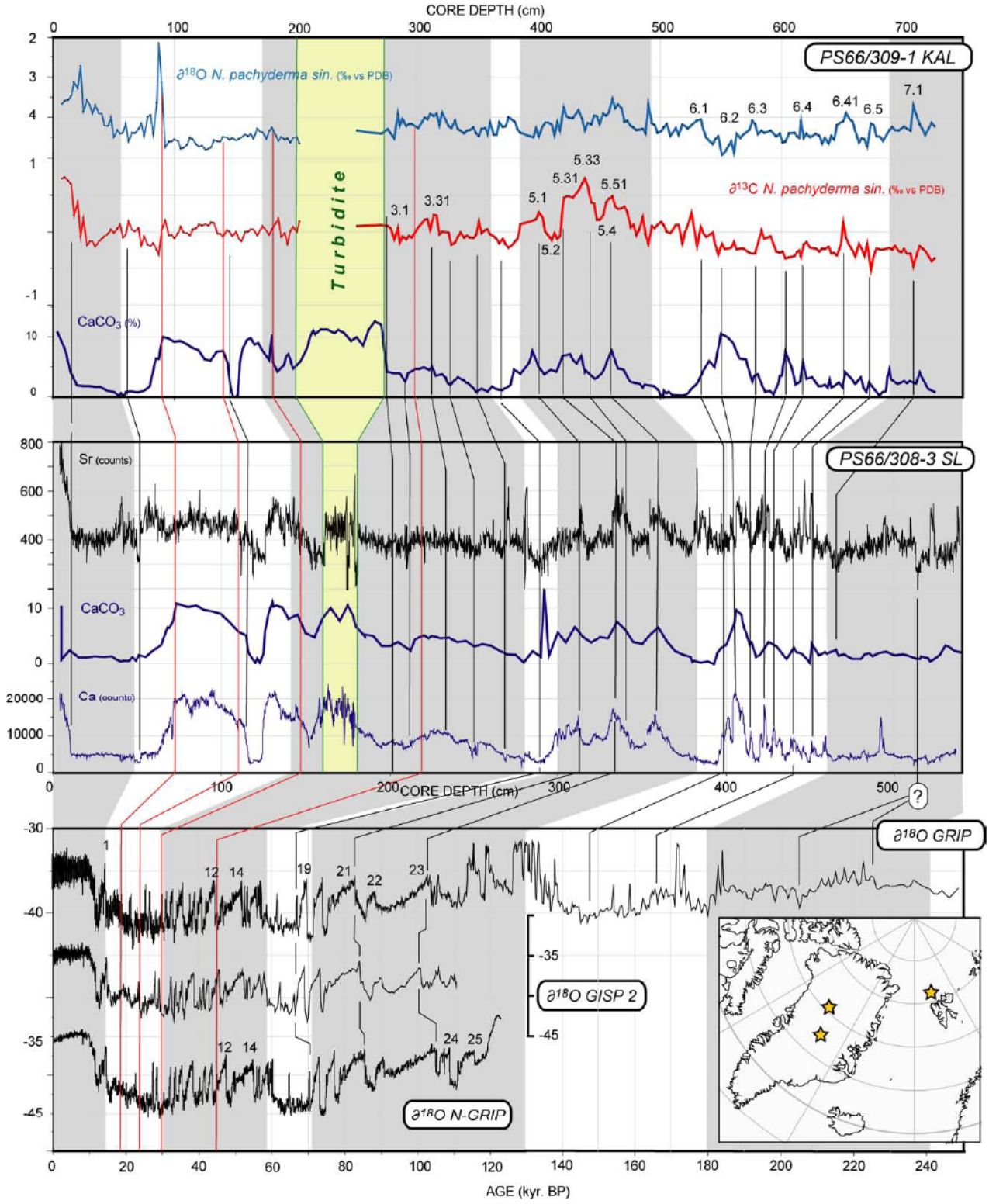

Figure 10: Detailed correlation of cores PS66/309, PS66/308 and Greenland ice core records (GRIP, N-GRIP; Johnsen et al., 1997; N-GRIP Ice Core Project members, 2004). The age model of PS66/309 is transferred to PS66/308 by correlation of the Carbonate and Ca records. The correlation to the GRIP respectively N-GRIP is based upon $\partial^{13}C$ of *N. pachyderma sin.* as well as Sr contents of bulk sediment of the gravity cores.

supply to the growing (regional) ice sheet during solar insolation minimum. In contrast to the common view (see review by Rahmstorf, 2002) of a strong THC resulting in warmer climate, we see this mode as the cooling mode of the climate engine, being able to transport the tropical (solar induced) heat to high latitudes (to cool) in the most effective way. Furthermore, our concept sees the enhanced circulation mode as the driving force for large scale glaciations. Considering that large ice sheets as well as glaciers represent a dynamic equilibrium between accumulation and ablation, the large ice sheets need to be fed by excessive moisture supply (e.g. Charles et al., 1994). In that respect, these ice volume represent energy put there in the form of solid precipitation. This view is corroborated by models (e.g. Gildor & Tziperman, 2001, 2003; Li et al., 2005). The growing ice sheets alter progressively the local and regional climate pattern (negative thermal anomaly) with positive feedbacks from their albedo and attraction of low pressure systems (due to forming of local high pressure cells. This results in a descending equilibrium line altitude (ELA) which in turn promotes glacial advance. The intensity of the North Atlantic's THC plays the key role in combination with solar insolation. A strong overturning of the THC will ultimately cool the Atlantic surface waters at low latitudes. Hence the initial warming on W-Europe from THC intensification is followed by gradually cooling. The glacial response will lead to short-lived strong coolings and associated Heinrich layers. This circulation cycle may explain the prominent Dansgaard/Oeschger events in Greenland ice cores and within the Greenland Sea (c.f. Gildor & Tziperman, 2001, 2003; Rahmstorf, 2002; Li et al., 2005).

Taking the enhanced circulation mode as the cause for glaciations, the fact that the maximum extents of Eurasian ice sheets displays a retrogressive development (early eastern largest towards late western maximum extents; from N-Siberia to Scandinavia; c.f. Svendsen et al., 2004) can be explained by a retrograding THC. The onset of a strong THC cycle far reaching into the eastern sector of the Arctic Ocean would cause rapid and maximum glaciation there (Kara Sea-Ice Sheet, SBIS). With decreasing penetration, the THC would cause the maximum ice sheet extents to shift to western locations (SBIS, Scandinavia).

The mechanism that allows the THC to penetrate deeply into the Arctic Ocean might be explained by a strong haline controlled positive feedback in combination with enhanced surface cooling that results from wind-driven freshwater export from surface waters. Higher glacial storminess and lower surface temperatures supports this idea. The strong deep water formation would pull the THC further East causing expansion of open waters and evaporation. The THC's subsequent retreat might result from increasing freshwater supply by Eurasian rivers/growing ice sheets resulting in a THC perturbation.

The fact that most climate reconstructions for the full glacial mode (which usually refers to the LGM

around 19-20 cal. kyr. BP) do not show a far reaching (into the Arctic Ocean) THC arises from the fact that the LGM scenario (c.f. CLIMAP, 1976, 1981) display the stagnant terminal stage (maximum extents shortly before collapse) of a large glaciation. These scenarios do not correspond to the built-up phase (which for the LGM should start around 33-30 cal. kyr. BP; c.f. Lambeck et al., 2002).

The circulation scenarios described in our study, displaying a meridional overturning circulation similar to the modern operational mode (with short-lived perturbations) throughout the glacial and interglacial cycles stand in accordance with carbonate and dissolution records within the Norwegian-Greenland Seas (Henrich, 1998; Henrich et al., 2002) and modelling results (e.g. Butzin et al., 2005). Recent scientific results showing monostable circulation as the robust mode during glacial conditions (Prange et al., 2002; Romanova et al., 2004), Atlantic mid-depth warming (Rühlemann et al., 2004) and increase of atmospheric freshwater transport (e.g. By stronger trade winds; c.f. Lohmann, 2003) during reduced THC (e.g. slow down during H1 and the Younger Dryas; c.f. Rühlemann et al., 2004) fit into the presented conceptual circulation model. The ocean circulation model can explain the DO-events in Greenland's ice cores as has been suggested by Jouzel et al. (2007) and a proposed southward source location shift during cold phases (e.g. Masson-Delmotte et al., 2005).

Following our conceptual model, we understand that indication of high Atlantic water influx into the Arctic Ocean should not be accompanied by an elevated stable oxygen isotopic signal on Greenland. Thus the cold periods of the shut-down scenario in both records appear to be more reliable for correlation leading to a better tuned record (Figure 9). This adjusted age model results in less variable sedimentation rates. In addition, the trends in both records seem to corroborate our heat piracy circulation concept. We see a gradually long term cooling after rapid warming in the ice core records. This moderate cooling is terminated by a rapid drop in $\partial^{18}O$. Following our new age model, we see a syn-optical gradually long term warming that is terminated by a rapid and longer lasting cooling in the sedimentary record of the SW Sophia Basin.

Using this general relation of long term gradual sea surface temperature (SST) warming north of Spitsbergen and gradually long term cooling in the $\partial^{18}O$ record, we can assign a number of these circulation cycles throughout the last 240 kyr. (Figure 11). For some periods, however, we can observe a positive correlation despite the application of our conceptual model. These periods show a strong trend towards high temperatures during the MIS6/5 and 2/1 boundaries and a strong cooling trend during the MIS5/4 boundary and into early MIS4 coincident with a rapid decrease of northern high-latitude insolation reaching a minimum around 72 kyr. BP (Berger & Loutre, 1991). Thus, and in concert with solar insolation curves we interpret this fact as a shift towards a (negative) solar control within the climate

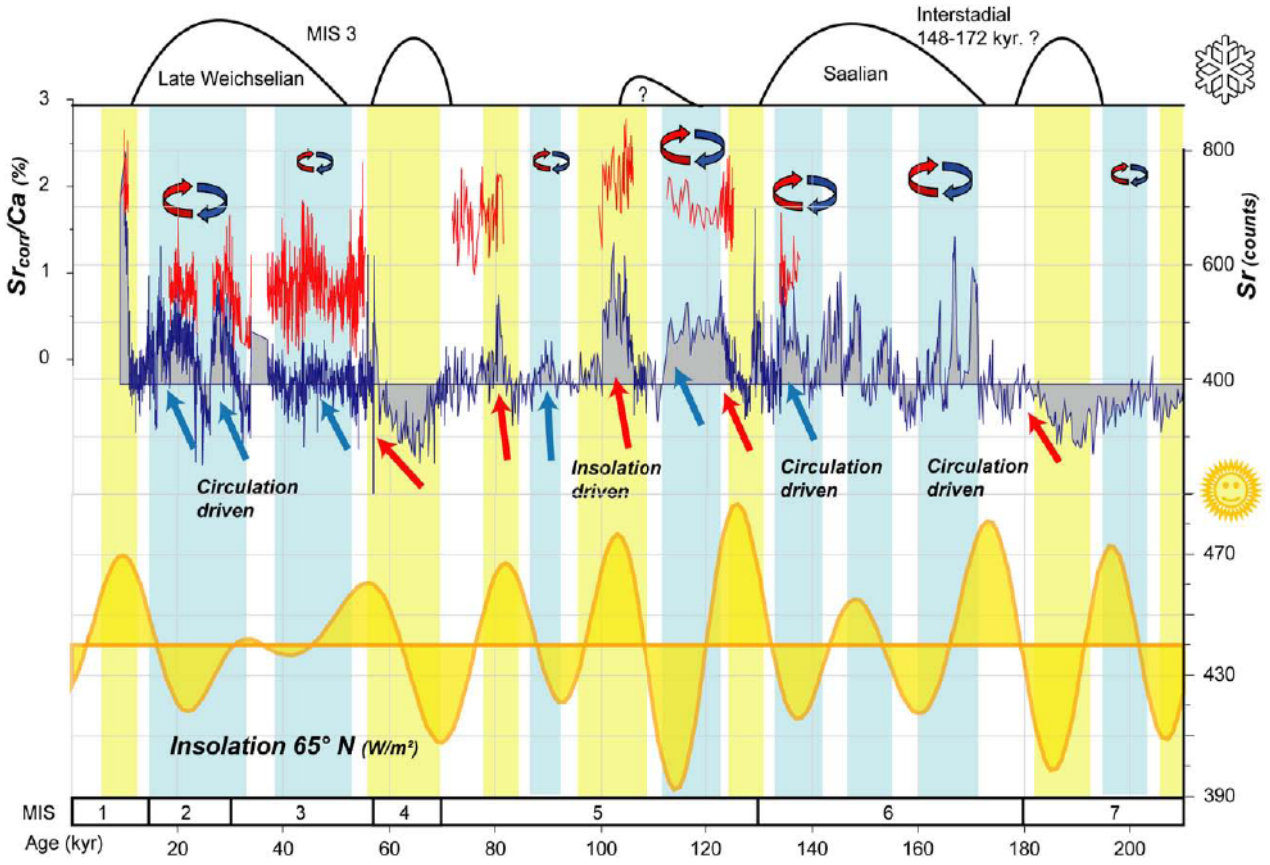

Figure 11: Summary interpretation of the Sr record of core PS66/308-3 with indication of glaciations, circulation events and solar forcing (insolation according to Berger & Loutre, 1991). Note circulation events in phase with solar maxima and minima and the two types of glaciations (circulation or solar controlled).

system. This interpretation includes the possibility of an additional contribution to the negative insolation budget from the largest Quaternary eruption of the Toba super volcano (e.g. Oppenheimer, 2002; and references therein). The eruption related sulphur spike has been dated within the GISP2 core to 71 kyr. BP according to the GISP2 age model (Zielinski et al., 1996; Zielinski, 2000). This event occurred prior to Dansgaard-Oeschger event 19 (DO19) at the MIS5a/4 transition around 74 ± 2 kyr. BP according to recent research including the new N-GRIP time scale (Oppenheimer, 2002; N-GRIP Ice Core Project members, 2004). Therefore we can summarize a circulation driven climate system for the North Atlantic, GIN Seas, eastern Arctic Ocean and adjacent continental areas (Greenland, Europe, NW-Asia) that is forced by extreme minimum solar insolation.

For the last interglacial we see the transition from a solar forced system towards a circulation-driven system. The high Arctic Sophia Basin was able to profit from the onset of an circulation cycle which resulted in warm water influx, higher productivity during the early MIS 5d.

Paleoceanographic Record of the Sophia Basin

MIS7

The MIS 7 exhibits moderate carbonate, relatively high C/N and Sr/Ca ratios and fairly low Sr contents of the bulk sediment indicate moderately glaciated conditions around 200 kyr. BP with increasing trend towards the MIS 7/6 boundary. The interval is characterised by Atlantic water inflow at probably lower temperatures and lower associated productivities and a declining trend into a period of enhanced ice rafting around 189-185 kyr. BP. This IRD event is accompanied by higher C/N and Sr/Ca ratios and might reflect an early ice sheet advance. The following interval displays Atlantic water inflow and increasing glacial activity into upper MIS 7. The associated moisture supply of this late inflow probably contributed to the early build-up of Saalian ice-sheets (e.g. Spielhagen et al., 2004).

MIS 6

The Latest MIS 7 and early MIS 6 is characterised by a proxy suite characteristic for extensive glaciation. The records exhibit similarities to the Middle Weichselian glaciation in terms of duration and forcing of a solar minimum. (Figure 11). An intensive ice rafting event preceded by terrigeneous input event 5 indicates the termination of this cold period. The following period between ~172-148 kyr BP displays almost an interstadial character with high Atlantic water influx similar to MIS 3. This confirms findings of Hebbeln & Wefer (1997), Hebbeln et al. (1998) and Spielhagen et al. (2004) concluding an Atlantic water inflow around 160 kyr. BP. However, heavy $\partial^{18}O$, frequent and intensive ice rafting and elevated Sr/Ca ratios indicate somewhat colder conditions. A drop to heavier $\partial^{18}O$ values around 4,5 ‰ indicates the rapid build-up of the SBIS and the onset (or culmination) of the Late Saalian glaciation. The proceeding intensive terrigeneous input (event 4; Figure 7) reflects the extensions of ice sheets onto the shelf edge with associated calving from ice streams. The build-up of the SBIS was again promoted by the intensive moisture supply from the inflowing Atlantic waters (c.f. Full glacial conditions are characterised by high Atlantic water influx, increased evaporation with associated colder surface temperatures and higher productivity. The ice-sheet extents and configuration of the Saalian glaciation(s) are not well known since terrestrial and shelf records provide little information and difficulties arising from (mainly luminescence) dating techniques complicate the stratigraphic work (see discussion in Spielhagen et al., 2004). The termination II (event 3; Figure 7), documented as Sr/Ca, Zr/Rb and C/N (which lacks a corresponding peak in the TOC record) peak contents and a carbonate minimum, follows with increased sedimentation rate, a tendency towards lighter $\partial^{18}O$ and a final melt water signal including IRD peak. It clearly depicts the disintegration of the SBIS.

MIS 5

This boundary is followed by a trend towards higher carbonate contents, lower TOC contents (below 0,7 wt. %) and C/N ratios below 8. Sr_{corr}/Ca ratios indicate warmer and increasing surface water conditions in accordance with stable isotopes. The trend reaches a maximum around 124 kyr. BP and endures with a minor perturbation until ~112 kyr. BP. This again reflects an Atlantic water inflow event during MIS 5.5 which initially started at a solar insolation maximum. Generally heavy oxygen values in early MIS 5 indicate moderate glaciation rather than full interglacial conditions. The abrupt end of this warmer episode leading into MIS 5.4 might indicate a (local) shut down or displacement of the Atlantic's THC. The MIS 5.3 displays another inflow event. Accompanied with peak insolation values it is documented with highest $\partial^{13}C$, Sr and Sr_{corr}/Ca values during MIS 5. The $\partial^{18}O$ values between 4,5 ‰ to 3,5 ‰ display a full glacial – interglaciel range during MIS 5 but are generally heavier than in the Holocene. Stage 5.3 in accordance with core records from PS2212-3 and PS1533-3 (Vogt et al., 2001; Spielhagen et al., 2004) appears to have been warmer than 5.5 north of Spitsbergen. Farther east, stage 5.5 seems a warmer period in the proxy record of core PS2138-1 from the Franz-Victoria-Trough (Knies et al., 2000) and might point to an enhanced circulation via the Barents Sea. MIS 5.3 is coincident with the onset of DO23 (Figures 7 and 10). MIS5.2 follows and might correspond to the termination of DO23. The long duration of this DO event on Greenland might be explained by the intensive warm water conditions of MIS 5.3 and resulting enhanced accumulation on Greenland. MIS 5.1 shows higher carbonate, Sr and Sr_{corr}/Ca ratios reflecting another inflow event and open water conditions (Nørgaard-Pedersen et al., 2007). Its onset most likely corresponds to the early DO21. The coincidence of circulation and accumulation onset points to a joint solar control (Figure 11).

IRD peaks in middle MIS 5 and in lower MIS 5.1, 5.2 and 5,4 indicate ice rafting. Low but persistent IRD contents prevail from Late MIS 5 into MIS 4. Obviously, the IRD signal does not necessarily match the terrigeneous signal and appears discoupled. A possible explanation is that ice bergs from the Norwegian and Greenland Seas drifting along the paleo-WSC are the dominant IRD source. In contrast to Mangerud et al. (1998), we see no extensive glacial advances in our sediment cores north off Svalbard. We rather can identify a long and enduring (de-)glacial activity throughout the early MIS 5 with minor glacial activity in upper MIS 5.4. Increasing glacial activity probably due to lower solar insolation and Atlantic water influx (Figure 11) characterises the upper MIS 5 and the MIS 5/4 boundary. The Toba supervolcano eruption around 74 kyr. BP might have had an additional impact on negative insolation values close to the MIS 5/4 boundary which we place to 71 kyr. BP according to Thompson & Goldstein (2006).

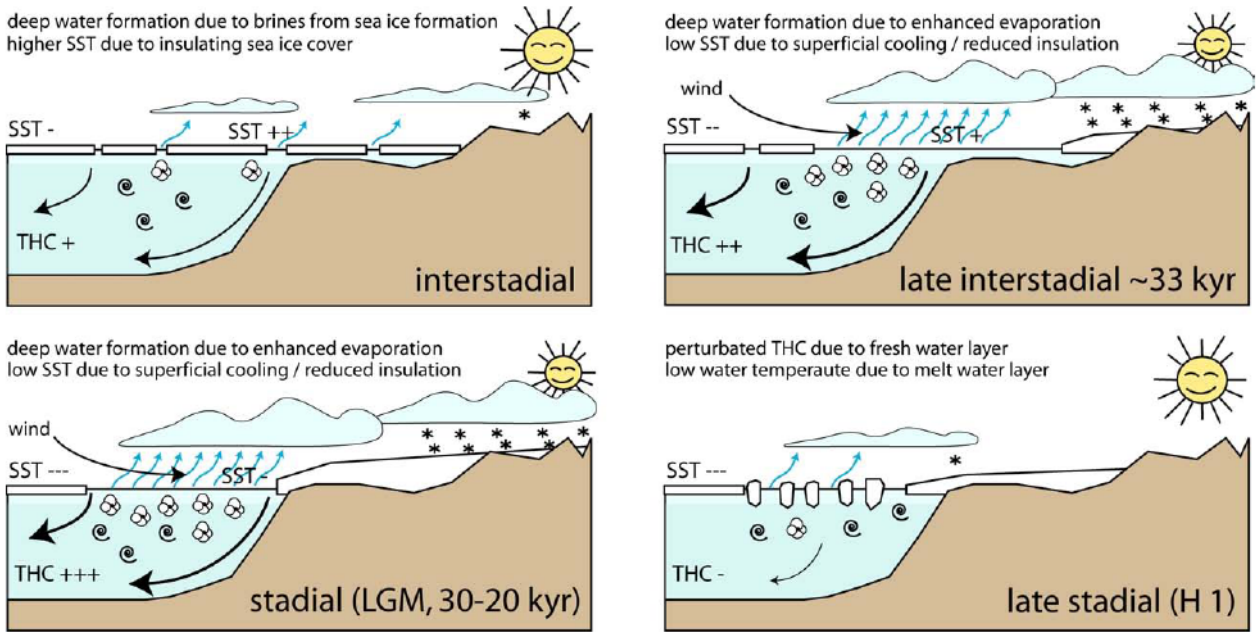

Figure 13: Summary interpretation of paleo-environmental conditions within the Sophia Basin north of Svalbard with strongest THC circulation events leading into major glaciations (Saalian, LGM: 30-20 kyr. BP.) by excess winter snowfall.

MIS 4

MIS 4 is characterised by the continued transition from mild into colder full glacial conditions in middle MIS 4. The $\partial^{18}O$ record displays heavy values above 4 ‰ throughout MIS 4 (Figure 7). The record of $\partial^{13}C$ exhibits a maximum (0,25 ‰) in lower MIS 4 followed by a minimum in upper MIS 4 (-0,25 ‰) and again increasing values into MIS 3. TOC peak contents coincide with peak C/N ratios as well as low carbonate contents in upper MIS 4. A subsequent C/N peak that is not reflected in the TOC contents marks the MIS 4/3 boundary and is accompanied by an IRD peak. In general, the MIS 4 is characetrised by persistent terrigeneous input (event 2; Figures 5 and 7) to the Sophia Basin, culminating at the MIS4/3 boundary and reflecting the extensive Mid Weichselian glaciation (glaciation E; cf. Mangerud et al., 1998, Svendsen et al., 2004) roughly between 75-55 kyr. BP. This glaciations appears to be different in terms of climatic preconditioning onset and duration. In analogue to the late MIS 7/early MIS 6, the glaciation was probably forced by a pronounced solar minimum that was not accompanied by intensive Atlantic water inflow. The inflow events during the upper MIS 5 (DO21, 20, 19) and associated open water conditions (e.g. Nørgaard-Pedersen et al., 2007; this study) provided moisture to the growing SBIS but weakened towards the middle MIS 4. The rather limited duration of the Mid Weichselian Glaciation and the related low sedimentation rates might be explained by this fact. The beginning termination of this glaciations characterises the MIS 4/3 boundary and the lowermost MIS 3 with peak IRD, C/N and Sr/Ca ratios around 60 cal. kyr. BP.

MIS 3

Early MIS 3 is characterised by an increase of carbonate contents, rather low and low variable TOC contents and C/N ratios. High IRD contents point towards increased glacial activity throughout the early and middle MIS 3. Both key cores (PS66/309-1 KAL and PS66/308-3 SL) show three maxima in early MIS 3. They all exhibit a similar pattern and point towards a well developed cyclycity of the IRD record during this time. The cyclic IRD peaks that characterise the MIS 3 might correspond to the Daansgaard-Oeschger-Events (DO-events) in Greenland ice cores and their relation to the Heinrich events (H-events) that are well described in marine records of the North Atlantic and Nordic-Seas (e.g. Bond et al., 1992; Voelker, 1999, 2000; Mix et al., 2001). In contrast to sediment cores off Greenland (Kierdorf, 2006), these events are not imprinted on the TOC records. One probable explanation is the drift of icebergs coming from Greenland with the paleo-WSC towards the south-western Sophia Basin during MIS 3. Both carbonate record and the cyclic IRD peaks point to meridional circulation conditions (e.g. Vogt et al., 2001). The identified at least two episodes with sediment and iceberg transport from south to north via the paleo-WSC based on detailed mineralogic analysis. The source region of their OLEM-events has been inferred to be the Jurassic hot shales of the Spitsbergenbanken, western Barents Sea (Storfjord Trough). Taken modern circulation pattern as an analogue, the Greenland iceberg discharge signal (DO/H-events) might have been recirculated in the Norwegian Sea, transported to the south-western Sophia Basin. This concept is supported by conclusions of Pirrung et al. (2002) that identified a counter-clockwise iceberg drift during the colder stages of the Holocene with its implication for MIS 3. There are 7 distinct discharge events during the time window of D/O 6-18 including H4-6 in our cores. H6 as well as H2 are recorded as terrigeneous input events in our Sr/Ca record (Figure 5). However, a local source appears not probable for the remaining IRD events since they are not reflected as terrigeneous input events. Relatively high carbonate and Sr contents indicate persistent Atlantic water inflow events throughout MIS 3 with decreasing Sr_{corr}/Ca ratios (mirroring sea surface temperatures) and only minor perturbations. This further corroborates the meridional circulation and associated IRD interpretation.

The increasing Atlantic water inflow documented as high productivity events led to a significant moisture supply to the rapidly growing SBIS (c.f. Hebbeln et al., 1994; Dokken & Hald, 1996; Knies et al., 2000; Hald et al., 2001; Spielhagen et al., 2004) probably in combination with stronger inter-latitudinal temperature gradients (Alfano et al., 2003; Vettoretti & Peltier, 2003; .Kukla & Gavin, 2005) The rapidly changing environment associated with this ice-sheet growth caused the Hinlopen/Yermak Megaslide (Winkelmann & Stein, 2007). Therefore, the upper MIS 3 contains a hiatus of variable depth/time interval due to erosion by the marginal turbidite and/or debris flow of the Hinlopen/Yermak Megaslide event (c.f.

Winkelmann et al., 2006a; 2007). Accordingly, the interval roughly between 42-30 cal. kyr. BP is missing in the records. Maximum ice volumes were probably already reached around 30 cal. kyr. PB (Lambeck et al., 2002; Peltier & Fairbanks, 2006). The MIS 3/2 boundary follows closely the submarine megaslide event and exhibits Atlantic water inflow at low surface temperatures with fair terrigeneous input and ice rafting.

MIS 2

Following the continuation of uppermost MIS 3 conditions and reaching of maximum extensions of the extensive SBIS, the lower MIS 2 is characterised by terrigeneous input event 1 with peaks in the TOC, C/N, Sr/Ca, Zr/Rb, Ti/Rb records and IRD contents while carbonate contents are lowest or absent (Figures 5 and 7). Planktonic $\partial^{18}O$ display heavy values around 4,5 ‰. $\partial^{13}C$ values are close to the standard (0 ‰ vs PDB). This interval mirrors the major glacial advance to the shelf edge including local ice streams from the SBIS with associated iceberg discharge. Our closest AMS radiocarbon date some cm above gives 23379 ± 394 cal. kyr. BP dating the very early LGM ice extent in the area, equivalent with H2. A larger perturbation of Atlantic water inflow probably accompanied this event. The following interval is characterised by rather stable conditions with TOC contents <0,5 wt.% and C/N ratios <8. Consistently higher IRD contents indicate ice stream activity while high carbonate and Sr values indicate enhanced Atlantic water inflow during the LGM. High productivity at lowest surface temperatures (Sr_{corr}/Ca) consistent with the reconstruction of Nørgaard-Pedersen et al. (2003) and reduced terrigeneous input is documented in our cores for this interval. A strong IRD peak starting around 19 cal. kyr. BP is not accompanied by elevated C/N ratios nor TOC contents and might indicate an early disintegration signal of distal ice-sheets transported by the paleo-WSC into the south-western Sophia Basin. It foreshadows the proceeding termination.

Highest IRD peaks accompanied by a clear melt water signal ($\partial^{18}O$ of 2,2 ‰ and $\partial^{13}C$ of -0,7 ‰) and a radiocarbon date of 18491 ± 237 cal. kyr. BP mark the initial disintegration of late Weichselian ice-sheets during the Oldest Dryas (Figures 2, 4 and 7). It represents Termination 1a and H1 (e.g. Bond et al., 1993) respectively in our cores and coincides with a warming period in marine and terrestrial records of the North Atlantic realm (e.g. Denton et al., 1999 and references therein) and a first stepwise strengthening of NADW production (documented e.g. in the south-eastern Atlantic, Piotrowski et al., 2004). $\partial^{13}C$ values increasing from -0,05 to 0,16 ‰ between 19 and 18,75 cal. kyr. BP indicate this strengthening, while, however, sudden drops to very low values around 18,3 and 16,7 might point to perturbations of the THC. Decreased bottom current speeds have been reported from the western Yermak Plateau between 16,3 and

15,5 cal. kyr. BP (Birgel & Hass, 2004). Generally increasing $\partial^{13}C$ values between 18,2 and 15,7 cal. kyr. BP indicate intensification of the THC while a trend to heavier $\partial^{18}O$ values indicate cold surface waters. This is corroborated by findings of Rassmussen et al. (2007) who suggest a strong bottom warming (7°C on the shelf and 2°C on the slope) and a stronger stratification of the upper water column west of Spitsbergen. The surface temperatures, were probably lower than in the succeeding Bølling period (Svendsen et al., 1996).

Pronounced peaks in the Sr/Ca, Zr/Rb, TOC and C/N records, accompanied by low and lowest carbonate contents follow the initial disintegration signal and characterise the intensive terrigeneous input event 0 (Figure 5). Termination 1b follows subsequently (around 17,3 cal.. kyr. BP) with less pronounced melt water characteristic but a strong IRD peak. This first deglacial stage (17–14,7 cal. kyr. BP) in northern Europe/Arctic Ocean was probably triggered by a global sea level rise leading to a quick disintegration of the marine-based parts of the SBIS (Elverhøi et al., 1995; Andersen et al., 1996).

The initially strong and decreasing IRD signal in our cores contrasts the minor melting resulting in no significant IRD deposition close to the Svalbard archipelago as reported by (Svendsen et al. (1996). This, again, might be explained by the paleo-WSC transporting icebergs northward via strong slope currents and carrying away the IRD-bearing icebergs (Andersen et al., 1996; Dowdeswell & Elverhøi, 2002). On their way north into the Sophia Basin, subsurface melting in the relatively warm Atlantic waters released their ice rafted material from sea-ice and icebergs.

MIS 1

The initial strong warming of the Bølling/Allerød (B/A) warm period around 14,6 cal. kyr. BP (DO 1) which coincides with the uppermost MIS 2. The B/A is characterised by highest Mn contents reflecting either the oxidation front between 40 and 50 cm core depth (c.f. Thomson et al., 1996; Mangini et al., 2001) and/or a strong deep oceanic ventilation event. This deep ventilation with stronger current regime and relatively high and stable bottom water salinities reported from the western Yermak Plateau (Birgel & Hass, 2004), the western (Ślubowska-Woldengren et al., 2007) and northern shelf (Koç et al., 2002; Ślubowska et al., 2005) of Spitsbergen was accompanied by high sedimentation rates and relatively cold surface waters (Rasmussen et al., 2007). A decreasing trend in $\partial^{13}C$ values and Sr contents indicates a steady weakening of the THC from 14,2 cal. kyr. BP towards the end of the B/A interval. Low carbonate, increasing $\partial^{18}O$ values and little ice rafting might point to increasing sea ice coverage and resulting less productivity throughout this interval.

Meltwater peak 1a follows around 12,9 cal. kyr. BP shortly after this warm interval and introduces the following Younger Dryas (YD) cold period (12,7-11,5 cal. kyr. BP). The strong terrigeneous input signal (event 0) with highest peaks in Sr/Ca, Zr/Rb, TOC and C/N records endures between 17,4 and 10,6 and reflects ongoing or retarded local deglaciation. An intensive perturbation of Atlantic water inflow might have accompanied this discharge events. The lowermost interval of the YD is characterised by high but decreasing Mn contents possibly indicating still well oxygenated deep water conditions. Low $\partial^{13}C$ values reflect a weaker or dislocated THC while relatively light $\partial^{18}O$ values might result from increasing melt water contribution. Decreasing bottom current activity has been reported from the Hinlopen Strait (Koç et al., 2002; Ślubowska et al., 2005) and on the western Yermak Plateau (Birgel & Hass, 2004). While surface waters opened shortly after (Koç et al., 2002) and remained open and productive in Fram Strait (Birgel & Hass, 2004). Birgel & Hass (2004). explained this discrepancy by open water conditions of a polynya environment due to “Föhn”-like winds.

While open water conditions (with increasing marine biomarkers) in the eastern Fram Strait endured throughout the YD, a period of harshening climate in N-Europe with west-ward shifting of the polar front (e.g. Klitgaard-Kristensen et al., 1998) advancing glaciers (e.g. Renssen & Isarin, 2001; Bondevik & Mangerud, 2002) was probably related to major perturbations in the Atlantic's THC. Considering the relation of moisture supply and glacial accumulation, glacial advances should have occurred on Svalbard too following the disappearance of glaciers by the end of the Allerød (Mangerud & Svendsen, 1990; Svendsen & Mangerud, 1992; Svendsen et al., 1996). End moraines succeeding the LGM were found to be from the Holocene Little Ice Age (LIA)(Mangerud & Svendsen, 1990; Svendsen & Mangerud, 1992). Svendsen & Mangerud (1992) suggest that glaciers on W-Svalbard might have already taken modern dimensions during the YD. However, glacial advances smaller in scale (and older) than during the LIA on Svalbard might remain difficult to detect. The fact that the YD coincided with maximum solar insolation can explain partly the lack of glacial activity on Svalbard. Colder and dryer conditions with higher temperature seasonal gradients, reduced cloudiness and altered storm tracks have been considered to too (see discussion in Birgel & Hass, 2004). The more important aspect might be the perturbated circulation that did not succeed in supplying sufficient amounts of moisture to the Svalbard archipelago. Glacier grew in northern Scandinavia (Renssen & Isarin, 2001; Bondevik & Mangerud, 2002) where the proximity to open waters and associated moisture supply was provided (open water conditions along the Norwegian coastline, e.g. Koç et al., 1993).

The following abrupt warming (DO 0) roughly between 11.9 and 10 cal. kyr. BP is characterised by a trend towards lighter $\partial^{18}O$ values with distinct perturbations and melt-water signals. Accompanied by increasing

carbonate and TOC contents at low C/N values and low or absent ice rafting, we speculate whether these perturbations superimposed on an overall warming trend coincide with well documented coolings in the North Atlantic sector (PBO, the 8.2 kyr-Event, c.f. Barber et al., 1999, etc.) towards and during the early Holocene. Whether the colder surface and bottom waters in the Hinlopen Strait reported by Koç et al. (2002) and Ślubowska et al. (2005) might represent a local or regional signal remains to be answered, since our age control relies on linear interpolation between 18,5 and 10,9 with some uncertainties for the correlated younger datum. Therefore, we refuse to further interpret these environmental changes. However, this uppermost interval with high and highest Sr_{corr}/Ca, carbonate, Sr, $\partial^{13}C$ and $\partial^{18}O$ values certainly reflects the early warm Holocene.

Global Warming Perspectives

Following our circulation controlled scenario and lowered and further decreasing solar insolation, our modern climate should be characterised by strong advection of Atlantic water to the Nordic Seas and into the Arctic with local climate being moderate, mainly controlled by the ocean warming (and related low pressure systems).

On the shelf north of Svalbard, the first post-LGM strong sub-surface inflow of Atlantic waters is documented in core NP94-51 during the Bölling/Alleröd interstadial around 15 cal. kyr. BP (Ślubowska et al., 2005). This documented circulation event was strongly perturbated or even terminated during the Younger Dryas. The following strong inflow of Atlantic water culminated during the Early Holocene and declined gradually during the Mid-Holocene, being weakest between 4,5 and 1,1 cal. kyr. BP (Ślubowska et al., 2005). During the last kyr. Sub-surface Atlantic water inflow increased again.

Following this Early Holocene circulation event (and initially warm pattern, c.f. Lockwood, 2001 and refernces therein), a rapid growth of glaciers and minor ice sheets might be expected starting from East Eurasia and developing towards the West. This scenario can be interpreted as the cause for the onset of modern glacier advances around 2.4 kyr BP. This so-called Neoglaciation is documented roughly between 5,7 and 4 with intensification around 2,4 cal. kyr. BP in a variety of places in both hemispheres (e.g. Porter, 2000; Nesje et al., 2000; Kirkbride & Dugmore, 2001; Matthews et al., 2005; Miller et al., 2005; Magny et al., 2006; Jouzel et al., 2007). Around 3,7 cal. kyr. BP a period with slightly warmer but generally more unstable conditions follows the early Holocene thermal maximum and the subsequent cooler phase (6,5-3,7 cal. kyr. BP) in the northern North Atlantic (Moros et al., 2004). The cooler phase might correspond to the advanced stage of the early Holocene circulation event with efficient heat piracy and might explain steadily decreasing surface temperatures in the north-east Atlantic (Marchal et al.,

2002) and major wet shifts recorded in peat bog surface wetness on the British Isles (Barber et al., 2003; Langdon et al., 2003). As outlined by Moros et al. (2004), the neoglaciation may not only be attributed to declining summer insolation but also to increased snow precipitation during generally milder winters. In combination with declining summer insolation the circulation around 2,4 cal. kyr. BP probably delivered the necessary moisture for the increasing mass balance of advancing glaciers. Glacial initiation on Severnaya Zemlya, Franz Joseph Land, Svalbard and Scandinavia may be explained by this circulation scenario. The onset of the contour current on the western shelf of Spitsbergen estimated to ~2,6 cal. kyr. BP (Andruleit et al., 1996) dates into this times and might corroborate our interpretation. The faunal changes in core NP94-51 during the last 4,5 cal. kyr. BP (Ślubowska et al., 2005) mirror environmental changes towards this Neoglaciation. During the later stage of this circulation event growing glaciers might have led to local cooling and enhanced freshwater forcing might have imprinted the THC circulation. This might be seen in the strongest reduction of Atlantic water inflow around Svalbard before 1,1 cal. kyr. BP (c.f. Ślubowska et al., 2005).

However, with the termination of a standard temporal duration of the circulation events of 8-10 kyr., (a possible multiple of the 1500 year cycle; c.f. Bond et al., 1997) we should expect a final (probably freshwater induced) cooling trend in our global climate during the last centuries. This trend might already have started with the onset of the Little Ice Age (LIA). In contrast to other Holocene coolings (c.f. Lockwood, 2001 and refernces therein), the LIA exhibits aside global glacier advances (Lowell, 2000) the geographic pattern of the YD and the main glacial maximum (Broecker, 2000). Strongest glacial advances characterise the LIA on Baffin Island since the last 7 cal. kyr. BP (Miller et al., 2005), since the last 9 cal. kyr. BP in Norway (Matthews et al., 2005) and comparable with early neoglacial advances on Iceland (Kirkbride & Dugmore, 2001). On Svalbard glacier advances during the LIA are documented as end moraines. Considering that no end moraines were found from the YD cold period on Svalbard (in contrast to other places in Europe; c.f. Mangerud & Svendsen, 1990; Svendsen & Mangerud, 1992), this glacier advance represents the largest during the Holocene.

This glacial advances in the North Atlantic sector may already mark the natural end of our interglacial leaving the abrupt warming of the last century as a human impact. If true, this human warming compound would be much greater, camouflaged by a descending natural temperature curve of the global climate during the last ~120 years. This would put the excessive combustion of fossil fuels into a new light and would point to an unprecedented stage of our climate system which future behaviour will be difficult to forecast.

However, the causes for the LIA have been discussed controversially. The step-wise cooling during the LIA might reflect minor perturbations of the THC (c.f. Lamb, 1979), or other forcings like the Maunder solar minimum (e.g. Nesme-Ribes & Mangeney, 1992; Stuiver et al., 1997; Fischer et al., 1998) or to major volcanic eruptions (Mann et al., 1998; Briffa et al., 1998; Bertrand et al., 1999; Crowley & Kim, 1999; D'Arrigo et al., 1999; Crowley, 2000; Zielinski, 2000). The volcanic forcing seems to fail to explain the long cooling trend of the LIA (Stuiver et al., 1997; Fischer et al., 1998; Luterbacher et al., 2001; Shindell et al., 2003). Solar forcing in combination with the Atlantic's THC (Bond et al., 1997; Barber et al., 1999; Broecker, 2000; Lockwood, 2001; Luterbacher et al., 2001) might be the most likely causes.

Recent current measurements of the WSC in the Fram Strait document a strengthening of the THC since the 1960ies and especially during the 1990ies indicating the onset of another circulation event (Schauer et al., 2004; Polyakov et al., 2005; Walczowski & Piechura, 2006). Half of the increased net heat transport towards the Arctic Ocean (from 16 ± 12 to 41 ± 5 TW at 78°55´N between 1997 and 1999) was caused by higher surface water temperatures while the other half was due to enhanced flow (Schauer et al., 2004).

The recent warming of the Arctic can partly be attributed to this enhanced inflow of Atlantic water meaning the introduction of thermal anomalies (e.g. Morison et al., 2000; Schauer et al., 2004; Polyakov et al., 2005). Travel time of heat anomalies have been estimated to ~1,5 years from the Norwegian Sea into Fram Strait region and 4,5-5 years more to reach the continental slope of the Laptev Sea (Polyakov et al., 2005).

Considering that the increased heat transport into the Arctic Ocean was strongest during winter and not balanced by higher heat export through Fram Strait (Schauer et al., 2004), that the resulting warming leads to open water condition (e.g. Winkelmann & Knies, 2005) and that cold air masses travelling over relatively warm waters will cause extreme snowfall, the strong inflow might result in enhanced precipitation. Since we can expect this precipitation to be snow in the Arctic realm it might cause glacier advances further east. As demonstrated for the interior of Antarctica (e.g. Morgan et al., 1991), the relation of an cold environment and enhanced moisture supply leading to enhanced accumulation and glacial advances is relevant for our modern times. Keeping this points in mind, recent global warming at negative solar forcing (c.f. Landscheidt, 2003) might lead into a major glaciation faster than expected. To what degree this effect might be compensated by atmospheric warming from increased greenhouse gases remains open for modelling.

Conclusion

- The cores from Sophia Basin in concert with sediment cores of the eastern Yermak Plateau (PS2212, PS1533) generally show a consistent climate history.
- The bulk sediment Sr/Ca ratios reflects fluctuations in terrigeneous input in the Sophia Basin.
- Higher Sr/Ca ratios (>6%) indicate terrigeneous input events. These events are accompanied by higher concentrations of TOC, higher C/N ratios and due to dilution lower carbonate, lower Ca and Sr concentrations.
- These terrigeneous events are considered as synchronous and can be used as time marker.
- The Sr contents probably reflect primary productivity due to inflow of Atlantic water.
- Corrected bulk sediment Sr_{corr}/Ca ratios may be used as a proxy for SST remaining to be scaled.
- The positive correlation between planktic $\partial^{13}C$ of *N. Pachyderma sin.* and Sr contents can be used for fast establishments of age models for sediment cores of the region. Thus expanding the applicability of the XRF scanning method.
- The Sr record can be directly correlated to Greenland's ice core records.
- Correlation of minima appears as the preferred method for this purpose.
- The North Atlantic climate system changed between circulation controlled and solar forced modes during the last ~240 kyr. BP.
- Peak glaciations of the Late Saalian (MIS6.2) and Late Weichselian (around 33-18 kyr. BP) occurred during and probably due to a circulation driven mode.
- The Mid Weichselian glaciation (MIS4/3) occurred during forcing of a solar minimum insolation.
- The early Weichselian glaciation is not documented in our sediment cores. Thus, northern Svalbard was probably not experiencing an extensive glaciation between 115-100 kyr. BP (Glaciation C of the Svalbard glaciation curve; cf. Mangerud et al., 1998) possibly due to remnant glacial inundation. This stands in accordance with both terrestrial and marine records.
- Therefore we proposed a revised version of the Svalbard Glaciation curve of Mangerud et al. (1998).
- The recent Arctic warming accomplished by oceanic circulation might lead to enhanced precipitation with onsetting glaciation earlier than expected.

Acknowledgement

This study was funded by the German Research Foundation (DFG, STE 412/17). We are thankful to the scientific shipboard party and the captain and crew of RV "Polarstern" during ARK-XX/3.

References

Alfano, M.J., Barron, E.J., Pollard, D., Huntley, B., Allen, J.R.M. (2003): Comparison of climate model results with European vegetation and permafrost during oxygen isotope stage three, Quaternary Research 59, 97–107.

Anand, P. & Elderfield, H. (2005): Variability of Mg/Ca and Sr/Ca between and within the planktonic foraminifers Globigerina bulloides and Globorotalia truncatulinoides, Geochemistry Geophysics Geosystems 6 (11), doi: 10.1029/2004GC000811.

Andersen, E.S., Dokken, T.M., Elverhøi, A., Solheim, A., Fossen, I. (1996): Late Quaternary sedimentation and glacial history of the western Svalbard margin, Marine Geology 133, 123–156.

Andersen, K.K., Svensson, A., Johnsen, S.J., Rasmussen, S.O., Bigler, M., Röthlisberger, R., Ruth, U., Siggaard-Andersen, M.L., Steffensen, J.P., Dahl-Jensen, D., Vinther, B.M., Clausen, H.B. (2006): The Greenland Ice Core Chronology 2005, 15–42 ka. Part 1: constructing the time scale, Quaternary Science Reviews 25, 3246–3257.

Andersson T., Forman, S.L., Ingólfsson, Ó., Manley, W. (1999): Late Quaternary environmental history of Prins Karls Forland, western Svalbard, Boreas 28, 292-307.

Andruleit, H., Freiwald, A., Schäfer, P. (1996): Bioclastic carbonate sediments on the south-western Svalbard shelf, Marine Geology 134, 163-182.

Barber, D.C., Dyke, A., Hillaire-Marcel, C., Jennings, A.E., Andrews, J.T., Kerwin, M.W., Bilodeau, G., McNeely, R., Southon, J., Morehead, M.D., Gagnon, J.-M. (1999): Forcing of the cold event of 8,200 years ago by catastrophic drainage of Laurentide lakes, Nature 400, 344–348.

Barber, K.E., Battarbee, R.W., Brooks, S.J., Eglinton, G., Haworth, E.Y., Oldfield, F., Stevenson, A.C., Thompson, R., Appleby, P.G., Austin, W.E.N., Cameron, N.G., Ficken, K.J., Golding, P., Harkness, D.D., Holmes, J.A., Hutchinson, R., Lishman, J.P., Maddy, D., Pinder, L.C.V., Rose, N.L., Stoneman, R.E. (1999): Proxy records of climate change in the UK over the last two millennia: documented change and sedimentary records from lakes and bogs, Journal Geological Society 156, 369–380.

Barber, K.E., Chambers, F.M., Maddy, D. (2003): Holocene paleoclimates from peat stratigraphy: macrofossil proxy climate records from three oceanic raised bogd in England and Irland, Quaternary Science Reviews 22, 521-539.

Berger, A. & Loutre, M.F. (1991): Insolation values for the climate of the last 10 million years, Quaternary Science Reviews Volume 10 (4), Pages 297-317, doi:10.1016/0277-3791(91)90033-Q.

Bertrand, C., van Ypersele J.P., Berger, A. (1999): Volcanic and Solar Impacts on Climate since 1700, Climate Dynamics 15, 355–367.

Birgel, D. & Hass, H.C. (2004): Oceanic and atmospheric variations during the last deglaciation in the Fram Strait (Arctic Ocean): a coupled high-resolution organic-geochemicaland sedimentological study, Quaternary Science Reviews 23, 29-47.

Bond, G.C., Heinrich, H., Broecker, W.S., Labeyrie, L.D., McManus, J., Andrews, J., Huon, S., Janschick, R., Clasen, S., Simet, C., Tedesko, K., Klas, M., Bonani, G., Ivy, S. (1992): Evidence for massive iceberg discharges in the North Atlantic Ocean during the last glacial period, Nature 360, 245-249.

Bond, G., Broecker, W.S., Johnsen, S.J., McManus, J., Labeyrie, L., Jouzel, J., Bonani, G. (1993): Correlations between climate records from North Atlantic sediments and Greenland ice, Nature 365, 143–147.

Bond, G., Showers, W., Cheseby, M., Lotti, R., Almasi, P., deMenocal, P., Cullen, H., Hajdas, I., Bonani, G. (1997): A pervasive millennial-scale cycle in North Atlantic Holocene and glacial climates, Science 278, 1257–1265.

Bondevik, S. & Mangerud, J. (2002): A calendar age estimate of a very late Younger Dryas ice sheet maximum in western Norway, Quaternary Science Reviews 21, 1661–1676.

Briffa, K.R., Jones, P.D., Schweingruber, F. H., Osborn, T.J. (1998): Influence of Volcanic Eruptions on Northern Hemisphere Summer Temperature over the Past 600 Years, Nature 393, 450–455.

Broecker, W.S. (2000): Was a change in the thermohaline circulation responsible for the Little Ice Age? Proceedings of the National Academy of Science USA 97: 1339-1347.

Butzin, M., Prange, M., Lohmann G. (2005): Radiocarbon simulations for the glacial ocean: the effects of wind stress, Southern Ocean sea ice and Heinrich events, Earth Planet. Science Letters 235, 45-61, doi:10.1016/j.epsl.2005.03.003.

Charles, C.D., Rind, D., Jouzel, J.,. Koster, R.D, Fairbanks, R.G. (1994): Glacial-interglacial changes in moisture sources for Greenland: Influences on the ice core record of climate, Science 263, (5146), 508-511.

Chivas, A.R., De Deckkler, P., Shelley, J.M.G. (1985): Strontium content of ostracods indicates lacustrine palaeosalinity, Nature 316, 251 - 253 ; doi:10.1038/316251a0.

Chivas, A.R., De Deckkler, P., Shelley, J.M.G. (1986): Magnesium and strontium in non-marine ostracod shells as indicators of palaeosalinity and palaeotemperature, Hydrobiologia 143, 135-142.

CLIMAP (1976):The surface of the Ice-Age Earth, Science 191, 1131-1137.

CLIMAP (1981): Seasonal reconstruction of the Earth's surface at the last glacial maximum. Geological Society of America, Map and Chart Series, Vol. C36.

Crowley, T.J. & Kim, K.Y. (1999): Modeling the Temperature Response to Forced Climate Change over the Past Six Centuries, Geophysical Research Letters 26, 1901–1904.

Crowley, T.J. (2000): Causes of Climate Change over the Past 1000 Years, Nature 289, 270–277.

Crüger, T., Fischer, H., von Storch, H. (2004): What do accumulation records of single ice cores in Greenland represent?, Journal of Geophysical Research 109, D21110, doi:10,1029/2004JD005014.

D'Arrigo, R.D., Jacoby, G.C., Free, M., Robock, A. (1999): Northern Hemisphere Temperature Variability for the Past Three Centuries: Tree-Ring and Model Estimates, Climate Change 42, 663–675.

de Vernal, A., Rosell-Melé, A., Kucera, M., Hillaire-Marcel, C., Eynaud, F., Weinelt, M., Dokken, T., Kageyama, M. (2006): Comparing proxies for the reconstruction of LGM sea-surface conditions in the northern North Atlantic, Quaternary Science Reviews 25 (21-22), 2820-2834.

de Villiers, S., Shen, G.T., Nelson, B.K. (1994): The Sr/Ca-temperature relationship in coralline aragonite: influence of variability in (Sr/Ca) seawater and skeletal growth parameters, Geochimica et Cosmochimica Acta 58, 197–208.

de Villiers, S. (1999): Seawater strontium and Sr/Ca variability in the Atlantic and Pacific oceans, Earth and Planetary Science Letters 171, 623–634.

Denton, G.H., Heusser, C.J., Lowell, T.V., Moreno, P.I., Andersen, B.G., Heusser, L.E., Schluchter, C., Marchant, D.R., (1999): Interhemispheric linkage of paleoclimate during the last glaciation. Geografiska Annaler Series A, Physical Geography 81A (2), 107–153.

Dokken, T.M. & Hald, M., 1996. Rapid climatic shifts during isotope stages 2–4 in the Polar North Atlantic. Geology 24 7 , 599–602.

Dowdeswell, J.A., Elverhøi, A. (2002): The timing of initiation of fast–flowing ice streams during a glacial cycle inferred from glacimarine sedimentation. Marine Geology 188, 3–14.

Duplessy. J.-C. (1978): Isotope studies, in: Gribbin. J.R. (Ed.) Climatic Change, pp. 46--67. Cambridge University Press, Cambridge, U.K.

Duplessy. J.-C. (1982): Circulation des eaux profondes au cours du dernier cycle climatique. Bulletin h~stitute Geologique Bassin d'Aquitaine, 31. 379-391.

Duplessy, J.-C.. Shackleton, N.J., Matthews, R.K., Prell, W., Ruddiman. W.F., Caralp, M. and Hendy, C.H. (1984): Carbon-13 record of benthic foraminifera in the last interglacial ocean: Implications for the carbon cycle and the global deep water circulation, Quaternary Research 21, 225-243.

Duplessy, J.-C. and Shackleton. N.J. (1985): Response of global deep-water circulation to the Earth's climatic change 135,000 -107,000 years ago, Nature. 316, 500-507.

Elderfield, H., Cooper, M., Ganssen, G. (2000): Sr/Ca in multiple species of planktonic foraminifera: Implications for reconstructions of seawater Sr/Ca, Geochemistry Geophysics Geosystems 1, (Paper number: 1999GC000031).

Elderfield, H., Vautravers, M., Cooper, M. (2002): The relationship between shell size and Mg/Ca, Sr/Ca, $\partial^{18}O$ and $\partial^{13}C$ of species of planktonic foraminifera, Geochemistry Geophysics Geosystems 3 (8), doi: 10.1029/2001GC000194.

Elverhøi, A., Andersen, E.S., Dokken, T., Hebbeln, D., Spielhagen, R.F., Svendsen, J.I., Sørflaten, M., Rørnes, A., Hald, M., Forsberg, C.F. (1995): The growth and decay of the Late Weichselian Ice Sheet in western Svalbard and adjacent areas based on provenance studies of marine sediments, Quaternary Research 44, 303–316.

Fischer, H., Werner, M., Wagenbach, D., Schwager, M., Thorsteinnson, T., Wilhelms, F., Kipfstuhl, S., Sommer, S. (1998): Little Ice Age clearly recorded in northern Greenland ice cores, Geophysical Research Letters 25, 1749– 1752.

Forman, S.L. (1999): Infrared and Red Stimulated Luminescence Dating of Late Quaternary Near-shore Sediments from Spitsbergen, Svalbard, Arctic, Antarctic and Alpine Research, 31 (1), 34-49.

Forman, S.L. & Ingólfsson, Ó. (2000): Late Weichselian glacial history and postglacial emergence of Phippsøya, Sjuøyane, northern Svalbard: a comparison of modelled and empirical estimates of a glacial-rebound hinge line, Boreas 29, 16-25.

Gabitov, R.I. & Watson, E.B. (2006): Partitioning of Sr between calcite and fluid, Geochemistry Geophysics Geosystems 7 (11), doi:10.1029/2005GC001216.

Gaetani, G. & Cohen, A.L. (2006): Element partitioning during precipitation of aragonite from seawater: A framework for understanding paleoproxies, Geochimica et Cosmochimica Acta 70, 4617-4634.

Gildor, H. & Tziperman, E. (2001): A sea ice climate switch mechanism for the 100-kyr glacial cycles, Journal of Geophysical Research 106, 9117-9133.

Gildor, H. & Tziperman, E. (2003): Sea ice switches and abrupt climate change, Phil. Trans. R. Soc. Lond. 361, 1935-1944, 10.1098/rsta.2003.1244.

Grimm, E.C., Watts, W.A., Jacobson Jr., G.L., Hansen, B.C.S., Almquist, H.R., Dieffenbacher-Krall, A.C. (2006): Evidence for warm wet Heinrich events in Florida, Quaternary Science Reviews 25, 2197–2211.

Grobe, H., 1987. A simple method for determination of ice rafted debris in sediment cores. Polarforschung 57 3 , 123–126.

Haake, F.W. & Plaumann, U. (1989): Late Pleistocene foraminiferal stratigraphy on the Vøring Plateau, Norwegian Sea, Boreas 18 (4), 343–356.

Haase-Schramm, A., Böhm, F., Eisenhauer, A., Dullo, W.C., Joachimski, M.M., Hansen, B., Reitner, J. (2003): Sr/Ca ratios and oxygen isotopes from sclerosponges: Temperature history of the Caribbean mixed layer and thermocline during the Little Ice Age, Paleoceanography 18 (3), 1073-1091, doi: 10.1029/2002PA000830.

Hald, M., Dokken, T., Mikalsen, G. (2001): Abrupt climatic change during the last interglacial–glacial cycle in the polar North Atlantic, Marine Geology 176, 121-137.

Halverson, G.P., Maloof, A.C., Schrag, D.P., Dudás, F.Ö., Hurtgen, M. (2007): Stratigraphy and geochemistry of a ca 800 Ma negative carbon isotope interval in northeastern Svalbard, Chemical Geology 237 (2007) 5–27.

Hampt, G. & Delaney, M. (1997): Influence on calcite Sr/Ca records from Ceara Rise and other regions: Distinguishing ocean history and calcite recrystallisation, in: Shackleton, N.J., Curry, W.B., Richter, C., Bralower, T.J. (Eds.), Proceedings of the ocean Drilling Program, Scientific Results 154(34), 491-500.

Hebbeln, D., Dokken, T., Andersen, E.S., Hald, M., Elverhøi, A. (1994): Moisture supply for northern ice-sheet growth during the Last Glacial Maximum, Nature 370, 357–359.

Hebbeln, D. & Wefer, G. (1997): Late Quaternary paleoceanography in the Fram Strait, Paleoceanography 12, 65-78.

Hebbeln, D., Henrich, R., Baumann, K.H. (1998): Paleoceanography of the last Interglacal/Glacial Cycle in the Polar North Atlantic, Quaternary Science Reviews 17, 125-153.

Henrich, R. (1998): Dynamics of Atlantic water advection to the Norwegian-Greenland Sea - a time-slice record of carbonate distribution in the last 300 ky, Marine Geology 145 95- 131.

Henrich, R., Baumann, K.H., Huber, R., Meggers, H. (2002): Carbonate preservation records of the past 3 Myr in the Norwegian^Greenland Sea and the northern North Atlantic: implications for the history of NADW production, Marine Geology 184, 17-39.

Hodell, D.A., Romero, O.E., Roehl, U., Channell, J.E., Exp. 303 Shipboard Scientific Party (2005): Detrital Carbonate (Heinrich-type) Layers During Glacial Stages of the Brunhes Chronozone at IODP Site 1308 (re-occupation of DSDP Site 609) , Eos Trans. AGU, 86(52), Fall Meet. Suppl., Abstract PP33A-1553.

Huybrechts, P. (2002): Sea-level changes at the LGM fromice-dynam ic reconstructions of the Greenland and Antarctic ice sheets during the glacial cycles, Quaternary Science Reviews 21, 203–231.

Jakobsson, M., Cherkis, N. Z, Woodward, J., Macnab, R., Coakley, B. (2000): New grid of Arctic bathymetry aids scientists and mapmakers; Eos, Transactions, American Geophysical Union, v. 81 (9), p. 89, 93, 96.

Jansen, E. (1989): The use of stable oxygen and carbon isotope stratigraphy as a dating tool, Quaternary International 1, 151-166.

Johnsen, S.J., Clausen, H.B., Dansgaard, W., Gundestrup, N.S., Hammer, C.U., Andersen, U., Andersen, K.K., Hvidberg, C.S., Dahl-Jensen, D., Steffensen, J.P., Shoji, H., Sveinbjörnsdóttir, A.E., White, J.W.C., Jouzel, J., Fisher, D. (1997): The $\partial^{18}O$ record along the Greenland Ice Core Pproject deep ice core and the problem of possible Eemian climatic instability, Journal of Geophysical Research 102, 26397-26410.

Jokat, W. (Ed.) (2000): The Expedition RKTIS-XV/2 of Polarstern in 1999, Berichte zur Polar- und Meeresforschung, 368, 128 pp, Alfred-Wegener-Institut, Bremerhaven.

Jouzel, J., Stiévenard, M., Johnsen, S.J., Landais, A., Masson-Delmotte, V., Sveinbjornsdottir, A., Vimeux, F., von Grafenstein, U., White, J.W.C. (2007): The GRIP deuterium-excess record, Quaternary Science Reviews 26, 1–17.

Kierdorf, C. (2006): Variability of organic carbon along the ice-covered polar continental margin of East Greenland, unpublished PhD thesis, University of Bremen, 241 pp.

Kirkbride, M.P. & Dugmore, A.J. (2001): Timing and significance of mid-Holocene glacier advances in northern and central Iceland, Journal of Quaternary Science 16, 145–153.

Klitgaard-Kristensen, D., Rasmussen, T.L., Sejrup, H.P., Haflidason, H., van Weering, T.C.E. (1998): Rapid changes in the oceanic fronts in the Norwegian Sea during the last deglaciation: implications for the Younger Dryas cooling event, Marine Geology 152 (1998) 177–188.

Knies, J. & Stein, R. (1998): New aspects of organic carbon deposition and its paleoceanographic implications along the northern Barents Sea margin during the last 30,000 years. Paleoceanography 13 4 , 384–394.

Knies, J., Vogt, C., Stein, R. (1999): Late Quaternary growth and decay of the Svalbard-Barents Sea ice sheet and paleoceanographic evolution in the adjacent Arctic ocean. Geo-Marine Letters 18, 195–202.

Knies, J., Nowaczyk, N.R., Müller, C., Vogt, C, Stein, R. (2000): A multiproxy approach to reconstruct the environmental changes along the Eurasian continental margin over the last 150 000 years. Marine Geology 163, 317-344.

Knies, J., Kleiber, H.P., Nowaczyk, N., Mathiessen, J., Muller, C., Niessen, F., Stein, R., Weiel, D. (2001): Marine ice-rafted debris records constrain maximum extent of Saalian and Weichselian ice-sheets along the northern Eurasian Margin. Global and Planetary Change 31, 45–64.

Koç, N., Jansen, E., Haflidason, H. (1993): Palaeoceanographic reconstructions of surface ocean conditions in the Greenland, Iceland and Norwegian Seas through the last 14 ka based on diatoms, Quaternary Science Reviews 12, 115–140.

Koç, N., Klitgaard-Kristensen, D., Hasle, K., Forsberg, C.F., Solheim, A. (2002):Late glacial paleoceanography of Hinlopen Strait, northern Svalbard, Polar Research 21, 307-314.

Kroopnick, P. (1980). The distribution of ~3C in the Atlantic Ocean, Earth and Planetary Science Letters 49, 469--484.

Kukla, G. & Gavin, J. (2005): Did glacials start with global warming?, Quaternary Science Reviews 24; 1547-1557.

Labeyrie, L.D. & Duplessy, J.-C. (1985): Changes in the oceanic I3C/12C ratio during the last 140,000 years: high latitude surface water records, Palaeogeography, Palaeoclimatology, Palaeoecology 50, 217-240.

Lamb, H.H. (1979): Climatic Variations and Changes in the Wind and Ocean Circulation. The Little Ice Age in the Northeast Atlantic, Quarternary Research 11, 1–20.

Lambeck, K., Yokoyama, Y., Purcell, T. (2002): Into and out of the Last Glacial Maximum: sea-level change during Oxygen Isotope Stages 3 and 2, Quaternary Science Reviews 21, 343-360.

Landscheidt, T. (2003): New Little Ice Age Instead of Global Warming? Energy & Environment, Volume 14, 327-350.

Landvik, J.Y., Bondevik, S., Elverhøi, A., Fjeldskaar, W., Mangerud, J., Salvigsen, O., Siegert, M.J., Svendsen J.I., Vorren, T.O. (1998): The last glacial maximum of Svalbard and the Barents sea area: ice sheet extent and configuration, Quaternary Science Reviews 17, 43-75.

Langdon, P.G., Barber, K.E., Hughes, P.D.M. (2003): A 7500-year peatbased palaeoclimatic reconstruction and evidence for an 1100-year cyclicity in bog surface wetness from Temple Hill Moss, Pentland Hills, southeast Scotland, Quaternary Science Reviews 22, 259– 274.

Li, C., Battisti, D.S., Schrag, D.P., Tziperman, E. (2005): Abrupt climate shifts in Greenland due to displacements of the sea ice edge, Geophysical Research Letters 32, L19702, doi:10.1029/2005GL023492.

Lisiecki, L.E., & Raymo, M.E. (2005): A Pliocene-Pleistocene stack of 57 globally distributed benthic ^{18}O records, Paleoceanography 20, PA1003, doi:10.1029/2004PA001071.

Lockwood, J.G. (2001): Abrupt and sudden climate transitions and fluctuations. A review, International Journal of Climatology 21, 1153–1179.

Lohmann, G. (2003): Atmospheric and oceanic freshwater transport during weak Atlantic overturning circulation, Tellus 55A, 438–449.

Lowell, T.V. (2000): As climate changes, so do glaciers, Proceedings of the National Academy of Science USA 97, 1351–1354.

Luterbacher, J., Rickli, R., Xoplaki, E., Tinguely, C., Beck, C., Pfister, C., Wanner, H. (2001): The late Maunder Minimum (1675–1715) – a key period for studying decadal scale climate change in Europe, Climatic Change 49: 441–462.

Magny M., Leuzinger, U., Bortenschlager, S., Haas, J.N. (2006): Tripartite climate reversal in Central Europe 5600–5300 years ago, Quaternary Research 65 (2006) 3-19.

Manabe, S. & Broccoli, A.J. (1985): The influence of continental ice sheets on the climate of an ice age, Journal of Geophysical Research 90 (D1), 2167-2190.

Mangerud, J. & Svendsen, J.I. (1990): Deglaciation chronology inferred from marine sediments in a proglacial lake basin, western Spitsbergen, Svalbard, Boreas 19, 249-272.

Mangerud, J., Bolstad, M., Elgersma, A., Helliksen, D., Landvik, J.Y., Lønne, I., Lycke, A.K., Salvigsen, O., Sandahl, T., Svendsen J.I. (1992): The last glacial maximum on Spitsbergen, Svalbard, Quaternary Research 38, 1-31.

Mangerud, J., Jansen, E., Landvik, J. (1996): Late Cenozoic history of the Scandinavian and Barents Sea ice sheets, Global and Planetray Change, 12, 11-26.

Mangerud, J., Dokken, T., Hebbeln, D., Heggen, B., Ingólfsson, Ó., Landvik, J.Y., Mejdahl, V., Svendsen, J.I., Vorren, T.O. (1998): Fluctuations of the Svalbard-Barents Sea ice sheet during the last 150 000 years, Quaternary Science Reviews 17: 11-42.

Mangini, A. Jung, M., Laukenmann, S. (2001): What do we learn from peaks of uranium and of manganese in deep sea sediments? Marine Geology 177, 63-78.

Mann, M.E., Bradley, R.S., Hughes, M.K. (1998): Global-Scale Temperature Patterns and Climate Forcing over the Past Six Centuries, Nature 392, 779–787.

Marchal, O., Cacho, I., Stocker, T.F., Grimalt, J.O. Calvo, E., Martrat, B., Shackleton, N., Vautravers, M., Cortijo, E., van Kreveld, S., Andersson, C., Koc, N., Chapman, M., Sbaffi, L., Duplessy, J.C., Sarnthein, M., Turon, J.L., Duprat, J., Jansen, E. (2002):Apparent long-termcooling of the sea surface in the northeast Atlantic and Mediterranean during the Holocene, Quaternary Science Reviews 21, 455–483.

Martin, P.A., Lea, D.W., Mashiotta, T.A., Papenfuss, T., Sarnthein, M. (1999): Variation of foraminiferal Sr/Ca over Quaternary glacial-interglacial cycles: evidence for changes in mean ocean Sr/Ca?, Geochemistry Geophysics Geosystems 1, paper number: 1999GC000006.

Martinson, D.G., Pisias, N.G., Hays, J.D., Imbrie, J., Moore, T.C., Shackleton, N.J. (1987): Age dating and the orbital theory of the ice ages: development of a high-resolution 0 to 300,000 years chronostratigraphy. Quaternary Research 27, 1–27.

Masson-Delmotte, V., Jouzel, J., Landais, J.A., Stievenard, M., Johnsen, S.J., White, J.W.C., Werner, M., Sveinbjornsdottir, A., Fuhrer, K. (2005): GRIP Deuterium Excess Reveals Rapid and Orbital-Scale Changes in Greenland Moisture Origin, Science 309, 118-121.

Matthews, J.A., Berrisforda, M.S., Dressera, P.Q., Nesje, A., Dahl, S.O., Bjune, A.E., Bakke, J., John, H., Birks, B., Lie, Ø., Dumayne-Peaty, L., Barnett, C. (2005): Holocene glacier history of Bjørnbreen and climatic reconstruction in central Jotunheimen, Norway, based on proximal glaciofluvial stream-bank mires, Quaternary Science Reviews 24, 67–90.

Miller, G.H., Wolfe, A.P., Briner, J.P., Sauer, P.E., Nesje, A. (2005): Holocene glaciation and climate evolution ofBaf fin Island, Arctic Canada, Quaternary Science Reviews 24, 1703–1721.

Mix, A.C. & Fairbanks, R.G. (1985): North Atlantic surface-ocean control of Pleistocene deep-ocean circulation, Earth and Planetary Science Letters. 73, 231-243.

Mix, A.C., Bard, E., Schneider, R. (2001): Environmental processes of the ice age: land, ocean, glaciers (EPILOG), Quaternary Science Reviews 20, 627-657.

Möller, P., Lubinski, D.J., Ingólfsson, Ó., Forman, S.L., Seidenkrantz, M.S., Bolshiyanov, D.Y., Lokrantz, H., Antonov, O., Pavlov, M., Ljung K., Zeeberg, J., Andreev, A. (2006): Severnaya Zemlya, Arctic Russia: a nucleation area for Kara Sea ice sheets during the Middle to Late Quaternary, Quaternary Science Reviews 25, 2894-2936.

Morgan, V.I., Goodwin, I.D., Etheridge, D.M., Wookey, C.W. (1991): Evidence from Antarctic ice cores for recent increases in snow accumulation, Nature 354 (6348), 58-60.

Morison, J., Aagaard, K., Steele, M. (2000): Recent Environmental Changes in the Arctic: A Review, Arctic 53 (4), 359-371.

Moros, M., Emeis, K., Risebrobakken, B., Snowball, I., Kuijpers, A., McManus, J., Jansen, E. (2004): Sea surface temperatures and ice rafting in the Holocene North Atlantic: climate influences on northern Europe and Greenland, Quaternary Science Reviews 23, 2113–2126.

Nesje, A., Dahl, S.O., Andersson, C., Matthews, J.A. (2000): The lacustrine sedimentary succession in Sygneskardvatnet, western Norway: a continuous, high-resolution record of the Jostedalsbreen ice cap during the Holocene, Quaternary Science Reviews 19, 1047–1065.

Nesme-Ribes, E. & Mangeney, A. (1992): On a plausible physical mechanism linking the Maunder minimum to the Little Ice Age, Radiocarbon Volume 34, 263-270.

North Greenland Ice Core Project members (2004): High-resolution record of Northern Hemisphere climate extending into the last interglacial period, Nature 431, 147-151.

Nørgaard-Pedersen, N., Spielhagen, R.F., Thiede, J., Kassens, H. (1998): Central Arctic surface ocean environment during the past 80,000 years, Paleoceanography 13 2 , 193–204.

Nørgaard-Pedersen, N., Spielhagen, R.F., Erlenkeuser, H., Grootes, P.M., Heinemeier, J., Knies, J. (2003): The Arctic ocean during the Last Glacial Maximum: atlantic and polar domains of surface water mass distribution and ice cover, Pleoceanography 18, 1-19.

Nørgaard-Pedersen, N., Mikkelsen, N., Lassen, S.J., Kristoffersen, Y., Sheldon, E. (2007): Reduced sea ice concentrations in the Arctic Ocean during the last interglacial period revealed by sediment cores off northern Greenland, Paleoceanography 22, PA1218, doi:10.1029/2006PA001283.

Nyland, B.F., Jansen, E., Elderfield, H., Andersson, C. (2006): Neogloboquadrina pachyderma (dex. and sin.) Mg/Ca and $\partial^{18}O$ records from the Norwegian Sea, Geochemistry Geophysics Geosystems 7 (10), doi: 10.1029/2005GC001055.

Oppenheimer, C. (2002): Limited global change due to the largest known Quaternary eruption, Toba ≈74 kyr BP? Quaternary Science Reviews 21, 1593-1609.

Ottesen, D., Dowdeswell, J.A., Rise, L. (2005): Submarine landforms and the reconstruction of fast-fl owing ice streams within a large Quaternary ice sheet: The 2500-km-long Norwegian-Svalbard margin (57°–80°N), GSA Bulletin, 117 (7/8), 1033–1050, doi: 10.1130/B25577.1.

Owrid, G., Socal, G., Civitarese, G., Luchetta, A., Wiktor, J., Nöthig, E.M., Andreassen, I., Schauer, U., Strass, V. (2000): Spatial variability of phytoplankton, nutrients and new production estimates in the waters around Svalbard, Polar Research 19, 155–171.

Peltier, W.R. & Fairbanks, R.G. (2006): Global glacial ice volume and Last Glacial Maximum duration from an extended Barbados sea level record, Quaternary Science Reviews 25, 3322–3337.

Piotrowski, A.M., Goldstein, S.L., Hemming, S.R., Fairbanks, R.G. (2004): Intensification and variability of ocean thermohaline circulation through the last deglaciation, Earth and Planetary Science Letters 225, 205– 220.

Pflaumann, U. Sarnthein, M., Chapman, M., dÀbreu, L., Funnel, B., huels, M., Kiefer, T., Maslin, M., Schulz, H., Swallow, J., van Kreveld, S., Vautravers, M., Vogelsang, E., Weinelt, M. (2003): Glacial North Atlantic: Sea-surface conditions reconstructed by GLAMAP 2000, Paleoceanography 18, doi: 10.1029/2002PA000774.

Pirrung, M., Fütterer, D., Grobe, H., Matthiessen, J., Niessen, F. (2002): Magnetic susceptibility and ice-rafted debris in surface sediments of the Nordic Seas: implications for Isotope Stage 3 oscillations, Geo-Marine Letters 22, 1-11.

Polyakov, I.V., Beszczynska,A., Carmack, E.C., Dmitrenko, I.A., Fahrbach, E., Frolov, I.E., Gerdes, R., Hansen, E., Holfort, J., Ivanov, V.V., Johnson, M.A., Karcher, M., Kauker, F., Morison,J., Orvik, K.A., Schauer, U., Simmons, H.L., Skagseth, Ø., Sokolov, V.T., Steele, M., Timokhov, L.A., Walsh, D., Walsh, J.E. (2005): One more step toward a warmer Arctic, Geophysical Research Letters 32, L17605, doi:10.1029/2005GL023740.

Porter, S.C. (2000): Onset of Neoglaciation in the Southern Hemisphere, Journal of Quaternary Science 15, 395–408.

Prange, M., Romanova, V., Lohmann, G. (2002): The glacial thermohaline circulation: Stable or unstable?, Geophysical Research Letters 29, 2028 (doi:10.1029/2002GL015337).

Rahmstorf, S. (2002): Ocean circulation and climate during the past 120,000 years, Nature 419, 207-214.

Rasmussen, T., Thomsen, E., Ślubowska, M., Jessen, S., Solheim, A., Koç, N. (2007): Paleoceanographic evolution of the SW Svalbard margin (76°N) since 20,000 ^{14}C yr BP, Quaternary Research 67, 100-114.

Renssen, H. & Isarin, R.F.B. (2001): The two major warming phases of the last deglaciation at ~14.7 and ~11.5 ka cal B.P. in Europe: climate reconstructions and AGCM experiments, Global and Planetary Change 30, pp. 117–153.

Rickaby, R.E.M., Schrag, D.P., Zondervan, I., Riebesell, U. (2002): Growth rate dependence of Sr incorporation during calcification of Emiliana huxleyi, Global Biogeochemical Cycles 16 (1), doi: 10.1029/2001GB001408.

Ritz, C., Fabre, A., Letr!eguilly, A. (1997): Sensitivity of a Greenland ice sheet model to ice flow and ablation parameters: consequences for the evolution through the last glacial cycle, Climate Dynamics 13, 11–24.

Ritz, C., Rommelaere, V., Dumas, C. (2001): Modeling the Antarctic ice sheet evolution of the last 42,0000 years: implication for altitude changes in the Vostok region, Journal of Geophysical Research106, 31,943– 31,964.

Romanova, V., Prange, M., Lohmann, G. (2004): Stability of the glacial thermohaline circulation and its dependence on the background hydrological cycle, Climate Dynamics 22, 527-538.

Rosenthal, Y., Lear, C.H., Oppo, D.W., Linsley, B.K. (2006): Temperature and carbonate ion effects on Mg/Ca and Sr/Ca ratios in benthis foraminifera: Aragonite species *Hoeglundina elegans*, Paleoceanography 21, doi:10.1029/2005PA001158.

Rühlemann, C., Mulitza, S., Lohmann, G., Paul, A., Prange M., Wefer, G. (2004): Intermediate depth warming in the tropical Atlantic related to weakened thermohaline circulation: Combining paleoclimate and modeling data for the last deglaciation, Paleoceanography 19, PA1025, doi: 10.1029/2003PA000948.

Schäfer, C. (2005): Untersuchungen zu Menge und Zusammensetzung des Organischen Kohlenstoffs in spätquartären Sedimenten des Yermak-Plateaus (Arktischer Ozean) und Umweltbedingungen, Master thesis, Univ. of Trier, 105 pp.

Schauer, U., Fahrbach, E. Osterhus, S, Rohardt, G. (2004): Arctic warming through Fram Strait: Ocean heat transport from 3 years of measurement, Journal of Geophysical Research 109 (C06026), doi: 10.1029/2003JC001823.

Sclanger, S.O. (1988): Strontium storage and release during deposition and diagenesis of marine carbonates related to sea-level variations, in: Lennan, A. & Meybeck, M. (Eds.) Physical and Geochemical Whethering in Geochemical Cycles, NATO ASI Series, Ser. C, Math. Phys. Sci. 251, 323-340.

Schlichtholz, P. & Houssais, M.N. (1999): An inverse modeling study in Fram Strait. Part 1: dynamics and circulation, Deep-Sea Research 46 (II), 1083-1135.

Schneider, R., Bard, E., Mix, A.C. (2000): Last Ice Age global ocean and land surface temperature: the EPILOG initiative, PAGES newsletter 8, 19-21.

Schrag, D.P., DePaolo, D.J., Richter, F.M. (1995): Reconstruction past sea surface temperatures: correcting for diagenesis of bulk marine carbonate, Geochimica et Chosmochimica Acta 59, 2265-2278.

Shackleton, N.J., Backman, J., Zimmerman, H., Kent, D.V., Hall, M.A., Roberts. D.G., Schnitker. D., Baldauf, J., Desprairies, A., Homrighauscn. R., Huddlcstun, P.. Keene. J.B., Kaltcnback, A.J., Krumsiek, K.A.O.. blot'ton, A.C., Murray. J.W., Westberg-Smith, J. (1984): Oxygen isotope calibration of the onset of ice-rafting and history, of glaciation in the North Atlantic region, Nature. 307,620--623.

Shen, C.C., Lee, T., Chen, C.Y., Wang, C.H., Dai, C.F., Li, L.A. (1996): The calibration of D[Sr/Ca] versus sea surface temperature relationship for Porites corals, Geochimica Cosmochimica Acta 60, 3849–3858.

Shindell, D.T., Schmidt, G.A., Miller, R.L., Mann, M.E. (2003): Volcanic and solar forcing of climate change during the preindustrial era, Journal of Climate 16, 4094– 4107.

Siegel, F.R., Galasso, J.L., Kravitz, J.H. Basinger, W.D. (2000): The Svalbard western coast: site of baseline geochemistry and incipient contamination, Environmental Geology 39 (7), 816-822.

Ślubowska, M.A., Koç, N., Rasmussen, T.L., Klitgaard-Kristensen, D. (2005): Changes in the flow of Atlantic water into the Arctic Ocean since the last deglaciation: evidence from the northern Svalbard continental margin, 80°N, Paleoceanography 20, 1-15, doi:10.1029/2005PA001141.

Ślubowska-Woldengen, M., Rasmussen, T.L., Koç, N., Klitgaard-Kristensen, D., Nilsen, F., Solheim, A. (2007): Advection of Atlantic Water to the western and northern Svalbard shelf since 17,500 cal yr BP, Quaternary Science Reviews 26, 463-478.

Sosdian, S., Gentry, D.K., Lear, C.H., Grossman, E.L., Hicks, D., Rosenthal, Y. (2006): Strontium to calcium ratios in the marine gastropod Conus ermineus: Growth rate effects and temperature calibration, Geochemistry Geophysics Geosystems 7, Q11023, doi:10.1029/2005GC001233.

Spielhagen, R.F., Baumann, K.H., Erlenkeuser, H., Nowaczyk, N.R., Nørgaard-Pedersen, N., Vogt, C., Weiel, D. (2004): Arctic Ocean deep-sea record of northern Eurasian ice sheet history, Quaternary Science Reviews 23, 1455-1483.

Stein, R. (Ed.), 2005: Scientific Cruise Report of the Arctic Expedition ARK-XX/3 of RV "Polarstern" in 2004: Fram Strait, Yermak Plateau and East Greenland Continental Margin, Reports on Polar and Marine Research 517.

Stocker, T.F. (1998): The seesaw effect, Science 282, 61–62.

Stocker, T.F. & Marchal, A. (2000): Abrupt climate change in the computer: is it real? Proceedings of the National Academy of Science USA 97, 1362–1365.

Stoll, H.M. & Schrag, D.P. (1996): Evidence for glacial control of rapid sea level changes in the early Cretaceous. Science 272, 1771–1774.

Stoll, H.M. & Schrag, D.P. (1998): Effect of Quaternary sea level cycles on the Sr budget of the ocean. Geochimica et Cosmochimica Acta, 62, 1107-1118.

Stoll, H.M., Schrag, D.P., Clemens, S.C. (1999): Are seawater Sr/Ca variations preserved in Quaternary foraminifera?, Geochimica et Cosmochimica Acta 63 (21), 3535-3547.

Stoll, H.M. & Schrag, D.P. (2000): Coccolith Sr/Ca as a new indicator of coccolithophorid calcification and growth rate. Geochemistry Geophysics Geosystems 1, 1–24.

Stoll, H.M., Rosenthal, Y., Falkowski, P. (2002): Climate proxies from Sr/Ca of coccolith calcite: Calibrations from continuous culture of *Emiliania huxleyi,* Geochimica et Cosmochimica Acta 66 (6), 927–936.

Stoll, H. & Bains, S. (2003): Coccolith Sr/Ca records of productivity during the Paleocene-Eocene Thermal Maximum from the Weddel Sea, Paleoceanography, 18 (2), 27-1.

Stuiver, M., Braziunas, T.F., Grootes, P.M., Zielinski, G.A (1997): Is There Evidence for Solar Forcing of Climate in the GISP2 Oxygen Isotope Record?, Quaternary Research 48, 259–266, QR971931.

Svendsen, H.A., Beszczynska-Møller, A., Hagen, J.O., Lefauconnier, B., Tverberg, V., Gerland, S., Bischof, K., Papucci, C., Zajaczkowski, M., Azzolini, R., Bruland, O., Wiencke, C., Winther, J.G., Dallmann, W. (2002): The physical environment of Kongsfjorden-Krossfjorden, an Arctic fjord system in Svalbard, Polar Research 21(1): 133-166.

Svendsen, J.I. & Mangerud, J. (1992):Paleoclimatic inferences from glacial fluctiations on Svalbard during the last 20 000 years, Climate Dynamics 6, 212-220.

Svendsen, J.I., Elverhøi, A., Mangerud, J. (1996): The retreat of the Barents Sea Ice Sheet on the western Svalbard margin, Boreas 25, 244–256.

Svendsen, J.I., Alexanderson, H., Astakhov, V.I., Demidov, I., Dowdeswell, J.A., Funder, S., Gataullin, V., Henriksen, M., Hjort, C., Houmark-Nielsen, M., Hubberten, H.W., Ingólfsson, Ó., Jakobsson,´M. Kjær, K.H., Larsen, E., Lokrantz, H., Lunkka, J.P., Lyså, A., Mangerud, J., Matiouchkov, A., Murray, A., Möller, P., Niessen, F., Nikolskaya, O., Polyak, L., Saarnisto, M., Siegert, C., Siegert, M.J., Spielhagen, R.F., Stein, R. (2004): Late Quaternary ice sheet history of northern Eurasia, Quaternary Science Reviews 23, 1229–1271.

Svensson, A., Andersen, K.K., Bigler, M., Clausen, H.B., Dahl-Jensen, D., Davies, S.M., Johnsen, S.J., Muscheler, R., Rasmussen, S.O., Röthlisberger, R., Steffensen, J.P., Vinther, B.M. (2006): The Greenland Ice Core Chronology 2005, 15–42 ka. Part 2: comparison to other records, Quaternary Science Reviews 25, 3258–3267.

Swart, P.K., Elderfield, H., Greaves, M.J. (2002): A high-resolution calibration of Sr/Ca thermometry using the Caribbean coral Montastraea annularis, Geochemistry Geophysics Geosystems 3 (11), doi: 10.1029/2002GC000306.

Tjallingii, R., Röhl, U., Kölling, M., Bickert, T. (2007): Influence of the water content on X-ray fluorescence core-scanning measurements in soft marine sediments, Geochemistry, Geophysics, Geosystems 8 (2), doi:10.1029/2006GC001393.

Thompson, W.G. & Goldstein, S.L. (2006): A radiometric calibration of the SPECMAP timescale, Quaternary Science Reviews 25, 3207–3215.

Thomson, J., Higgs, N.C., Colley, S. (1996): Diagenetic redistributions of redox-sensitive elements in northeast Atlantic glacial/interglacial transition sediments, Earth and Planetary Science Letters 139, 365-377.

Vettoretti, G. & Peltier, W.R. (2003): Post-Eemian Glacial Inception, Part II: Elements of a Cryospheric Moisture Pump, Journal of Climate 16, 912–927.

Vogt, C., Knies, J., Spielhagen, R.F., Stein, R. (2001): Detailed mineralogical evidence for two nearly identical glacial/deglacial cycles and Atlantic water advection to the Arctic Ocean during the last 90,000 years. Global and Planetary Change 31, 23-44.

Voelker, A.H.L., Sarnthein, M., Grootes, P.M., Erlenkeuser, H., Lay, C., Mazaud, A., Nadeau, M.J., Schleicher, M. (1998): Correlation of marine ^{14}C ages from the Nordic Seas with the GISP2 isotope record: implications for ^{14}C calibration beyond 25 ka BP. Radiocarbon 40 (1), 517–534.

Voelker, A.H.L. (1999): Zur Deutung der Dansgaard-Oeschger Ereignisse in ultra-hochauflösenden Sedimentprofilen aus dem Europäischen Nordmeer, DSc dissertation, University of Kiel, Germany: Berichte-Reports, Institut für Geowissenschaften, Univerität Kiel, nr. 9:278p.

Voelker, A.H.L., Grootes, P.M., Nadeau, M.J., Sarnthein, M. (2000): Radiocarbon levels in the Iceland Sea from 25–53 kyr and their link to the earth's magnetic field intensity, Radiocarbon 42, 437–452.

Walczowski, W. & Piechura, J. (2006): New evidence of warming propagating toward the Arctic Ocean, Geophysical Research Letters 33, L12601, doi:10.1029/2006GL025872.

Weinelt, M., Vogelsand, E., Kucera, M., Pflaumann, U., Sarnthein, M., Voelker, A. (2003): Variability of North Atlantic heat transfer during MIS 2, Paleoceanograpy 18, doi: 10.1029/2002PA000772.

Wien, K., Kölling, M., Schulz, H.D. (2005): Close correlation between Sr/Ca ratios in bulk sediments from the southern Cape Basin and the SPECMAP record, Geo-Marine Letters 25, 265-271, doi: 10.1007/s00367-005-0211-8.

Winkelmann, D. & Knies, J. (2005): Recent distribution and accumulation of organic carbon on the continental margin west off Spitsbergen, Geochemistry, Geophysics, Geosystems 6 (9), doi:10.1029/2005GC000916.

Winkelmann, D., Jokat, W., Stein, R., Winkler, A. (2006a): Age and extent of the Yermak Slide north of Spitsbergen, Arctic Ocean, Geochemistry, Geophysics, Geosystems 7 (6), doi:10.1029/2005GC001130.

Winkelmann, D., Jokat, W., Niessen, F., Stein, R., Winkler, A. (2006b): Dynamic and Timing of the Yermak/Hinlopen Slide, Arctic Ocean, European Geosciences Union General Assembly 2006 Vienna, Austria, 02 – 07 April 2006.

Winkelmann, D. & Stein, R. (2007): Triggering of the Hinlopen/Yermak Megaslide in relation to paleoceanography and climate history of the continental margin north of Spitsbergen, Geochemistry, Geophysics, Geosystems 8 (6), Q06018, doi:10.1029/2006GC001485.

Winkelmann, D., Geissler, W., Schneider, J., Stein, R. (2007): Dynamic and timing of the Hinlopen/Yermak Megaslide north of Spitsbergen, Arctic Ocean, Marine Geology (under review).

Zielinski, G.A., Mayewski, P.A., Meeker, L.D., Whitlow, S., Twickler, M.S., Taylor, K. (1996): Potential atmospheric impact of the Toba mega-eruption 71,000 years ago, Geophysical Research Letters 23, 837-840.

Zielinski, G.A. (2000): Use of paleo-records in determining variability within the volcanism-climate system, Quaternary Science Reviews 19, 417-438.

Chapter VI

Summary & Conclusion

Summary

The dynamics of submarine failure events north of Svalbard have been elucidated within the ESF EUROMARGIN Project “Slope stabilities on Europe's passive continental margin”. We identified an enormous submarine slide north of Spitsbergen confirming an earlier and discussed scientific publication by Cherkis et al. (1999). Based on high-resolution acoustic data (Hydrosweep swath-bathymetry and PARASOUND) and seismic data, we revised the extent and firstly characterise the true geometry of the megaslide.

Geometry

This huge slope failure consists of one main event (megaslide) and a number of comparably small-scaled events visible as younger debris flows on top of the main slide debris body. The megaslide involved more than 2400 km³ of sedimentary material and affected an area exceeding 10.000 km² (Winkelmann et al., 2006). The runout length exceeds 275 km at an total drop height of more than 3750 m. Thus, we established the geometrical parameter in describing submarine slides.

Sedimentological and physigraphical characterisation

The megaslide is result of a partial shelf collapse at the termination of a cross shelf trough. The failed sediments were part of the associated trough mouth fan (TMF) and their continuation and transition into “normal” hemi-pelagic glacio-marine sediments to the east.

The event left the highest headwalls (up to 1400 m and 1600 m combined headwall height) so far reported for glacier-fed continental margins and probably world-wide. Tens of rafted blocks reaching extensions of more than 3 km and up to 450 m relief are present within the main debris body inside the Sophia Basin.

Dynamic

The megaslide developed as a multi-stage single main retrogressive slope failure. The slide process is characterised by an initial rapid evacuation process that led to excess debris input into the Sophia Basin. The slide had to funnel out into the Nansen Basin through the Littke Channel – a submarine narrow channel between the “Polarstern Seamount” and the adjacent continental slope. This funnelling process consumed a large portion of its kinetic energy and resulted in the multi-stage character of the megaslide. Following this first excess evacuation, a secondary evacuation led to secondary headwalls and escarpments in the north-western Sophia Basin inside the slide's debris. This secondary evacuation is associated with differential subsidence inside the basin.

Following this multi-stage megaslide event, a number of small-scale failure events have been recognised. They are documented as younger debris flows and most likely correspond to adjusting multiple headwalls of the eastern headwall area. This eastern headwall area appears to be subject to ongoing failure processes related to a retrogressive headwall development. The whole continental slope bordering the Sophia Basin to the east appears to be still adjusting to the removal of the TMF. Soft sediment deformation and presence of decollements are documented in the geophysical and sedimentological data.

Age

The Yermak Megaslide occurred around 30 calendar kyr. BP (Winkelmann et al., 2006). The minor events (younger debris flows) have not been dated.

Paleo-environmental conditions

Based on our dating, the megaslide occurred during the rapid onset of peak glaciation around 30 calendar kyr. BP which was associated with a drastic sea level drop (ca. 50 m in less than 1 kyr.; Lambeck et al., 2002) that were probably amplified by a local isostatic rebound and fore bulge development of the growing Svalbard-Barents Sea-Ice Sheet (SBIS). Coinciding with this sea-level drop, enhanced Atlantic water inflow occurred leading to higher surface water temperatures, open water conditions and thus, higher primary productivity and higher moisture supply to the growing regional ice sheet.

Preconditioning and Triggering

The preconditioning of this mega-scale failure event includes transition of TMF-sediments into normal hemi-pelagic glaciomarine sediments (spatial and lithological), increasing glacio-tectonic activity, rapid sea-level drop, possible de-stabilisation of (possible) gashydrates due to ocean warming, tectonic stress amplification due to increasing ice load and an (probably unprecedented) high speed of these environmental changes. The Yermak Slide was probably triggered by an amplified earthquake positioned near the bottle neck of the headwall area. The earthquake must have had an impact on tectonic movements along the Hinlopen cross shelf trough (fault zone).

Conclusion

This most prominent Hinlopen/Yermak Megaslide has successfully been geometrically described and dated. Based on these findings its character in relation to the climate history of Svalbard has been discussed. Thus the main objectives of this study have been achieved. Apart from these main objectives, the south-western Sophia Basin has been characterised a an excellent climate archive, and the application of Sr concentrations within the marine sediments have been shown to provide precious information on sea surface temperature and therefore Atlantic water inflow in the area. Further results of this study give constraints on the structure and tectonic behaviour of the Sophia Basin.

In more detail, the conclusion of this study are:

1. The extent and geometry of the Yermak Slide has been identified. It affected an area of more than 10.000 km² and involved an estimated sedimentary volume of 2.400 km³.
2. Thus the Yermak Slide is to be ranked among the largest exposed submarine slides worldwide and constitutes an end-member in a variety of geometrical aspects.
3. The Slide originated at the termination of the Hinlopen cross shelf trough and developed into the semi-enclosed Sophia Basin.
4. The slide consists of one major event (megaslide) and has been followed by several minor events.
5. This megaslide is to be characterised as a highly dynamic multiple-phase slope failure that lead to both compressional and extensional features within the Sophia Basin.
6. The slide process has been divided into 5 phases.
7. The megaslide as well as the following minor failure events developed retrogressive and created the cauliflower structure of the headwalls.
8. Physical appearance of both headwalls and slide debris point towards a major shelf collapse rather than a slide within less consolidated material.
9. Therefore a tectonic control on the megaslide seems favourable.
10. The first slide event (megaslide) has been dated into MIS 3 around 30 kyr. BP.
11. Thus the megaslide occurred during the rapid transition of the Kapp Ekholm Interstadial into Glaciation G on Svalbard, during enhanced inflow of Atlantic water, rapidly falling sea level and drastically increasing glacio-tectonic activity.
12. The trigger-mechanism, thus seems to be most likely connected with the development of a fore bulge

on the outer shelf as well as an asymmetrical ice-loading of the hinterland. And due to that, with enhanced tectonic activity along the fault zone below the Hinlopen trough. The final trigger is assumed to be an earthquake that may have been amplified by glacial loading.

13. The sedimentary record of the south-western Sophia Basin constitutes an excellent climate archive and provides evidence for numerous events of Atlantic water inflow during the last 240 kyr. BP.

14. Sr contents of sediments from this area mainly reflect sea surface temperature and thus Atlantic water inflow.

15. Elevated and peak Sr/Ca ratios mainly reflect terrigeneous events within the Sophia Basin.

Some concluding remarks may be granted to clarify the inconsistent nomenclature of the Yermak Slide: The Slide was first described by Cherkis et al. in 1999. They did not assign a name to the slope failure. Until the start of the ESF project and even after, the slide has been mentioned as Malene or Malene Bukta Slide in several papers (Vogt et al., 1999; Haflidason et al., 2004). Within the ESF project the slide was assigned the term "Yermak Slide" and was called according to this draft name until 2006 (Winkelmann et al., 2004; Vanneste et al., 2005; Winkelmann et al.. 2006). However, in 2006 the Norwegian project partners decided to re-name the slide into "Hinlopen Slide" (cf. Vanneste et al., 2006) despite these earlier publications and despite an earlier agreement. Following this developement, we decided to address the slide with a double name to reduce confusion and keep track within earlier publications. Therefore, the Yermak Slide is named "Hinlopen/Yermak Megaslide" in the third and second publication.

References

Cherkis, N.Z., Max, M.D., Vogt, P.R., Crane, K., Midthassel, A., Sundvor, E. (1999): Large-scale mass wasting on the north Spitsbergen continental margin, Arctic Ocean. Geo-Marine Letters 19, 131-142.

Haflidason, H., Sejrup, H.P., Nygard, A., Mienert, J., Bryn, P., Lien, R., Forsberg, C.F., Berg, K., Masson, D. (2004): The Storegga Slide: architecture, geometry and slide development, Marine Geology 213, 201-234.

Vanneste, M., Bünz, S., Mienert, J. (2005): Multi-phase submarine mega-sliding on the Arctic Continental Margin north of Svalbard: characteristics, morphology and volume estimates, NGF Abstracts and Proceedings of the 2nd International Conference “Submarine Mass Movements and Their Consequences”, 5-7 September 2005, Oslo, Norway.

Vogt, P.R., Gardner, J., Crane, K. (1999): The Norwegian-Barents-Svalbard (NBS) continental margin: Introducing a natural laboratory of mass wasting, hydrates and ascent of sediment, pore water and methane, Geo-Marine Letters 19, 2-21.

Winkelmann, D., Stein, R., Niessen, F. (2004): The Yermak Slide north of Svalbard (Arctic Ocean) - Preliminary Results, 2nd EUROMARGINS Conference, Palau de les Heures, 11-13 Nov., Barcelona, Spain.

Winkelmann, D., Jokat, W., Niessen, F., Stein, R., Winkler, A. (2006a): Age and extent of the Yermak Slide north of Spitsbergen, Arctic Ocean, Geochemistry Geophysics Geosystem, 7, Q06007, doi:10.1029/2005GC001130.

Chapter VII

Outlook

Outlook

Questions

With respect to the accomplished scientific work, there are a number of questions remaining or raising:

1. What are the precise ages of minor failure events that left smaller debris flows on the main debris of the Hinlopen/Yermak Megaslide and in what paleo-environmental context are they to be seen?
2. What is the outer extent of the Hinlopen/Yermak Slide in the Nansen Basin?
3. What did the associated tsunami of such an enormous megaslide looked like (wave height, and wave length, duration)?
4. Which areas were affected by the tsunami?
5. Are there tsunami deposits on Svalbard or the adjacent shelf (surviving the last glacial maximum, LGM)?
6. Can these potential deposits help to reconstruct the correct tsunami geometries?
7. What role do gashydrates play in preconditioning and configuration of the Hinlopen/Yermak Slide?
8. Are mega-scale slope failure events common for the Arctic realm?
9. How big can these slides and their tsunamis be?
10. Are slide frequencies of large-scale failures related to glacial cycles (to onset, duration or/and termination; and their related environmental changes like sea-level variations, tectonic effects or climate-controlled sedimentological changes)?
11. Can Arctic areas be classified as “prone to failure” (according to their sediments) or “endangered by tsunamis” (according to their geographic position)?
12. What types of submarine slides do exist (volcanic-, sea-level-, tectonic, climate-related,...)?
13. How can these slides be predicted?
14. Is there a general relation of Sr contents in (polar) marine sediments and other paleo-climate proxies like the stable oxygen isotopes of ice cores and stable carbon isotopes of planktic foraminifers?

Approach

1. Recovery of new sediment cores from the younger debris flows for AMS radiocarbon dating of the related failure events.
2. Planning and execution of a new cruise with RV “Polarstern” to the Nansen Basin and eastern Yermak Plateau with focus on recovery of new geophysical data and sediment cores from the outer slide.
3. Survey of the adjacent shelf to search and identify possible tsunami deposits.
4. Land-based screening for possible relict-deposits of the tsunamis.
5. Generation of a numerical tsunami model based on bathymetric data and dynamic modelling.
6. Tuning of the tsunami model to the tsunami deposit geological evidence.
7. Detailed geophysical and geochemical investigation of the headwall area of this unique slide.
8. Bathymetric mapping of the accessible Arctic shelves (general survey).
9. Scientific characterisation and classification based on statistical analysis of slide-related parameter.
10. Classification of Arctic areas based on their geographic position, sediment characteristic and tsunami hazard potential (GIS-based).
11. Development of regional prediction scenarios based on these classifications (GIS-based).
12. Launch of a pilot study related to the Sr contents of marine sediments and other environment-related proxies with focus on recent sedimentation processes, around Svalbard and in other polar regions. This study should focus on both surface sediments and ultra-high-resolution of longer sediment cores.

Chapter VIII

Acknowledgment

Acknowledgements

Zunächst möchte ich mich bei Herrn Prof. Dr. Rüdiger Stein für die Anregung zu dieser Arbeit und die Betreuung bedanken. Seine Diskussionsbereitschaft zu jeder Zeit hat mir in den letzten Jahren sehr geholfen.

Herrn Prof. Dr. Rüdiger Henrich danke ich für die Übernahme des Korreferats.

Ganz besonderer Dank gilt Dr. Wilfried Jokat für die vielen fachlichen Diskussionen, Kommentare und Anregungen während meiner gesamten Zeit am AWI und für die kritische Durchsicht meiner Arbeit in der Endphase.

Prof. Dr. Rüdiger Stein und Dr. Frank Niessen danke ich für die Überlassung unveröffentlichter Daten.
Allen Mitarbeitern der Arktisgruppe (Klaus Dittmers, Kirsten Fahl, Sabine Hanisch, Jens Hefter, Beate Hollmann, Walter Luttmer, Jens Matthiessen, Cornelia Saukel, Christoph Kierdorf, Christoph Schäfer, Frank Schoster, Dominik Weiel, Petra Weller), Kapitän und Besatzung der “Polarstern” während der ARK-XX/3 sowie Graham Eagles, Wolfram Geissler, Jörn Hatzky, Veit Helm und Andreas Winkler, danke ich für das angenehme Arbeitsklima während der letzten Jahre. Sie haben alle auf dem einen oder anderen Weg zum Gelingen dieser Arbeit beigetragen.

Ein ganz besonderer Dank gilt meinen Verwandten in Deutschland und in Argentinien, die mich in allen Lebenslagen uneingeschränkt unterstützt haben.

Dir Denise, danke ich am meisten. Deine Unterstützung und Dein Verständnis ist die beste Motivation. Ich danke Dir von ganzem Herzen.

Chapter IX

Appendix

Appendix

The corresponding data sets for the publications of the previous chapters
will be available via the PANGAEA online data bank system (http://www.pangaea.de).